## General Disclaimer

One or more of the Following Statements may affect this Document

- This document has been reproduced from the best copy furnished by the organizational source. It is being released in the interest of making available as much information as possible.

- This document may contain data, which exceeds the sheet parameters. It was furnished in this condition by the organizational source and is the best copy available.

- This document may contain tone-on-tone or color graphs, charts and/or pictures, which have been reproduced in black and white.

- This document is paginated as submitted by the original source.

- Portions of this document are not fully legible due to the historical nature of some of the material. However, it is the best reproduction available from the original submission.
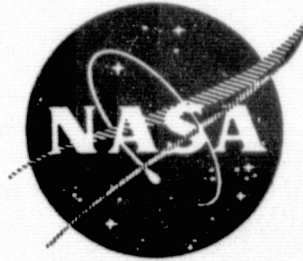
Produced by the NASA Center for Aerospace Information (CASI)

WIND TUNNEL TEST OF MODEL TARGET THRUST REVERSERS

FOR THE PRATT & WHITNEY AIRCRAFT JT8D-100 SERIES ENGINES

INSTALLED ON A 727-200 AIRPLANE

by D. Hambly

BOEING COMMERCIAL AIRPLANE COMPANY

A DIVISION OF

THE BOEING COMPANY

Prepared for

NATIONAL AERONAUTICS AND SPACE ADMINISTRATION

NASA Lewis Research Center
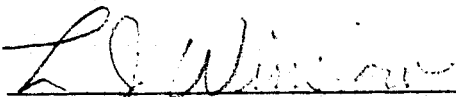
Contract NAS3-17842

1. Report No. DR-134709	2. Government Accession No.	3. Recipient's Catalog No.
4. Title and Subtitle Wind Tunnel Test of Model Target Thrust Reversers for the Pratt & Whitney Aircraft JT8D-100 Series Engines Installed on a 727-200 Airplane		5. Report Date September 1974
		6. Performing Organization Code
7. Author(s) D. Hambly		8. Performing Organization Report No. D6-41900
		10. Work Unit No.
9. Performing Organization Name and Address Boeing Commercial Airplane Company P. O. Box 3707 Seattle, Washington 98124		11. Contract or Grant No. NAS3-17842
		13. Type of Report and Period Covered
12. Sponsoring Agency Name and Address National Aeronautics and Space Administration Washington, D. C. 20546		14. Sponsoring Agency Code

15. Supplementary Notes

V/STOL and Noise Division Chief, R. W. Schroeder
NASA Lewis Research Center, Cleveland, Ohio 44135

16. Abstract

This report presents the results of a low speed wind tunnel test of 0.046 scale model target thrust reversers, for the Pratt & Whitney Aircraft JT8D-100 series engines, installed on a 727-200 model airplane. The full airplane model was mounted on a force balance, except for the nacelles and thrust reversers, which were independently mounted and isolated from it. The installation had the capability of simulating the inlet airflows and of supplying the correct proportions of primary and secondary air to the nozzles. The objectives of the test were to assess the compatibility of the thrust reversers target door design with the engine and airplane. This was accomplished by making the following measurements: hot gas ingestion at the nacelle inlets; model lift, drag and pitching moment; hot gas impingement on the airplane structure and a qualitative assessment of the rudder effectiveness. Two configurations were tested in detail to obtain the above information. A total of twelve were tested to determine hot gas ingestion characteristics.

The major parameters controlling hot gas ingestion were found to be thrust reverser orientation, engine power setting, and the lip height of the bottom thrust reverser doors on the side nacelles. A negative thrust reverser orientation (side nacelle thrust reversers rotated inward towards the vertical tail at the top) is required to achieve acceptable ingestion velocities. The thrust reversers tended, in general, to increase the model lift, decrease the model drag and decrease the model pitching moment. No hot gas impingement problems on the airplane structure appear to exist based on the thermocouple readings. A substantial loss of rudder effectiveness occurs at -20° reverser orientation and a smaller one at -10°.

Selection of a suitable thrust reverser configuration and assessment of stopping capability, compared with the current clamshell/deflector door installation on the 727 airplane, will be based on a landing roll study, and involve resolution of the conflicting hot-gas ingestion and airplane controllability requirements.

17. Key Words (Suggested by Author(s)) 727 Airplane Target Thrust Reverser Airplane Refanned JT8D Engine Controllability Hot Gas Ingestion Aerodynamic Interference Hot Gas Impingement	18. Distribution Statement Unclassified - Unlimited		
19. Security Classif. (of this report) Unclassified	20. Security Classif. (of this page) Unclassified	21. No. of Pages 154	22. Price*

FOREWORD

The low-speed wind tunnel test described in this report was performed by the Propulsion Technology Staff of the Boeing Commercial Airplane Company, a division of The Boeing Company, Seattle, Washington. The work, sponsored by NASA Lewis Research Center and reported herein, was performed between March 1974 and June 1974.
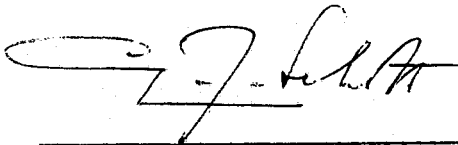
This report has been reviewed and is approved by:

_____
L. J. Winslow, Group Engineer
Propulsion Technology Staff

Date 15 July 1975

_____
G. J. Schott
Chief, Staff Technology
JT8D Refan Program

Date JULY 21 1975

_____
K. P. Rice
Program Manager
JT8D Refan Program

Date 7/22/5

TABLE OF CONTENTS

1.0 SUMMARY

The use of the JT8D Refan engine on the 727 airplane requires a new thrust reverser. A target type thrust reverser was selected for the new design compared with a clamshell/deflector door design of the current installation. The new thrust reversers will be required to reverse approximately 50% more air flow at lower nozzle pressure ratios and will be located further aft compared with the current 727 installation. In order to determine the performance of the target design and assess its compatibility with the engine and airplane restraints and requirements, a series of model tests and a landing roll analysis are required. The results of one of these model tests, a wind tunnel test, with objectives stated below, are presented in this report.

The objectives of the wind tunnel test were:

o To measure the hot gas ingestion characteristics at the nacelle inlets for a series of thrust reverser configurations and orientations.

o To measure the effect of thrust reverser use on the airplane lift, drag and pitching moment for use in the landing roll studies.

o To measure the hot gas impingement on the airplane structure and determine a thrust reverser configuration and orientation that will keep impingement within acceptable temperature limits.

1

o To obtain a qualitative assessment of the effect of thrust reverser
   use on the airplane rudder effectiveness.

A 0.046 scale full airplane model of a 727-200 airplane was manufactured for
this test and twelve thrust reverser configurations were tested. The test
was conducted in the Boeing Low-Speed Wind Tunnel 'A', located at Boeing
Field, Seattle, Washington from March 20 through June 3, 1974 under author-
ization of NASA Contract NAS3-17842.

Interpretation of the test results requires definition of the following terms
Ingestion velocity is defined as the average of the wind tunnel velocities at
which a local temperature rise of 10°F occurs on any one of the inlet thermo-
couples for each of the two side nacelles. A low ingestion velocity is de-
sirable. Orientation refers to the "clocking" angle of the thrust reversers
on the side nacelles only. The center thrust reverser remained in the hori-
zontal position for all testing. A negative orientation has the top reverser
doors on the side nacelles rotated toward the vertical tail.

Initial testing with Configuration 1 (3.5 inch full scale lip height) indi-
cated excessively high ingestion velocities (i.e., 131 knots at 0° orienta-
tion with 40° flaps and nozzle primary pressure ratio [PPR] of 1.8). Follow-
ing the initial testing, a series of runs were made to determine a configura-
tion that would reduce the ingestion velocity to practical levels. The cur-
rent clamshell/deflector door installation allows operation down to 70 knots.
These runs indicated that the major parameters controlling ingestion velocity

are reverser orientation, power setting and the lip height of the bottom reverser doors on the side nacelles. Further, smaller reductions could be achieved by raising the trailing edge flaps to the 25° position. Two configurations were then selected for more comprehensive ingestion testing and to measure the effect of the thrust reversers on model lift, drag and pitching moment, hot gas impingement on the airplane structure and airplane rudder effectiveness. These were Configuration 12 (1.5 inch full scale lip height) and Configuration 7 (no lips on the two side thrust reversers and 3.5 inch full scale lips on the center engine).

The following conclusions were drawn from this test:

o To achieve a stopping capability comparable to the current 727 installation will require a lip height at all engine positions sufficient to produce equivalent static reverse thrust performance and a negative thrust reverser orientation to give a practical ingestion velocity.

o The force balance data, in general, indicates trends in the airplane aerodynamic parameters which diminish the installed stopping capability of the thrust reversers, i.e., an increase of model lift, a decrease of model drag and a decrease of pitching moment. The significance of these changes will be determined from an airplane landing roll study, though only the drag loss will be of any consequence.

o Based on the thermocouple coverage, no hot gas impingement problems on the airplane structure appear to exist for a thrust reverser

orientation range of 0° to-20° for Configurations 12 and 7. The highest measured temperatures occur on the lower surface of the airplane fuselage.

o Qualitative assessment of the rudder effectiveness data indicates that a serious loss of local rudder dynamic pressure occurred at -20° orientation for all configurations and engine power settings tested, making the rudder ineffective. The data indicates a much greater rudder dynamic pressure at the -10° orientation. Further testing of this orientation is required to assess its acceptability.

Selection of a suitable thrust-reverser configuration and substantiation of stopping capability compared with the current 727 installation will be based on a landing roll study and involve satisfactory resolution of the conflicting hot-gas ingestion and airplane controllability requirements.

2.0 INTRODUCTION

2.1 BACKGROUND

The Pratt and Whitney Aircraft JT8D-100 engine is a derivative of the basic JT8D turbofan engine modified to incorporate a new, larger diameter, single-stage fan with a bypass ratio of 2.0 and two supercharging low-pressure compressor stages. The modification lowers jet noise, increases takeoff and cruise thrust, and lowers specific fuel consumption. The use of JT8D-100 series engines (-109, -115, and -117), also referred to as refanned JT8D engines, on the Boeing 727 airplane will require a new thrust reverser design.

A target type thrust reverser was selected for the new design, compared with the clamshell/deflector door type of the current installation. The design criteria for the new thrust reverser are as follows:

        o Static performance equal to current installation

        o No adverse effects on airplane controllability

        o Reingestion improved over the current 727

        o No increase in cruise drag

        o Reliability improved over the current 727

The new installation will be required to reverse approximately 50% more airflow at lower nozzle pressure ratios, compared with the current installation, while being located further aft relative to the airplane structure. Table I compares the more pertinent parameters of the JT8D-15 engine with its refanned derivative, the JT8D-115. The -115 engine was selected for thrust reverser development since it was representative of the -100 series engine spectrum.

To confirm the target door design and to determine its compatibility with the

JT8D-100 series engines and the 727 airplane, a series of model tests are required. The results of these tests are then incorporated into an airplane landing roll analysis to assess the acceptability of the candidate reverser configurations.

Briefly, the tests are as follows:

o A static test to determine reverse performance and engine airflow match of the target design (Reference 1).

o A wind tunnel test with thrust reversers mounted on a model airplane to develop a configuration that is compatible with the 727 airplane and the JT8D-100 series engines (hot-gas ingestion). This report presents the results of this test.

o A wind tunnel test to assess the effect of the thrust reversers on airplane stability and control characteristics (Reference 2).

2.2 TEST OBJECTIVES

The objectives of the wind tunnel test were:

o To measure the hot gas ingestion at the engine inlets and select a thrust reverser configuration and orientation that will best keep ingestion within allowable temperature distortion limits at reasonable airplane speeds.

o To measure the effect of thrust reverser operation on airplane model lift, drag and pitching moment for use in the landing roll studies.

o To measure the hot gas impingement on the airplane structure and determine a thrust reverser configuration and orientation that will

6

keep impingement within acceptable temperature limits.

o   To obtain a qualitative assessment of the effect of thrust reverser

operation on airplane rudder effectiveness.

The test was performed at Boeing Field, Seattle, Washington from March 20

thru June 3, 1974 under authorization of NASA Contract NAS3-17842.

3.0   NOMENCLATURE

$\bar{c}$	Mean aerodynamic chord of the wing, FT
CD, C_D	Airplane drag coefficient, drag/q Sw
CL, C_L	Airplane lift coefficient, lift/q Sw
CM, C_M	Pitching moment coefficient about the quarter MAC, positive-airplane nose up, pitching moment/q Sw $\bar{c}$
CR	Cruise configuration
D	Nozzle exit diameter, IN
FPR	Fan pressure ratio, P_{TF}/P_{SG}
MAC	Mean aerodynamic chord of the wing, FT
PPR	Primary pressure ratio, P_{TP}/P_{SG}
P_{SG}	Ground plane static pressure, PSIA
P_{TF}	Mean of three fan total pressure probes, PSIA
P_{TP}	Mean of three primary total pressure probes, PSIA
q	Dynamic pressure based on tunnel velocity, PSF
REV	Reverse configuration
S	Reverser setback distance, IN
Sw	Wing reference area, FT^2
T_A	Ambient temperature, °F
T/R	Thrust Reverser
$T_{T/C}$	Impingement temperature, °F
T_{TF}	Fan total temperature, °F
T_{TP}	Primary total temperature, °F
V	Tunnel velocity, KNOTS
V1,V2,V3	Vertical tail velocities, KNOTS

PRECEDING PAGE BLANK NOT FILMED

4.0 MODEL HARDWARE, TEST FACILITY AND DATA REDUCTION

4.1 MODEL HARDWARE AND INSTRUMENTATION DESCRIPTION

4.1.1 AIRPLANE MODEL

A 0.046 scale model of the Boeing 727-200 airplane was manufactured for this test. The model was mounted on a simulated ground plane which was installed approximately 20 inches above the tunnel floor. The fuselage was set at an angle of 0° relative to the ground plane. The trailing edge flaps were adjustable to the 5°, 25°, and 40° positions and the spoilers to the 45° extended position. For all testing the leading edge flaps and slats were in the extended position and the horizontal tail was maintained at a fixed angle of attack. Figure 1 shows an overall view of the model installed in the wind tunnel.

To allow aerodynamic forces to be measured, the model was constructed with the engine nacelles isolated and independently mounted from the airplane body. The fuselage and vertical and horizontal tails were constructed of fiberglas and the wings and flaps from aluminum. The model was mounted on a force balance which was attached to the ground plane. The force balance was calibrated for lift, drag and pitching moment measurements.

The engine nacelles were mounted to a pipe of semi-circular section which ran the length of the fuselage. The pipe was routed through the ground plane and tunnel floor and connected to a vacuum pump to extract the inlet flows entering the nacelle inlets. This pipe also

provided support for instrumentation lines and the pipework supplying the nozzle exhaust flows. The center engine nozzle was mounted off the nozzle flow pipework. Figure 2 shows the model arrangement.

Each nacelle was supplied with separate fan and primary airflows. Choke plates were installed in each airflow line prior to mixing in the nozzles. Three total pressure probes were installed in each fan and primary flow downstream of the choke plates. Fan and primary nozzle charging station pressures were determined by averaging the three total pressures. For the purposes of setting up test conditions, one fan and one primary probe from each engine were monitored. Fan and primary total temperatures for each nacelle, together with the delivery pressures, were measured upstream of the chokeplates.

Twenty thermocouples were located as in Figure 3 to measure the hot gas impingement on the airplane structure during reverse thrust operation. These were located to measure local air temperature close to the airplane structure.

The effect of thrust reverser operation on airplane rudder effectiveness was evaluated by measuring velocities at three locations in close proximity to the vertical tail. The velocities were determined from total and static pressure measurements located as in Figure 3 and shown in Figure 4.

Airflow was drawn through the inlets to simulate the flow field. The
amount of inlet suction could be set to the desired value which was
dependent upon the engine power setting. The total inlet airflow (3
nacelles) was measured at a single position, and the distribution be-
tween the three inlets was assumed to be in proportion to the inlet
throat areas. A static pressure port was located at the throat of
each inlet to assess the throat Mach number; i.e., flow distribution.
Each inlet was instrumented with 13 thermocouples to detect the inges-
tion of hot exhaust gases. The thermocouples were arranged, as shown
in Figure 5, with one at the center and two concentric rings of six
each located in the plane of the inlet throat. The inner seven ther-
mocouples were located to measure the temperature of the ingested gas
that would pass through the engine primary system. The thermocouples
were located in this manner in an attempt to compare the ingestion
with the engine manufacturer's allowable temperature distribution lim-
its, which are a function of radial location in the inlet.

4.1.2   THRUST REVERSER MODELS

The model thrust reversers were assembled with a fixed spacing distance
(i.e., distance between nozzle exit plane and the thrust reverser door
on the engine centerline, S/D = 0.966) and with the doors in the fully
extended position only. The internal door contour represented that of
the revised configuration tested for static performance, Reference 1.
They were designed to be readily attachable and removable from the

engine nozzles and rotatable about the nozzle centerline. The center
engine reverser was mounted in the horizontal position only while the
side engines were capable of attachment at various "clocking" angles
between -20° and +30° in 5° increments. A negative "clocking" angle
indicates that the side nacelle reverser top doors are rotated toward
the vertical tail while a positive "clocking" angle has the top doors
rotated away from the vertical tail. Figure 4 shows the port nacelle
thrust reverser installed at 0° "clocking" angle.

The models were designed to have easily changeable lips and fences.
Thrust reverser configurations are defined by various combinations of
lips and fences and differences in these combinations between engine
positions. Figure 6 defines the thrust reverser door components, and
Figure 7 shows the model components. Two sets of fences and six sets
of lips were manufactured although not all were tested. Twelve con-
figurations were tested, the details of which are given in Table 2 and
Figure 6.

4.2   TEST FACILITY AND INSTRUMENTATION DESCRIPTION
The test was conducted in the Low Speed Wind Tunnel 'A' facility lo-
cated at Boeing Field. Atmospheric air was drawn through the tunnel
bellmouth, flow straighteners and test section by a variable pitch pro-
peller driven by an Allison 501-D13 gas turbine engine. The test sec-
tion is nominally 9 foot by 9 foot. Tunnel velocities up to

approximately 160 knots were set during this test.

Plant air was used to supply the fan and primary airflows. The system allowed individual fan and primary flows for each nacelle to be supplied to the model. The total fan airflow was measured by an ASME nozzle located upstream of the three-way split to each nacelle. Each line had a control valve installed to allow the same pressure ratio to be set on each nacelle. The plant facility supplied the fan air at the desired temperature. The primary airflow was supplied from a different, unheated plant source. The primary airflow was then heated by a burner at the tunnel site. A bypass system allowed the burner to be started without air flowing through the model. An ASME nozzle installed upstream of the burner measured total primary airflow. The burner fuel flow was added to the airflow in the data reduction program. Downstream of the burner the airflow was split three ways with each line having a control valve. Model construction limited the primary temperature to approximately 750°F.

The inlet airflow was simulated by sucking the inlets by means of a vacuum pump and was adjusted during the test to equal that supplied to the nozzles. The total inlet airflow was measured by a venturi installed in the suction line.

The tunnel velocity was determined from total and static pressure

measurements at the exit of the tunnel bellmouth. Two total pressure probes were located in the tunnel sidewall and roof in a plane halfway along the model. Suitably placed static pressure ports were located in the tunnel wall for each of the total pressure probes. A 10 probe total pressure rake was installed on the ground plane ahead of the port wing together with a static pressure port on the ground plane.

4.3   ACCURACY OF MEASUREMENTS

Where accuracy is expressed as a percentage below, it represents the percentage of the full range value.

Measurement	Range	Accuracy
Tunnel total pressure	0 - 0.5 PSI	± 0.25%
Tunnel static pressure	0 - 1 PSI	± 0.25%
Primary nozzle upstream pressure	0 - 150 PSI	± 0.25%
Primary nozzle pressure drop	0 - 20 PSI	± 0.25%
Fan nozzle upstream pressure	0 - 100 PSI	± 0.25%
Fan nozzle pressure drop	0 - 20 PSI	± 0.25%
Venturi static pressure	0 - 5 PSI	± 0.25%
Venturi pressure drop	0 - 5 PSI	± 0.25%
Primary exit total pressure	0 - 30 PSI	± 0.5%
Fan exit total pressure	0 - 25 PSI	± 0.5%
Ground plane static pressure	0 - 1 PSI	± 0.25%
Vertical tail total pressure	0 - 1 PSI	± 0.5%

Measurement	Range	Accuracy
Vertical tail static pressure	0 - 5 PSI	± 0.5%
Tunnel total temperature	20 - 60°F	± 2°F
Venturi total temperature	20 - 70°F	± 2°F
Primary total temperature	AMB - 1000°F	± 4°F
Fan total temperature	AMB - 1000°F	± 4°F
Airplane impingement temperature	AMB - 500°F	± 4°F
Inlet ingestion temperature	AMB - 500°F	± 4°F
Airplane lift	0 - 300 LB	± 0.5%
Airplane drag	0 - 200 LB	± 0.5%
Airplane pitching moment	0 - 1000 IN LB	± 0.5%
Tunnel velocity	0 - 160 KNOTS	± 2%

4.4   TEST PROCEDURES AND TEST CONDITIONS

Following the installation of the model in the tunnel, three calibration tests were performed prior to testing. These were: 1) calibration of the model and force balance for lift, drag and pitching moment; 2) calibration of the inlet flow simulation system; and 3) determination of the fan and primary nozzle flow characteristics. A post calibration of the model and force balance was performed for lift and drag only.

Five types of runs were accomplished to satisfy the test objectives.

1. Baseline runs to determine the airplane aerodynamic parameters and

airplane rudder characteristics without the thrust reversers installed. Data were recorded for flap settings of 5°, 25° and 40° over a velocity range of 20 - 160 knots, in 20 knot increments. These runs were conducted with ambient air flowing through the nozzles and simulated inlet flow. Data were recorded following a stabilization period of 30 seconds.

2. Deceleration runs were made to determine the ingestion characteristics. After setting the desired test conditions and following a 30 second stabilization period, the tunnel velocity was reduced in a steady manner from velocities in the region of 140 knots to 20 knots in approximately 45 seconds. Ingestion temperatures were recorded on oscillographs as described in Section 4.5. Runs were made to determine the effect of thrust reverser configuration, reverser orientation, flap setting and engine power setting. One run was made for each test configuration.

3. Steady state velocity runs were performed to determine the airplane aerodynamic parameters and rudder effectiveness with operating thrust reversers. Data were recorded for selected thrust reverser configurations only. The effect of flap setting, reverser orientation and engine power setting was determined for these configurations. One run was made for each configuration. Ambient air was used in the nozzles for this series of runs since it had been

determined that heated air through the model resulted in force
balance shifts. Data were recorded over a tunnel velocity range
of 20 - 140 knots following a 30 second stabilization period at
each condition.

4. Steady state velocity runs were performed, with heated air flowing
through the nozzles, to determine the steady state ingestion char-
acteristics and hot gas impingement temperatures. Data were re-
corded for selected thrust reverser configurations only. Runs
were made to determine the effect of flap setting, reverser orien-
tation and engine power setting. One run was made for each con-
figuration. The fan temperatures were set to the required fan
total temperature to ambient temperature ratio and the primary
temperatures to approximately 750°F. The oscillographs were also
run during some of these runs to determine steady state ingestion
temperatures. Data were recorded over a tunnel velocity range of
40 - 120 knots following a stabilization period of 30 seconds at
each condition.

5. Flow visualization runs were performed, using steam, to provide a
qualitative aid to interpretating hot gas ingestion, hot gas im-
pingement, aerodynamic interference and rudder effectiveness data.
These runs were performed for two selected configurations only;
the effects of flap setting, reverser orientation and engine power

setting were observed. Two types of runs were performed, namely a deceleration type, as previously described, and a steady state type. These runs were performed over a velocity range of 40 - 120 knots. A high speed, black and white, front mounted movie camera was used to record the decelerations. Three black and white still cameras were used to record the steady state runs. Movies and photos were also recorded using wool tufts located on the ground plane, airplane fuselage and vertical tail for flow visualization.

Steam for the flow visualization runs was generated by heating the fan and primary airflows and injecting water into each fan and primary line. A single water pump with six delivery lines supplied the water to the fan and primary flows. Each water line was controlled with a hand valve. To give an indication of tunnel speed during these runs, a tunnel speed indicator was installed in the leading edge of the ground plane. The indicator was calibrated and marked in knots. Windows in the tunnel walls and roof allowed still and movie cameras to record the flow visualization runs.

The generalized test procedure is outlined below:
1. Set up desired test configuration, inspect instrumentation and make leak checks, etc.
2. Inspect model and facility.
3. Zero check instrumentation.

4. Start Allison 501 turboprop and warm up.

5. Set tunnel velocity to approximately 80 knots.

6A. For ambient flow in the nozzles, open individual fan and primary valves and adjust until the desired fan and primary pressure ratios are set on each nacelle.

6B. For heated flow in the nozzles, request desired fan temperature from plant facility. Close burner bypass valve, light burner, allow burner to stabilize and open bypass valve. Adjust the fan and primary flow valves until the desired fan and primary pressure ratios and primary temperatures are set on each nacelle.

7. Set vacuum pump to desired value to equal total nozzle airflow.

8. Increase tunnel velocity to 140 knots.

9. Recheck nozzle pressure ratios.

10. Allow 30 seconds for stabilization.

11. Close cut-off valves.

12. Activate scannivalves and record data.

13. After scan, open cut-off valves.

14. Reduce tunnel velocity in 20 knot increments down to 20 knots, repeating steps 9 - 13.

15. If model change is required, idle Allison 501 for 5 minutes and then shut down. If a run is required at different engine pressure ratios, go to step 5 without shutting down tunnel.

4.5   DATA REDUCTION

Data were recorded on the standard Low Speed Wind Tunnel data
acquisition system. This system, a Hewlett-Packard Dymec 2010D, is
a trap and scan scannivalve system with output on punched paper tape.

Final data reduction was accomplished by a computer, using a Boeing
data reduction program.

Acquisition of the inlet ingestion data was accomplished by recording
the individual inlet thermocouple temperatures as oscillograph traces.
Three oscillographs, one per nacelle, were used for this task. Each
roll of paper contained 13 thermocouple traces plus one trace repres-
enting tunnel velocity. The ingestion temperatures and velocities
were evaluated manually.

5.0 DISCUSSION OF TEST RESULTS

5.1 REVERSED GAS INGESTION

5.1.1 INGESTION VELOCITY DEFINITION

The estimated limiting temperature distortion at the engine inlet face for the JT8D-100 series engines, Reference 3, is a temperature difference $(T_{T2\ LOCAL} - T_A)$ of $20^\circ F$, constant from the fan hub to within 7 inches of the fan tip; from that position the limit rises non-linearly to $50^\circ F$ at the fan tip. This limit assumes no pressure distortion at the engine inlet and 100 percent takeoff airflow. Since the model was operated with the primary airflows limited to approximately $750^\circ F$ (for S.L., STD. DAY, takeoff conditions the primary temperature is $1,009^\circ F$) and with unknown inlet pressure distortion, a $10^\circ F$ local temperature rise was chosen as the probable model temperature distortion that would correlate with the full-scale limit of $20^\circ F$. The temperature rise to cause engine surge can only be determined from airplane taxi tests. The data from a taxi test of a 727-200 airplane equipped with JT8D-9 engines indicated that surges occurred with measured inlet temperature rises of about $18^\circ F$. Initial model testing indicated that the inlet temperature distribution was such that the area of the inlet in which a $20^\circ F$ temperature rise limit was permitted would be controlling. Little difference in ingestion velocity would result from the selection of a limit of $20^\circ F$ rather than $10^\circ F$ since the variation in inlet over-temperature with forward speed is very large in this over-temperature region.

The ingestion velocities used in this document were determined in the following manner. The three oscillographs recording the thermocouple temperature histories during a deceleration were analyzed to determine the tunnel velocities at which a $10^\circ F$ local temperature rise occurred on any one inlet thermocouple for each engine. The ingestion velocity was then computed as the average of the tunnel velocities for the two side nacelles. The test data showed that the side nacelle inlets always reached the $10^\circ F$ temperature rise limit at higher velocities than for the center nacelle inlet.

5.1.2   INITIAL DEVELOPMENT TESTING

Initial testing started with Configuration 1 (3.5 inch full-scale lip height) and indicated excessively high ingestion velocities of 99 knots at -20° orientation, 131 knots at 0° orientation and an estimated 160 knots at +20° orientation. The test conditions were 40° flaps and a nozzle primary pressure ratio (PPR) of 1.8, with only the primary airflows heated. Since the ingestion velocities with Configuration 1 were unacceptably high at any orientation, a series of deceleration runs were made to determine a reverser configuration that would significantly reduce these velocities and yet retain a level of reverse thrust performance comparable with the current installation. This testing was performed with the primary airflows heated to approximately 750°F. Initial testing had indicated little difference in ingestion velocities whether the fan airflows were heated or not. Facility scheduling during this period precluded the supply of heated fan airflows on a continuous basis. The effect of flap angle, reverser orientation and engine power setting were investigated during this testing, and the results are shown in Figures 8, 9, 10, and 11.

Figure 8 shows the effect of reverser orientation from +20° to -20° for Configurations 1, 2, 9, 12, and 13, for 40° flaps and a nozzle primary pressure ratio of 1.8. Configuration 1 indicated a 60 knot reduction in the ingestion velocity while Configuration 2 indicated a reduction of approximately 30 knots. The other configurations indicated reductions between the values for Configurations 1 and 2. Configuration 2 gave a 30 knot improvement compared with Configuration 1 at +20° orientation but none at-20°. The lowest levels of ingestion velocity, 15 knots lower than the next lowest configuration, were given by Configurations 9 and 13, both of which had no lips on the bottom doors of the thrust reversers located in nacelle positions 1 and 3. The lower door lip height of the side engine thrust reversers is the major parameter controlling the level of ingestion velocity. However, a configuration, with different lip heights between upper and lower reverser doors results in unacceptably high assymetric loading of the reverser

mechanism, Reference 1. The assymetric loading will also result in a moment that will tend to off-load the airplane nose gear.

The effect of engine power setting (plotted as nozzle primary pressure ratio) on ingestion velocity is given for Configurations 1, 7, 12, and 14 in Figure 9. Primary pressure ratios of 1.25 and 1.5 represent, respectively, 40 and 70 percent of gross takeoff thrust. The data is presented for test conditions of 40° flaps and 0° reverser orientation. Configurations 7 and 14 had the fan airflows heated to the correct fan total to ambient temperature ratio. An average reduction in ingestion velocity of 27 knots could be achieved by reducing the primary pressure ratio from 1.8 to 1.5. A further average reduction in ingestion velocity of 28 knots could be achieved by reducing the primary pressure ratio further to 1.25. Configuration 7 produced the lowest level of ingestion velocities but has a low reverse thrust performance.

The effect of raising the flaps from 40° to 25° is shown for Configurations 1, 9, and 12, in Figure 10, for a nozzle primary pressure ratio of 1.8. For Configuration 1 and 0° orientation, the effect of raising the flaps caused a 20 knot reduction of ingestion velocity. For Configuration 9, a reduction of ingestion velocities between 7 and 11 knots was measured over an orientation range of +20° to -20°. For Configuration 12, the reduction is between 7.5 and 12.5 knots over an orientation range of +20° to -20°. The primary landing flap setting is 40° with an alternate setting of 30°. The time required to raise the flaps to the 25° position may be too slow to achieve the potential ingestion velocity reduction.

Figure 11 shows the effect of full-scale lip height on ingestion velocity for test conditions of 40° flaps, a nozzle primary pressure ratio of 1.8 and reverser orientations of 0° and -20°. The lip height variable is that of the bottom lips on the side nacelles. At 0° orientation, reduction of the bottom lip height from 3.5 inches to zero reduces the ingestion velocity by 30 knots (i.e., Configuration 1 to Configuration 9). The reduction at -20° orientation is 25 knots. Configurations 12, 13, and 14, which are based on 1.5 inch

lips, show 5 knots lower ingestion speeds compared with the Configurations 1, 4, and 9, based on 3.5 inch lips. The difference is probably due to the influence of the center thrust reverser. A configuration with no lips on each thrust reverser is represented by Configuration 8 and gives a further 8 knot reduction in ingestion speed compared with the 1.5 inch lip configurations. It is important, however, to remember that as lip height is reduced so is the efficiency of the reverser.

From this initial testing, the following conclusions were made. A positive reverser orientation produced unacceptably high ingestion velocities. Some reduction could be achieved by raising the flaps. The lip height on the bottom of the side mounted thrust reversers was the major influence in controlling the ingestion velocity level. A configuration with different lip heights between top and bottom doors resulted in unacceptable assymetric loading of the reverser linkages, while a no lip configuration top and bottom results in a performance level that is probably too low (14% static reverse thrust at a nozzle primary pressure ratio of 1.8), see Reference 1.

5.1.3 INGESTION CHARACTERISTICS FOR CONFIGURATIONS 12 AND 7

Two configurations, namely 12 (with 1.5 inch lips and fences on all reversers) and 7 (with 3.5 inch fences on all reversers, 3.5 inch lips on the center position and no lips on the side doors) were selected for further testing to determine the effect of flaps, orientation, and engine power setting. Configuration 12 is estimated to have a static reverse thrust of 37.5% and Configuration 7 an estimated static reverse thrust of 24.6%, both at a nozzle primary pressure ratio of 1.8 (Reference 1). Initial testing of Configuration 7 indicated potential ingestion velocity gains to offset the lower reverse performance.

Results for Configuration 12 are presented in Figures 12, 13, and 14. Figure 12 presents ingestion velocities against nozzle primary pressure ratio for orientations of 0^0, -10^0, and -20^0. The data are for a 40^0 flap setting. The current 727 airplane with clamshell/deflector door thrust reverser allows operation down to 70 knots. In normal use, the engine power rating achieved, in reverse, is dependent upon the ambient temperature (constant power lever angle). A landing roll study will be required to compare the stopping capability of Configuration 12 with the various orientation and primary pressure ratio combinations with the stopping capability for the current installation. For example, at a nozzle primary pressure ratio of 1.5, it would be possible to operate down to velocities of 88.5, 73, and 64.5 knots at reverser orientations, respectively, of 0^0, -10^0, and -20^0. Figure 13 presents similar data for the 25^0 flap setting. At a nozzle primary pressure ratio of 1.8, a reduction of 13 knots and 11 knots occurred, for 0^0 and -20^0 orientations, respectively, due to the flap change. Little reduction was measured for a nozzle primary pressure ratio of 1.25. At a 1.5 nozzle primary pressure ratio, the ingestion velocities are, respectively, 84, 77.5, and 58 knots for reverser orientations of 0^0, -10^0, and -20^0. The data for the -10^0 orientation generally does not follow the same trends as for the 0^0 and -20^0 orientations. Ingestion velocities for a 5^0 flap setting are presented in Figure 14, for nozzle primary pressure ratios of 1.5 and 1.8 at reverser orientations of 0^0 and -20^0. Compared with the 25^0 flap data, a further reduction of ingestion velocity of 2 - 3 knots was measured at 0^0 orientation and 3 - 6 knots at -20^0 orientation.

Configuration 7 ingestion data is presented in Figures 15 and 16. Figure 15 gives ingestion velocities against nozzle primary pressure ratio for orientations of 0^0, -10^0, and -20^0 and a 40^0 flap setting. The Configuration 7 (Figure 15) ingestion velocities are lower than those for Configuration 12 (Figure 12) by 7 - 11 knots at 0^0 orientation; at -20^0 orientation the ingestion velocity is lower by 9 knots at a nozzle primary pressure ratio of 1.8 but higher by 9 knots at a 1.25 nozzle primary pressure ratio. At a nozzle primary pressure ratio of 1.5, the ingestion velocities are respectively 80, 76, and 66 knots for reverser orientations of 0^0, -10^0, and -20^0.

Figure 16 gives ingestion data for Configuration 7 at 25° flaps and -10° orientation. The ingestion velocities are generally several knots lower than for the 40° flap setting.

The ingestion velocities achieved by Configuration 7 were probably not low enough to offset its lower static performance compared with Configuration 12, though this will be determined from the landing roll analysis. A target thrust reverser configuration having comparable stopping capability with the current installation will probably require a negative reverser orientation and a lip height that will give a reverse thrust performance similar to the clamshell/deflector door design.

Test data for Configuration 15 (thrust reverser in the center position only with 3.5 inch full-scale lip height) indicated that this configuration could probably be operated at takeoff power rating to 0 knots.

5.2   FORCE BALANCE DATA

5.2.1   BASELINE DATA, DATA USE AND LIMITATIONS

Baseline aerodynamic parameters were measured without the thrust reversers installed. These data are presented as lift, drag and pitching moment coefficients against tunnel velocity on Figures 17, 18, and 19, respectively. Each parameter is given for 5°, 25°, and 40° trailing edge flap positions. All testing was performed with the leading edge flaps and slats extended and with all spoilers in the 45° extended position. The pitching moment coefficients are referred to the 25% MAC position.

The force balance data presented in the following sections show the effects of the thrust reverser operation on model lift, drag and pitching moment. These data will be used in a landing roll study to determine the aerodynamic interference effects on ground roll distance. The data are presented in forms that are readily usable in the landing roll computer program.

The data presented for tunnel velocities below 40 knots are probably questionable because of tunnel flow "break down" due to the reversed gas flow.

Calibration of the force balance after the test indicated fouling between the tail and nacelles with loading applied in the drag axis. This was caused by worn model mountings. The fouling resulted in balance errors up to 14% when increasing the applied load but 3% when decreasing the loading. The testing was performed from high velocity to low velocity, i.e. high load to low load. No fouling was evident during the force balance calibration prior to the test.

5.2.2   EFFECT OF THRUST REVERSERS ON MODEL LIFT

The effect of the use of thrust reversers on model lift is given in Figures 20 thru 32. Data are presented in the form of an incremental change of lift coefficient, compared to the baseline values of Figure 17, as a function of tunnel velocity for various nozzle primary pressure ratios. Figure 20 shows model C_L change for Configuration 1 and indicates an increase in lift above 85 knots and a loss of lift below that velocity. The test conditions are 40° flaps, 0° orientation and a PPR of 1.8. Repeat runs indicate good repeatability. Model C_L changes for Configuration 12 are presented in Figures 21 thru 28. The effect of flaps, reverser orientation and primary pressure ratio are given and several trends are discernible Decreasing flap angle results in a larger ΔC_L. With a more negative reverser orientation, the C_L changes are lower in magnitude and occur at lower velocities. Decreasing nozzle primary pressure ratio results in lower magnitude changes at lower velocities. Figures 29 thru 32 give the C_L changes for Configuration 7. The data given on Figures 30, 31, and 32 do not follow logical trends; this may be attributable to the model fouling problem. Figure 29 shows data for 40° flaps and 0° orientation and indicates little or no C_L change down to 80, 60 and 50 knots for primary pressure ratios, respectively, of 1.8, 1.5, and 1.25. Below these velocities, the change was negative.

An increase in airplane lift is undesirable and will tend to diminish the total retarding force. The effect of these lift changes in terms of ground roll distance will be evaluated by a landing roll analysis. Inspection of the data, however, indicates that the effect can be expected to be very small.

5.2.3 EFFECT OF THRUST REVERSERS ON MODEL DRAG

Figures 33 thru 45 indicate the effect of thrust reverser use on model drag. Data is presented in the form of an incremental change of drag coefficient, from the baseline values of Figure 18, as a function of tunnel velocity for various nozzle primary pressure ratios. Figure 33 gives the model C_D change for Configuration 1 and indicates a loss of model drag (detrimental to stopping distance) over the velocity range tested. The test conditions were 40° flaps and 0° orientation. The loss is equal to 28% of the baseline drag at 100 knots, 65% at 70 knots, and 100% at 40 knots. The two curves represent repeat runs and indicate good repeatability. Figures 34 thru 41 indicate the effect of Configuration 12 operation on model drag for various flap settings, reverser orientations, and nozzle primary pressure ratios. A loss of model drag was indicated for all flap and orientation combinations over most of the velocity range tested. The magnitude of the model drag reduction is diminished at lower flap angles and higher negative reverser orientations. For a PPR of 1.8 and 0° orientation, the model C_D change is -0.29 for 40° flaps and -0.06 for 25° flaps at 70 knots (from Figures 34 and 37). Comparing Figures 34, 35, and 36 at a PPR of 1.8, 40° flaps and 70 knots shows that the model C_D change is, respectively, -0.29, -0.18, and -0.13 for reverser orientations of 0°, -10°, and -20°. The incremental model C_D data for Configuration 7 is given in Figures 42 thru 45.

5.2.4 EFFECT OF THRUST REVERSERS ON MODEL PITCHING MOMENT

The effect of reverser use on model pitching moment is indicated in Figures 46 thru 58 for Configurations 1, 12, and 7. Data is presented in the form of an incremental change of pitching moment coefficient, compared with the baseline values of Figure 19, against tunnel velocity for various nozzle primary pressure ratios. Figure 46 presents data for Configuration 1 at 40° flaps

and 0° orientation. The C_M change is negative (tending to bring the aircraft nose down) over the velocity range tested. Repeat runs are shown which indicate good agreement. Configuration 12 data are shown on Figures 47 thru 54 indicating the effect of flaps, reverser orientation, and nozzle primary pressure ratio. The C_M change was generally negative in value except at low tunnel velocities. The largest C_M changes occurred at the 40° flap setting with the changes becoming less negative with increasing negative orientation. The C_M change for 25° and 5° flaps were generally of the same magnitude. Figures 55 thru 58 present data for Configuration 7.

In general, the model pitching moment change is negative compared with a positive pitching moment for the (no reverse) baseline. Positive pitching moment is a nose up attitude. The effect of these pitching moment changes, in terms of ground roll distance, will be determined from a landing roll analysis.

5.3 REVERSED GAS IMPINGEMENT

5.3.1 SCOPE, DATA PRESENTATION AND RESULTS

To assess potential reversed gas impingement problems on the airplane structure, twenty thermocouples were located as shown in Figure 3. Since the use of a model precludes measurement of actual structure temperatures, the thermocouples were attached to measure air temperatures close to the surface. The surface temperatures are not determinable by analysis from this data, but the data provides indication of potential hot spots which should be closely examined during taxi tests. The current clamshell/deflector door installation on the 72,-200 airplane is estimated to result in a maximum skin temperature of about $312^\circ F$, which is certified as structurally acceptable. The maximum skin temperatures occur on on the fuselage below the side-engine struts.

The impingement data are given in Figures 59 thru 79 with each figure presenting data for one of the twenty thermocouple positions. Since the model was not designed for primary airflow temperatures in excess of $750^\circ F$, data were recorded, for selected configurations, at nominal primary airflow temperatures of $400^\circ F$, $600^\circ F$, and $750^\circ F$ to establish a trend for extrapolation to the desired conditions.

The primary airflow temperature at takeoff rating for the JT8D-115 engine at sea level standard day conditions is 1,009°F. The impingement temperature data were recorded for both 0° and -20° orientations at a nozzle primary pressure ratio of 1.8 and a 40° trailing edge flap position. The data for 0° orientation was obtained using Configuration 14 with only the primary airflows heated while the data for -20° orientation was obtained using Configuration 12 with the fan airflows also heated to the correct value for the prevailing ambient temperature. The data are presented as the difference between thermo-couple and ambient temperatures ($T_{T/C}$ - T_A) against the difference between primary airflow total and ambient temperatures (T_{TP} - T_A) for tunnel veloci-ties of 100, 70, and 40 knots. Also presented on each figure are single point values at velocities of 100, 70, and 40 knots for Configurations 12 and 7 at 0° orientation and Configuration 7 at -20° orientation. It is assumed that the single point values could be extrapolated at the same slope as that established for each thermocouple position by the measurements at various primary airflow total temperatures.

Based on the thermocouple coverage of this test no reversed hot gas impinge-ment problems appear to exist for Configurations 12 and 7 at 0° and -20° orientations. The engine operating schedule during thrust reverser operation (i.e. power setting versus forward speed) is not definable at this time. Since the ingestion characteristics will probably preclude operation at a nozzle primary pressure ratio of 1.8, the extrapolated temperatures quoted below would not be achieved.

5.3.2   DISCUSSION OF TEST DATA

The hot gas impingement temperatures ($T_{T/C}$ - T_A) were found to vary linearly with the primary airflow total temperature (T_{TP} - T_A) for each of the thermo-couple locations. The slope is dependent upon the thermocouple location and tunnel velocity. At the 0° orientation the highest impingement temperatures were found to occur at the lowest velocities tested for both Configurations 12 and 7, except for the thermocouples located on the horizontal stabilizer. However, at the -20° orientation the tendency was for the highest impingement

temperatures to occur at velocities of 70 knots or higher, especially for Configuration 12 and for both Configurations 12 and 7 at thermocouple locations 15 thru 20. Comparison between the data for Configurations 12 and 7 shows that for thermocouples 1, 2 and 3 Configuration 12 temperatures are higher at both 0^0 and -20^0 orientations, while Configuration 7 temperatures are higher at both orientations for thermocouples 15 thru 20. For the thermocouples 4 thru 12, Configuration 7 temperatures were generally higher at 0^0 and Configuration 12 temperatures were generally higher at -20^0 orientation. Inspection of the data shows that the difference between Configurations 12 and 7 temperatures at both 0^0 and -20^0 orientation is generally less than 20^0F. The highest temperatures for both configurations occur generally at thermocouple locations 1 thru 7; i.e. the fuselage lower surface. For both configurations the readings for thermocouples 1 thru 4 and 9 thru 11 are higher at 0^0, and the readings for thermocouples 8, 14 and 15 are higher at -20^0 orientation. This trend with orientation is as expected.

Extrapolation of the data to JT8D-115 takeoff rating on a standard day, T_{TP} of $1,009^0F$, indicates an estimated maximum impingement temperature $(T_{T/C}-T_A)$ of 186^0F from the thermocouple at location 2 for Configuration 12 at 0^0 orientation. This results in an air temperature close to the surface of 245^0F. At -20^0 orientation $(T_{T/C}-T_A)$ is 168^0F for Configuration 12 and 175^0F for Configuration 7 at both 0^0 and -20^0 orientations. The highest impingement temperatures would occur on a hot day, $T_A = 130^0F$, and with the JT8D-117 engine. Maximum power rating under these conditions would produce a primary total temperature of $1,163^0F$ at a nozzle primary pressure ratio of 1.646. Extrapolation of the Configuration 12 data at 0^0 orientation indicates that $(T_{T/C}-T_A)$ would be approximately 200^0F, resulting in an impingement air temperature of 330^0F. The resulting skin temperatures will be less but are not determinable by analysis. Since the engine operating procedure during thrust reverser use is undefined at this time and will be until taxi tests are performed, the maximum impingement temperatures are difficult to estimate. However, because the hot gas ingestion characteristics will probably preclude engine operation at takeoff power rating in reverse, and some negative thrust reverser orientation may be required, the quoted maximum values would not be achieved.

To allow for the possibility that side spillage of the reversed gas would cause impingement problems on the fuselage immediately adjacent to the side nacelle mounted thrust reversers, one run was made with a thermocouple located close to the airplane surface at that position. The test conditions were Configuration 14, 40° flaps, 0° orientation and a nozzle primary pressure ratio of 1.8. The data are plotted as single point values for tunnel velocities of 100, 70 and 40 knots on Figure 64 and show that the impingement temperatures ($T_{T/C}-T_A$) are no higher than those occurring at other thermocouple locations.

Data is presented in Figure 79 to show the effect of engine power setting on impingement temperatures. The data is for thermocouple 6 and Configuration 12. Single point values at 100, 70, and 40 knots for nozzle primary pressure ratios of 1.8, 1.5 and 1.25 are given. Also shown on this figure are the nominal relationships between primary pressure ratio (PPR) and primary temperature ($T_{TP}-T_A$) for the JT8D-115.

5.4   AIRPLANE RUDDER EFFECTIVENESS

5.4.1   SCOPE, DATA PRESENTATION AND RESULTS

The thrust reversers deflect the engine exhaust gas forward causing a change to the airflow around the vertical tail. This change can result in a significant loss of rudder effectiveness, depending upon thrust reverser orientation and engine power setting. The effects of a loss of rudder effectiveness on the overall airplane controllability during landing roll can become important, especially when landing during crosswinds and on slippery runways. The magnitude of the loss of rudder effectiveness which can occur while still retaining acceptable airplane controllability is not readily definable and will require data from airplane taxi tests. However, to provide a qualitative comparative assessment of the effect of various thrust reverser configurations, orientations and engine power settings, instrumentation was provided to determine the velocity at three locations on the vertical tail, see Figure 3. A more comprehensive wind tunnel model test to determine the effect of thrust reverser use on airplane stability and control characteristics is reported in Reference 2.

34

The test data are presented as dynamic pressure ratio (reverse/cruise) against tunnel velocity for each of the three vertical tail locations. The dynamic pressure ratio is defined as the ratio of the dynamic pressure ($1/2 \rho v^2$) determined with the thrust reversers in use divided by the value determined in the cruise mode without the thrust reversers installed. Data were recorded for Configurations 1, 12, and 7 and show the effect of thrust reverser orientation and nozzle primary pressure ratio. All the data presented are for the 40° trailing edge flap setting. The test data indicate that rudder effectiveness, but not airplane handling, is independent of trailing edge flap setting. The dynamic pressure ratio values given are not considered to be absolute values but provide a reasonable basis for comparison between thrust reverser configurations, orientations and engine power settings. Two general trends were identifiable from the test data, one due to the velocity measurements at position 1 and the other due to the velocity measurements at positions 2 and 3. Since the probes at positions 2 and 3 are just forward of the rudder, they more closely represent the effect of thrust reverser use on the rudder, and the ensuing discussion will be limited to these two locations. The values of dynamic pressure ratio quoted below are computed as the average of the values determined at positions 2 and 3. As the dynamic pressure ratio approaches zero, the rudder effectiveness is reduced. It is reasonable to assume that for very low values of dynamic pressure ratio, the pilot would have difficulty controlling the airplane direction with the rudder.

Qualitative assessment of the rudder effectiveness with the thrust reversers operating indicates that a significant loss (dynamic pressure ratio 0.2 or less) of dynamic pressure occurs at the -20° orientation which could be unacceptable from the standpoint of airplane controllability. This condition was recorded for each of the configurations tested and at each of the engine power settings tested. This loss of dynamic pressure also occurred at a velocity higher than the estimated ingestion velocity for that condition. The configurations tested covered a range of full scale lip heights on the side nacelle reversers, from 0 to 3.5 inches, so the above condition would occur for any selected lip height. At the -10° orientation substantially more dynamic pressure was retained at the estimated ingestion velocities for both Configurations 12 and 7 for each engine power setting tested. The dynamic pressure

35

ratio is approximately 0.4 for Configuration 12 and approximately 0.8 for Configuration 7. It is beyond the scope of this test to assess the acceptability of the rudder effectiveness, except to point out that the data indicates substantially more dynamic pressure is retained at the -10° orientation compared with the -20° orientation. A full scale taxi test or a further stability and control model wind tunnel test will probably be required to make that assessment.

5.4.2   TEST RESULTS FOR CONFIGURATION 1

Data for Configuration 1 is presented in Figures 80 thru 84 for thrust reverser orientations of +20°, 0°, and -20° for a nozzle primary pressure ratio of 1.8 and for nozzle primary pressure ratios of 1.5 and 1.25 at 0° orientation. A significant loss of dynamic pressure is indicated as the thrust reverser orientation changes from +20° to -20°; e.g., at 100 knots and 1.8 nozzle primary pressure ratio the dynamic pressure ratio is 1.3, 0.48, and 0.13 respectively for thrust reverser orientations of +20°, 0°, and -20°. At the -20° orientation the dynamic pressure ratio is less than 0.2 over the velocity range 100 to 125 knots but then increases with decreasing velocity, reaching 0.7 at 50 knots. Comparison of the ingestion velocity data for Configuration 1 from Figures 8 and 9 with the rudder effectiveness data in Figures 80 thru 84 indicates that for the -20° orientation, a significant loss of dynamic pressure has occurred, dynamic pressure ratio less than 0.2, before the estimated ingestion velocity was reached. This condition does not occur for the +20° and 0° thrust reverser orientations.

5.4.3   TEST RESULTS FOR CONFIGURATION 12

Configuration 12 data is presented in Figures 85 thru 93 for thrust reverser orientations of 0°, -10°, and -20° and nozzle primary ratios of 1.8, 1.5, and 1.25. For a given nozzle primary pressure ratio the loss of dynamic pressure increases with increasing negative thrust reverser orientation; e.g., at 100 knots and a nozzle primary pressure ratio of 1.8, the dynamic pressure ratio values are 0.85, 0.44, and 0.1 respectively for thrust reverser orientations of 0°, -10°, and -20°. At -20° orientation and 1.8 nozzle primary pressure

ratio, the dynamic pressure ratio is zero between 70 and 90 knots but then increases with decreasing velocity below 70 knots (see Figure 87). An increase of dynamic pressure is indicated for each thrust reverser orientation with reduction of nozzle primary pressure ratio; e.g., at a thrust reverser orientation of -10° and 100 knots, the dynamic pressure ratio values are 0.44, 0.75, and 0.85 respectively for nozzle primary pressure ratios of 1.8, 1.5, and 1.25. Comparison of the ingestion velocity data for Configuration 12, from Figure 12, with the rudder effectiveness data of Figures 85 thru 93 indicates that for all nozzle primary pressure ratios tested at -20° orientation, a significant loss of dynamic pressure would have occurred, dynamic pressure ratio less than 0.2, before the estimated ingestion velocity was reached. For the -10° orientation the dynamic pressure ratio values at the estimated ingestion velocities were in the region of 0.35 to 0.5 for the three nozzle primary pressure ratios tested. At the 0° orientation little or no loss of dynamic pressure had occurred over the nozzle primary pressure ratio range tested.

5.4.4   TEST RESULTS FOR CONFIGURATION 7

Configuration 7 rudder effectiveness data is presented in Figures 94 thru 102 for thrust reverser orientations of 0°, -10°, and -20° and nozzle primary pressure ratios of 1.8, 1.5, and 1.25. For a given nozzle primary pressure ratio the loss of dynamic pressure increases with increasing negative thrust reverser orientation; e.g., at 100 knots and a nozzle primary pressure ratio of 1.8, the dynamic pressure ratio values are 1.33, 0.83, and 0.15 respectively for thrust reverser orientations of 0°, -10°, and -20°. The dynamic pressure falls off at a more rapid rate compared with Configurations 1 and 12 and does not show the increase at lower velocities which are characteristic of the other configurations. As was the case on Configuration 12, an increase of dynamic pressure generally occurs with decreasing nozzle primary pressure ratio; e.g., at a thrust reverser orientation of -10° and 100 knots, the dynamic pressure ratio values are 0.83, 0.87, and 0.96 respectively for nozzle primary pressure ratios of 1.8, 1.5, and 1.25. The dynamic pressure loss is generally less than for Configuration 12. Comparison of the ingestion velocity data from Figure 15 with the rudder effectiveness data of Figures 94 thru 102

indicates the following. For all nozzle primary pressure ratios at -20° orientation a significant loss of dynamic pressure would have occurred, dynamic pressure ratio less than 0.2, before the estimated ingestion velocity was reached. For the 0° and -10° orientations the estimated ingestion velocity was reached before a dynamic pressure ratio less than 0.5 was recorded.

5.5   FLOW VISUALIZATION

A series of runs were conducted for Configurations 12 and 7 with steam flowing through the nozzles with the reversers in the deployed mode. Photographs were taken showing the side and front views. Two representative front views are presented for each configuration. The figures show the extent of the reversed gas plumes at a tunnel velocity of 80 knots and also the effect of thrust reverser orientations of 0° and -20°. Figure 103 shows Configuration 12 and Figure 104 shows Configuration 7. The test conditions for both figures are a nozzle primary pressure ratio of 1.8 and a trailing edge flap setting of 40°.

6.0 CONCLUSIONS

The major parameters controlling hot gas ingestion to the engine inlets are thrust reverser orientation, engine power setting and the lip height of the bottom thrust reverser doors on the side engines. A reduction of ingestion velocity of up to 10 knots could be achieved by raising the trailing edge flaps to the 25° position from the 40° position.

Analysis of the force balance data, in general, indicates trends which diminish the installed stopping capability of the thrust reversers; i.e. an increase in airplane lift, a decrease in airplane drag and a decrease of positive pitching moment. The significance of these aerodynamic interference effects will be determined from a landing roll study. The magnitude of the changes in the aerodynamic parameters decreases as the thrust reverser orientation becomes more negative.

No hot gas impingement problems on the airplane structure exist, based on the thermocouple coverage for this test, for Configurations 12 and 7 and a thrust reverser orientation range of 0° to -20°. In general, the highest measured temperatures occur on the lower surface of the airplane fuselage.

Qualitative assessment of the rudder effectiveness data shows that the effectiveness is dependent upon thrust reverser orientation and engine power setting. A substantial loss of dynamic pressure in the vicinity of the rudder occurs at -20° orientation for all the configurations and engine power settings tested. The dynamic pressure remains at a higher level for the -10° orientation for both Configurations 12 and 7. Further model and full-scale (airplane taxi tests) testing will be required to assess the acceptability of different reverser orientations from the standpoint of airplane controllability.

Selection of a suitable thrust reverser configuration and substantiation of its installed stopping capability, compared with the current installation, will be based on a landing roll study and will involve satisfactory resolution of the conflicting hot gas ingestion and airplane controllability requirements.

7.0 TABLES AND FIGURES

42

TABLE 1

JT8D-15 /-115 ENGINE COMPARISON AND FAN AND PRIMARY PRESSURE RATIO RELATIONSHIPS

JT8D-15/-115 ENGINE COMPARISON

DESCRIPTION		JT8D-15	JT8D-115
TAKE-OFF CONDITION	THRUST, LBS.	15,500	17,500
SEA LEVEL, STATIC	BYPASS RATIO	1.034	2.000
STANDARD DAY	FAN PRESSURE RATIO	2.02	1.67
	PRIMARY PRESSURE RATIO	2.117	1.798
OVERALL BARE ENGINE LENGTH, IN.		119.88	127.20
FAN TIP DIAMETER, IN.		40.5	49.2
BARE ENGINE WEIGHT, LBS,		3,227	3,797
NOZZLE EXIT DIAMETER, IN.		29.79	38.02

TARGET FAN AND PRIMARY PRESSURE RATIO RELATIONSHIPS
(JT8D-115)
SEA LEVEL, Mn = 0.1, STANDARD DAY

PRIMARY PRESSURE RATIO	FAN PRESSURE RATIO
1.797	1.645
1.501	1.451
1.246	1.255

TABLE 2
DEFINITION OF THRUST REVERSER CONFIGURATIONS

CONFIG. NO.	LIP DEFINITION FULL SCALE HEIGHT-INCHES	FENCE DEFINITION FULL SCALE HEIGHT-INCHES	NACELLE VARIATION
1	3.5 constant, top and bottom.	3.5, 4 per reverser.	All positions the same.
2	3.5-1.75-1.0 tapered, top and bottom.	3.5, 2 per reverser.	All positions the same.
4	3.5 constant, top and 1.5 constant, bottom.	3.5, 2 per door top.1.5, 2 per door, bottom.	Position 3 as described. Positions 1 & 2 as Config.1.
6	1.5 constant, top. 3.5 constant, bottom.	1.5, 2 per door, top. 3.5, 2 per door, bottom.	Position 3 as described. Positions 1 & 2 as Config.1
7	No lips top and bottom.	3.5, 4 per reverser.	Positions 1 & 3 as described. Position 2 as Config.1.
8	No lips top and bottom.	3.5, 4 per reverser.	All positions the same.
9	3.5 constant, top. no lip bottom.	3.5, 4 per reverser.	Positions 1 & 3 as described. Position 2 as Config. 1.
11			Positions 2 & 3 as Config. 1. Position 1 as Config. 9.
12	1.5 constant, top and bottom.	1.5, 4 per reverser.	All positions the same.
13	1.5 constant, top. no lip bottom.	1.5, 4 per reverser.	Positions 1 & 3 as described. Position 2 as Config. 12.
14	1.5 constant, top. 0.68 constant, bottom.	1.5, 4 per reverser.	Positions 1 & 3 as described. Position 2 as Config. 12.
15			Positions 1 & 3 no reversers. Position 2 as Config. 1.
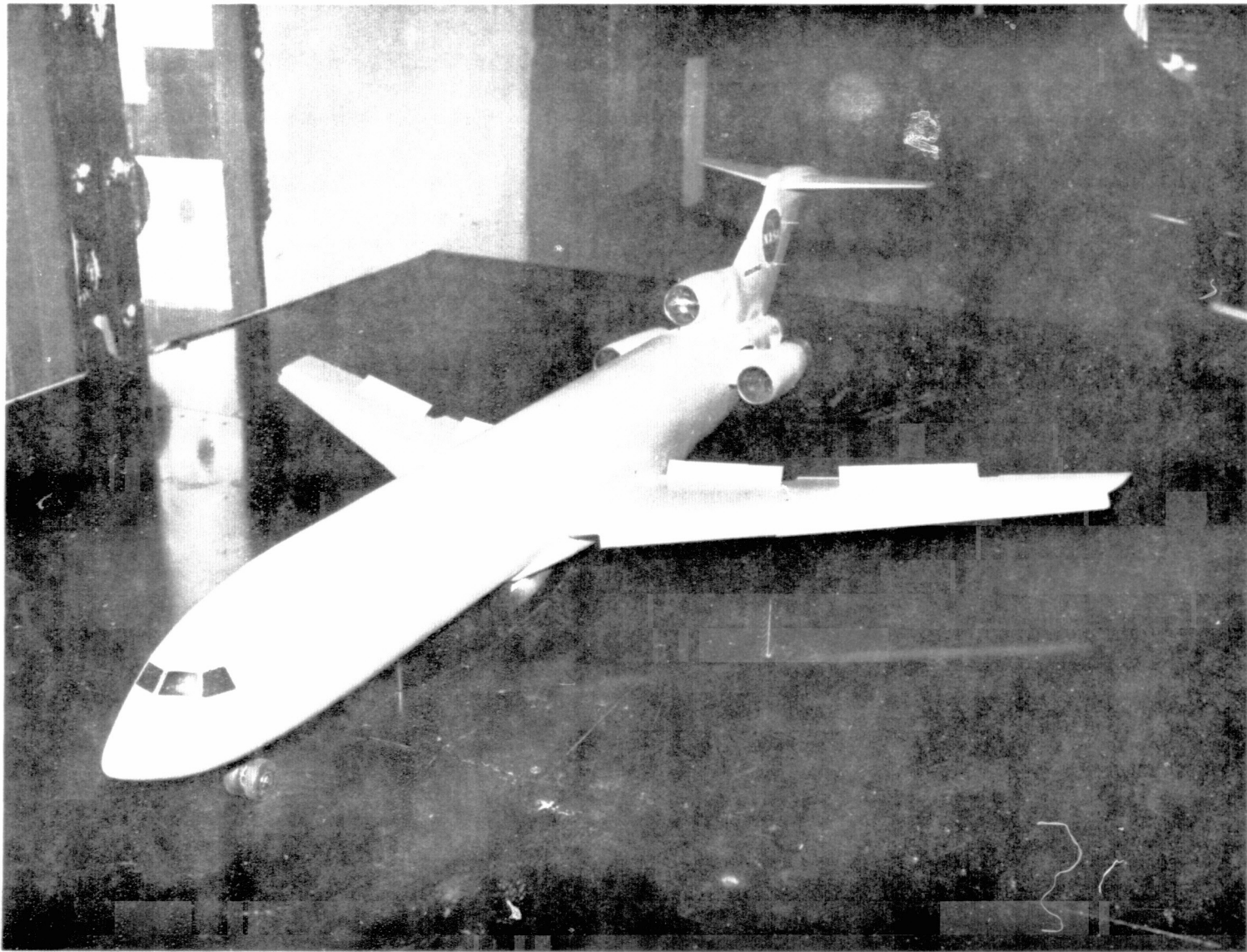
FIGURE 1. - 727-200 MODEL INSTALLED IN BOEING LOW SPEED WIND TUNNEL "A"

ON BALANCE

- - - - - OFF BALANCE

INLET
AIRFLOW

GROUND PLANE

FORCE BALANCE

TUNNEL FLOOR

INLET AIRFLOW
SIMULATION, THREE
ENGINES

NOZZLE AIR SUPPLY PIPES,
6 TOTAL, 3 FAN AND 3 PRIMARY.
(2 ONLY SHOWN)

TO VACUUM
PUMP
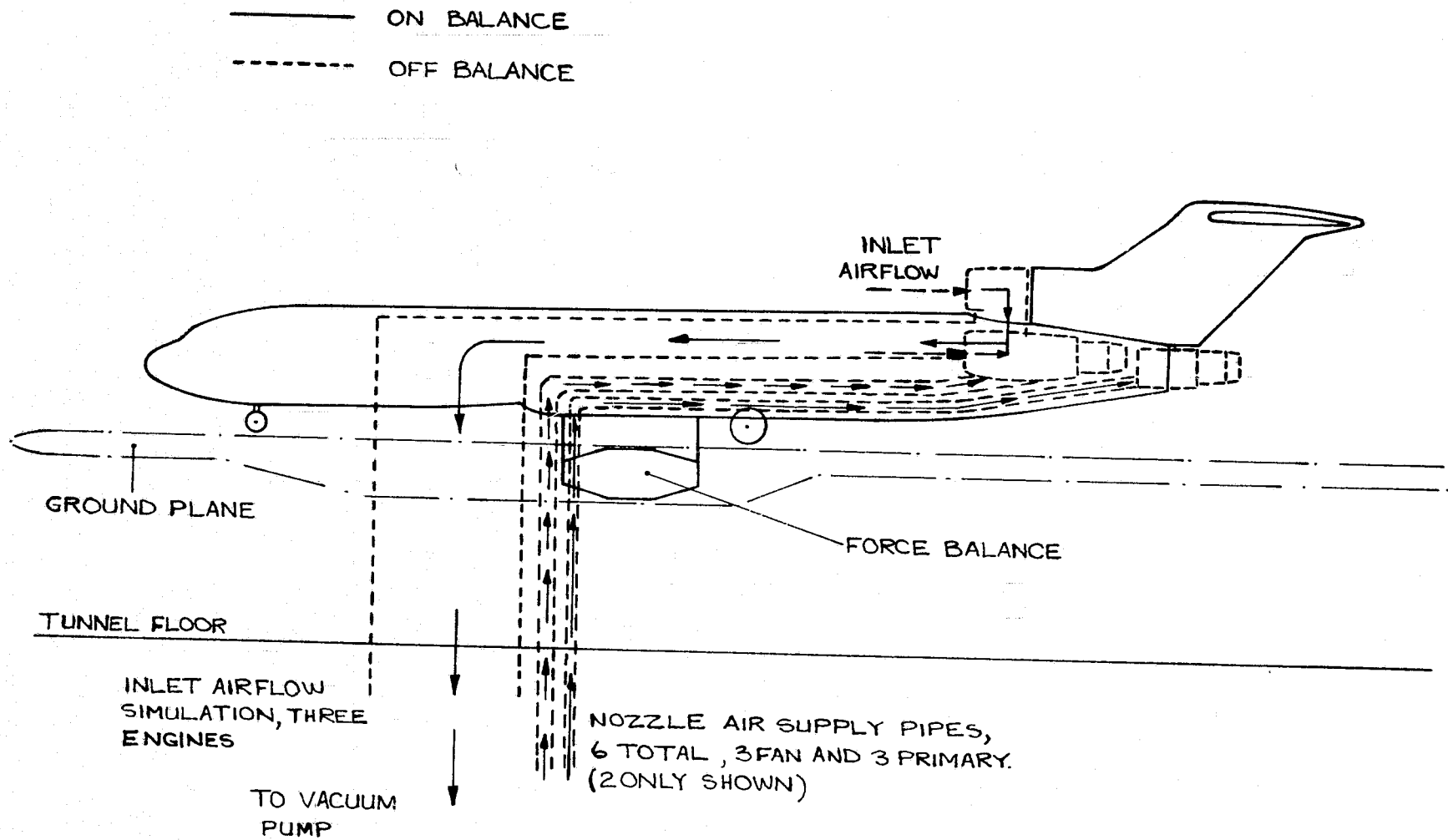
FIGURE 2 — SCHEMATIC OF MODEL INSTALLATION.
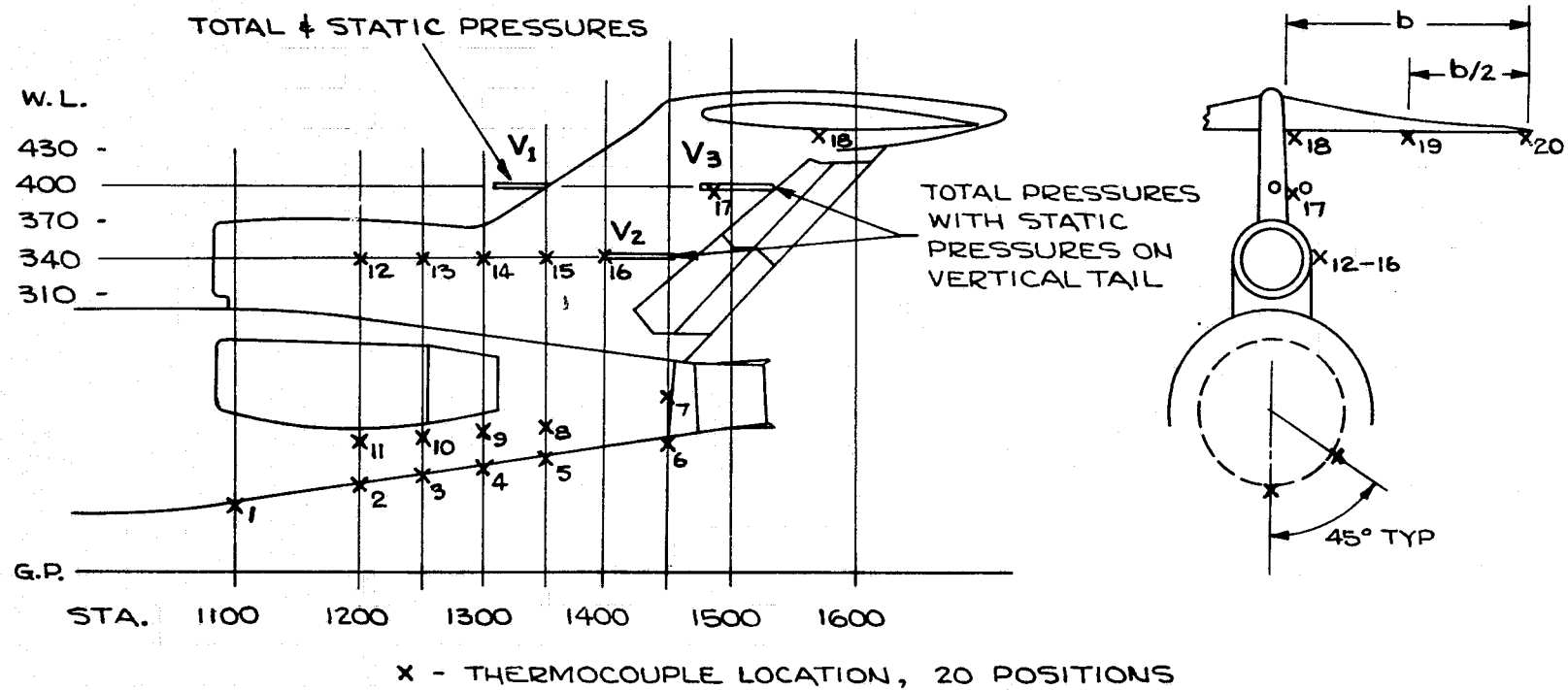
FIGURE 3 — LOCATION OF IMPINGEMENT THERMOCOUPLES AND VERTICAL TAIL TOTAL AND STATIC PRESSURE MEASUREMENTS.
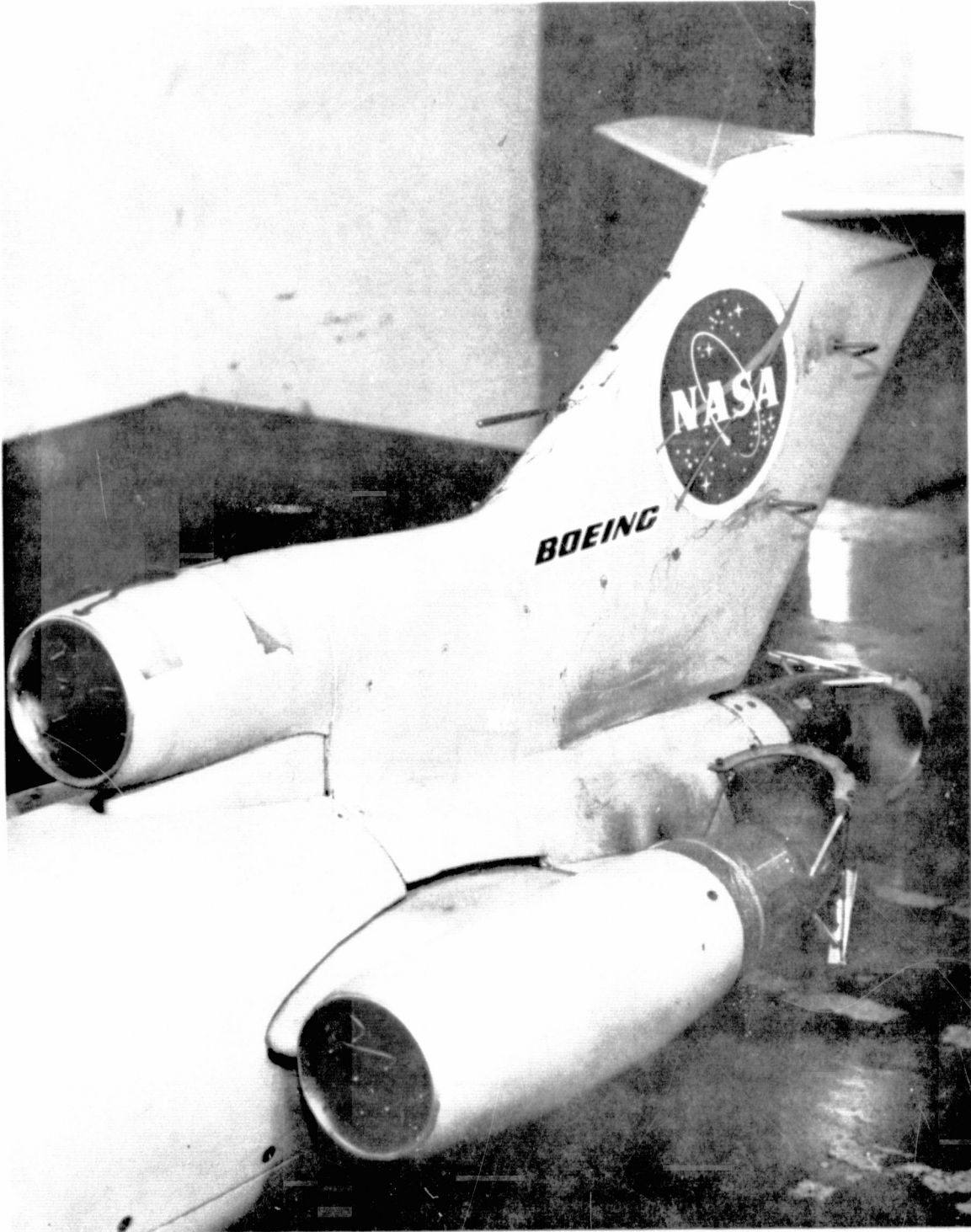
FIGURE 4. - MODEL VERTICAL TAIL AND NACELLES WITH THRUST REVERSERS INSTALLED

1.0 IN. RADIUS, 6 T/C AT 60° SPACING

0.65 IN. RADIUS, 6 T/C AT 60° SPACING

0.046 SCALE

X - THERMOCOUPLE LOCATION, 13 PER NACELLE

VERT. ₵
FRONT VIEW
NACELLE NO. 2
NACELLES 1 & 3 ROTATED 30°
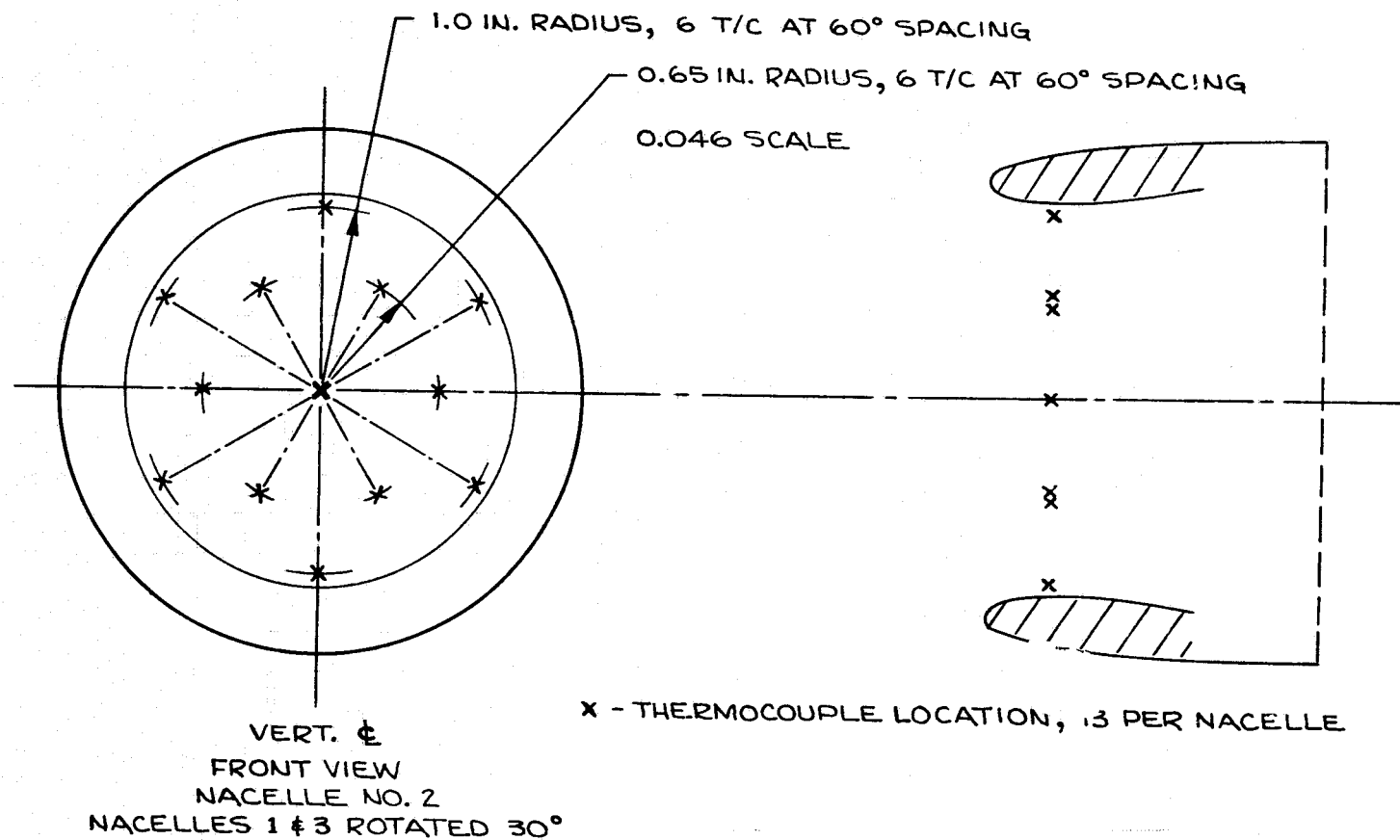
FIGURE 5 - INLET INGESTION THERMOCOUPLE LOCATIONS

POSITION 1

POSITION 2

POSITION 3

THRUST REVERSER ORIENTATION DEFINITION

CONSTANT LIP HEIGHT

TAPERED LIP HEIGHT

FENCE HEIGHT

LIP

TOP DOOR

FENCE

BOTTOM DOOR

LIP
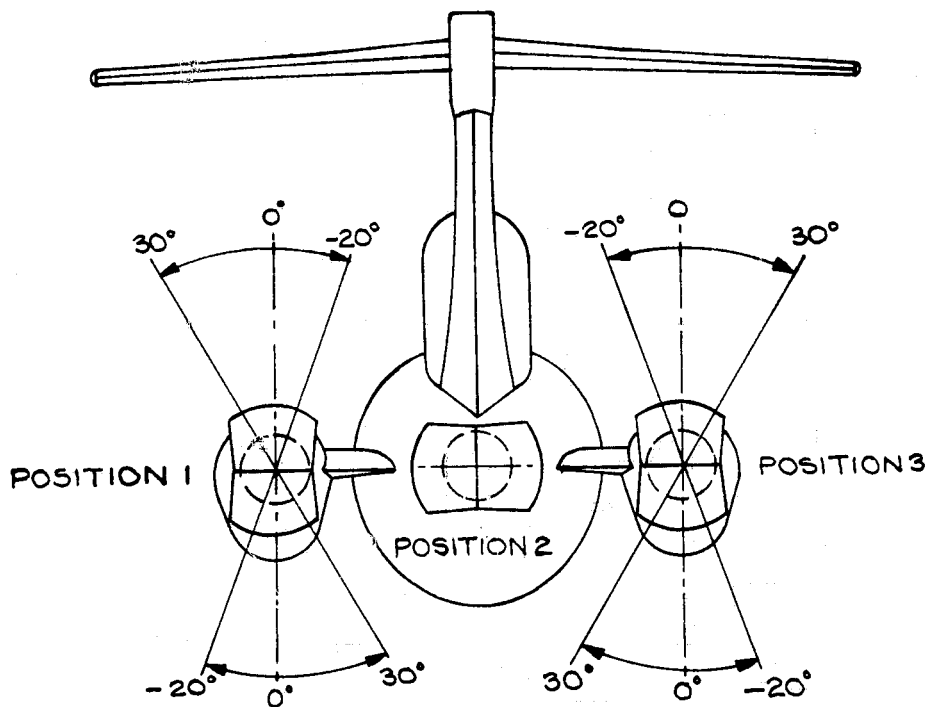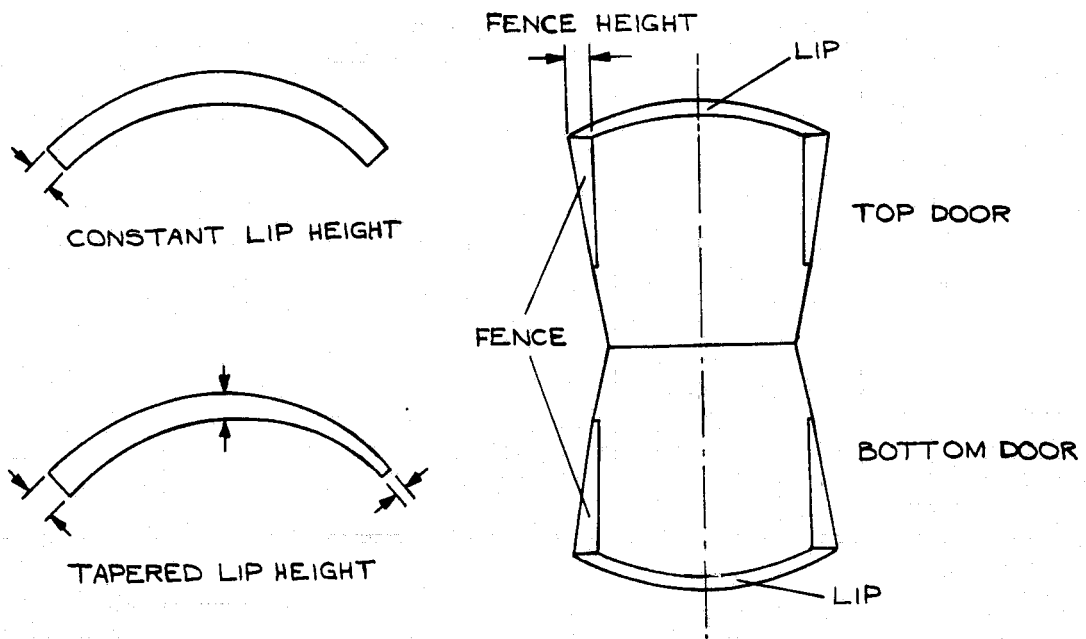
TARGET THRUST REVERSER DOOR COMPONENTS

FIGURE 6 — THRUST REVERSER ORIENTATION DEFINITION
AND TARGET DOOR COMPONENTS.
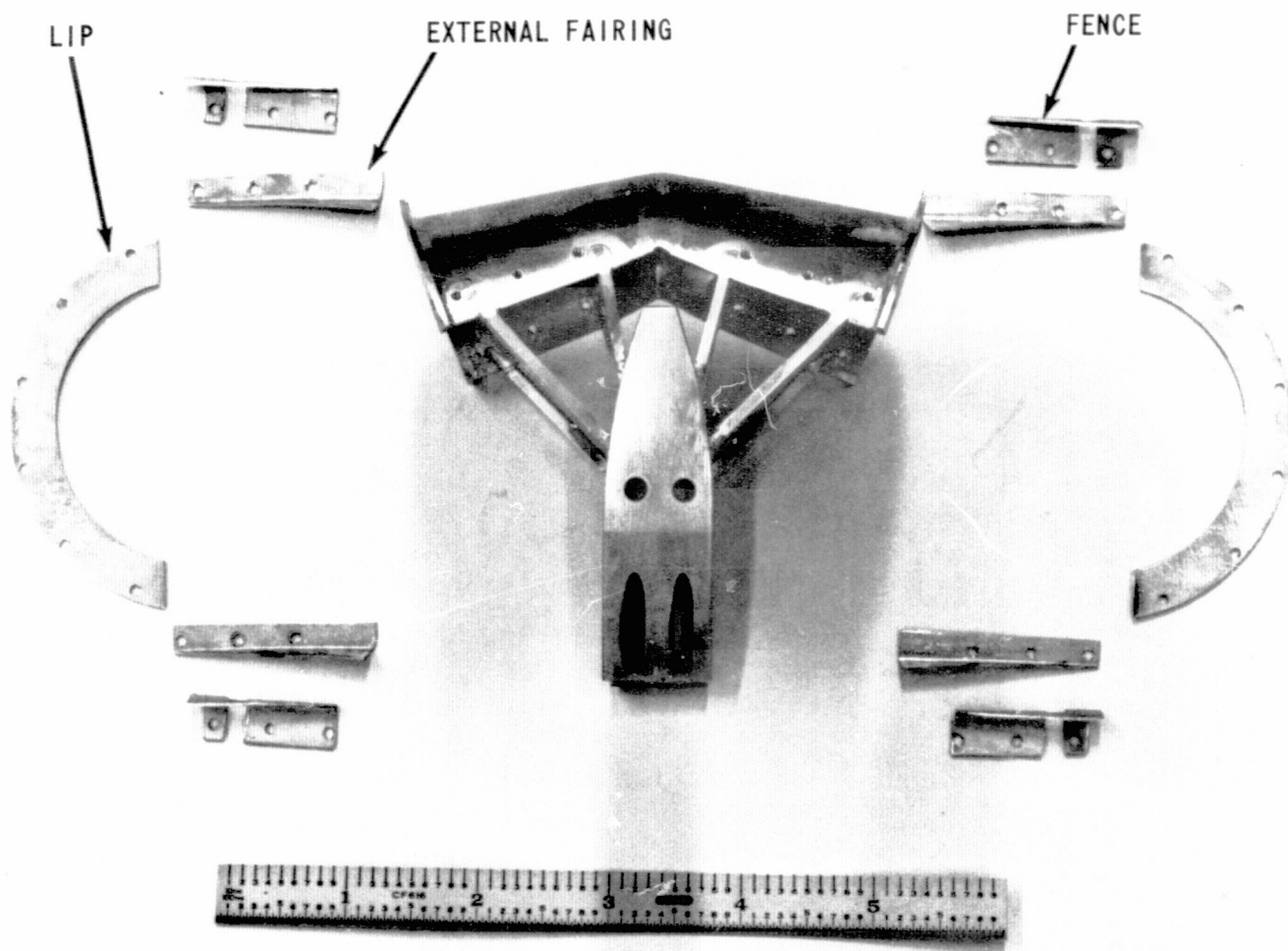
FIGURE 7. - MODEL THRUST REVERSER COMPONENTS
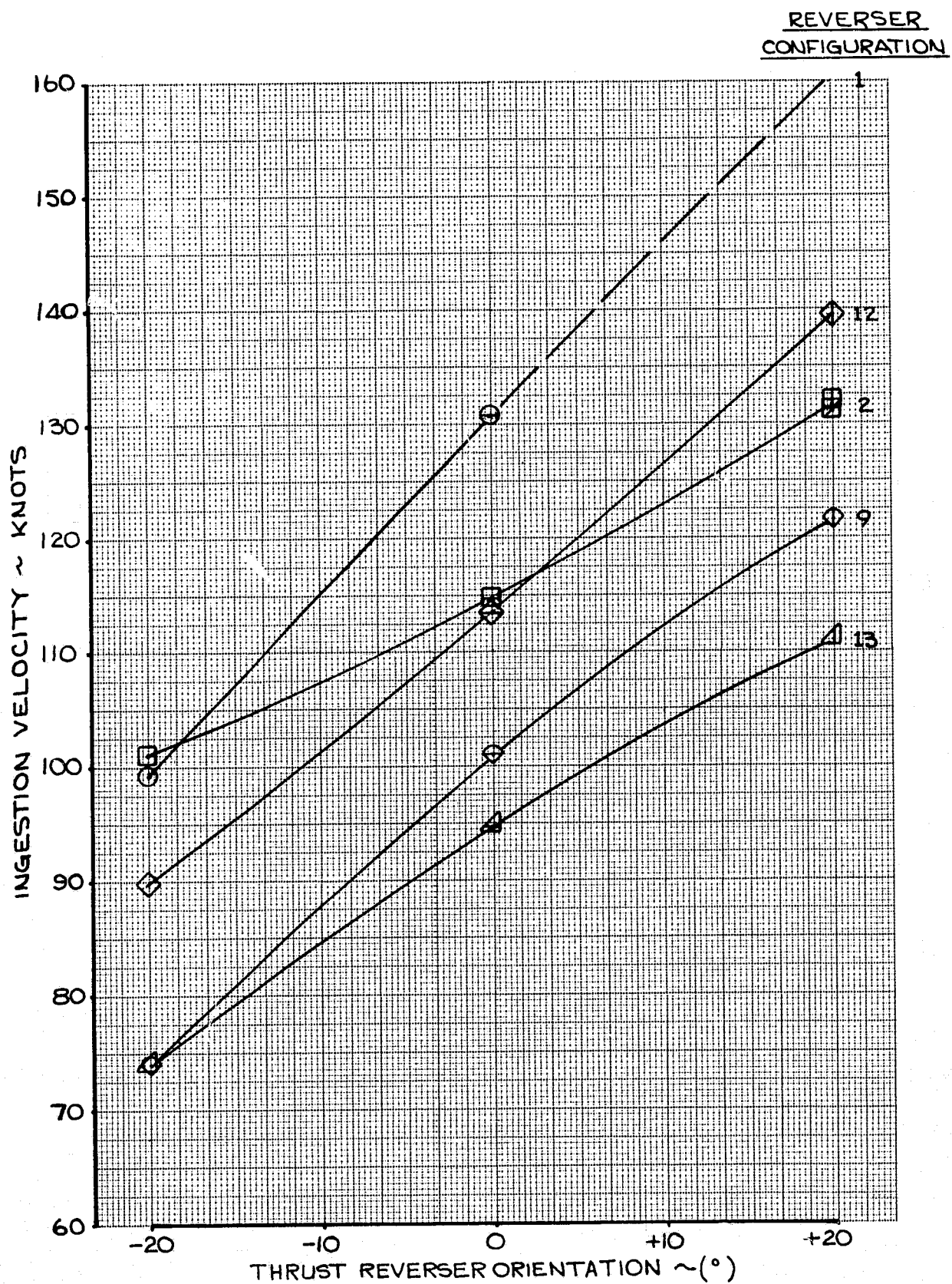
FIGURE 8 — EFFECT OF REVERSER ORIENTATION ON INGESTION VELOCITY, FOR 40°FLAPS AND PPR= 1.8
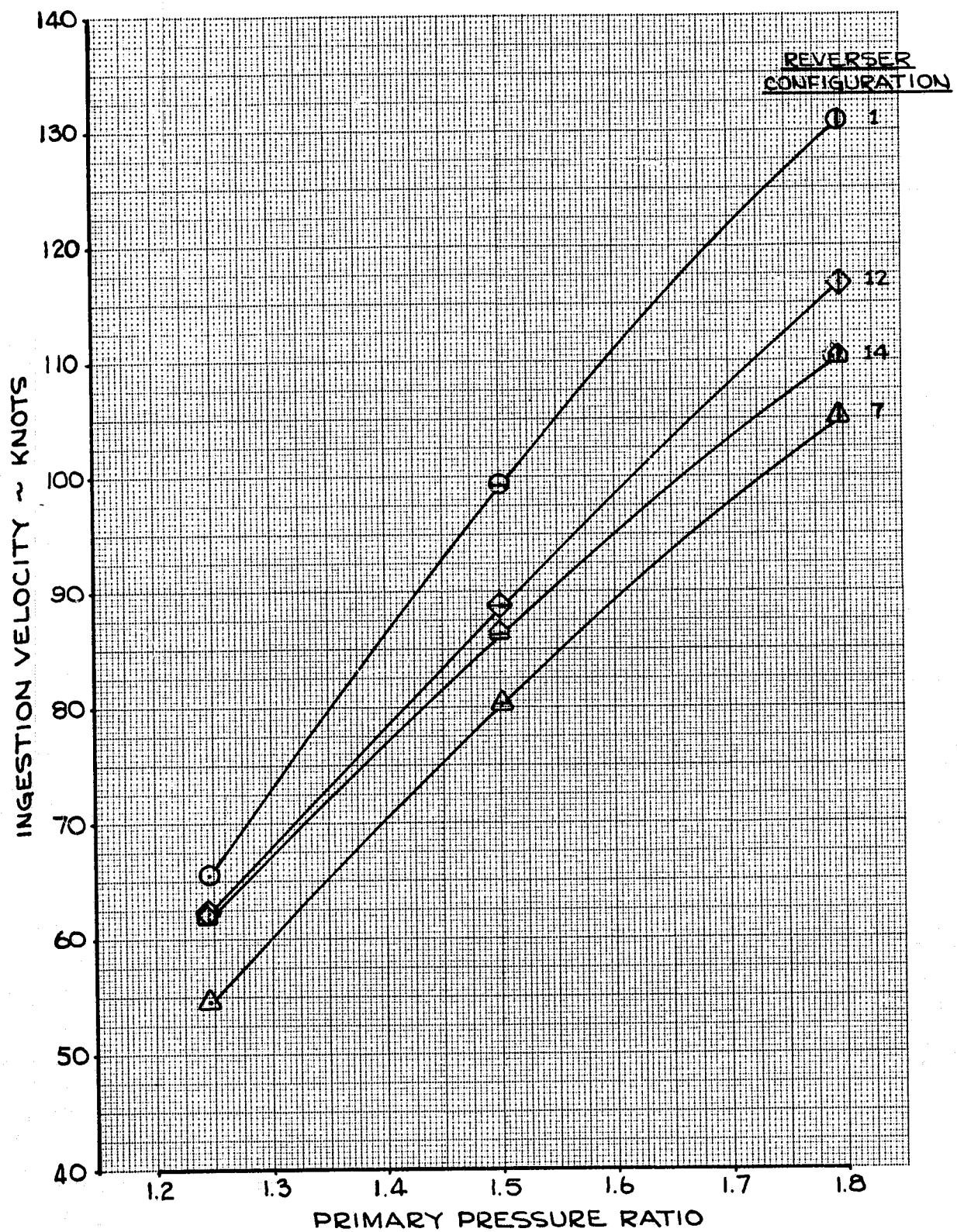
FIGURE 9 – EFFECT OF PRIMARY PRESSURE RATIO ON INGESTION VELOCITY AT 40° FLAPS AND 0° ORIENTATION
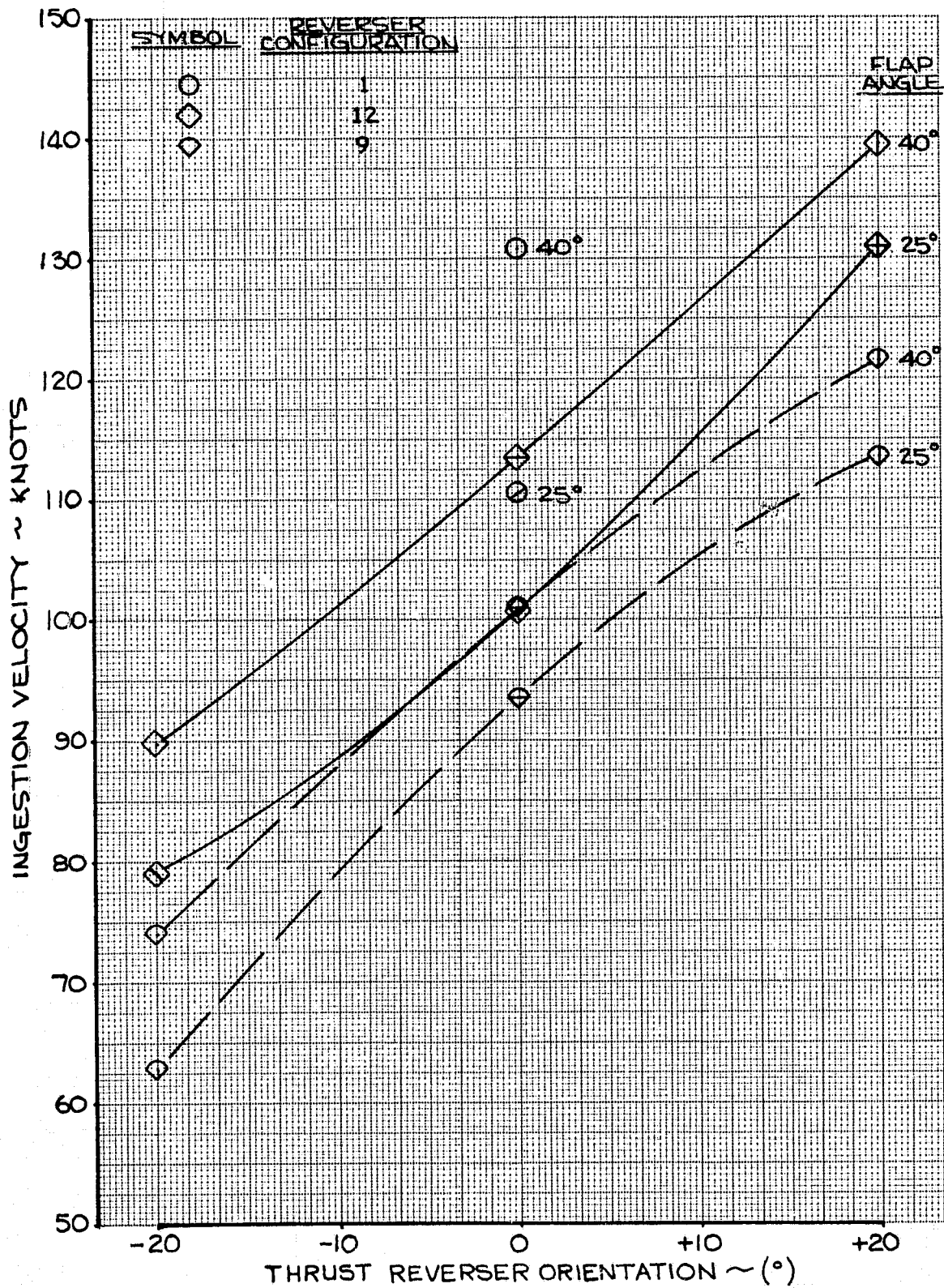
FIGURE 10 — EFFECT OF CHANGING FLAPS FROM 40° TO 25° ON INGESTION VELOCITY, PPR = 1.8
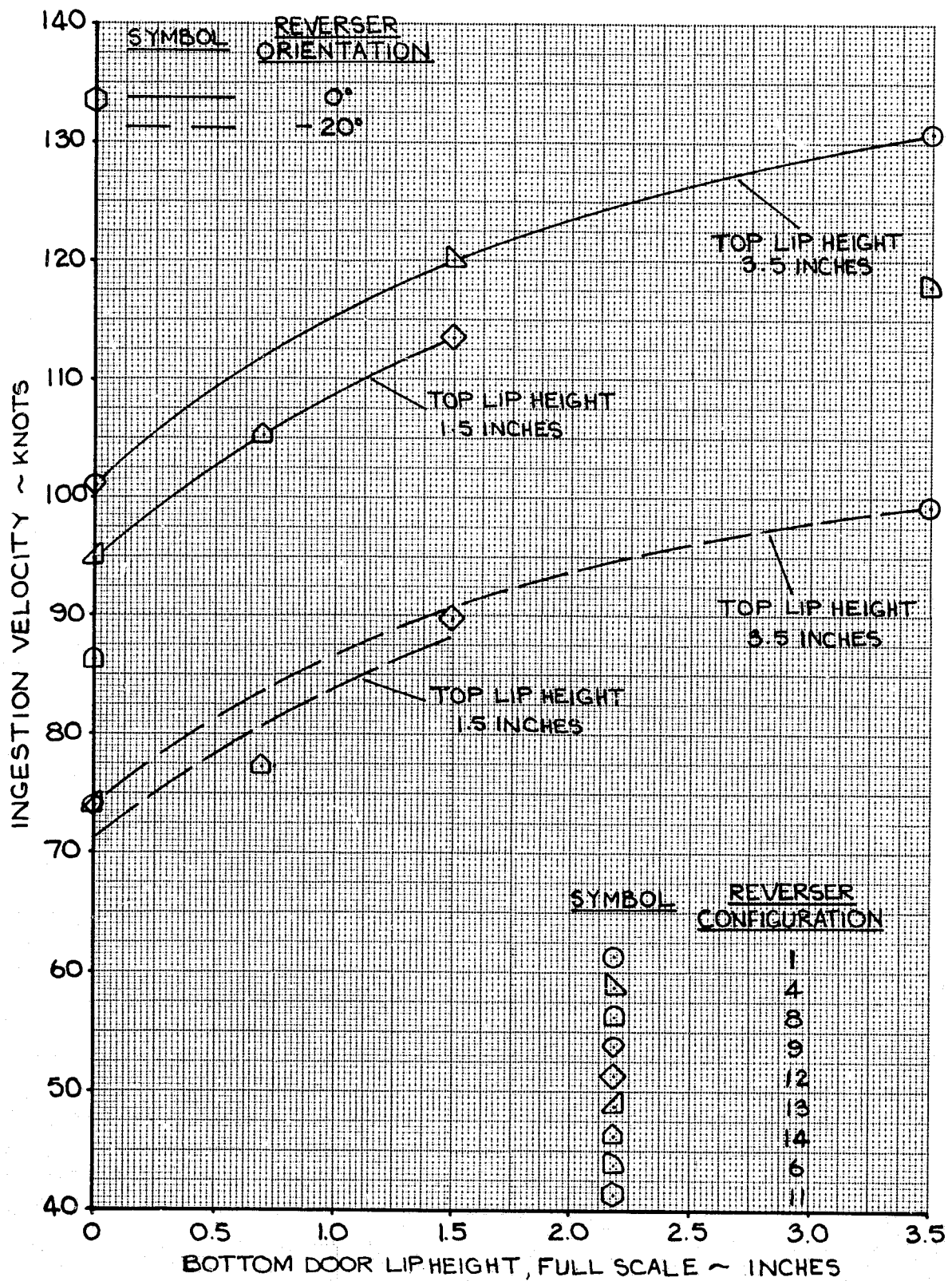
FIGURE 11 – EFFECT OF LIP HEIGHT ON INGESTION VELOCITY, 40° FLAPS AND PPR =1.8.
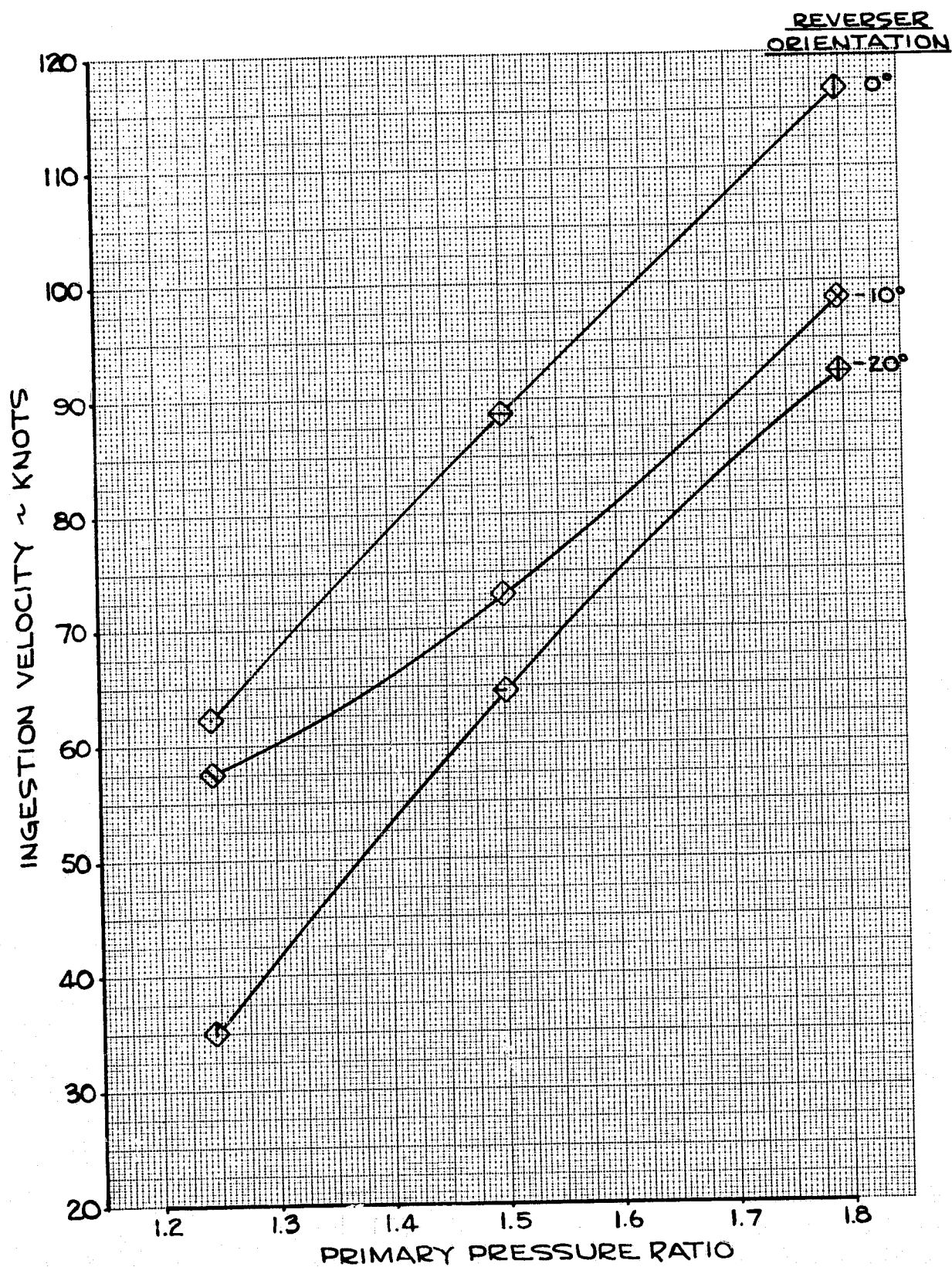
FIGURE 12 – INGESTION VELOCITIES FOR
CONFIGURATION 12, 40° FLAPS
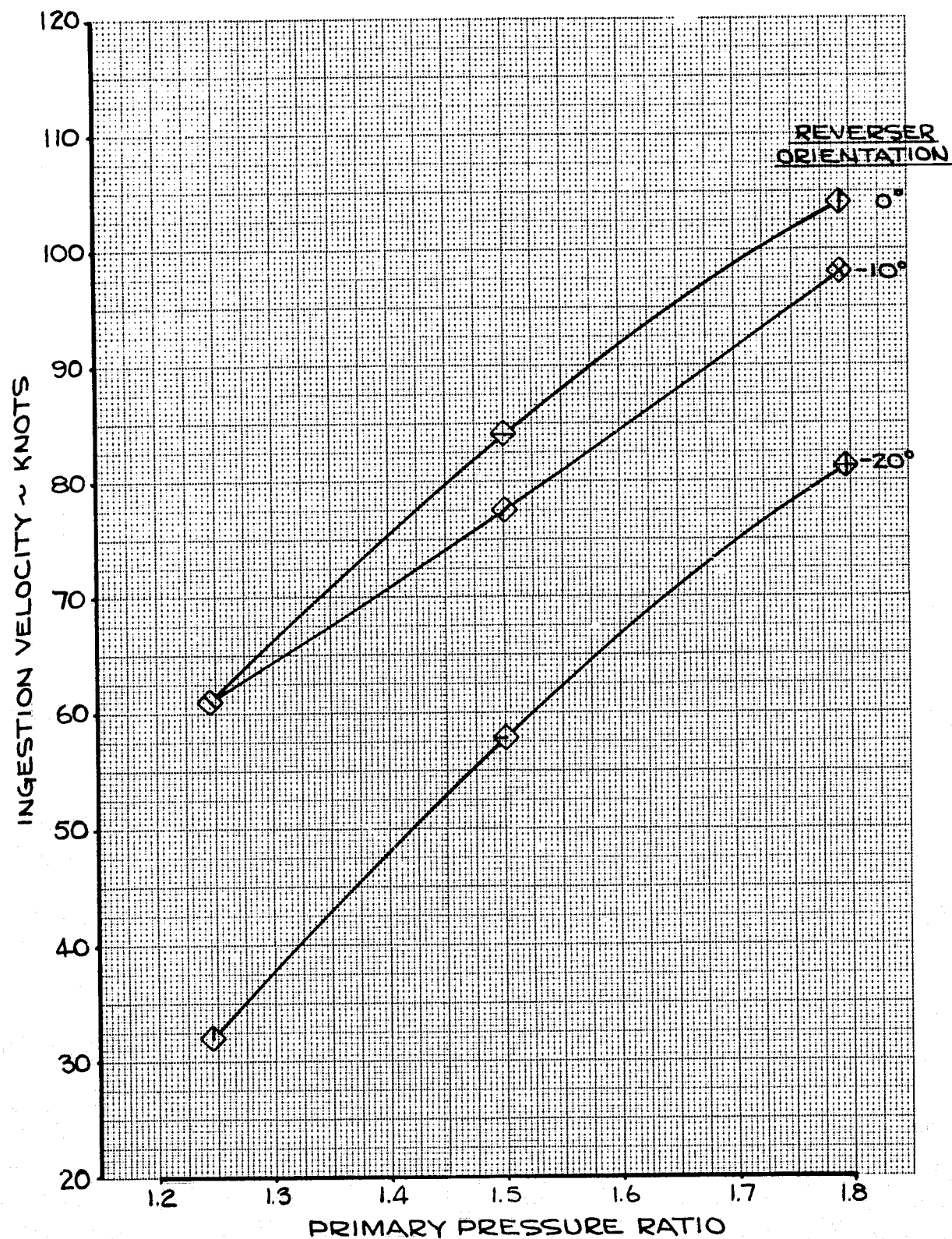
FIGURE 13 - INGESTION VELOCITIES FOR CONFIGURATION 12, 25° FLAPS
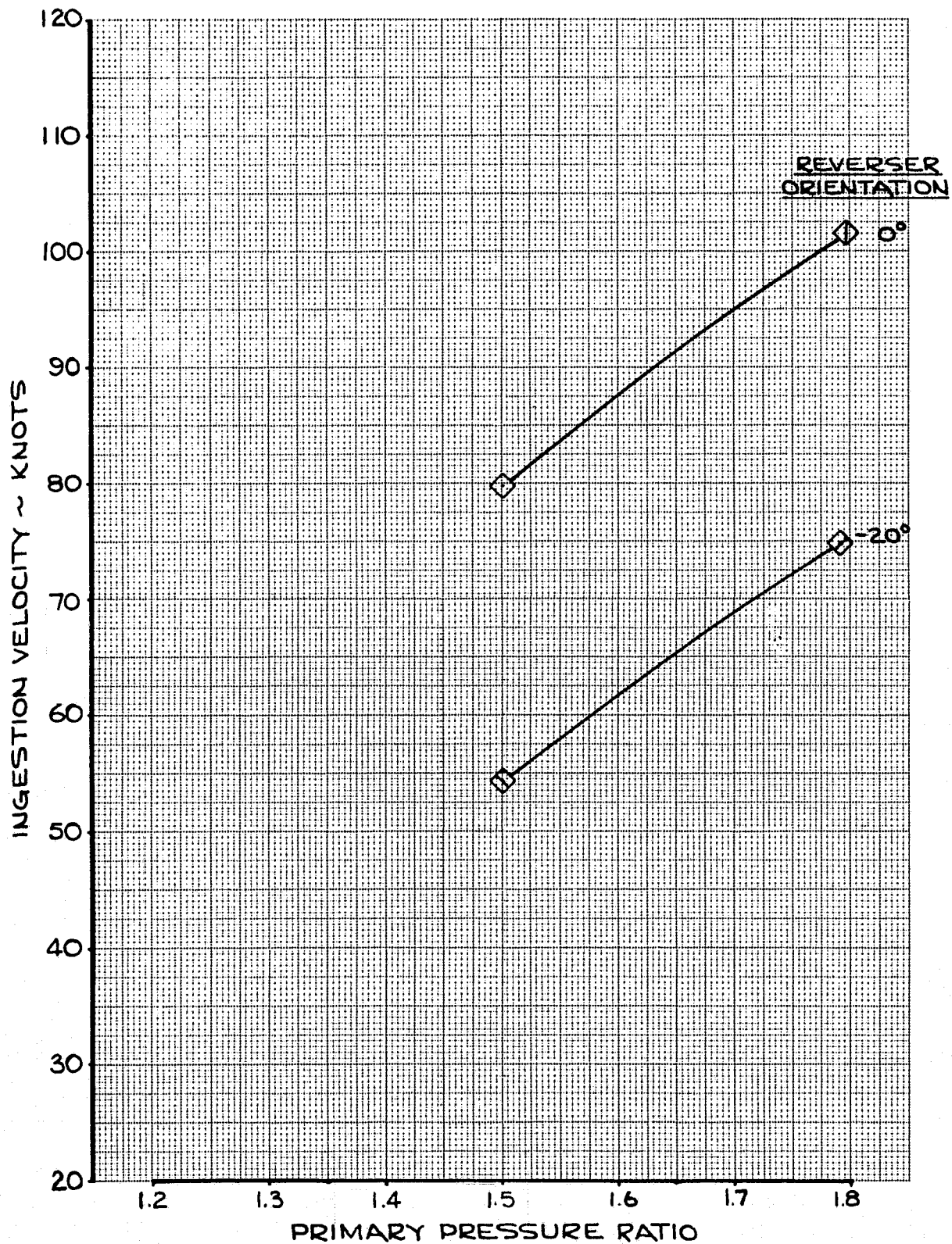
FIGURE 14 — INGESTION VELOCITIES FOR CONFIGURATION 12, 5° FLAPS
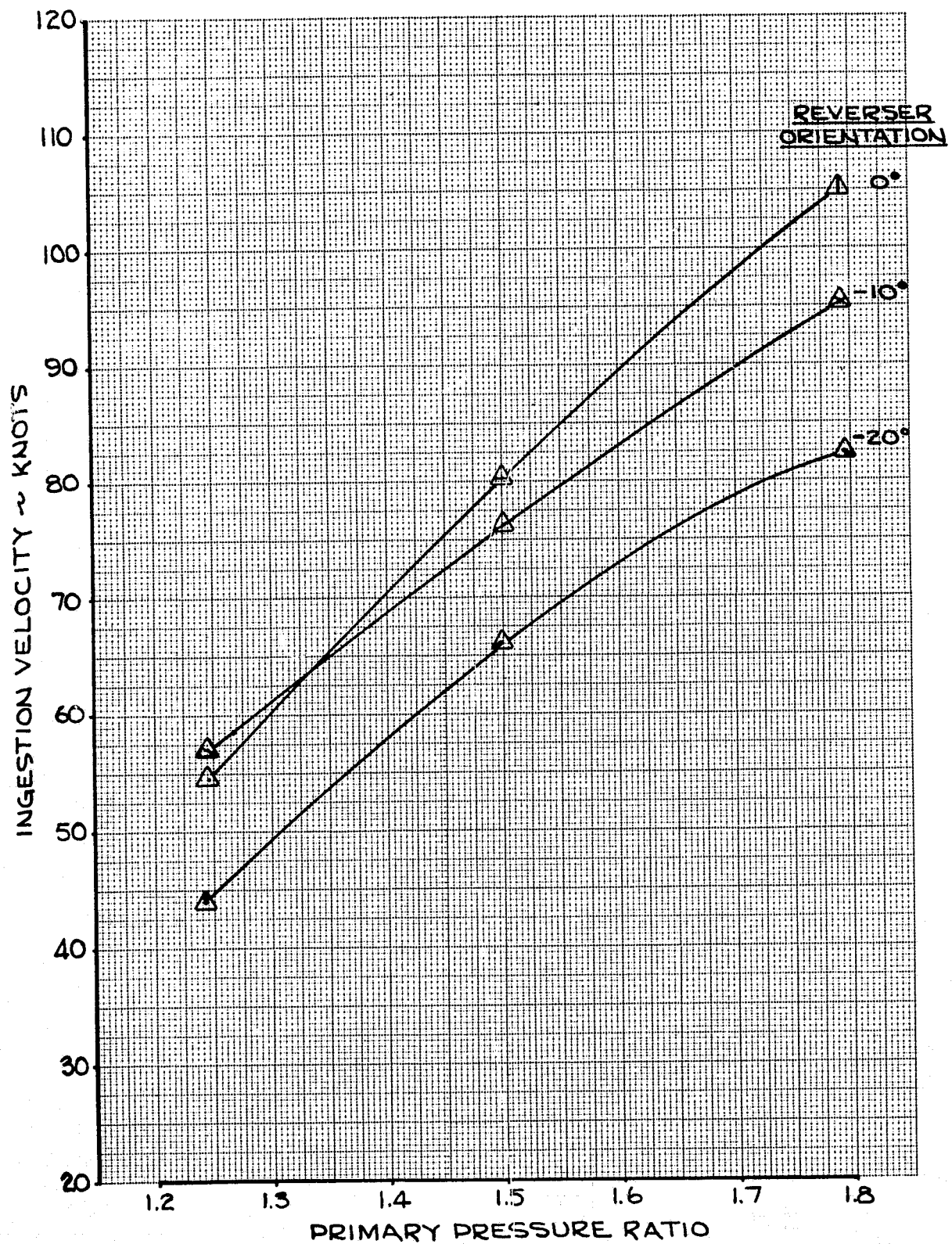
FIGURE 15 — INGESTION VELOCITIES FOR CONFIGURATION 7, 40°FLAPS
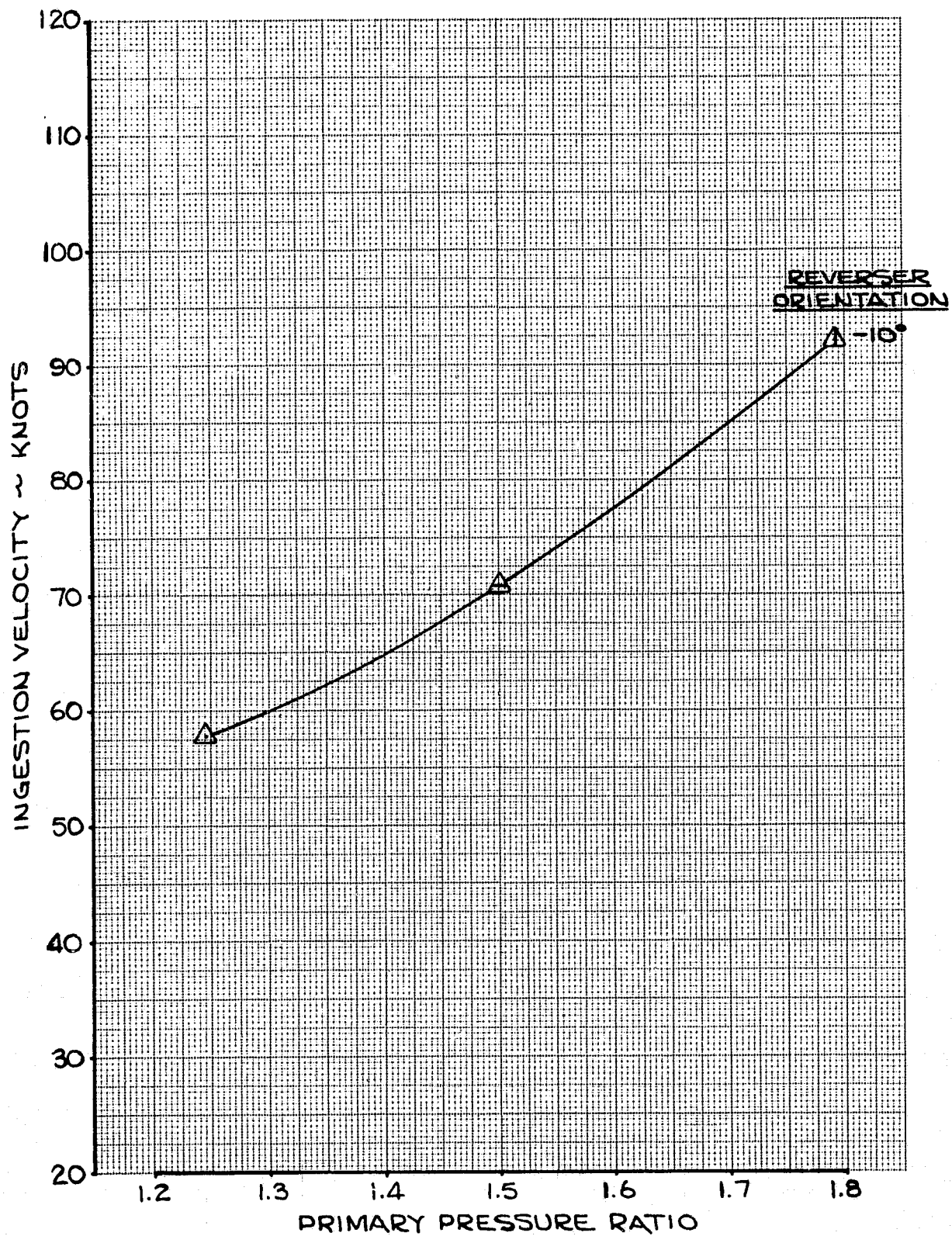
FIGURE 16 - INGESTION VELOCITIES FOR CONFIGURATION 7, 25° FLAPS
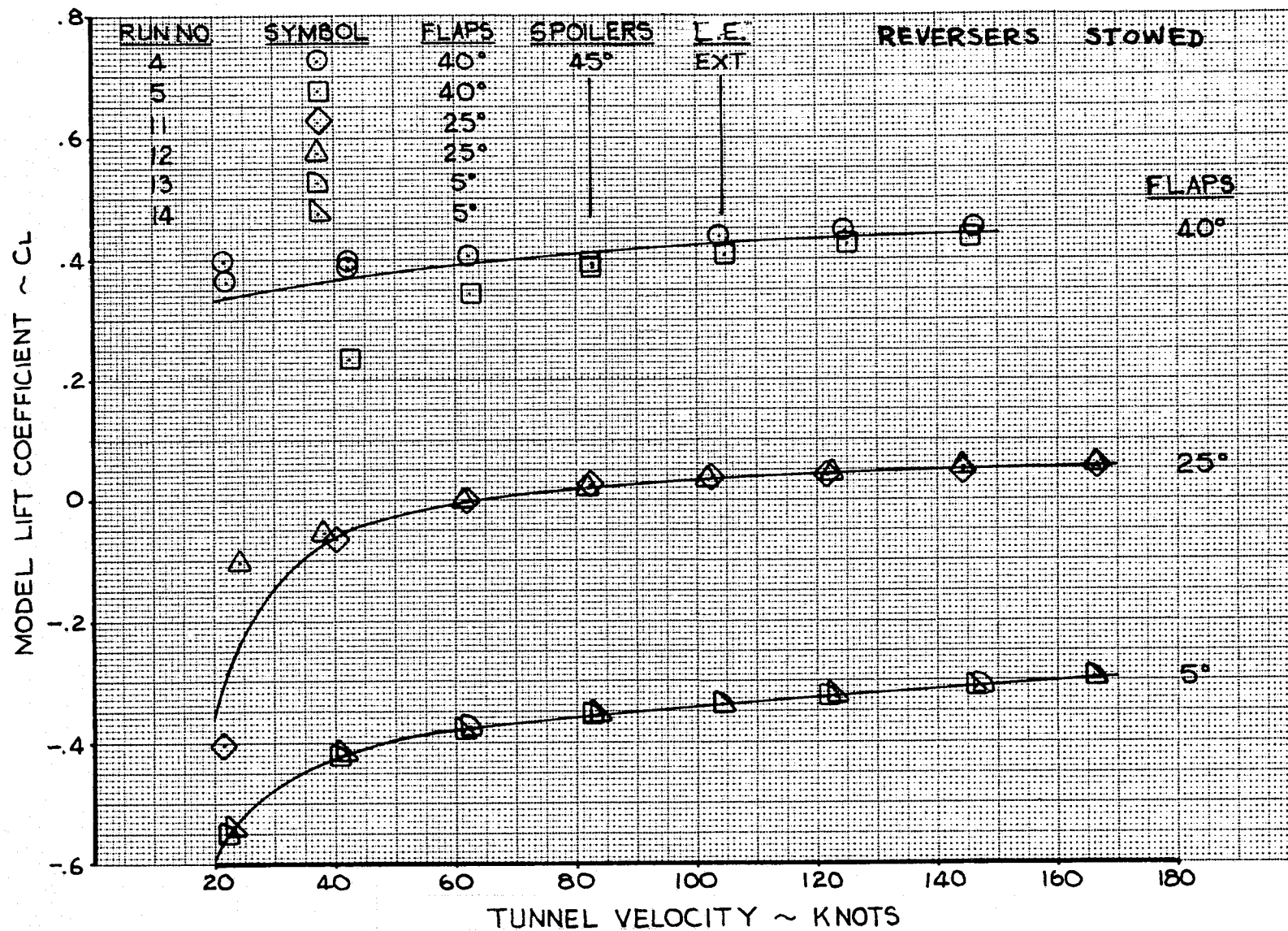
FIGURE 17 — MODEL LIFT COEFFICENTS-BASELINE
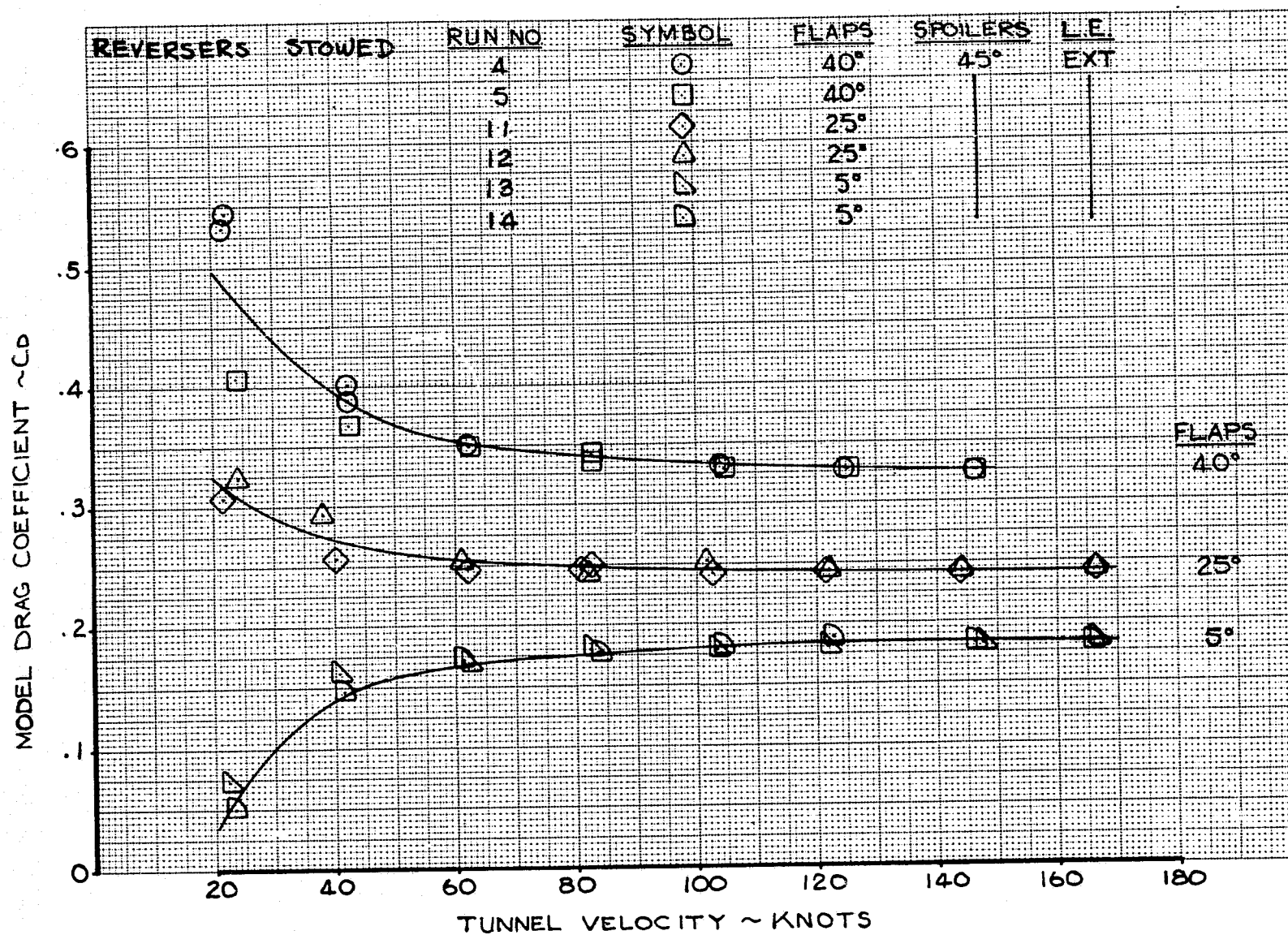
FIGURE 18 — MODEL DRAG COEFFICIENTS—BASELINE
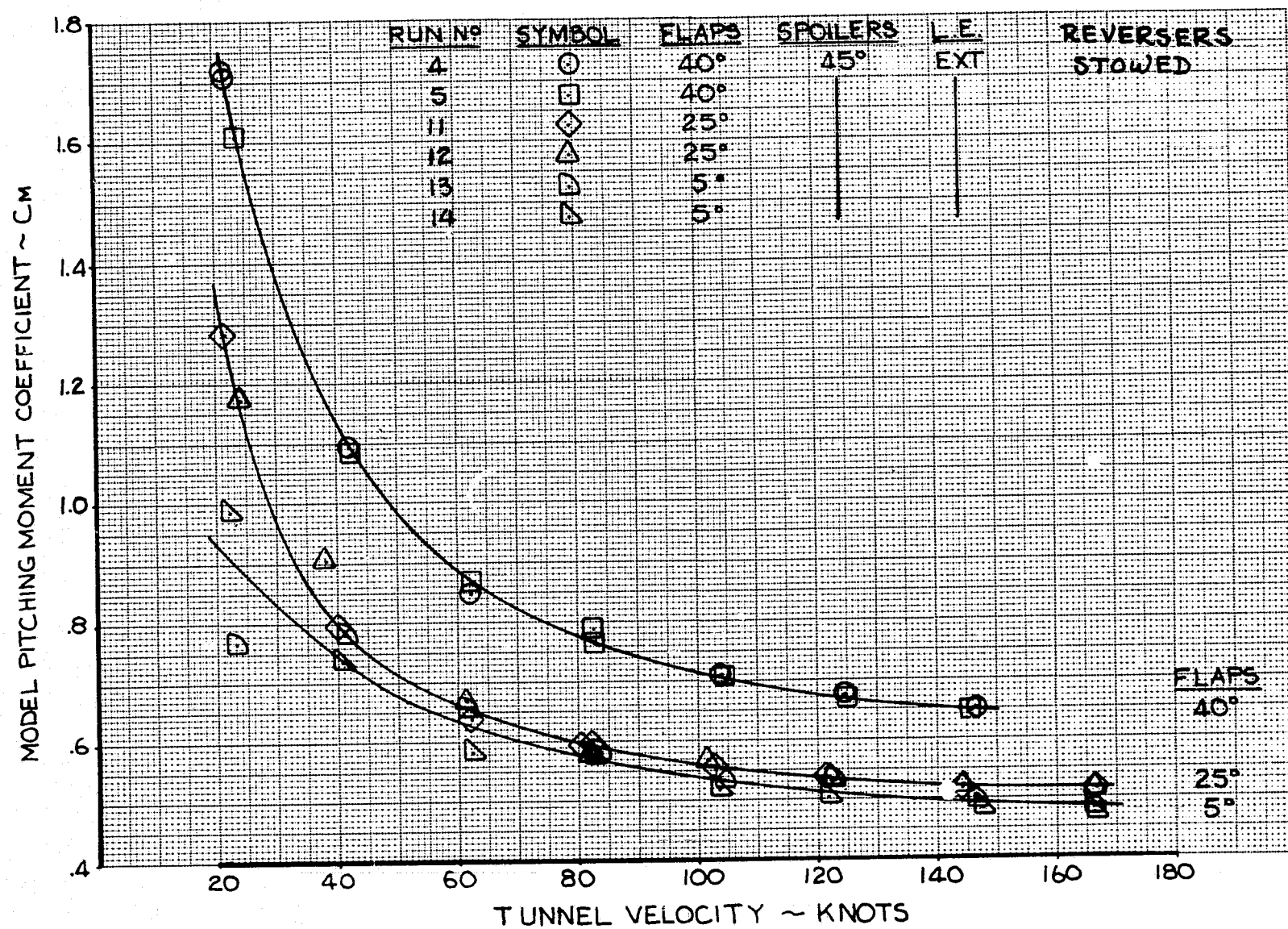
FIGURE 19 — MODEL PITCHING MOMENT COEFFICIENTS-BASELINE
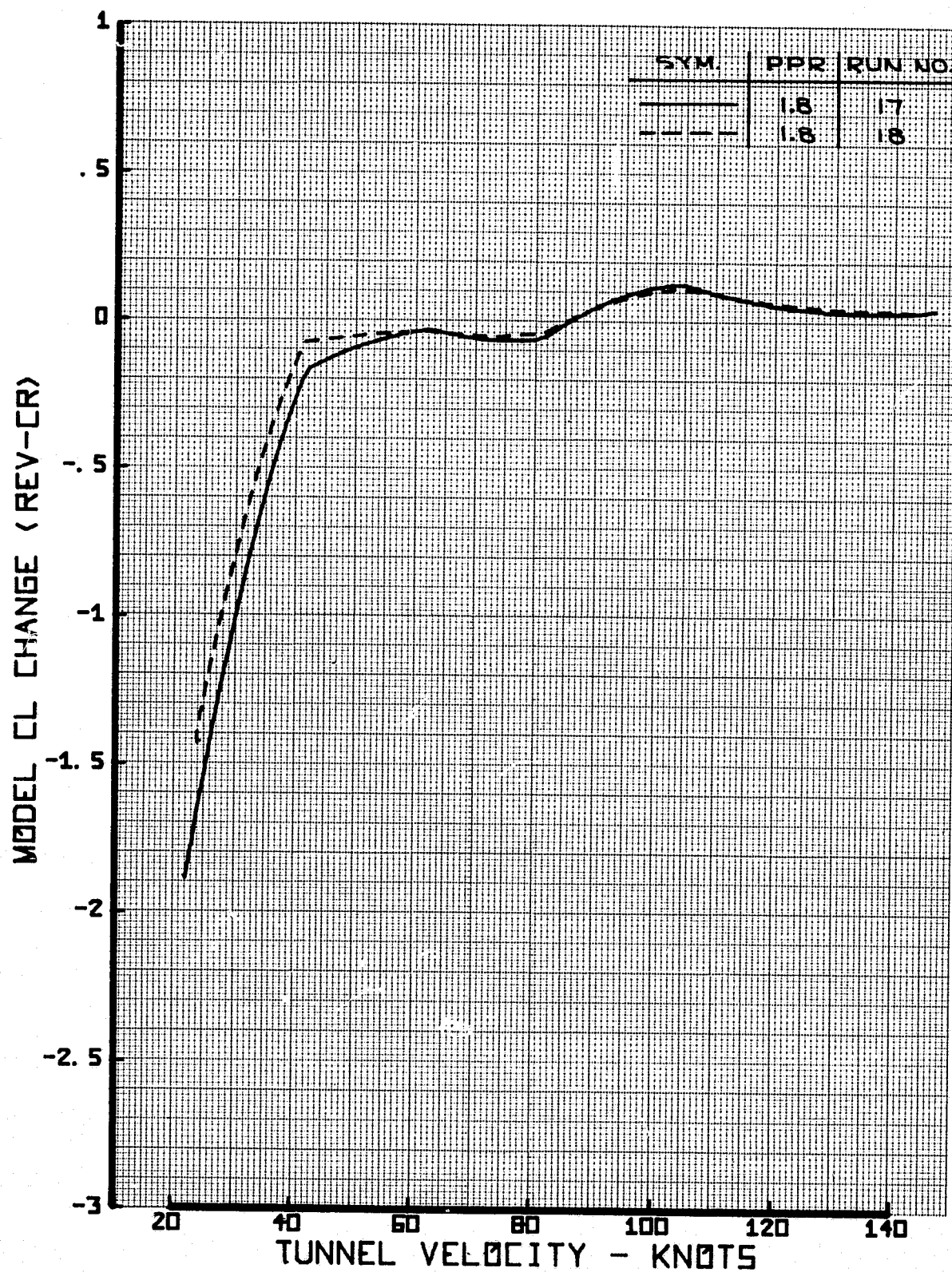
FIGURE 20 — MODEL C_L CHANGE, CONFIGURATION 1, 40° FLAPS, 0° ORIENTATION, PPR = 1.8.
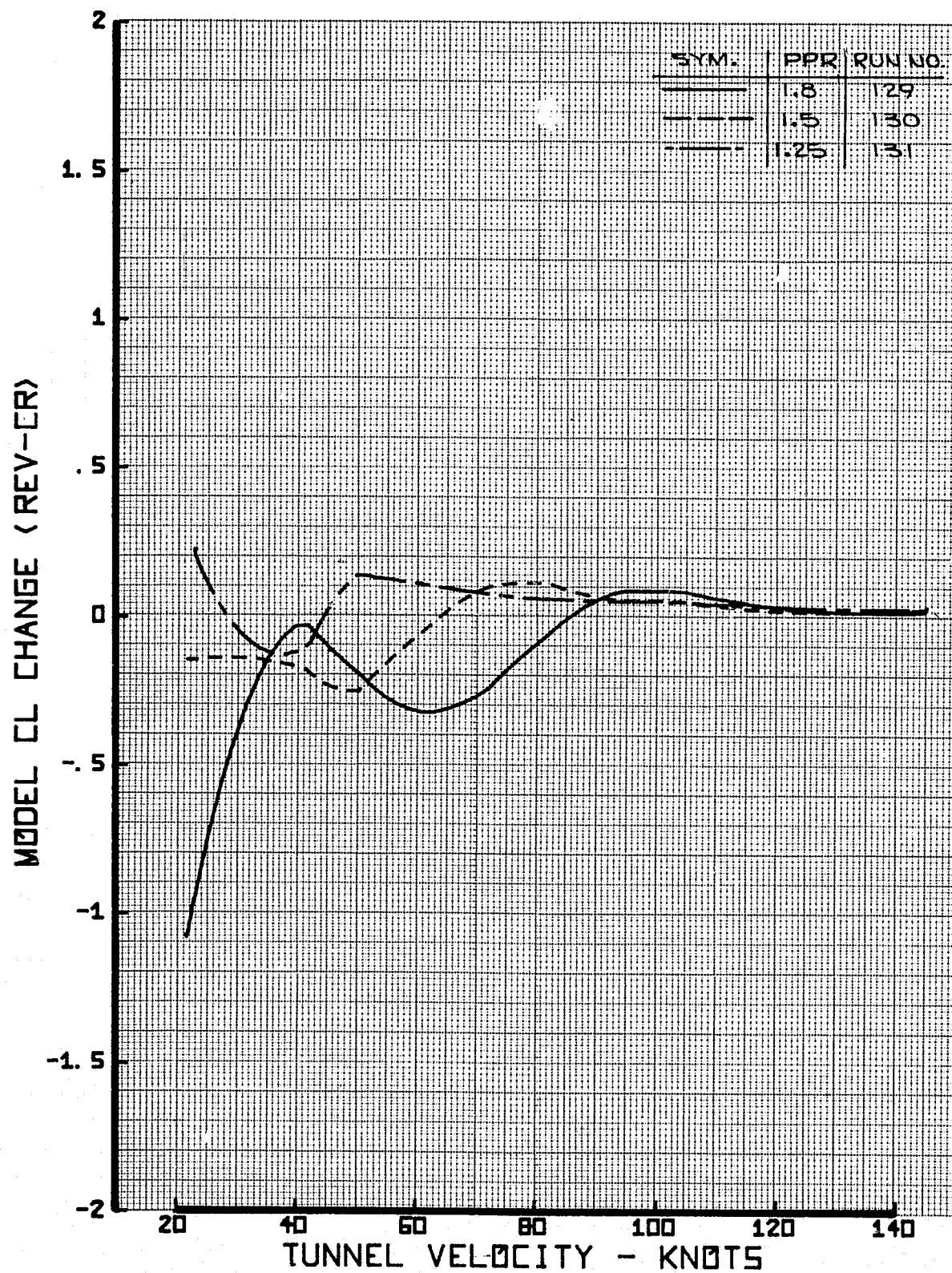
FIGURE 21 - MODEL CL CHANGE, CONFIGURATION 12, 40° FLAPS, 0° ORIENTATION

69
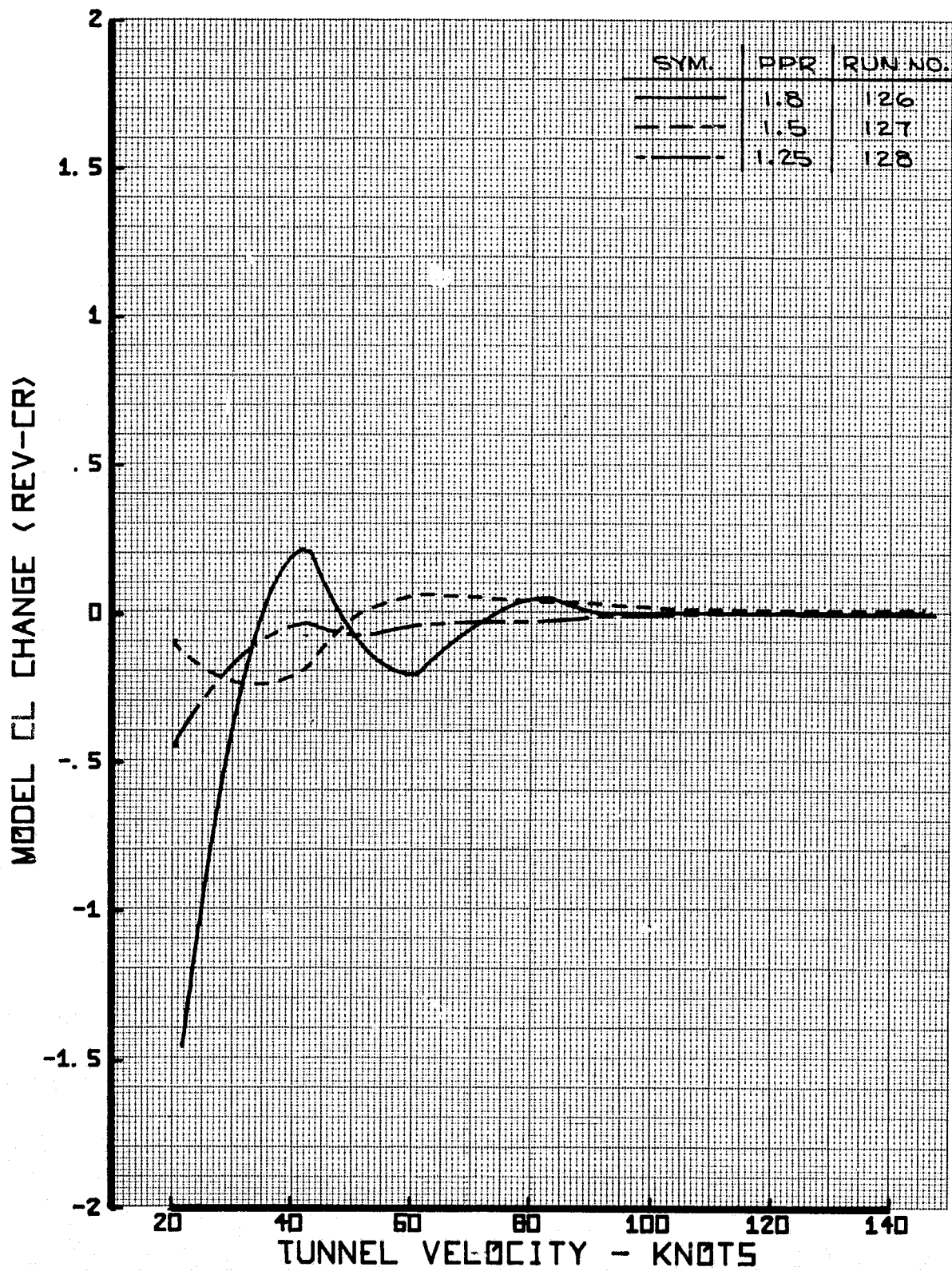
FIGURE 22 - MODEL CL CHANGE, CONFIGURATION 12, 40° FLAPS, -10° ORIENTATION
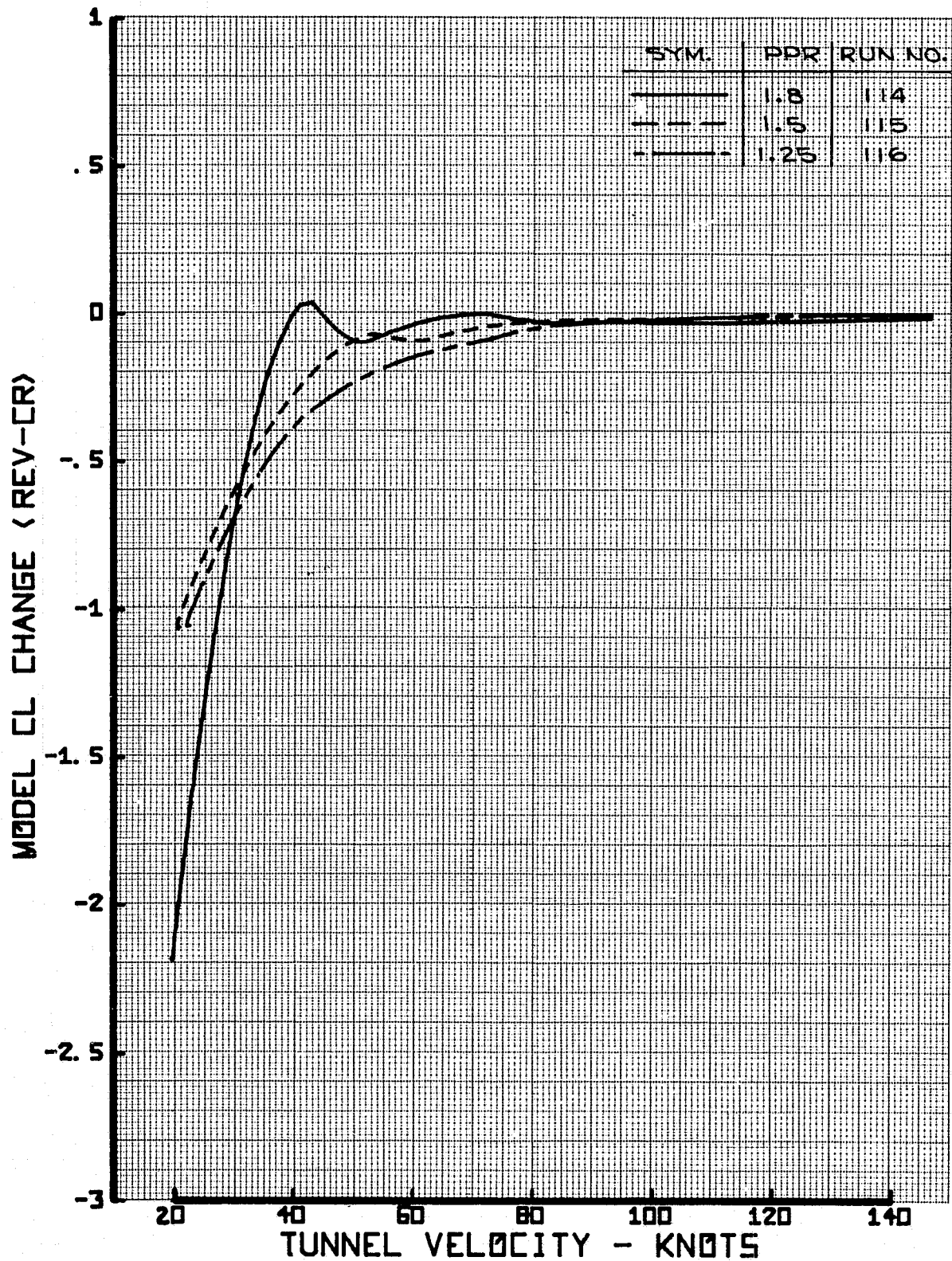
FIGURE 23 — MODEL CL CHANGE, CONFIGURATION 12,
40° FLAPS, −20° ORIENTATION
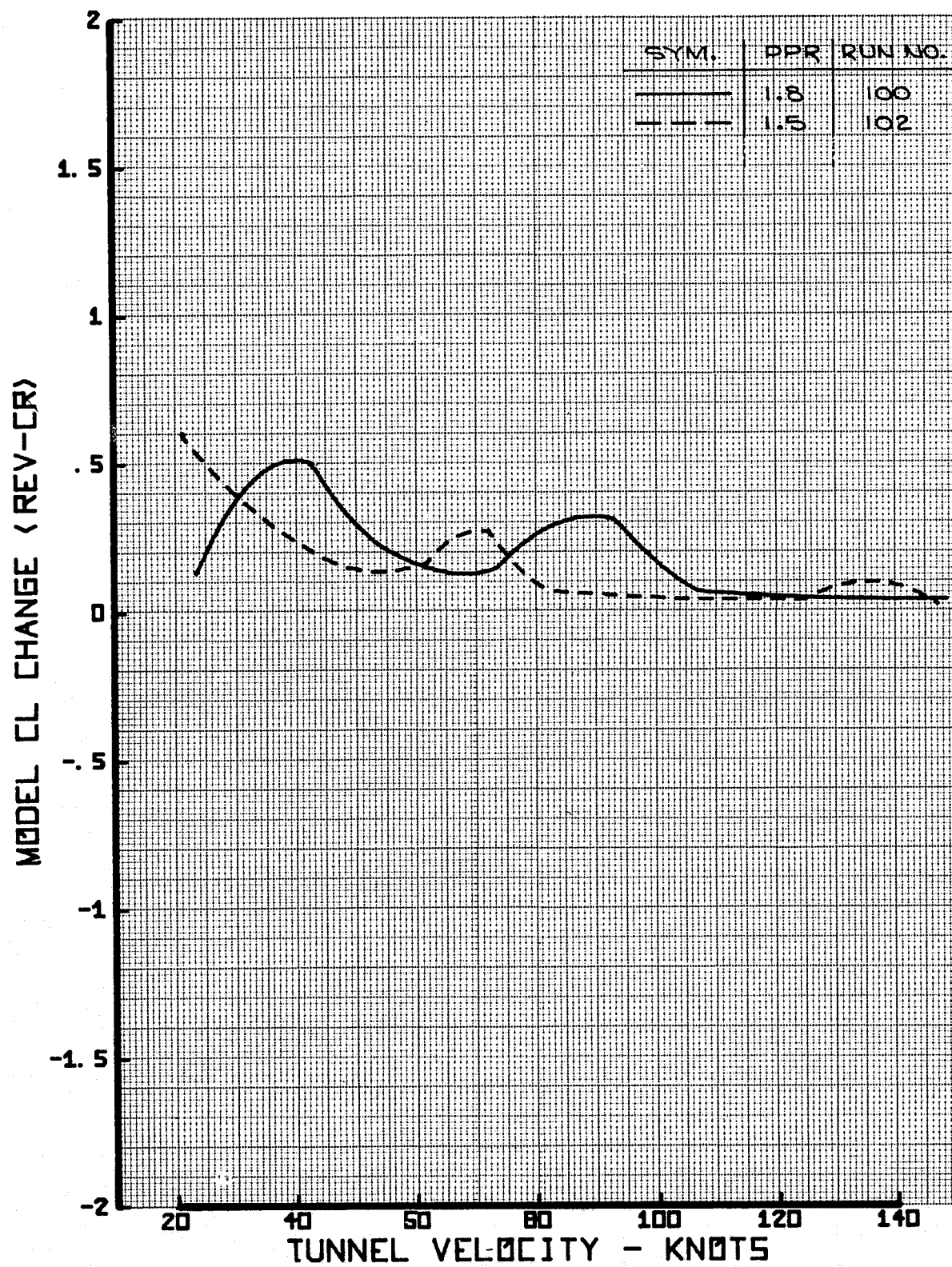
FIGURE 24 - MODEL C_L CHANGE, CONFIGURATION 12, 25° FLAPS, 0° ORIENTATION
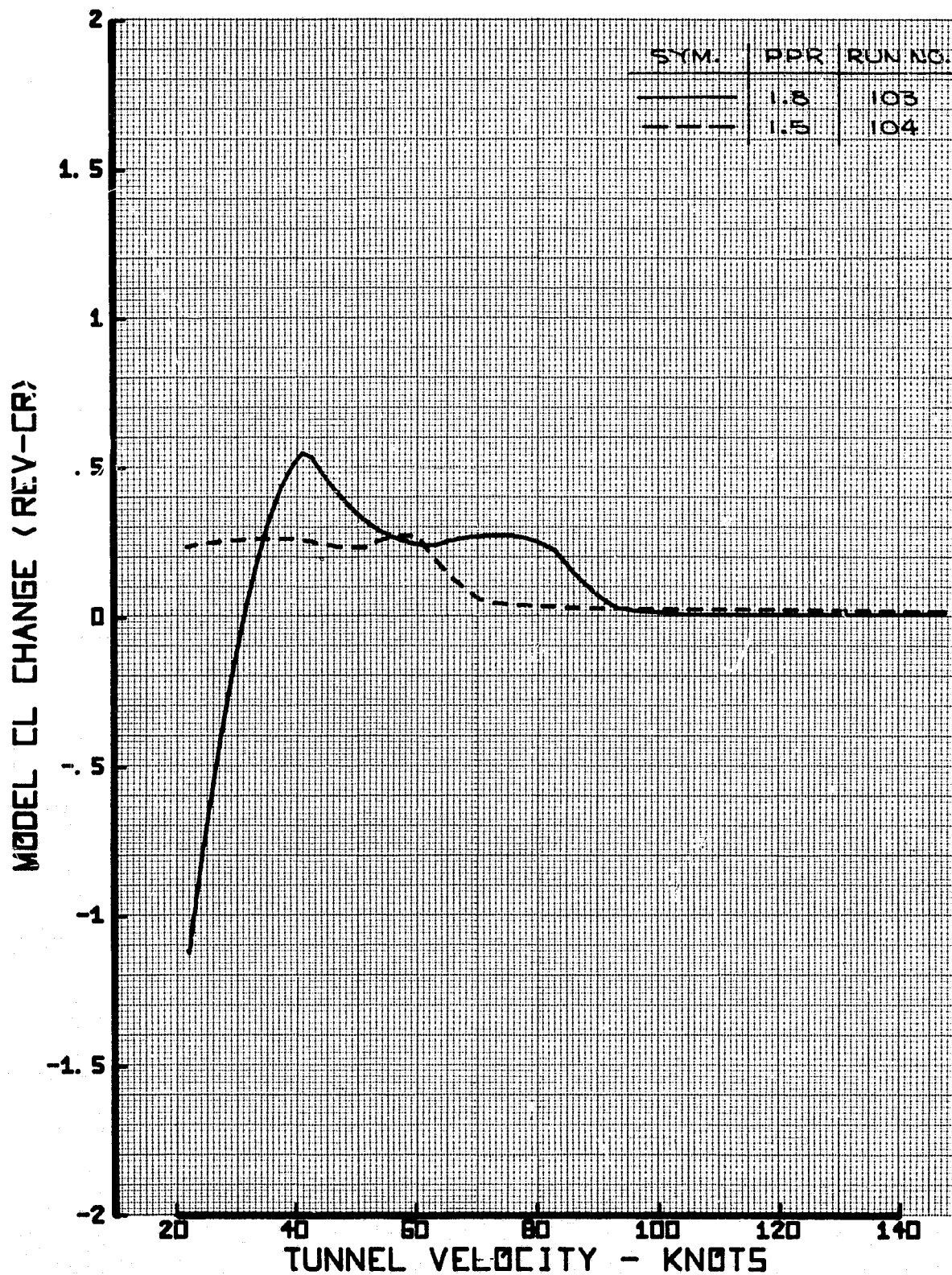
FIGURE 25 - MODEL CL CHANGE, CONFIGURATION 12, 25° FLAPS, -10° ORIENTATION

73
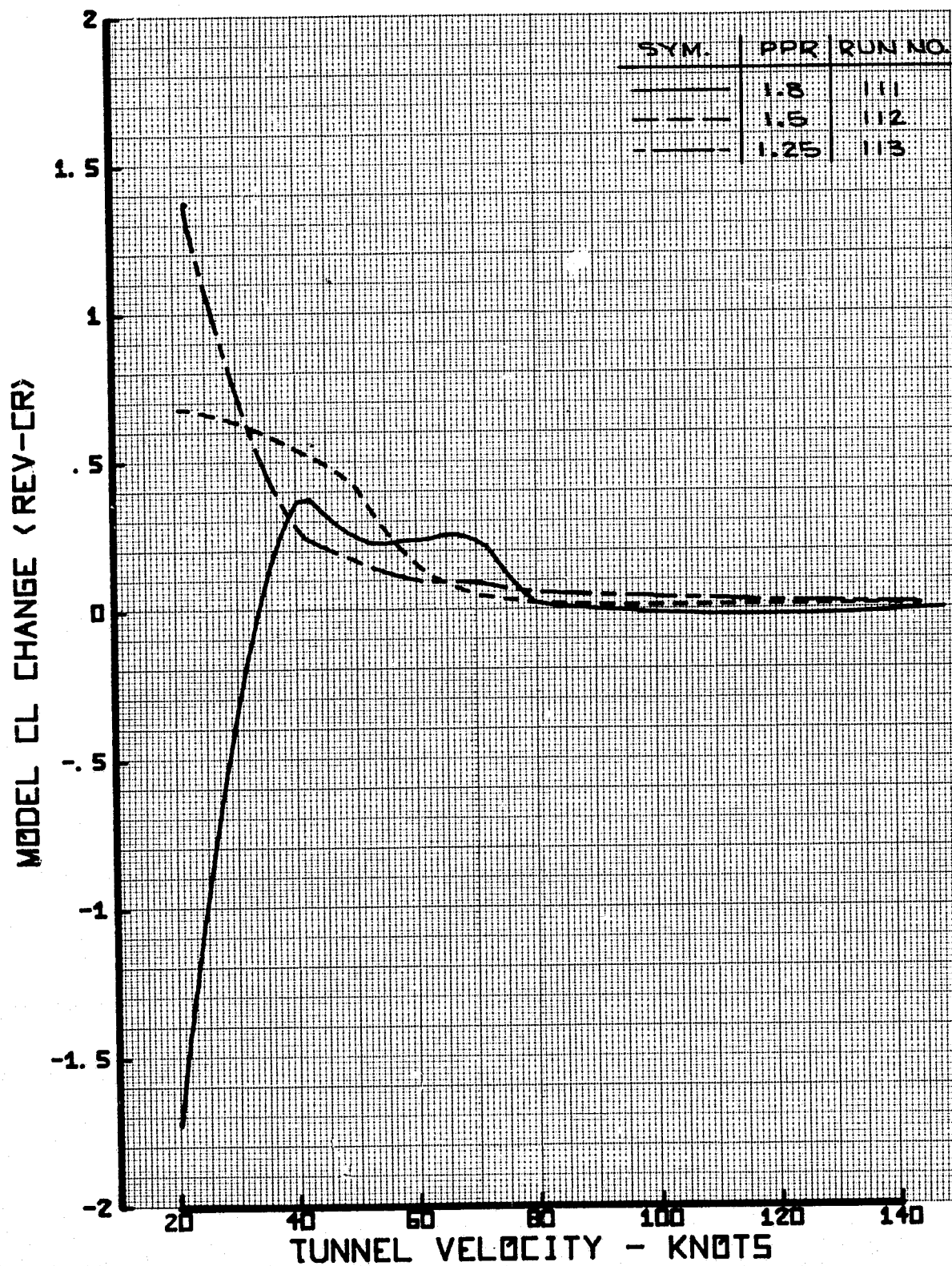
FIGURE 26 — MODEL CL CHANGE, CONFIGURATION 12
25° FLAPS, -20° ORIENTATION
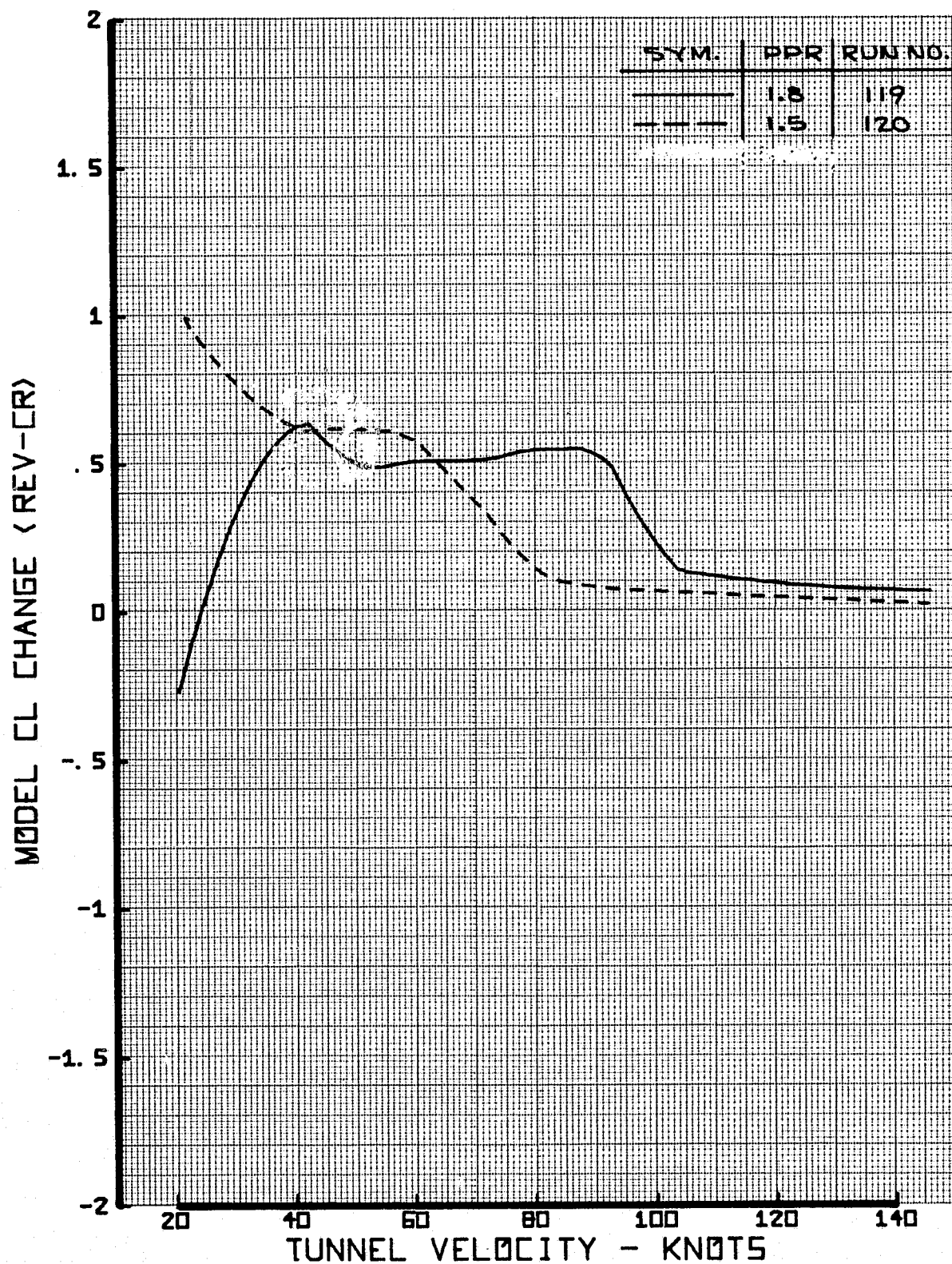
FIGURE 27 - MODEL C_L CHANGE, CONFIGURATION 12, 5° FLAPS, 0° ORIENTATION

75
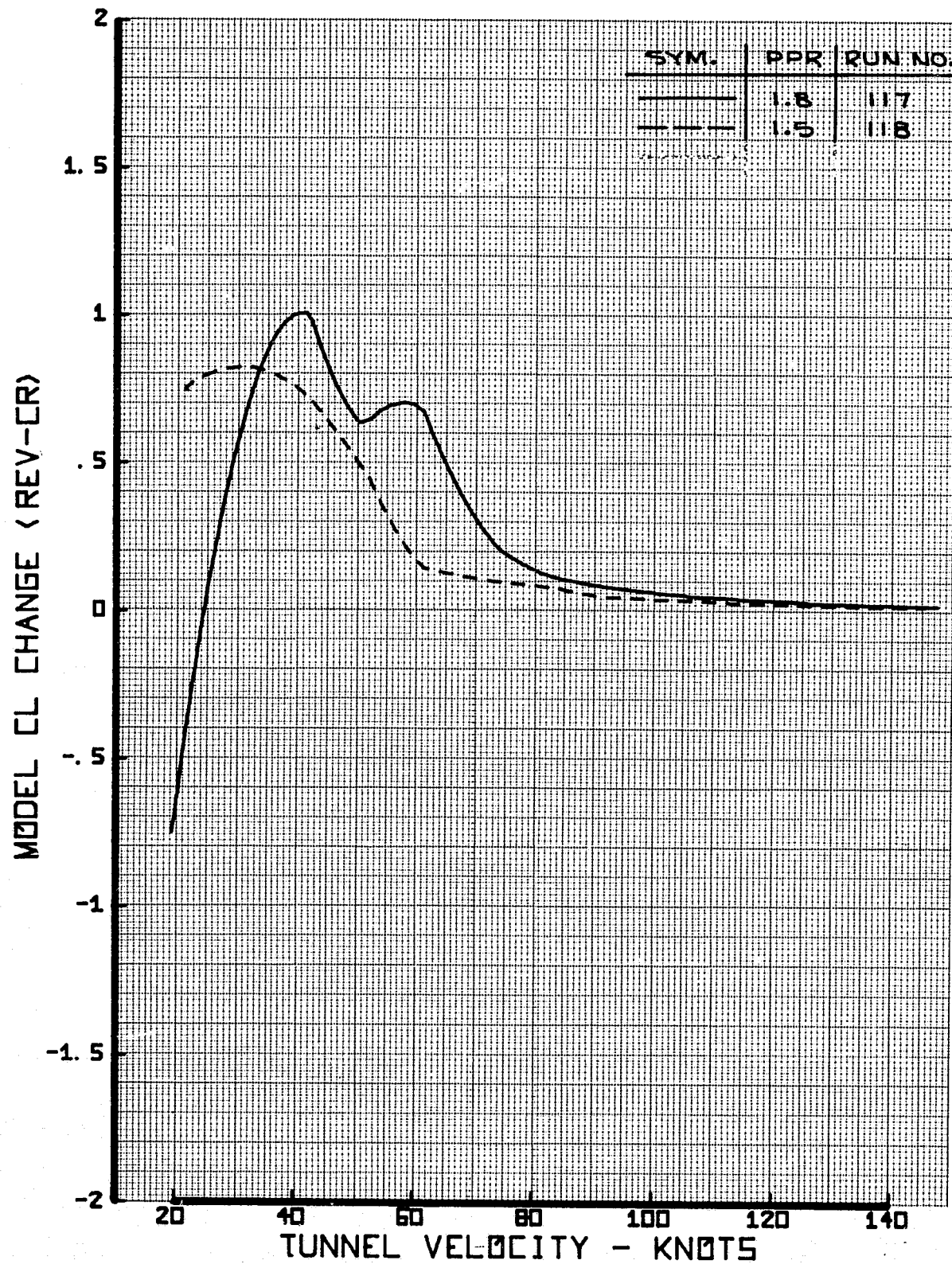
FIGURE 28 - MODEL C_L CHANGE, CONFIGURATION 12,
5° FLAPS, -20° ORIENTATION
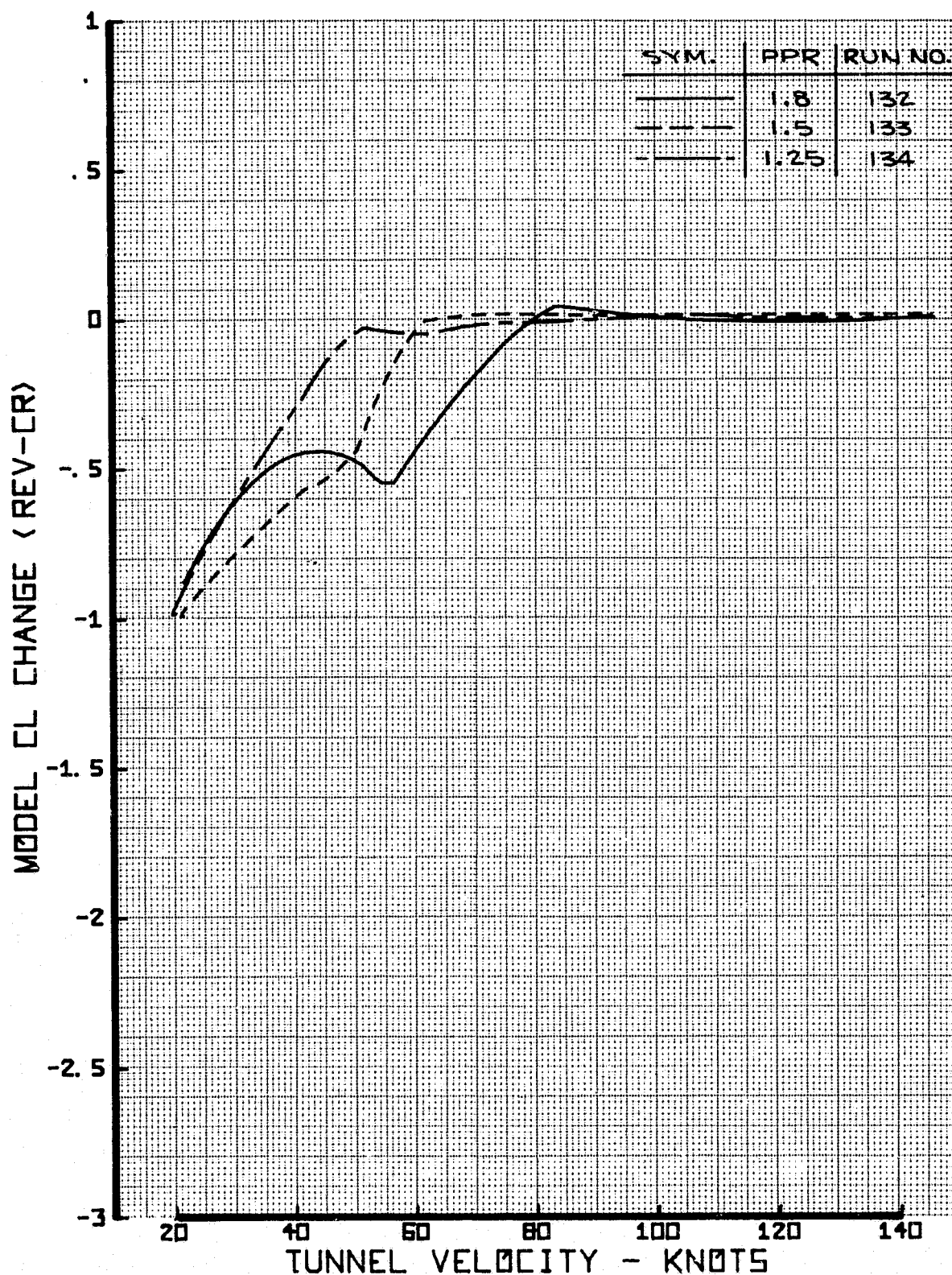
FIGURE 29 - MODEL C_L CHANGE, CONFIGURATION 7, 40° FLAPS, 0° ORIENTATION
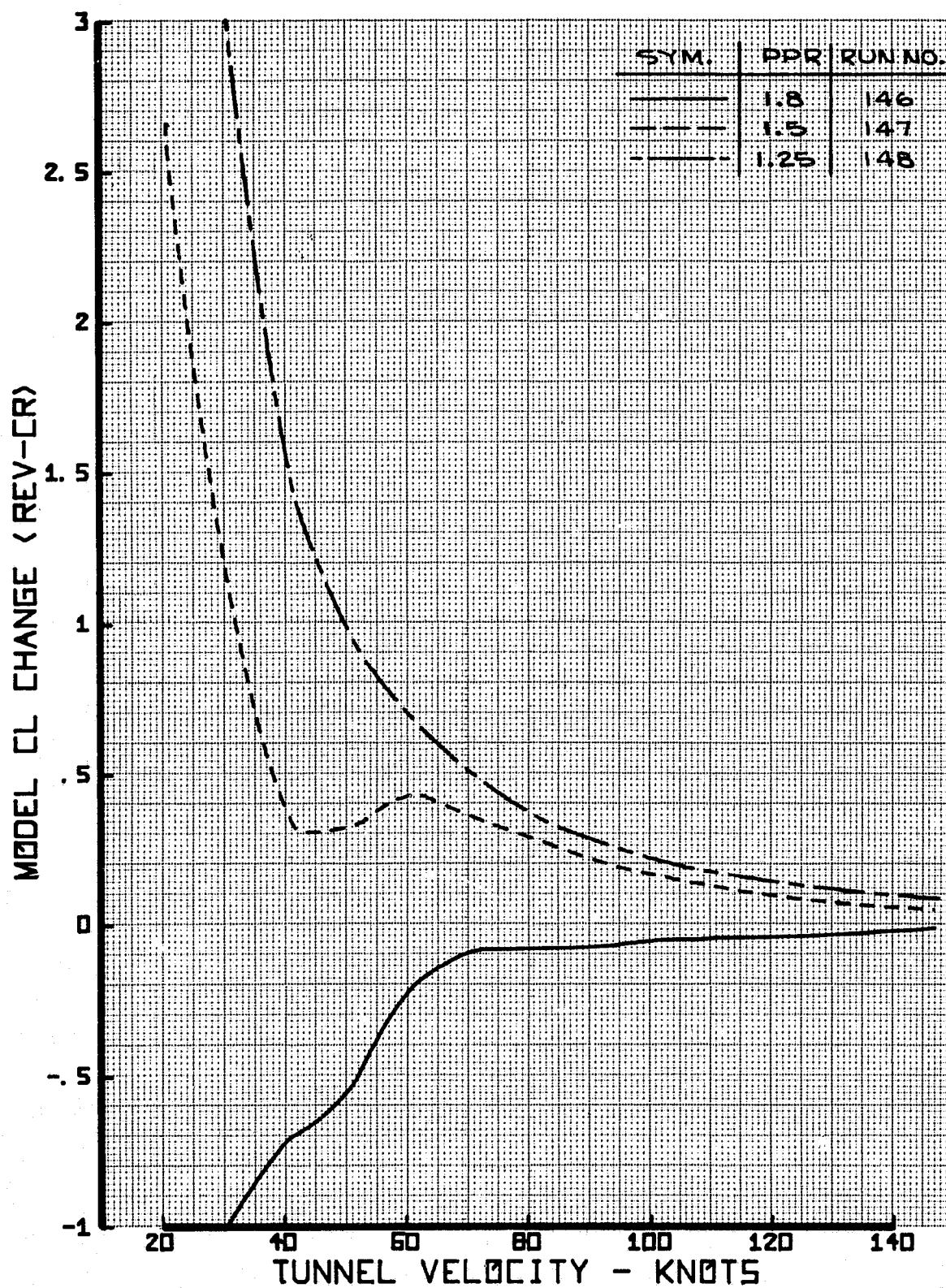
FIGURE 30 - MODEL C_L CHANGE, CONFIGURATION 7, 40° FLAPS, -10° ORIENTATION
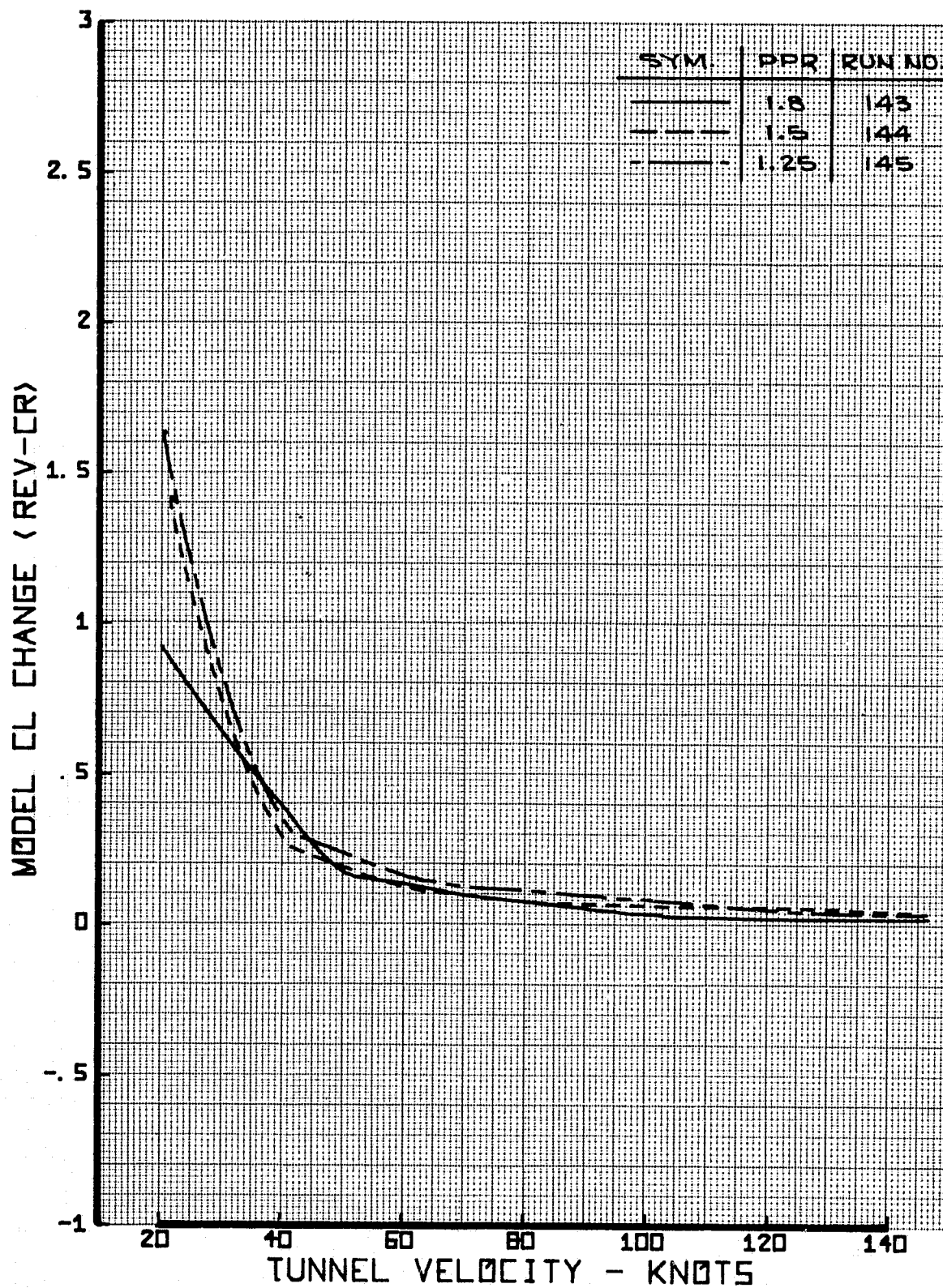
FIGURE 31 — MODEL CL CHANGE, CONFIGURATION 7, 40° FLAPS, −20° ORIENTATION
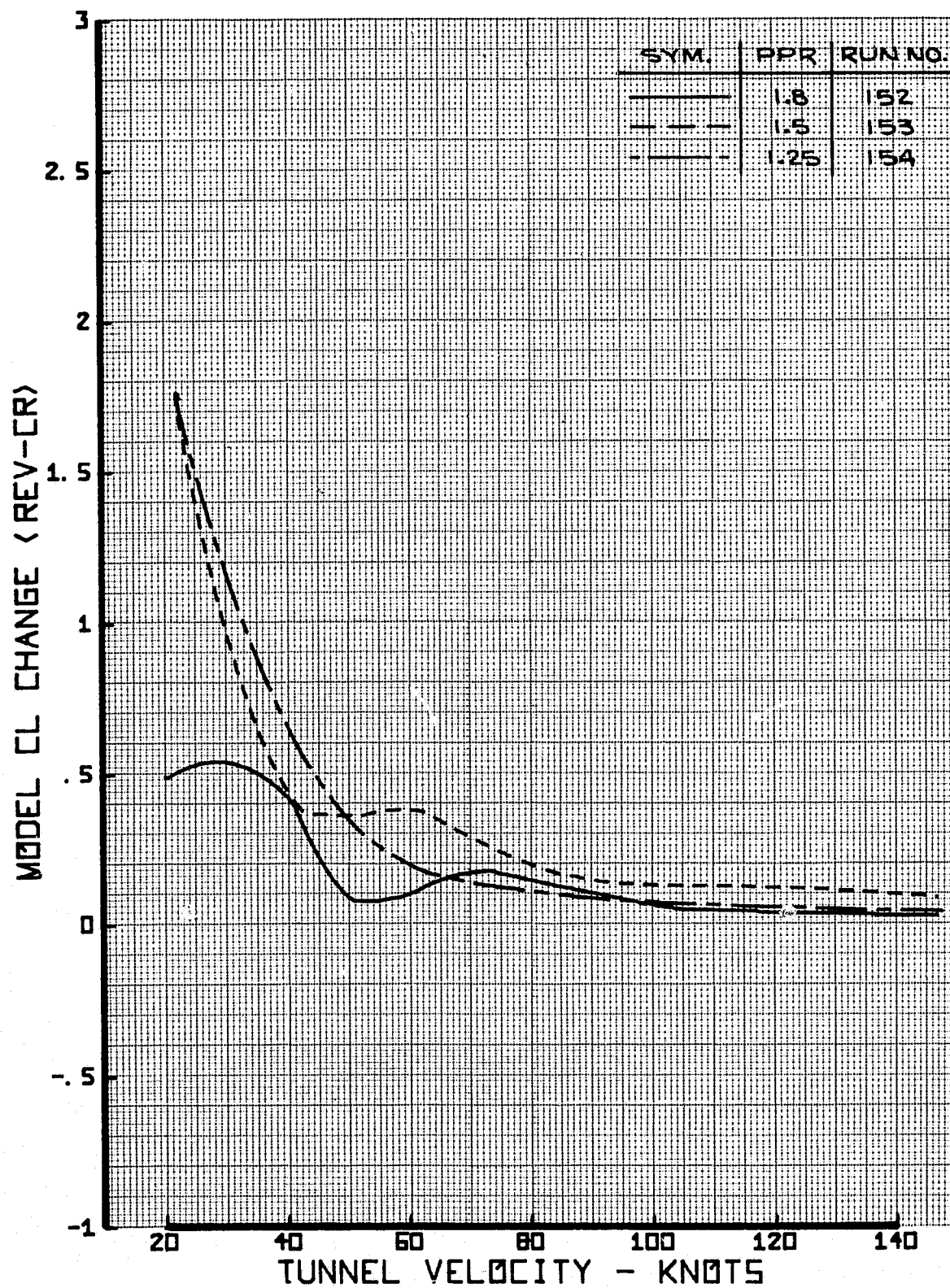
FIGURE 32 - MODEL CL CHANGE, CONFIGURATION 7, 25° FLAPS, -10° ORIENTATION
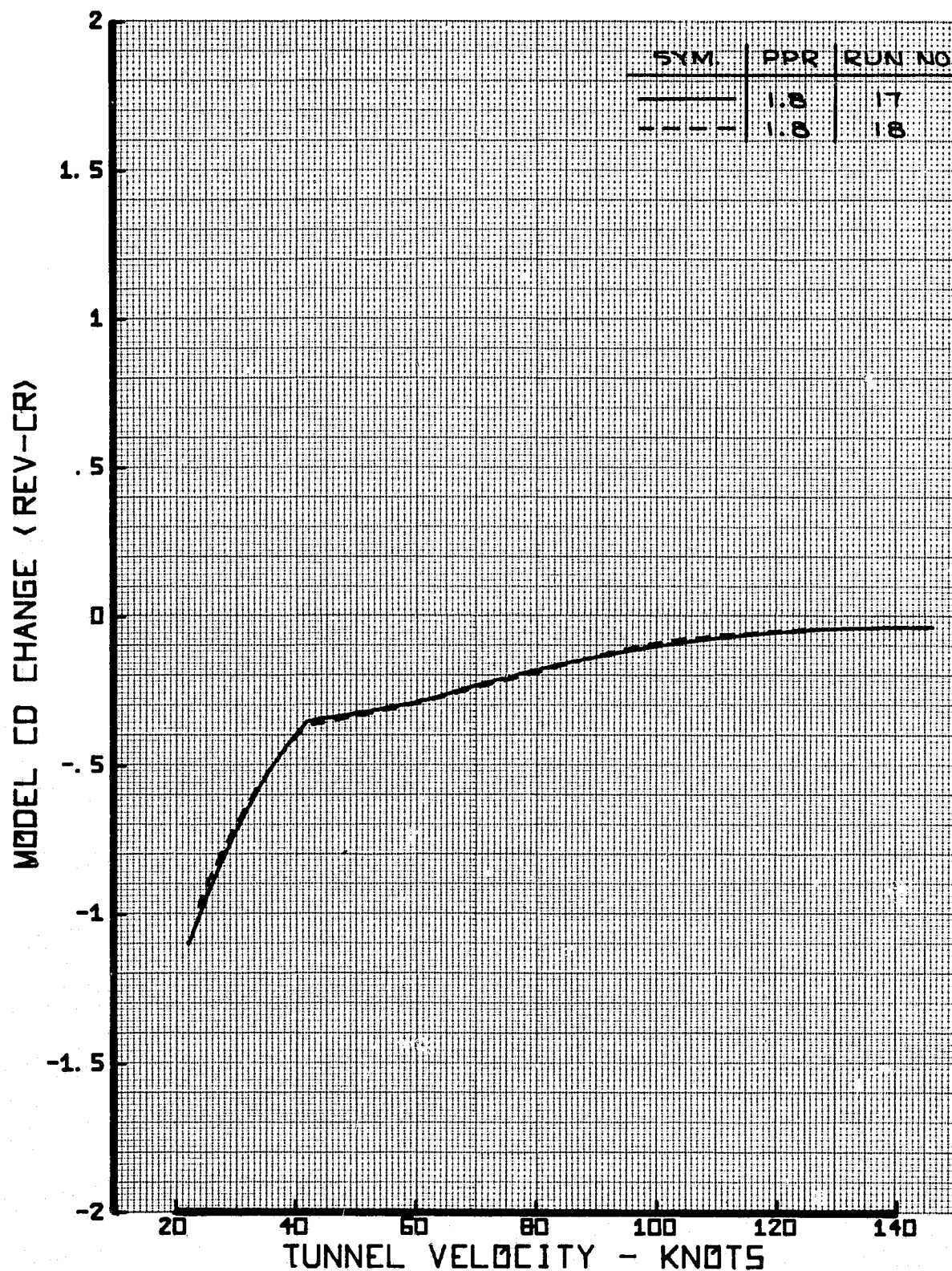
FIGURE 33 — MODEL C_D CHANGE, CONFIGURATION 1, 40° FLAPS, 0° ORIENTATION, PPR = 1.8.
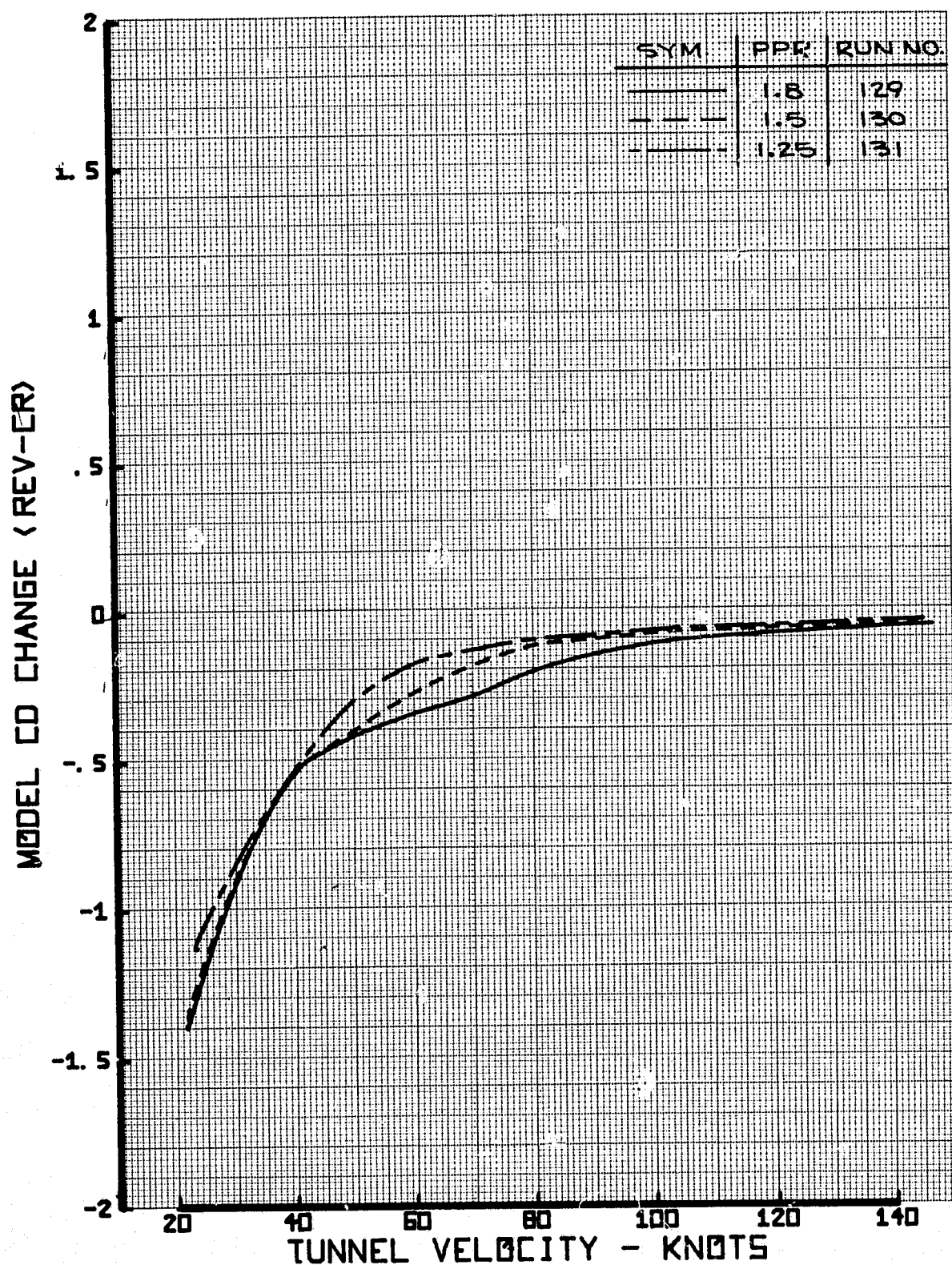
FIGURE **34** - MODEL C_D CHANGE, CONFIGURATION 12, 40° FLAPS, 0° ORIENTATION

82
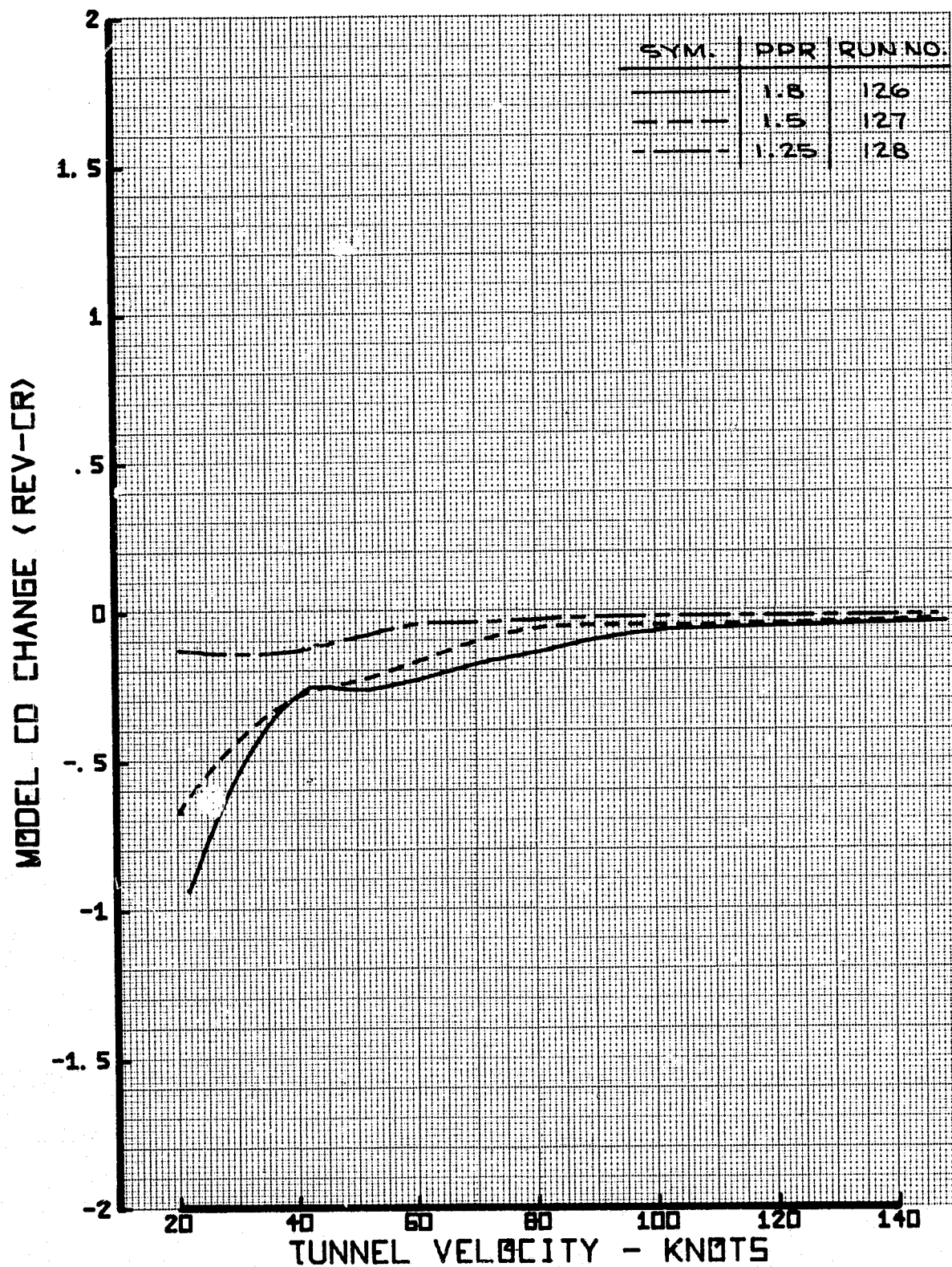
FIGURE 35 - MODEL C_D CHANGE, CONFIGURATION 12, 40° FLAPS, -10° ORIENTATION
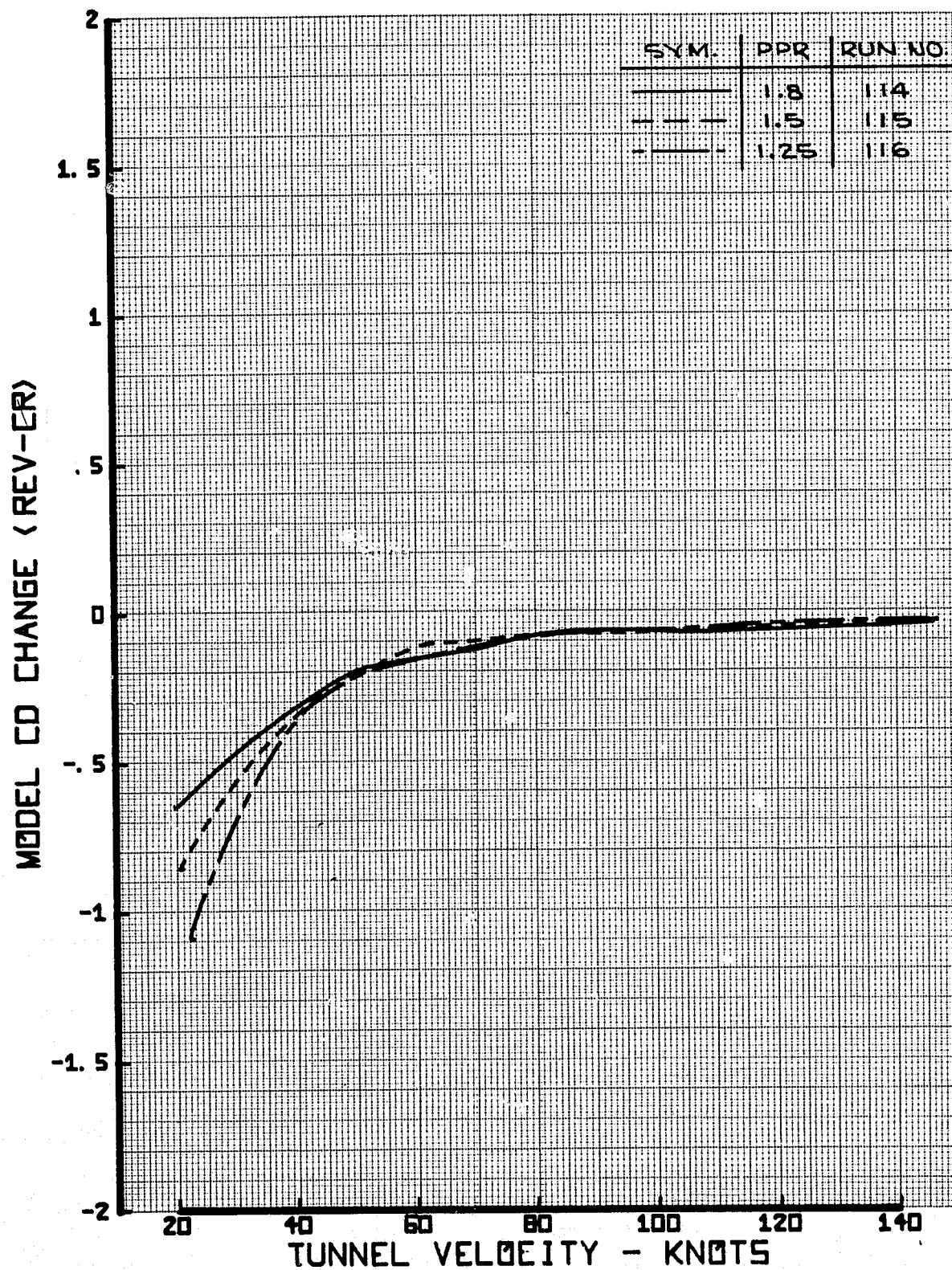
FIGURE 36 - MODEL C$_D$ CHANGE, CONFIGURATION 12, 40° FLAPS, -20° ORIENTATION
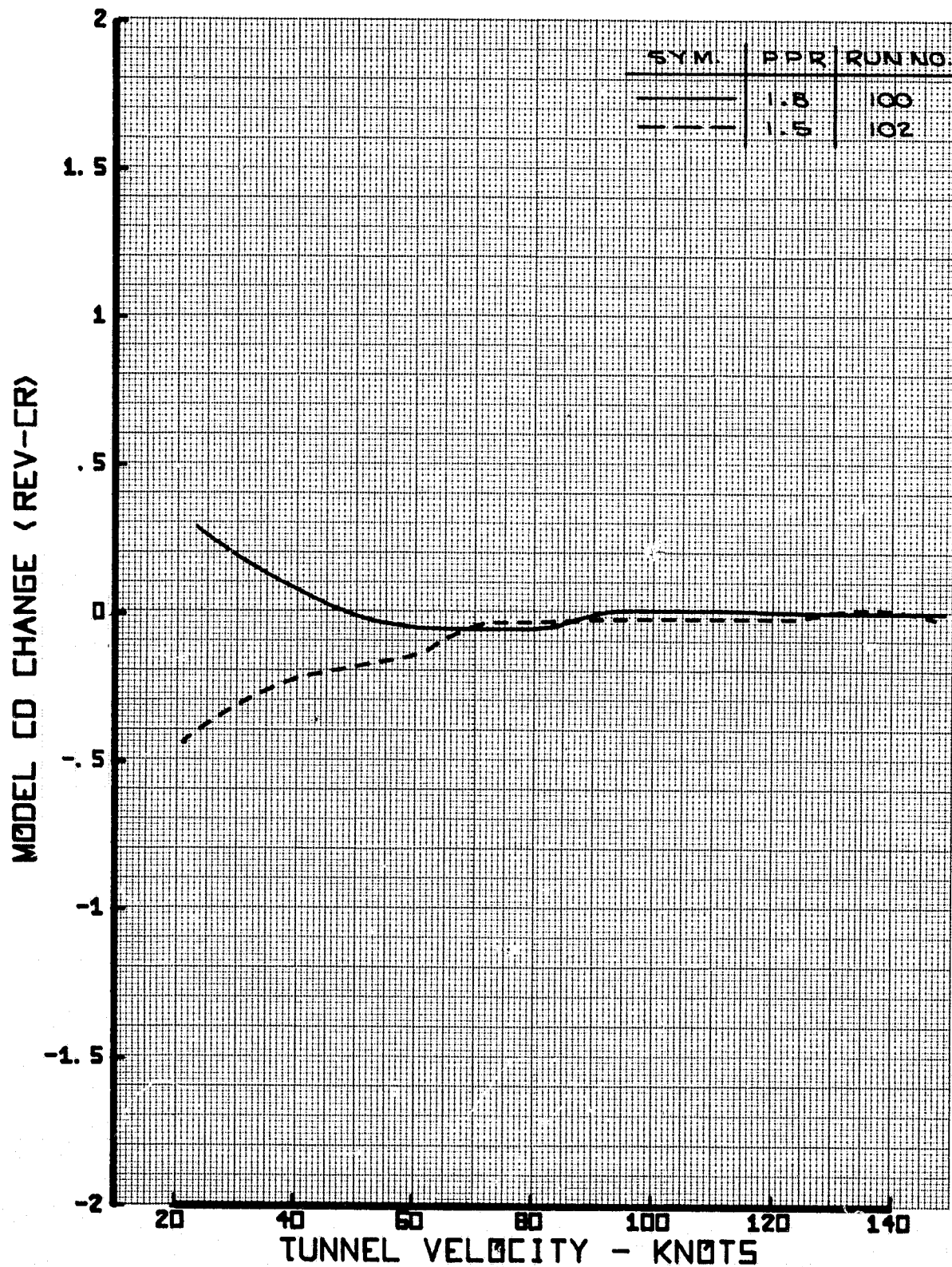
FIGURE 37 - MODEL C_D CHANGE, CONFIGURATION 12, 25° FLAPS, 0° ORIENTATION
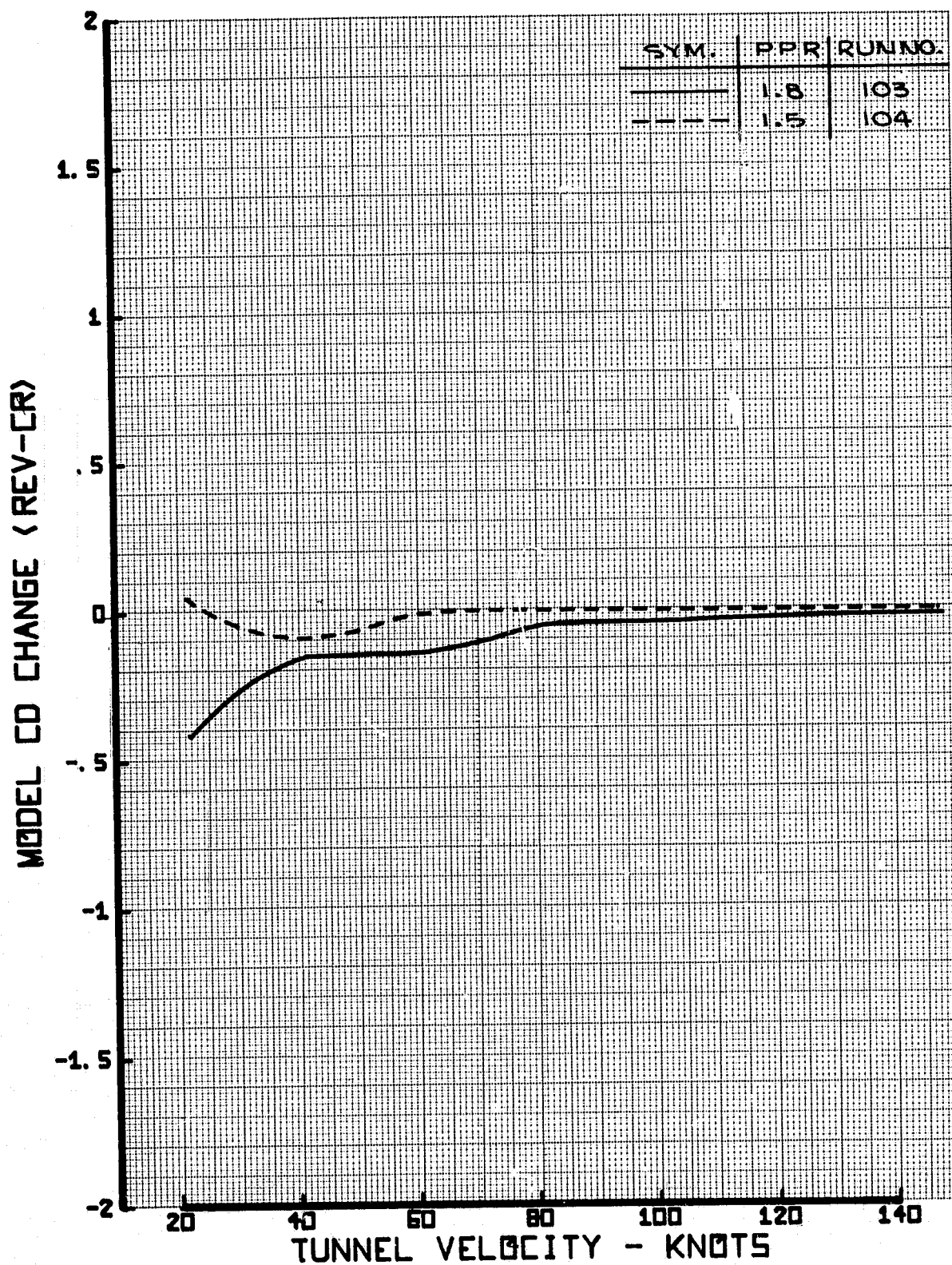
FIGURE 38 - MODEL C_D CHANGE, CONFIGURATION 12, 25° FLAPS, -10° ORIENTATION
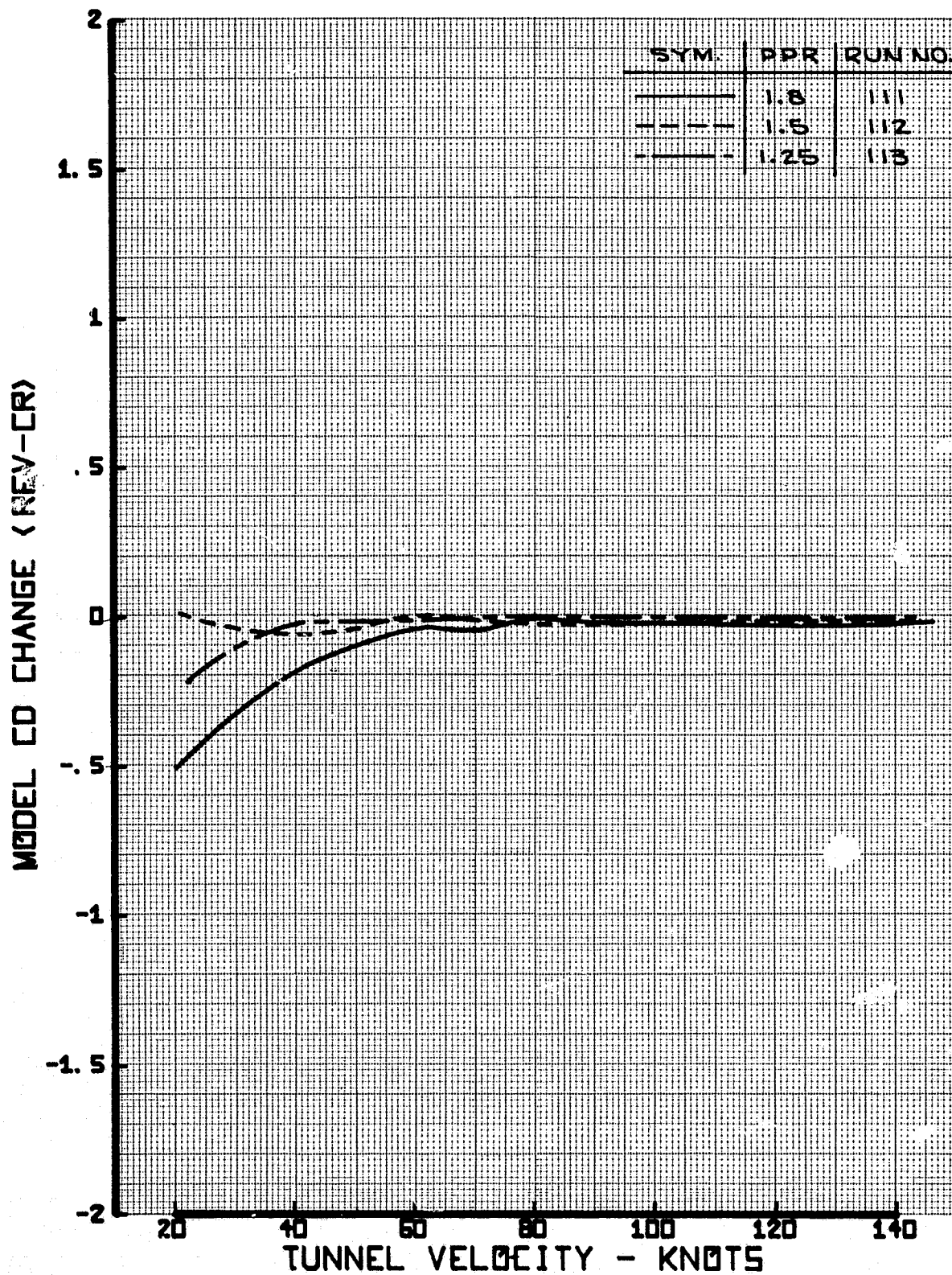
FIGURE 39 — MODEL C_D CHANGE, CONFIGURATION 12, 25° FLAPS, −20° ORIENTATION
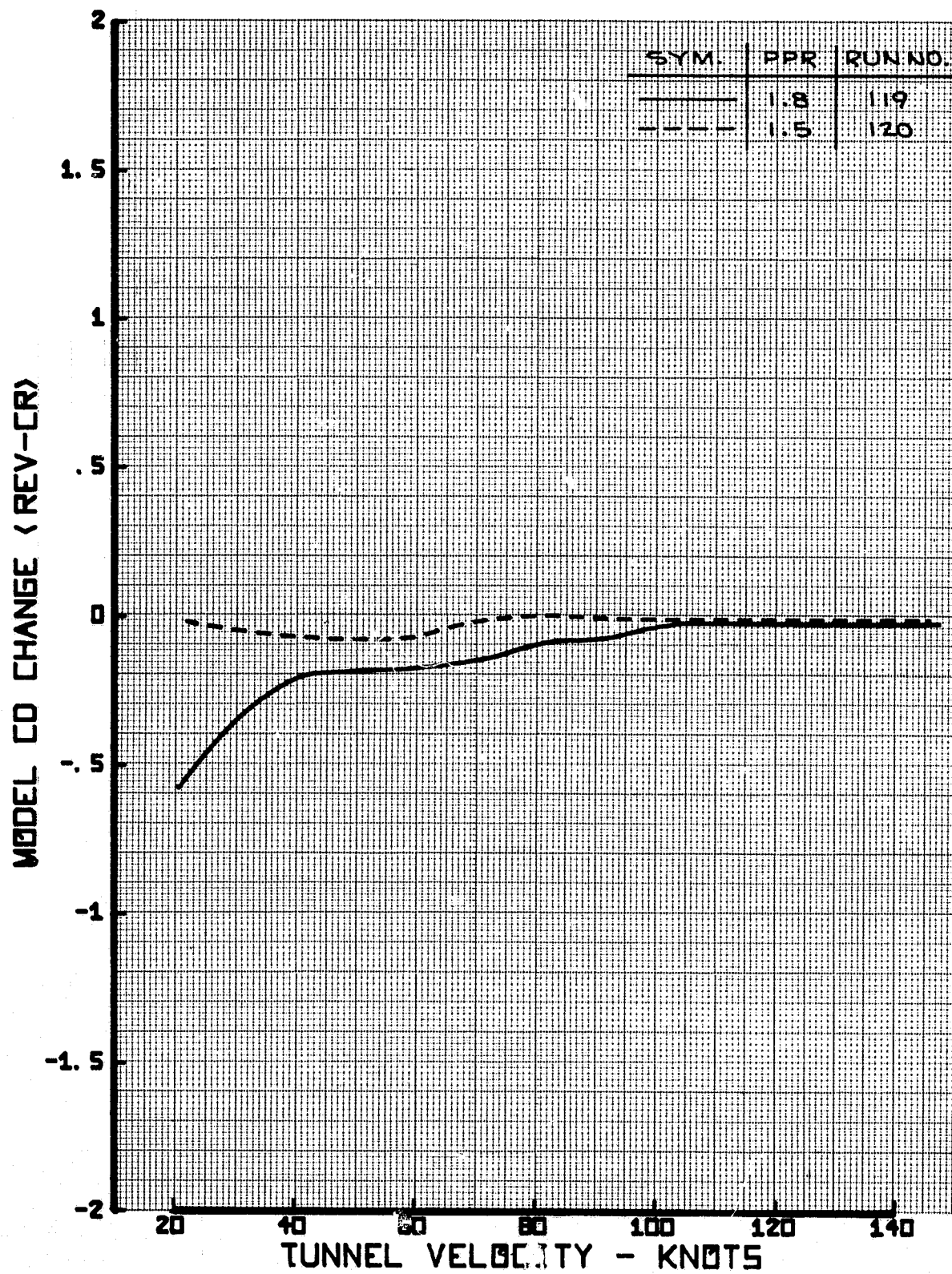
FIGURE 40 - MODEL C_D CHANGE, CONFIGURATION 12, 5° FLAPS, 0° ORIENTATION
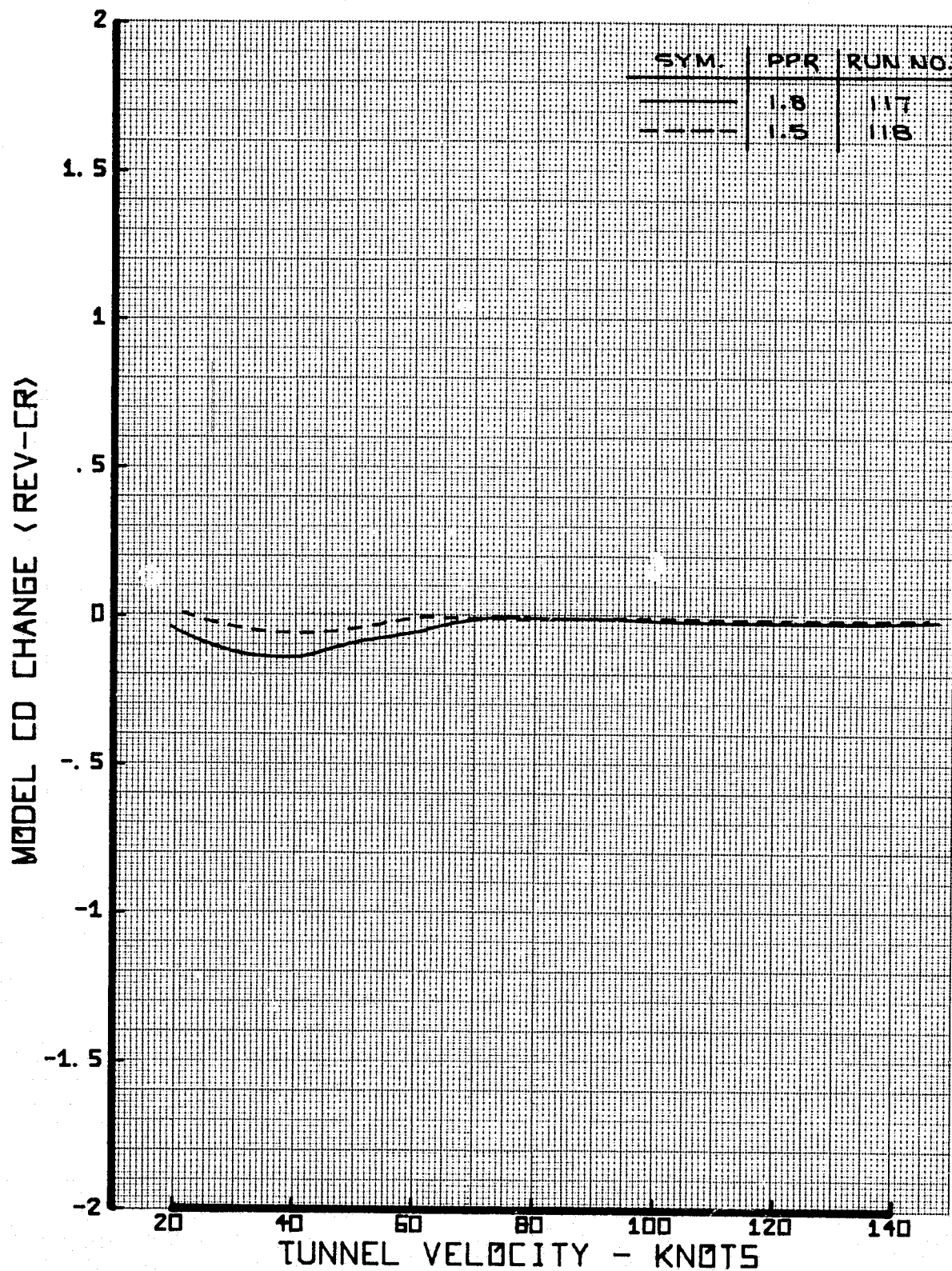
FIGURE 41 - MODEL C_D CHANGE, CONFIGURATION 12, 5° FLAPS, -20° ORIENTATION
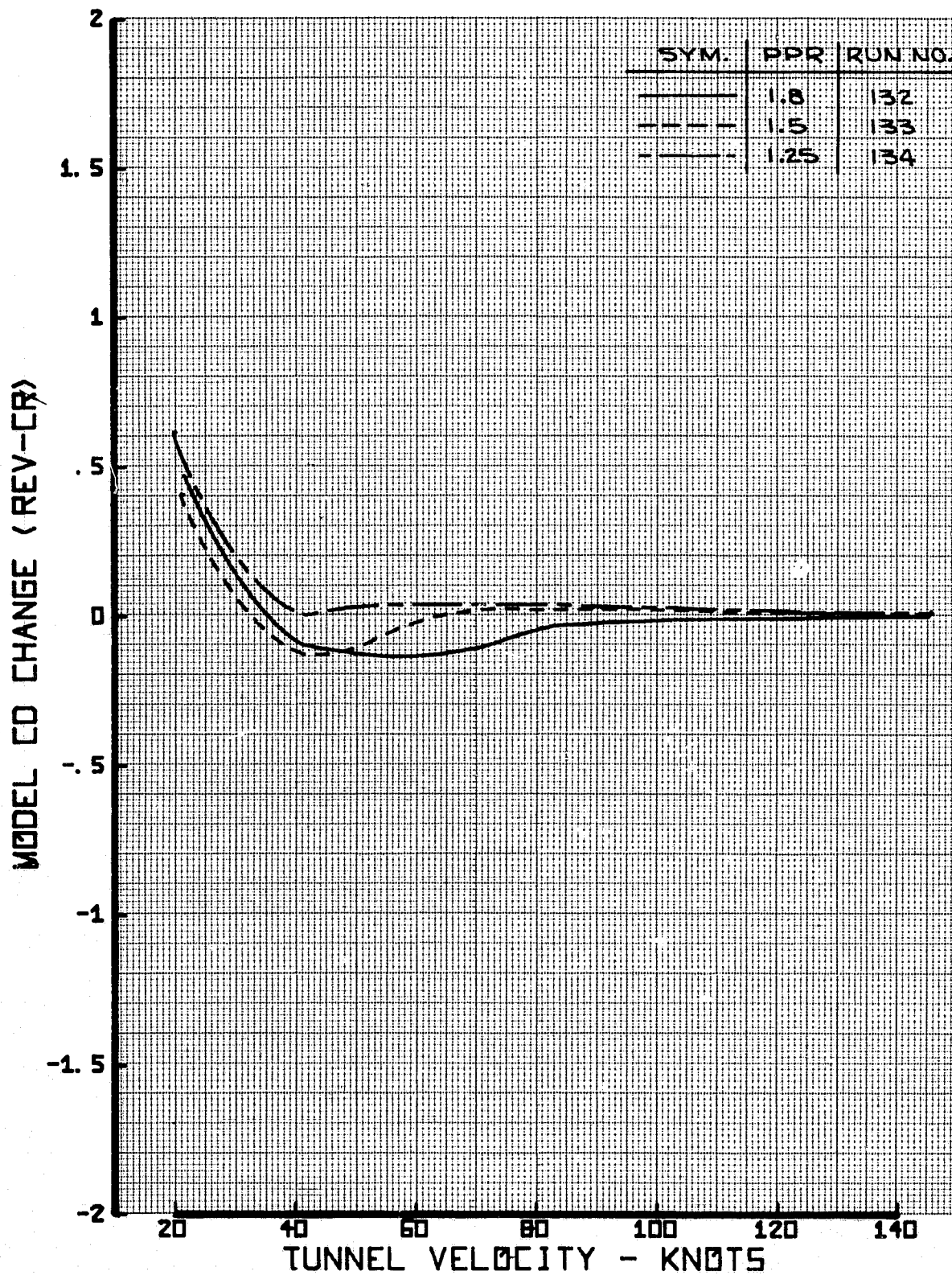
FIGURE 42 — MODEL C_D CHANGE, CONFIGURATION 7, 40° FLAPS, 0° ORIENTATION

The figure plots MODEL CD CHANGE (REV-CR) versus TUNNEL VELOCITY - KNOTS.

SYM.	PPR	RUN NO.
——	1.8	132
– – –	1.5	133
—·—	1.25	134

90

FIGURE 43 - MODEL C_D CHANGE, CONFIGURATION 7, 40° FLAPS, -10° ORIENTATION

SYM.	P.P.R.	RUN NO.
	1.8	146
	1.5	147
	1.25	148
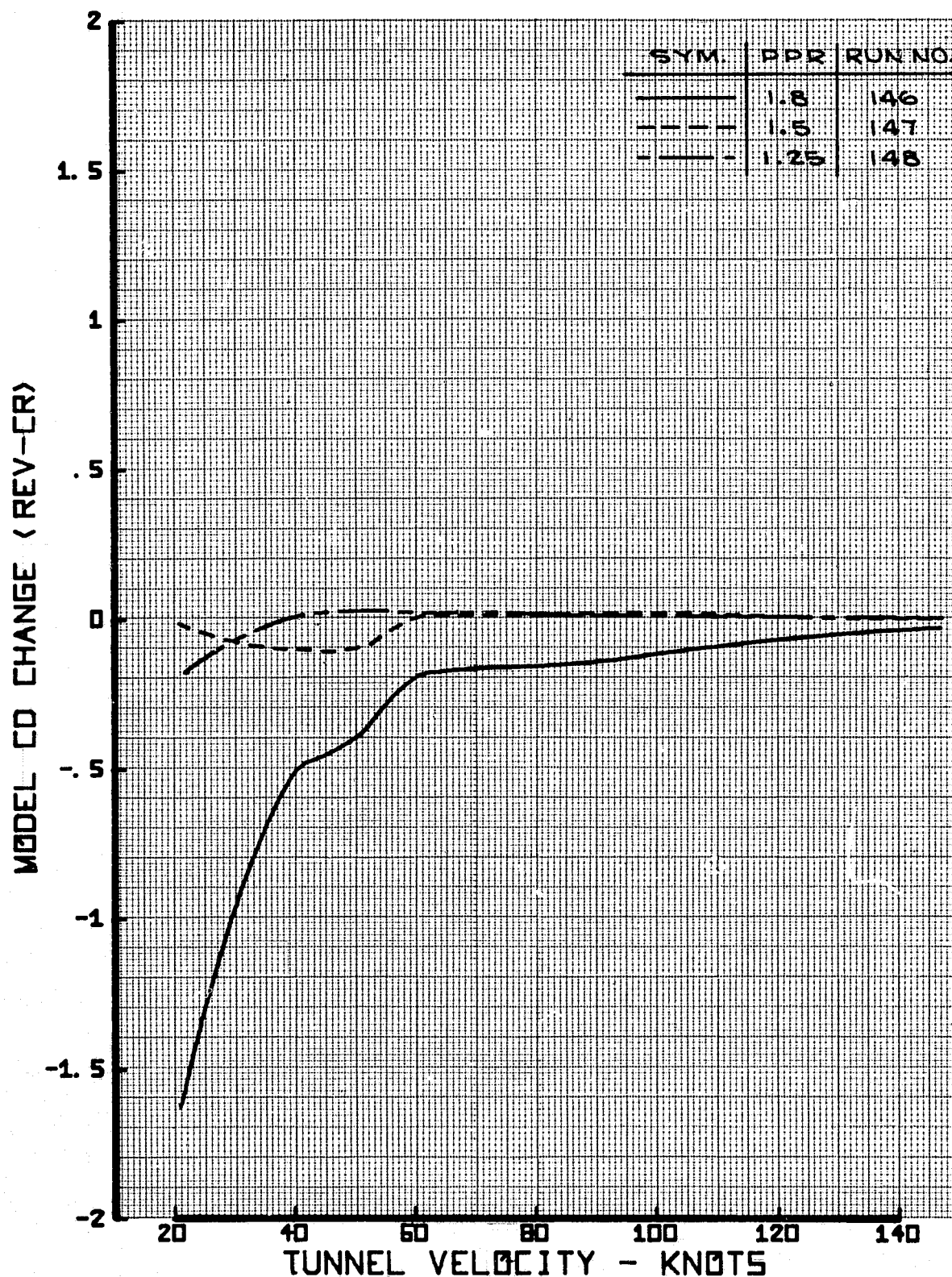
FIGURE 43 - MODEL C_D CHANGE, CONFIGURATION 7, 40° FLAPS, -10° ORIENTATION
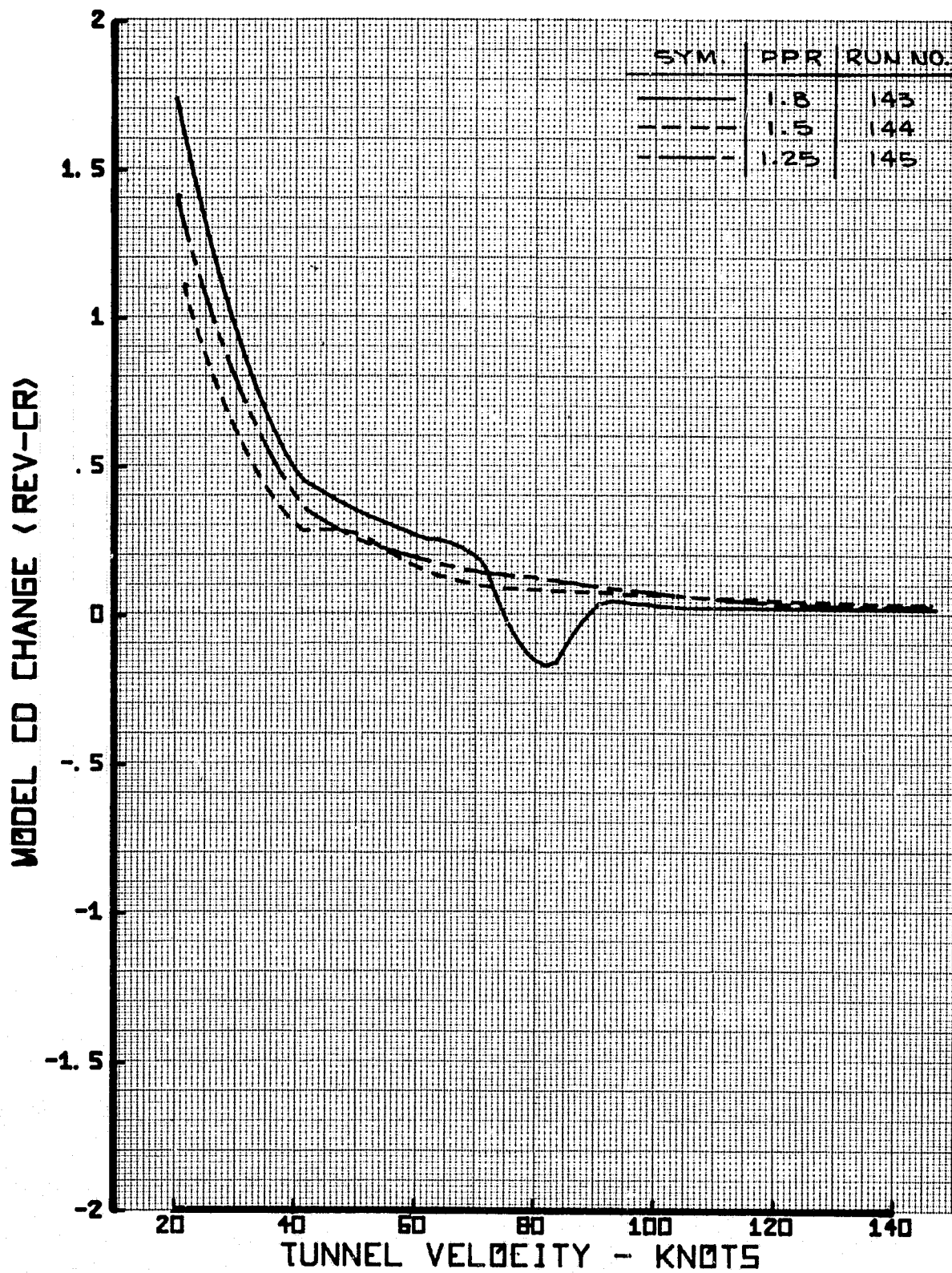
FIGURE **44** — MODEL C_D CHANGE, CONFIGURATION 7, 40° FLAPS, −20° ORIENTATION
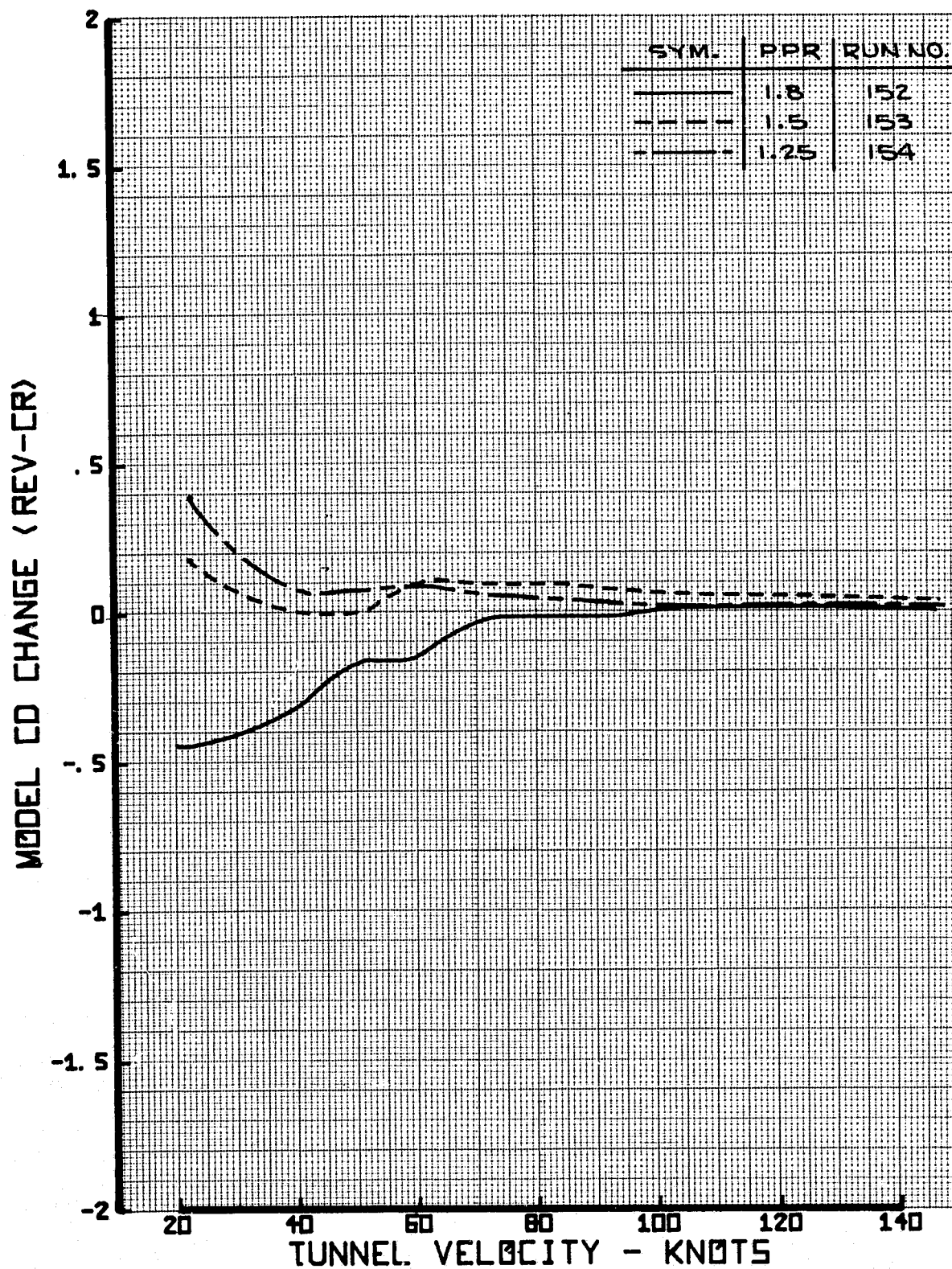
FIGURE 45 — MODEL C_D CHANGE, CONFIGURATION 7, 25° FLAPS, −10° ORIENTATION
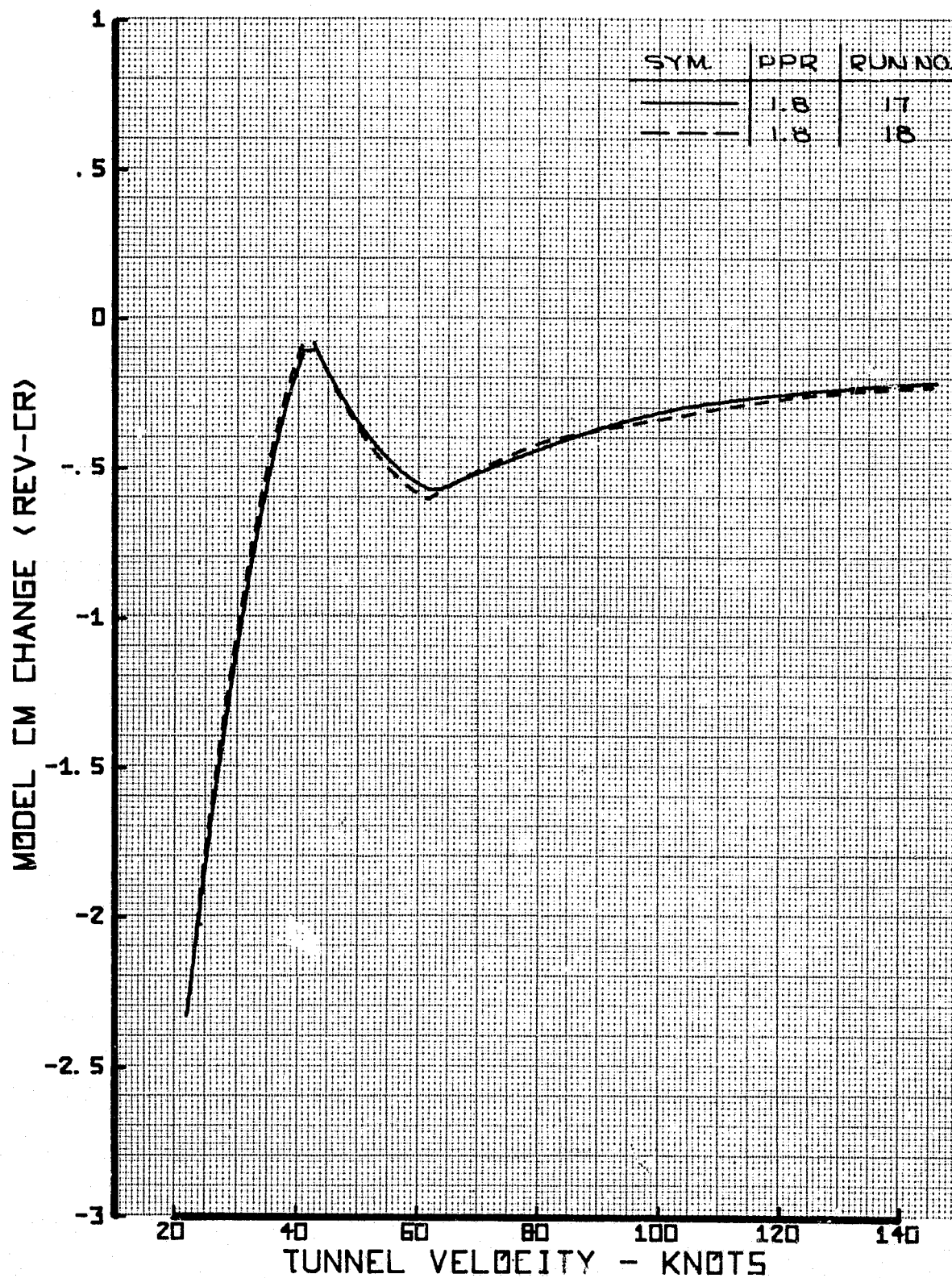
FIGURE 46 – MODEL C$_M$ CHANGE, CONFIGURATION 1, 40° FLAPS, 0° ORIENTATION, PPR = 1.8
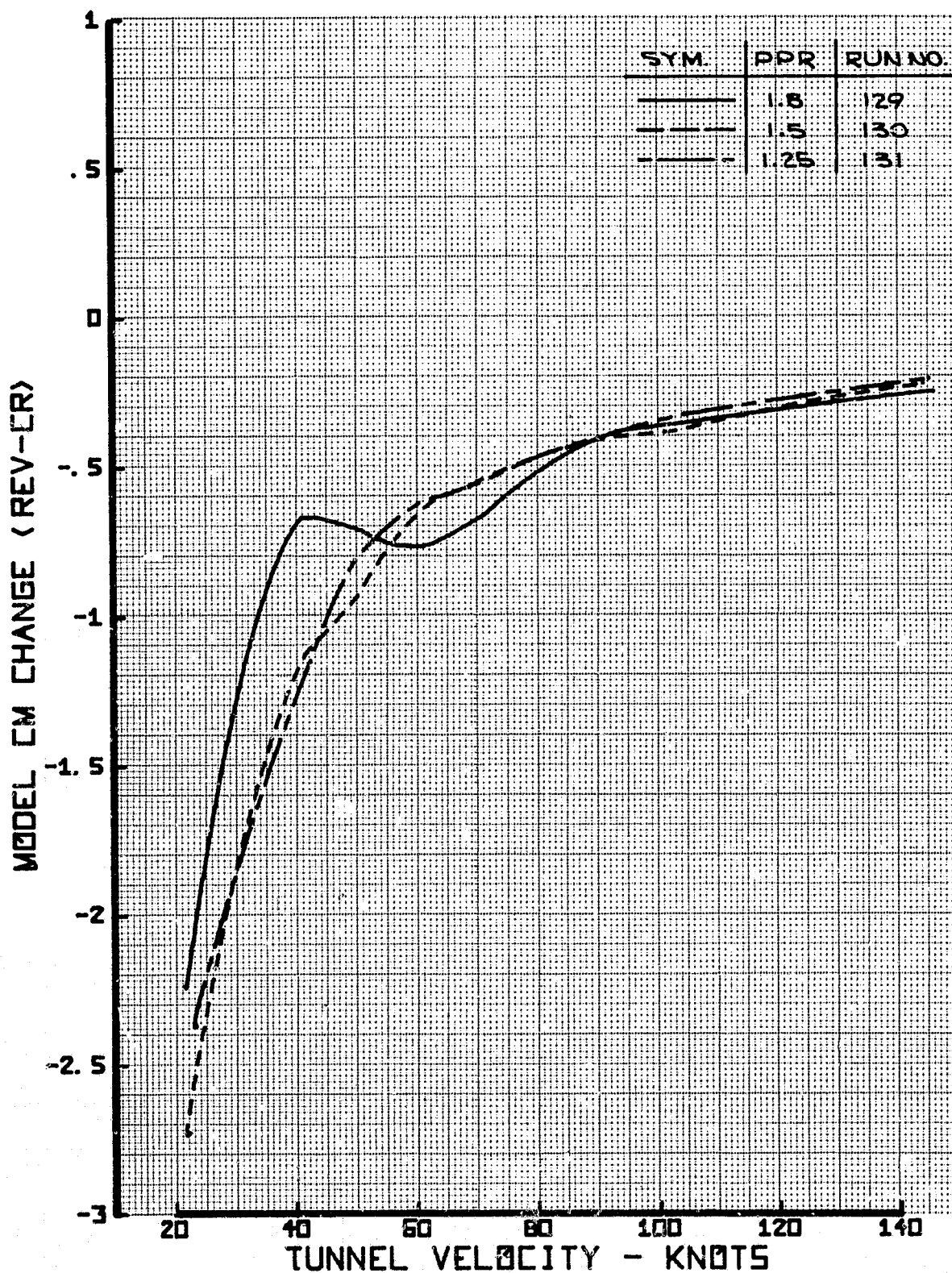
FIGURE 47 — MODEL C_M CHANGE, CONFIGURATION 12, 40° FLAPS, 0° ORIENTATION
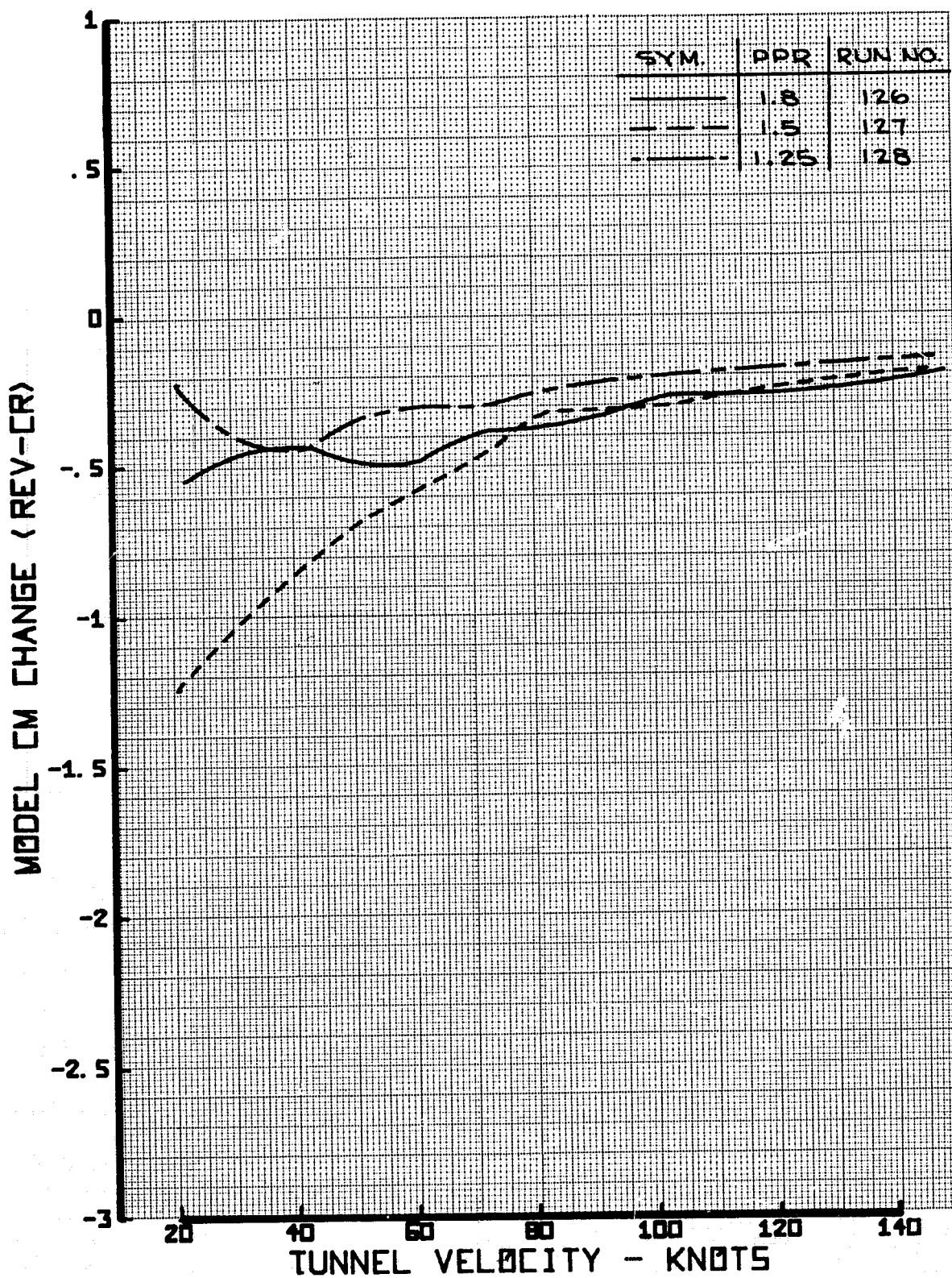
FIGURE 48 – MODEL Cm CHANGE, CONFIGURATION 12, 40° FLAPS, –10° ORIENTATION
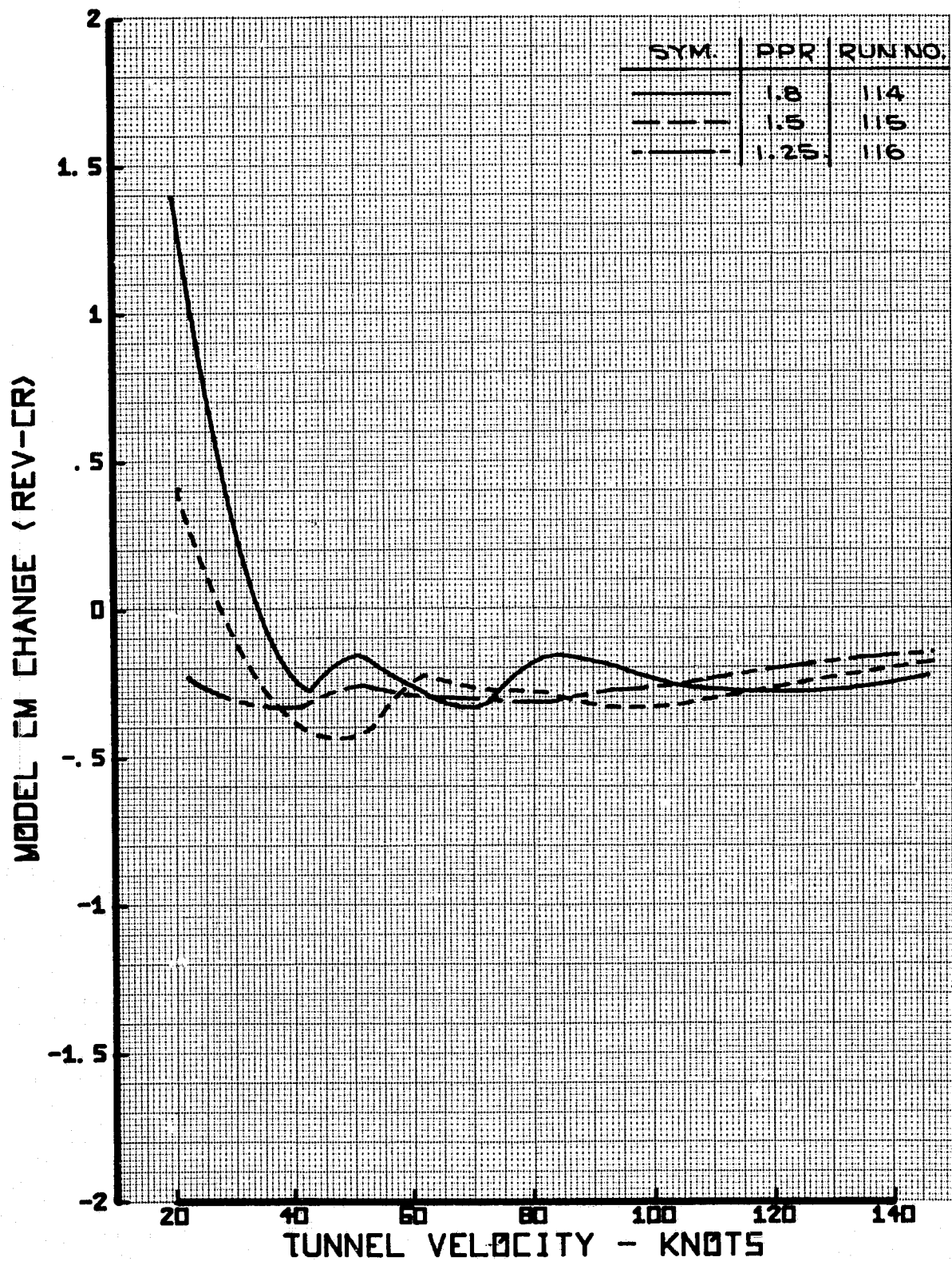
FIGURE 49 - MODEL CM CHANGE, CONFIGURATION 12,
40° FLAPS, -20° ORIENTATION
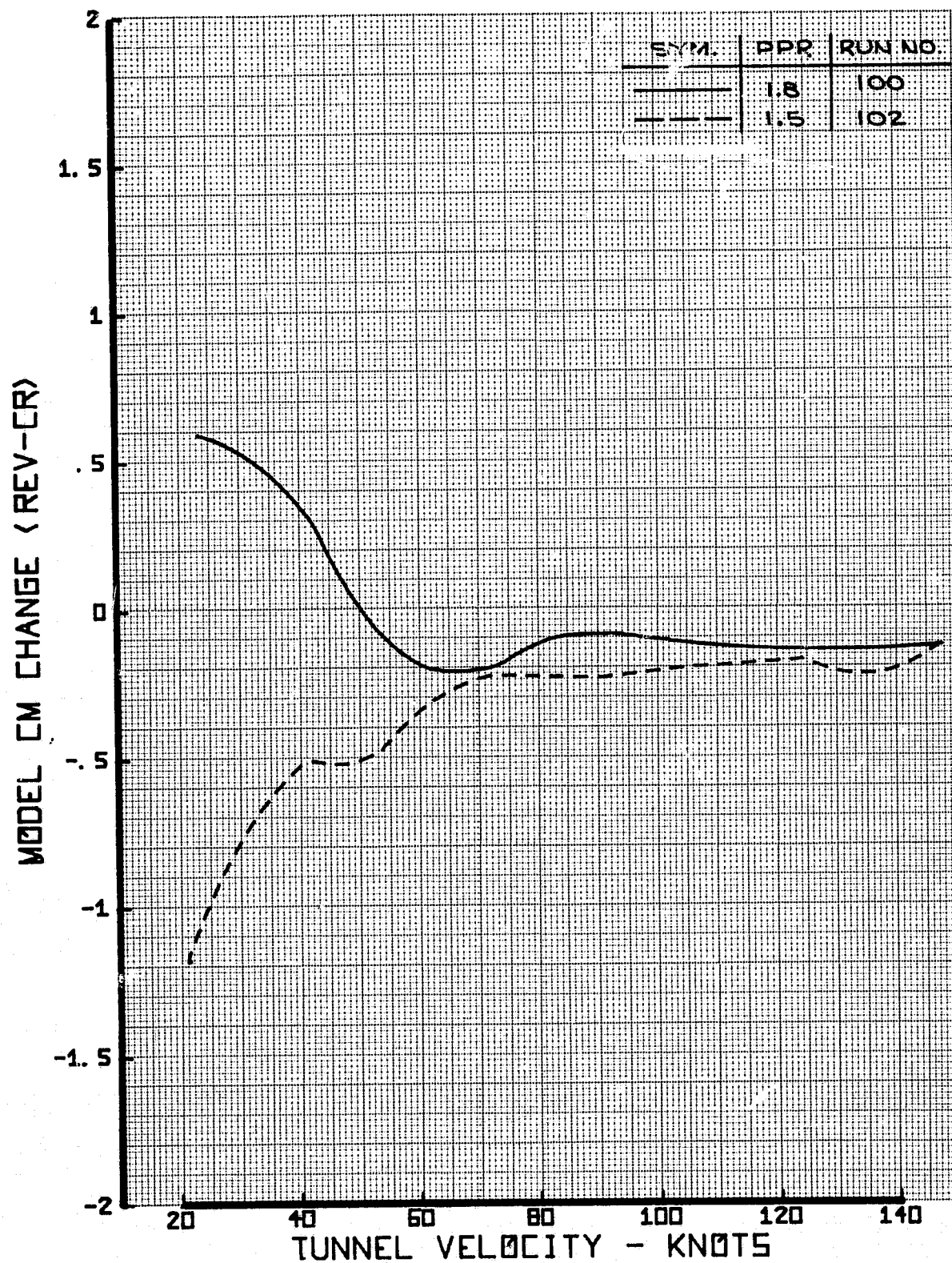
FIGURE 50 - MODEL CM CHANGE, CONFIGURATION 12, 25° FLAPS, 0° ORIENTATION

SYM	PPR	RUN NO.
——————	1.8	103
— — — —	1.5	104
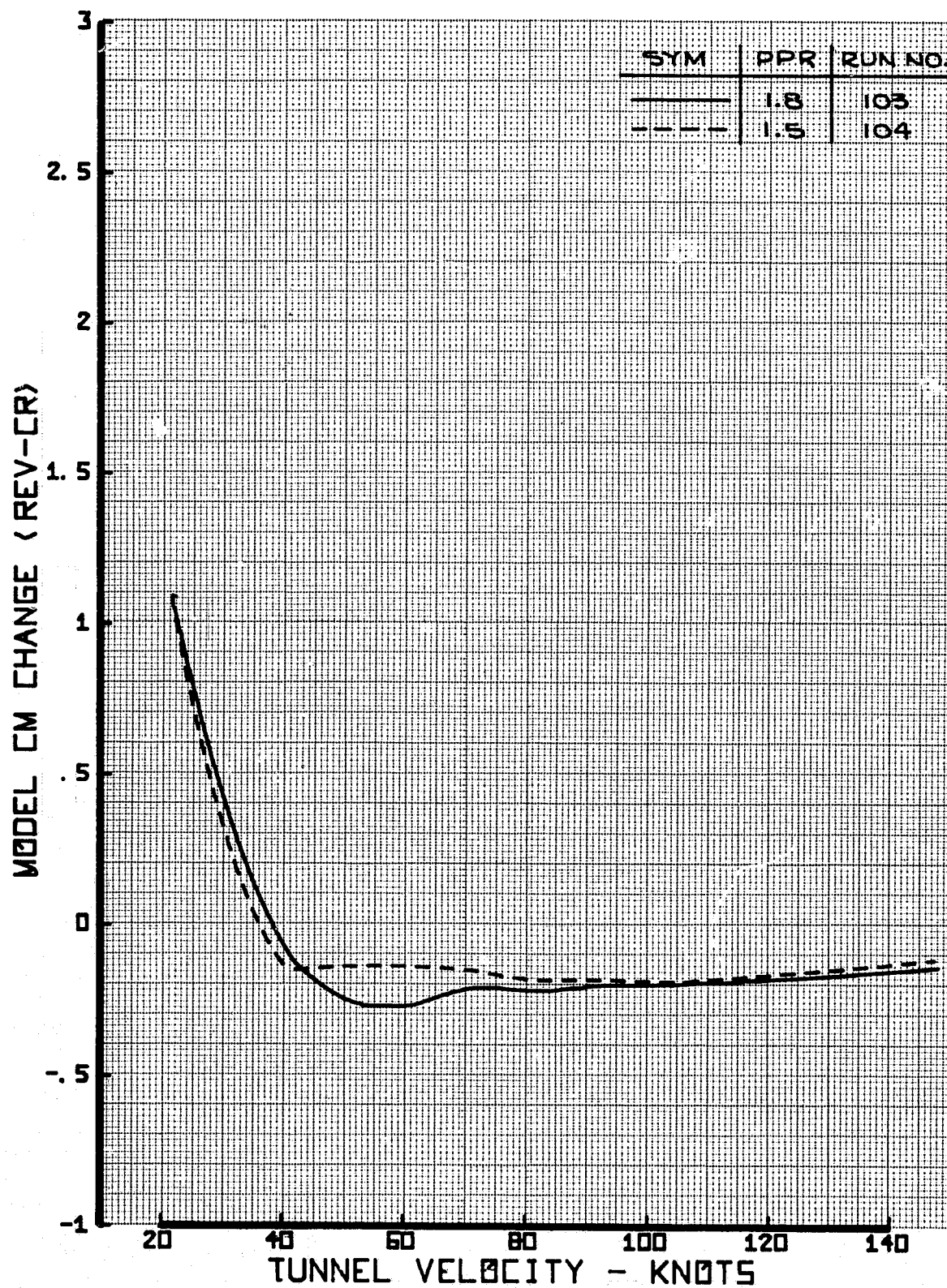
FIGURE 51 - MODEL C_M CHANGE, CONFIGURATION 12, 25° FLAPS, -10° ORIENTATION

SYM.	PPR	RUN NO.
————	1.8	111
– – – –	1.5	112
—–—–	1.25	113
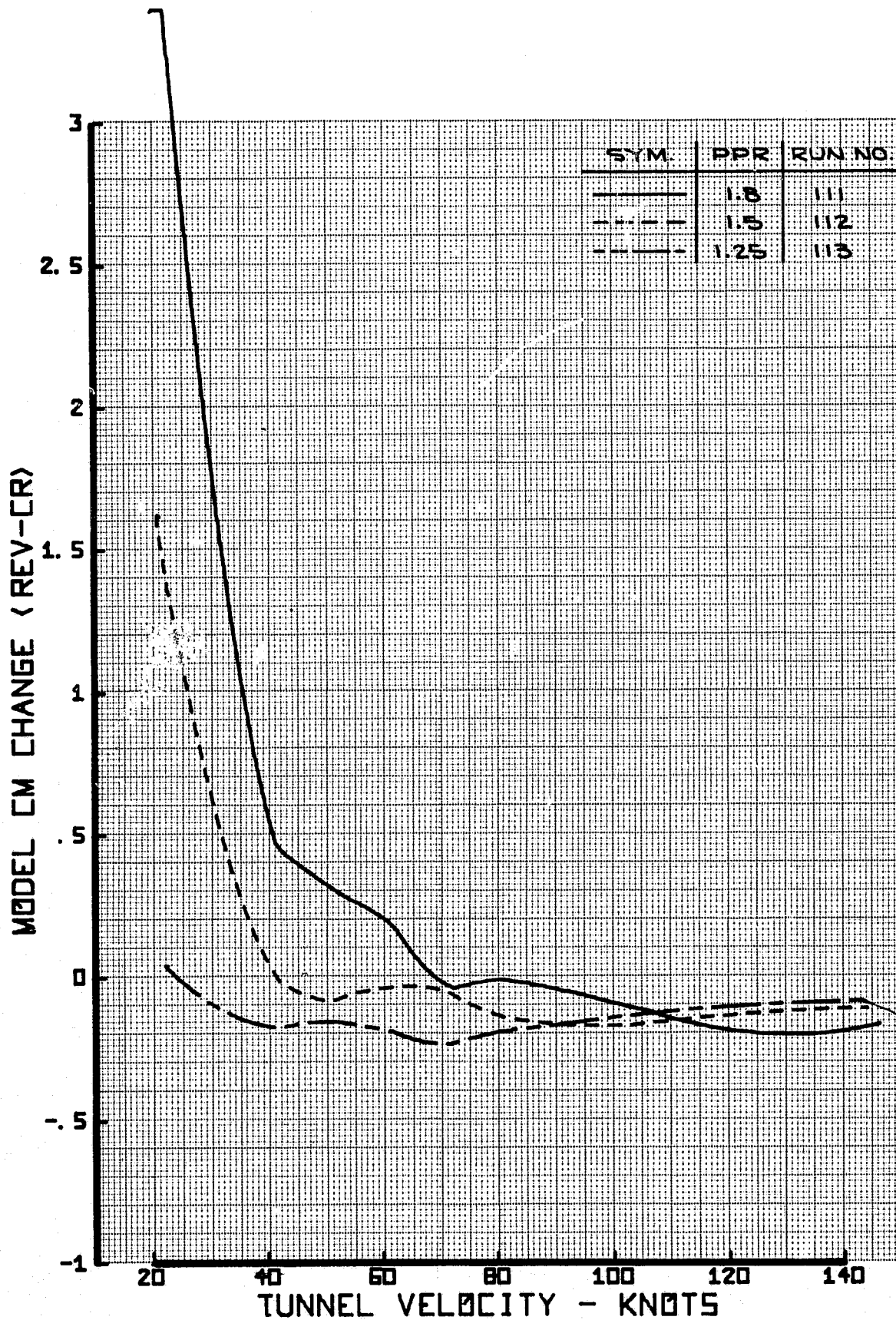
FIGURE 52 – MODEL C$_M$ CHANGE, CONFIGURATION 12, 25° FLAPS, -20° ORIENTATION
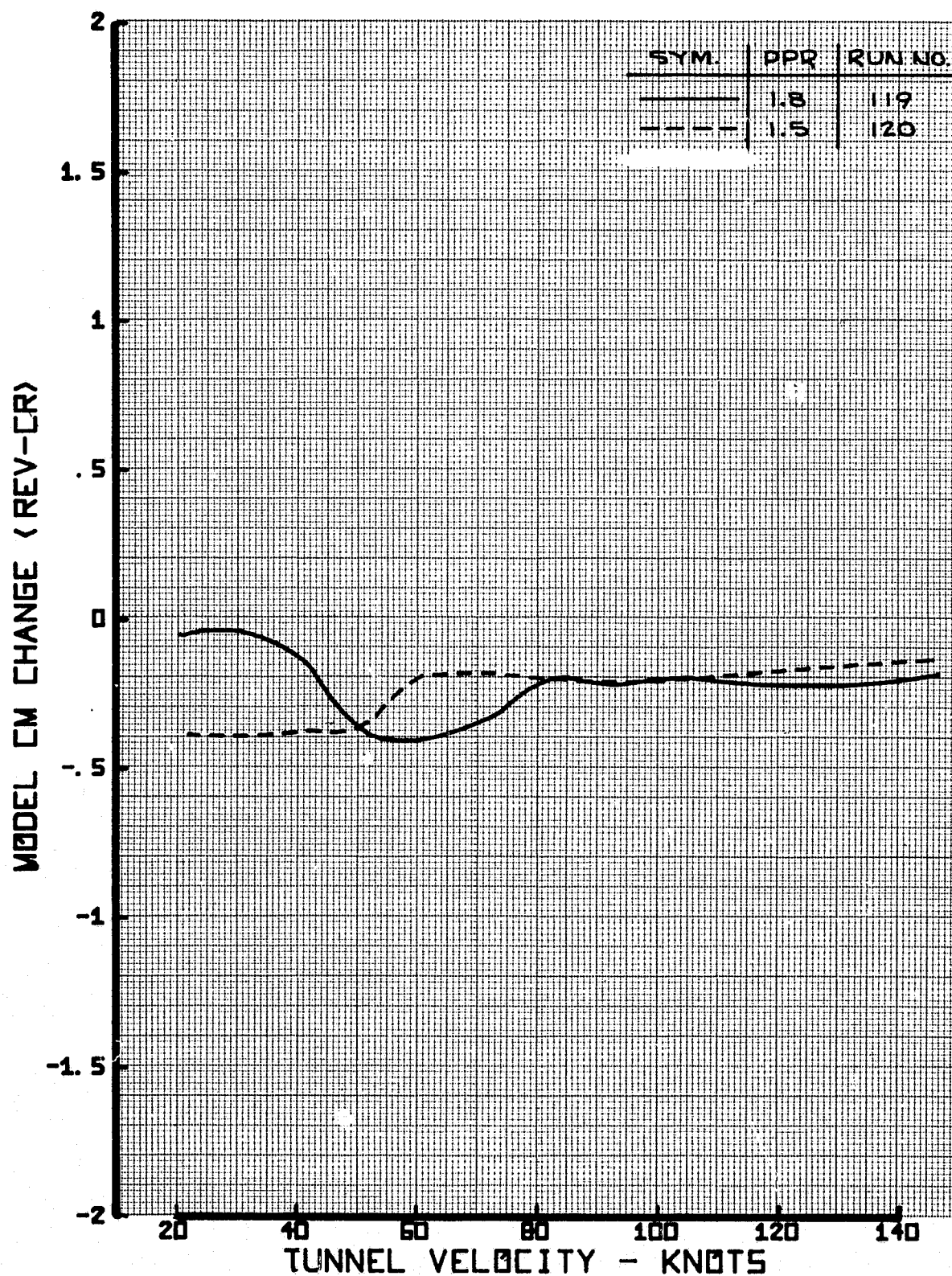
FIGURE 53 - MODEL C_M CHANGE, CONFIGURATION 12, 5° FLAPS, 0° ORIENTATION
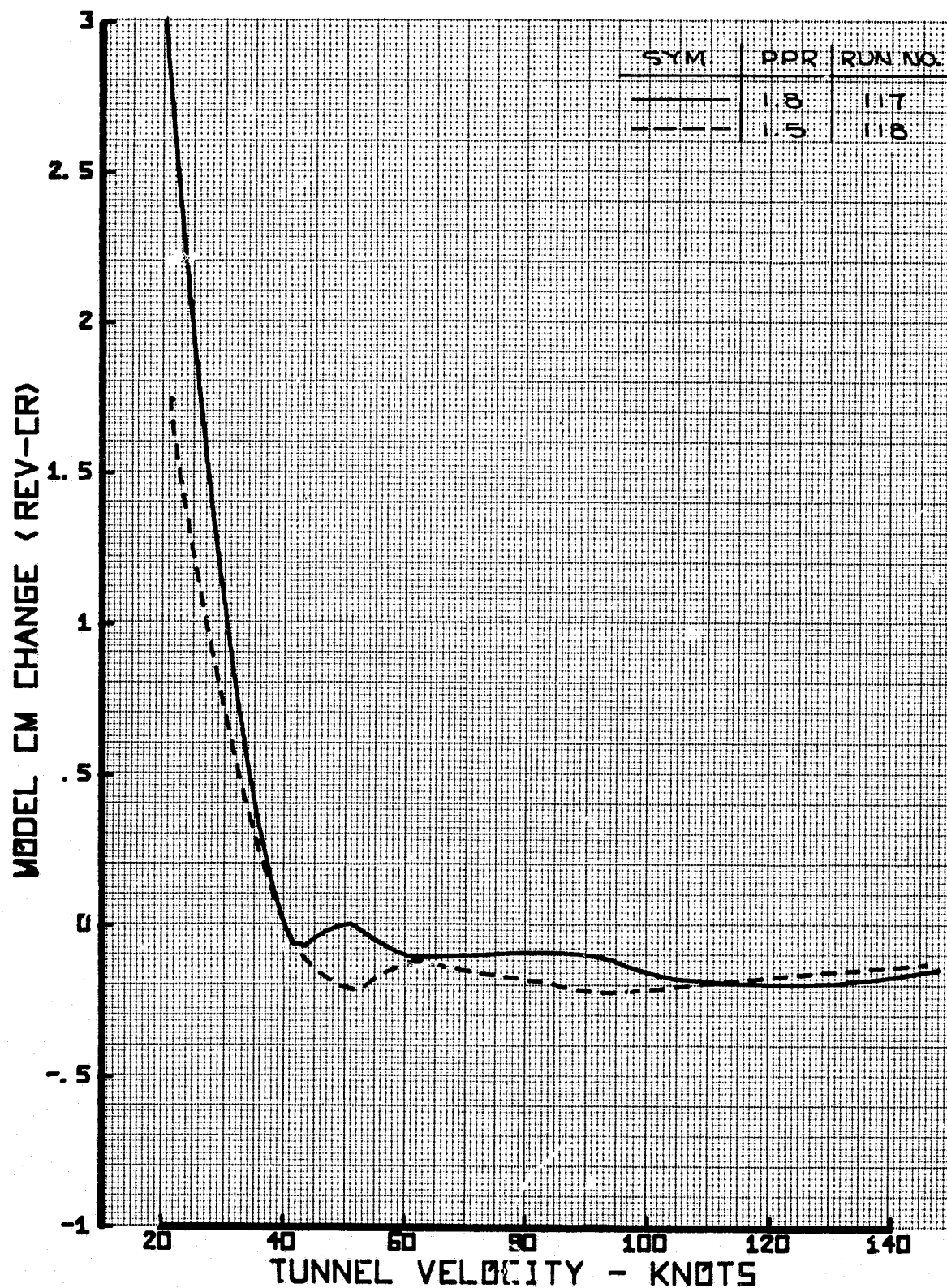
FIGURE 54 — MODEL C$_M$ CHANGE, CONFIGURATION 12, 5° FLAPS, -20° ORIENTATION
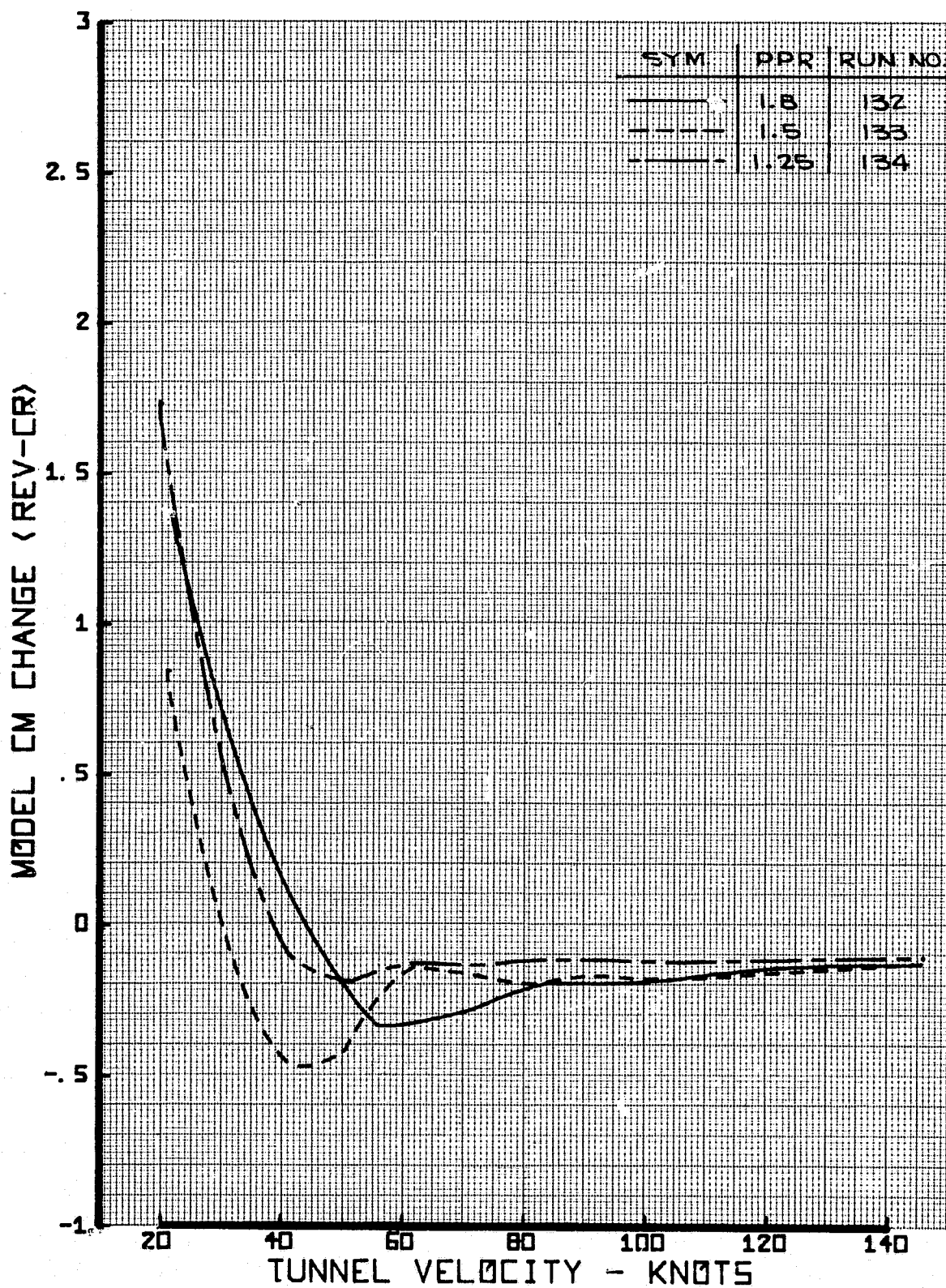
FIGURE **55** — MODEL C$_M$ CHANGE, CONFIGURATION 7, 40° FLAPS, 0° ORIENTATION
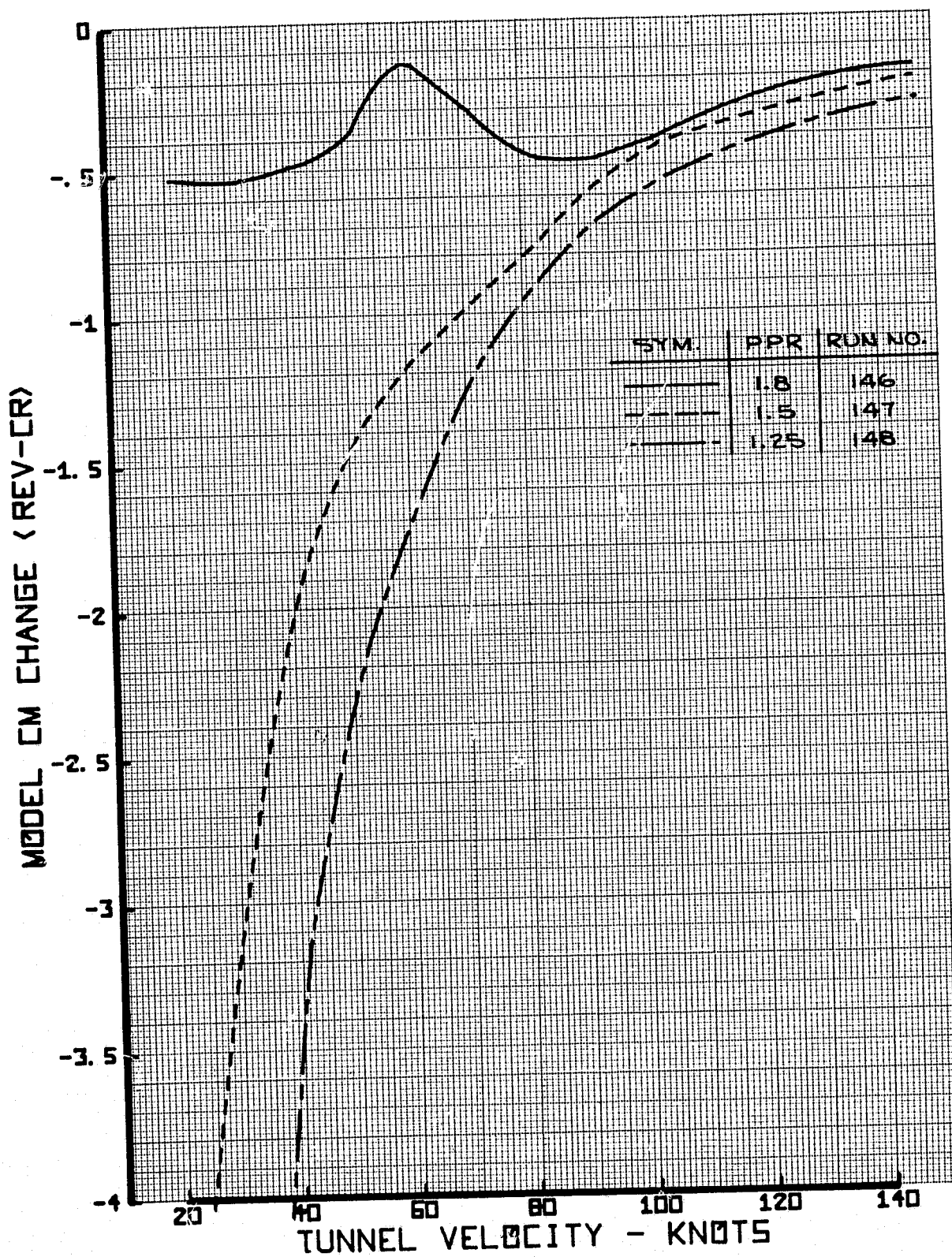
FIGURE 56 — MODEL Cₘ CHANGE, CONFIGURATION 7, 40° FLAPS, -10° ORIENTATION
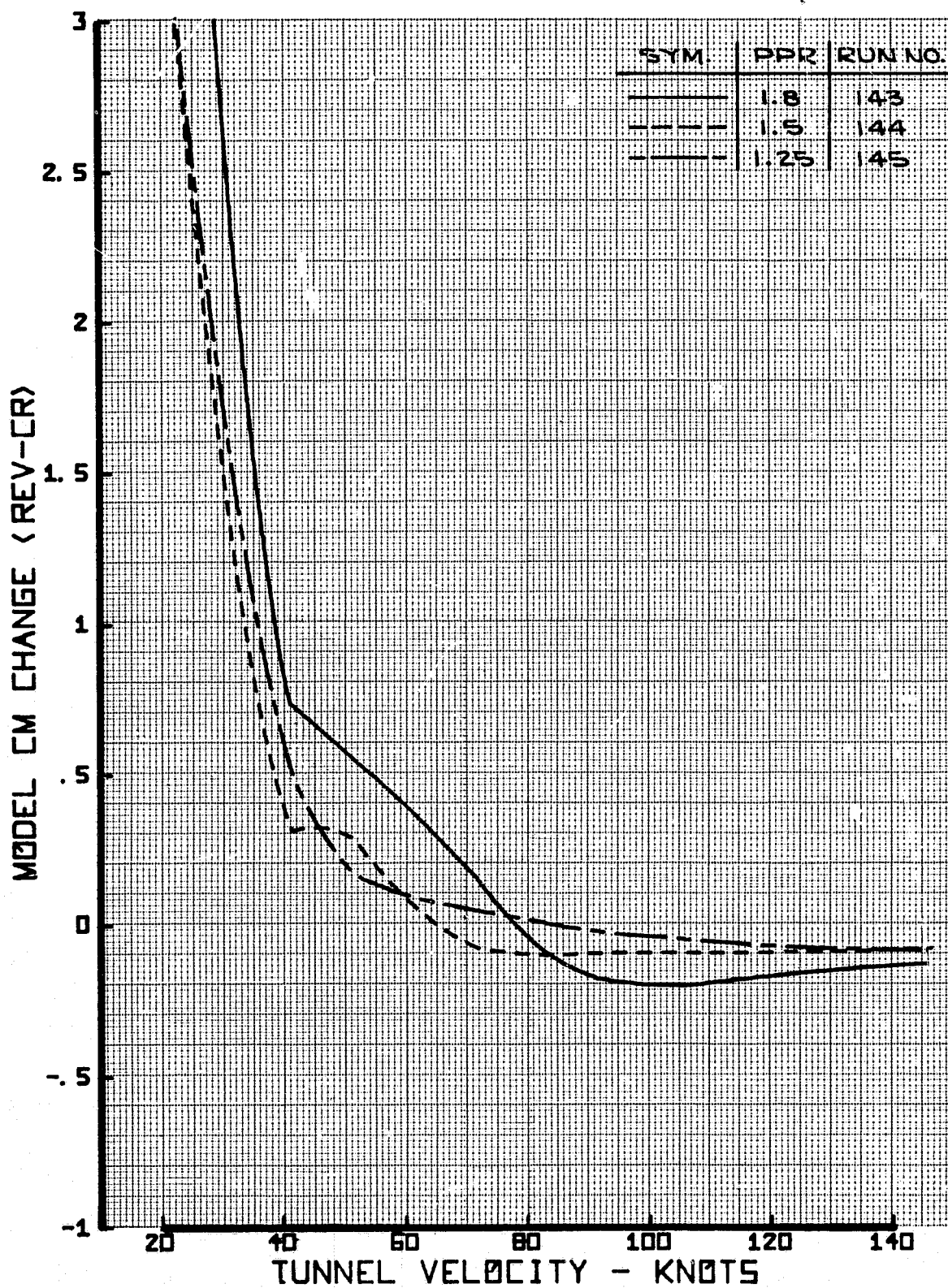
FIGURE 57 — MODEL C_M CHANGE, CONFIGURATION 7, 40° FLAPS, −20° ORIENTATION
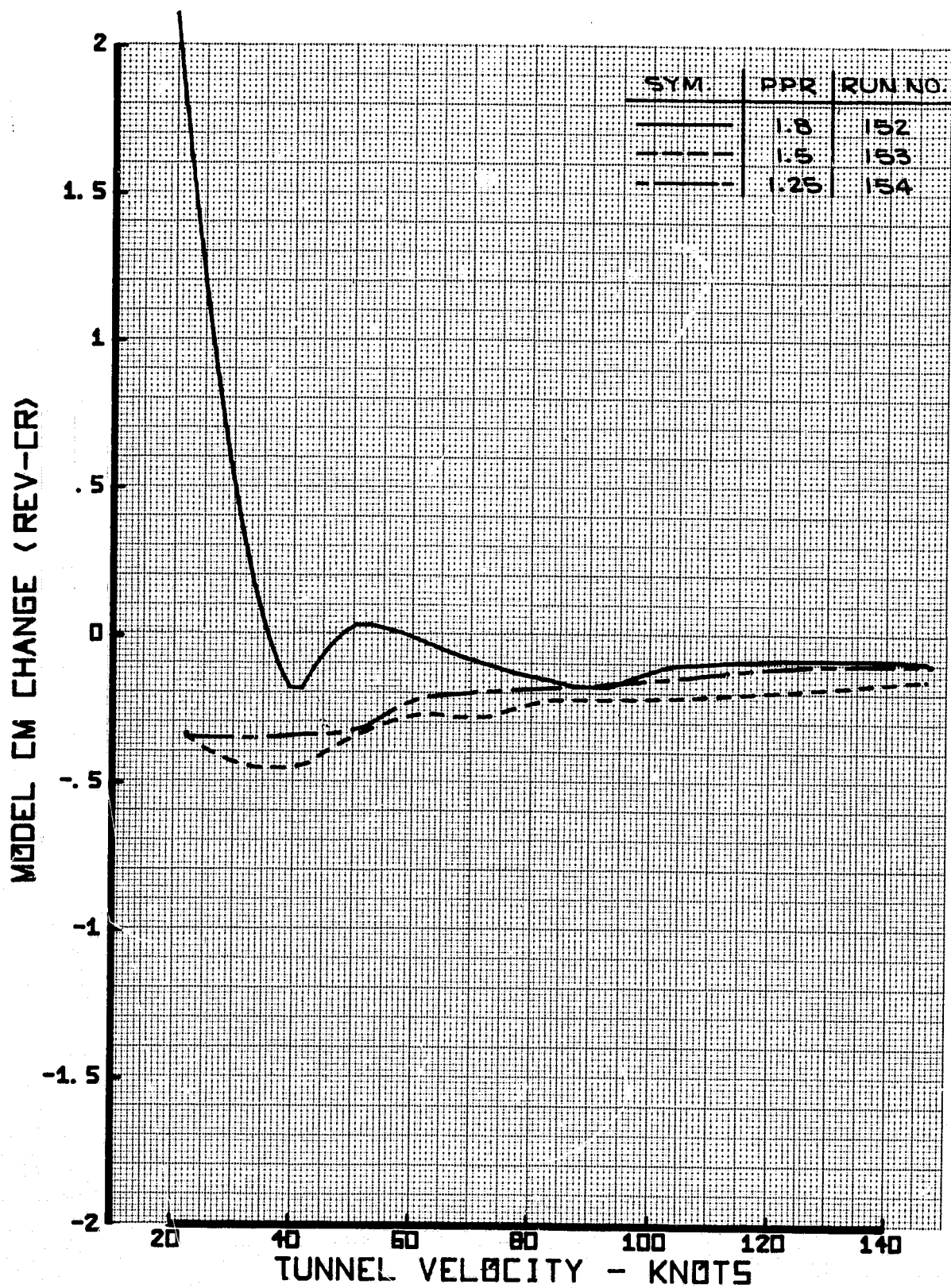
FIGURE 58 — MODEL C$_M$ CHANGE, CONFIGURATION 7, 25° FLAPS, -10° ORIENTATION
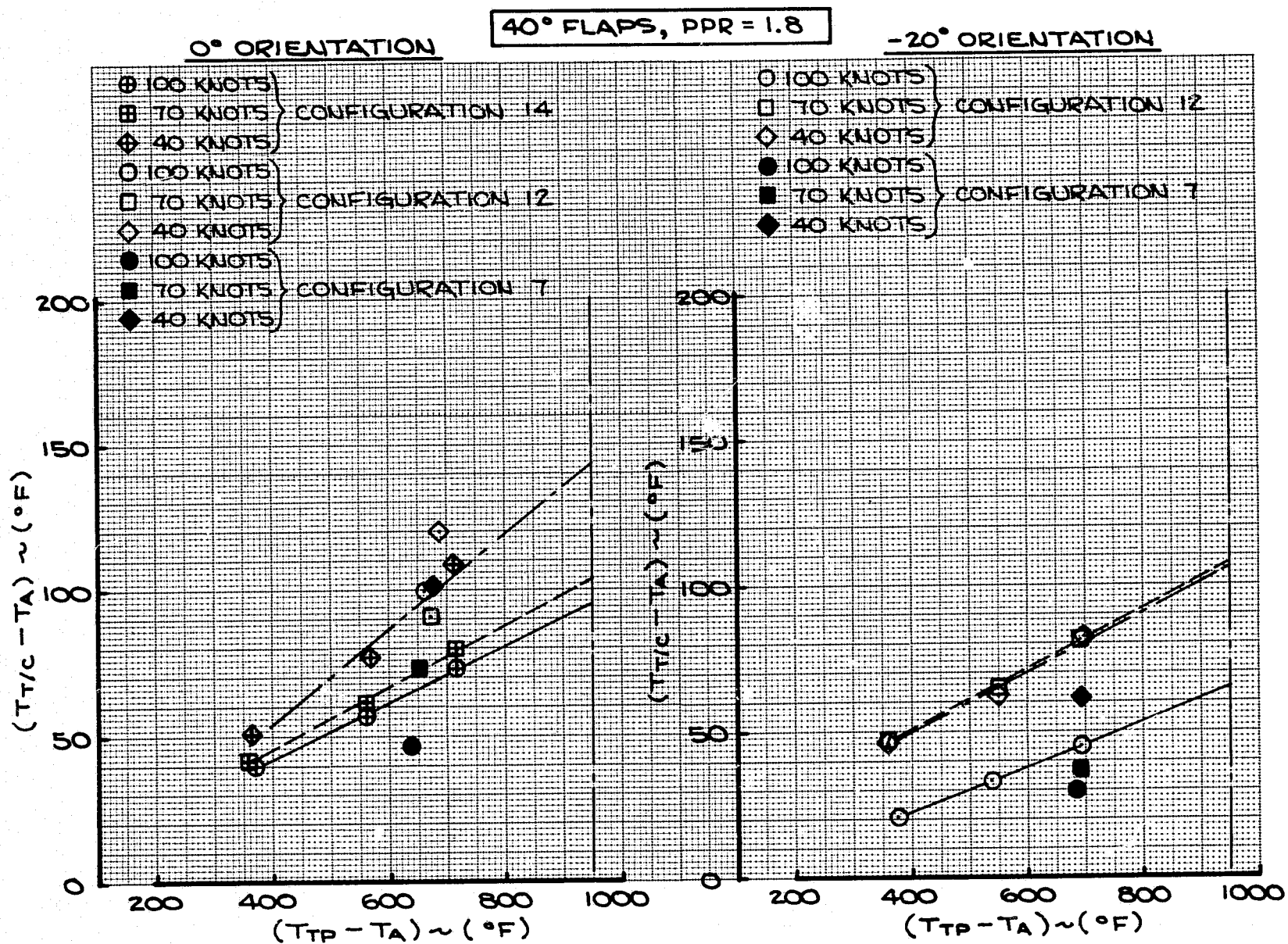
FIGURE 59 — IMPINGEMENT DATA FOR THERMOCOUPLE AT LOCATION 1
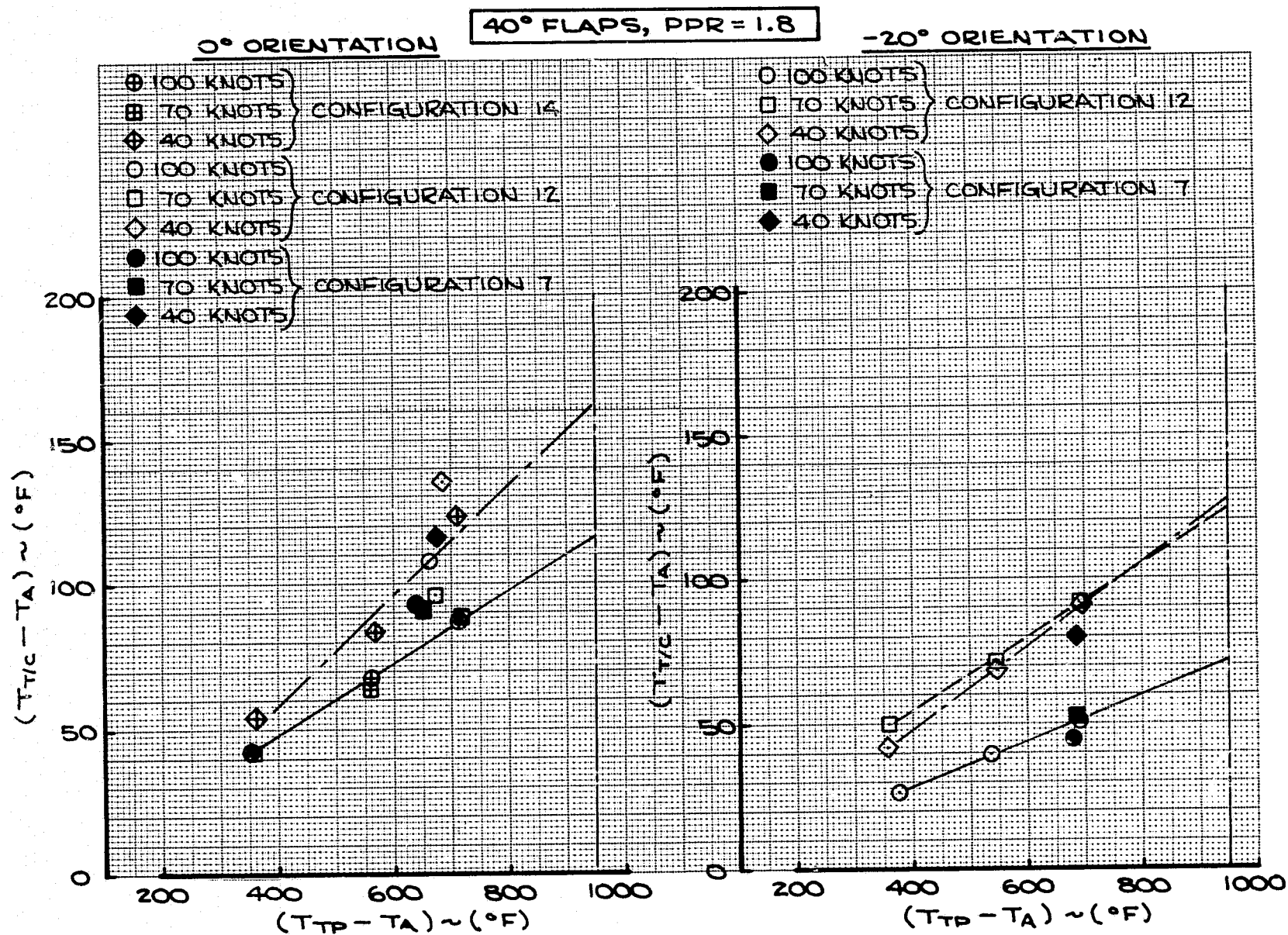
FIGURE 60 — IMPINGEMENT DATA FOR THERMOCOUPLE AT LOCATION 2
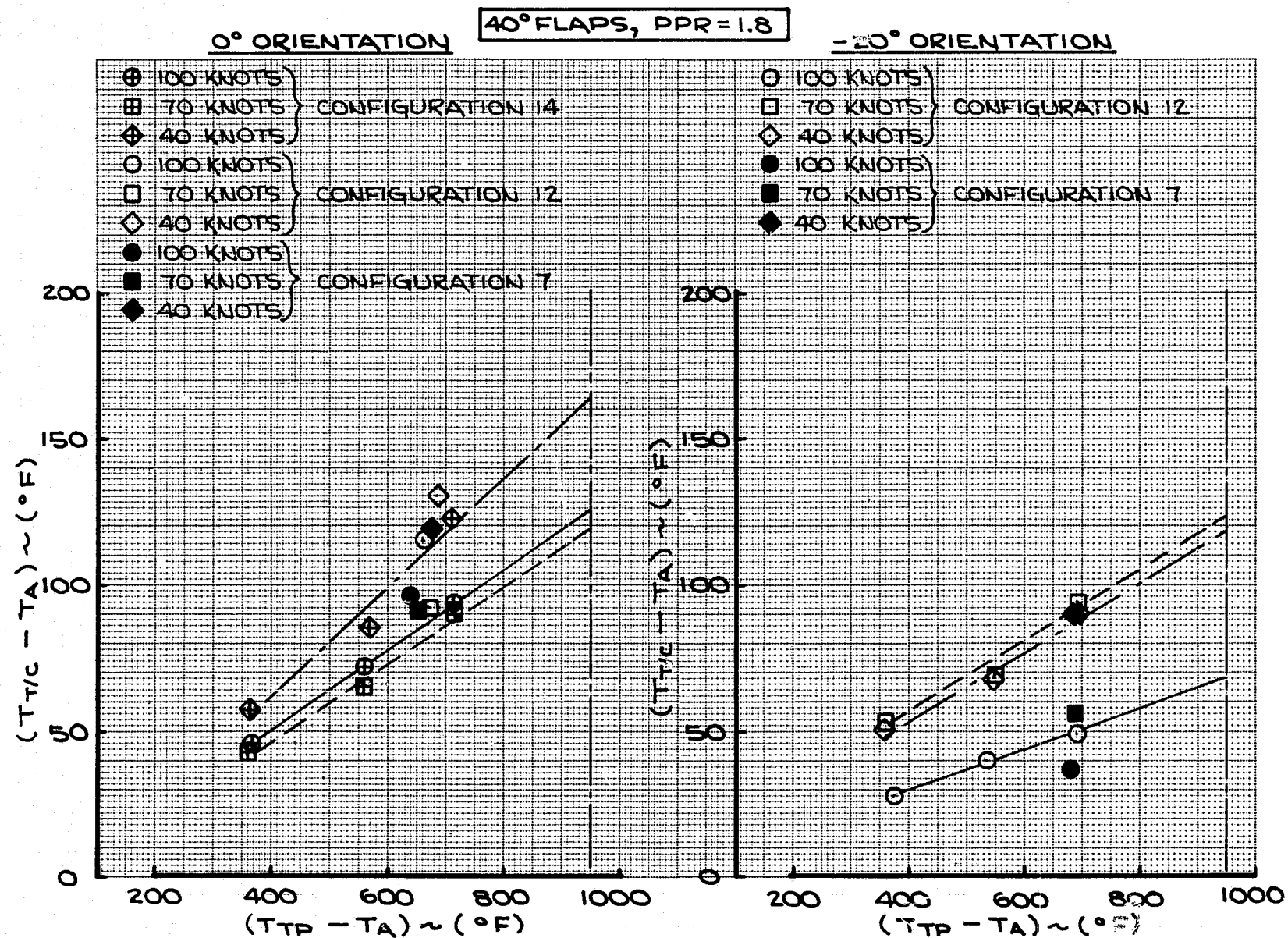
FIGURE 61 - IMPINGEMENT DATA FOR THERMOCOUPLE AT LOCATION 3
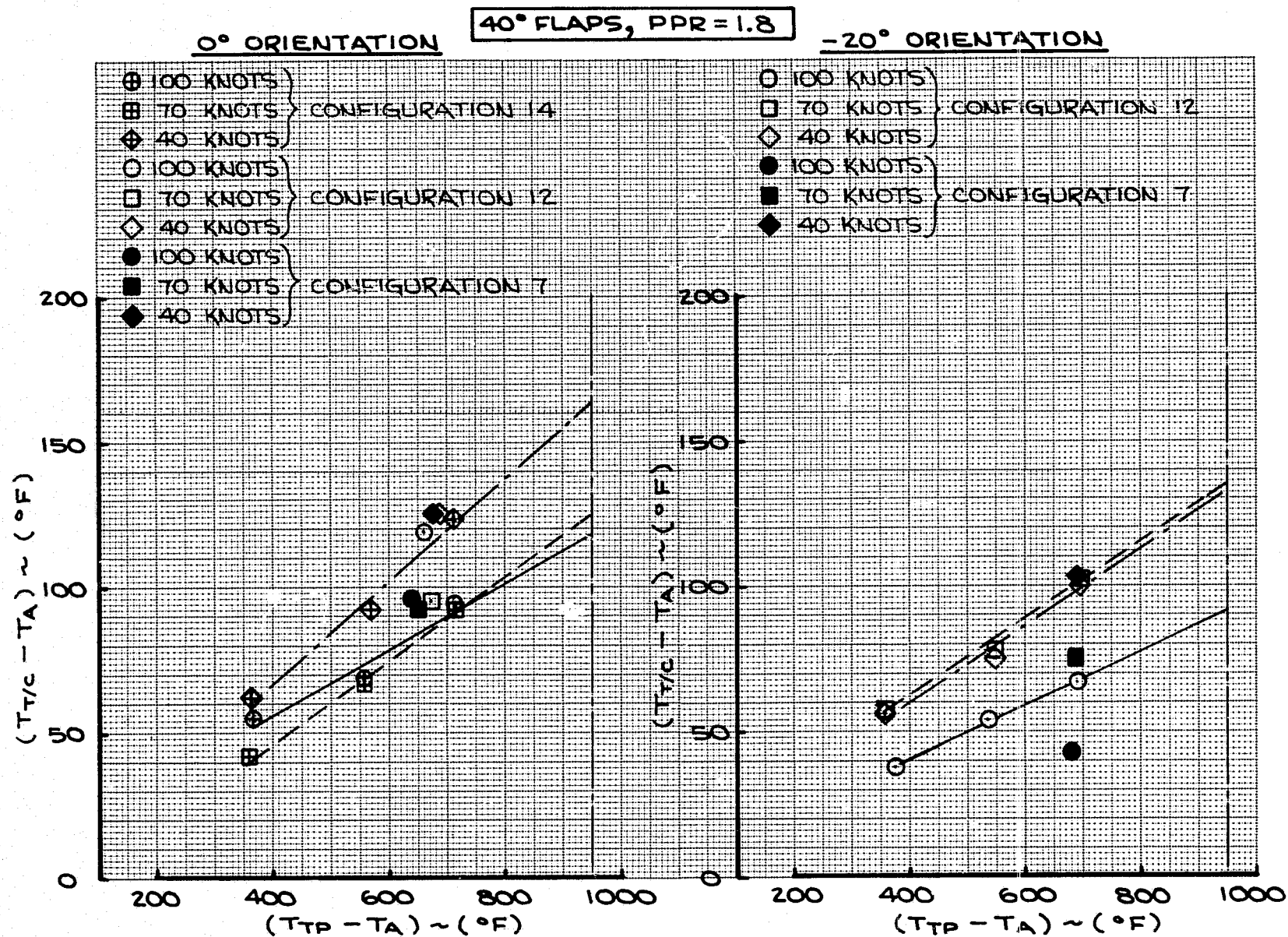
FIGURE 62 - IMPINGEMENT DATA FOR THERMOCOUPLE AT LOCATION 4
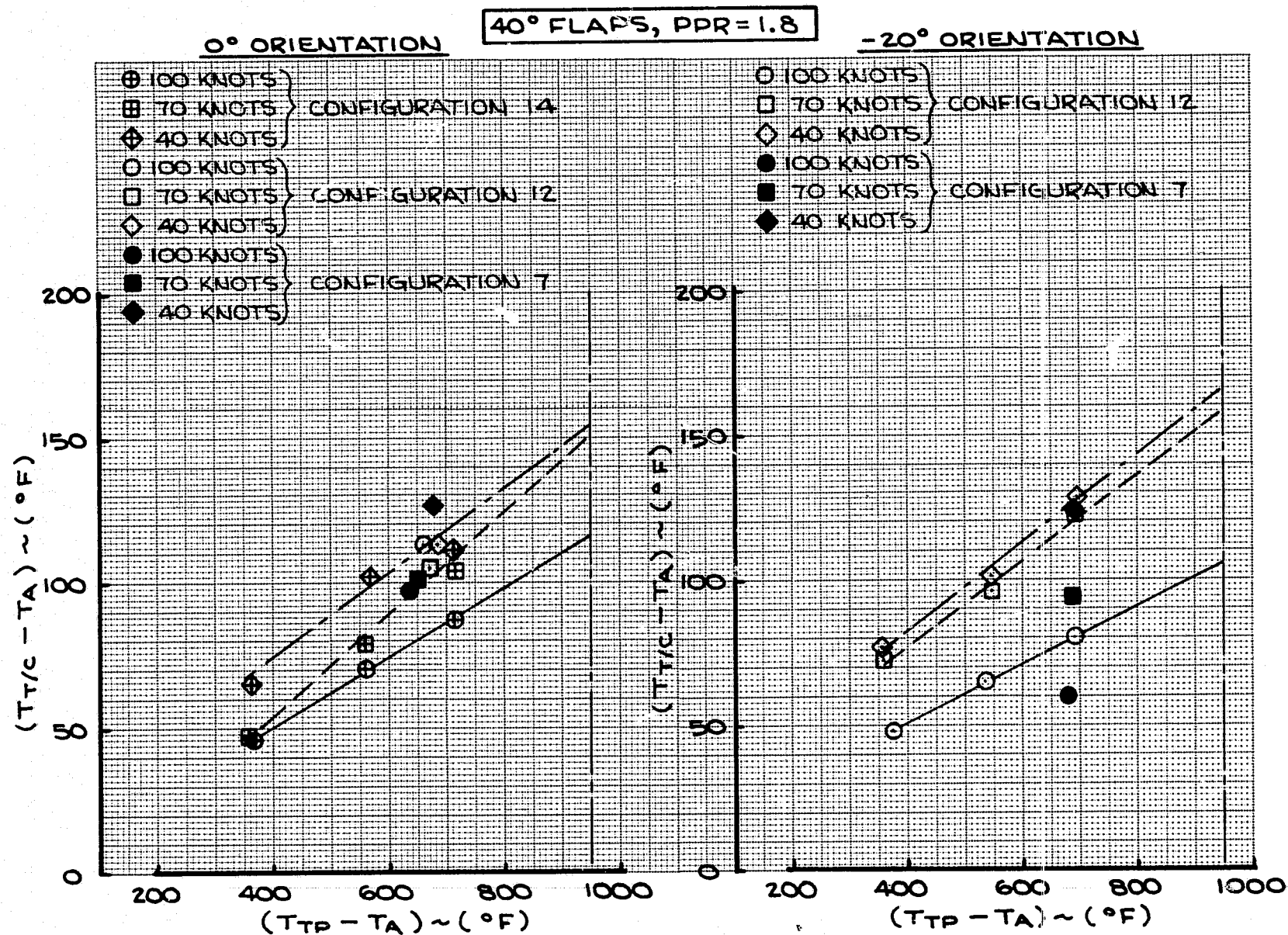
FIGURE 63 - IMPINGEMENT DATA FOR THERMOCOUPLE AT LOCATION 5
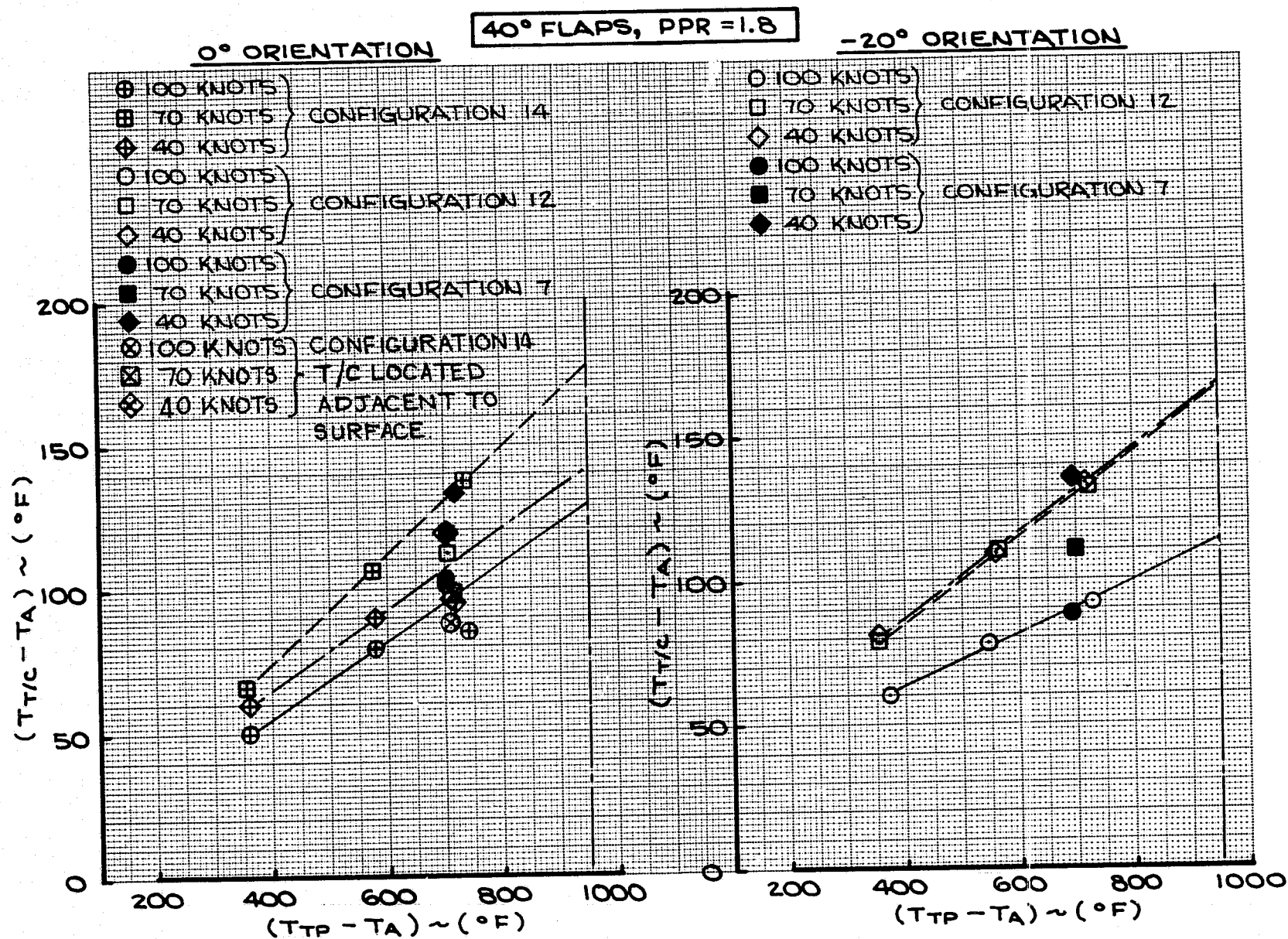
FIGURE 64 - IMPINGEMENT DATA FOR THERMOCOUPLE AT LOCATION 6
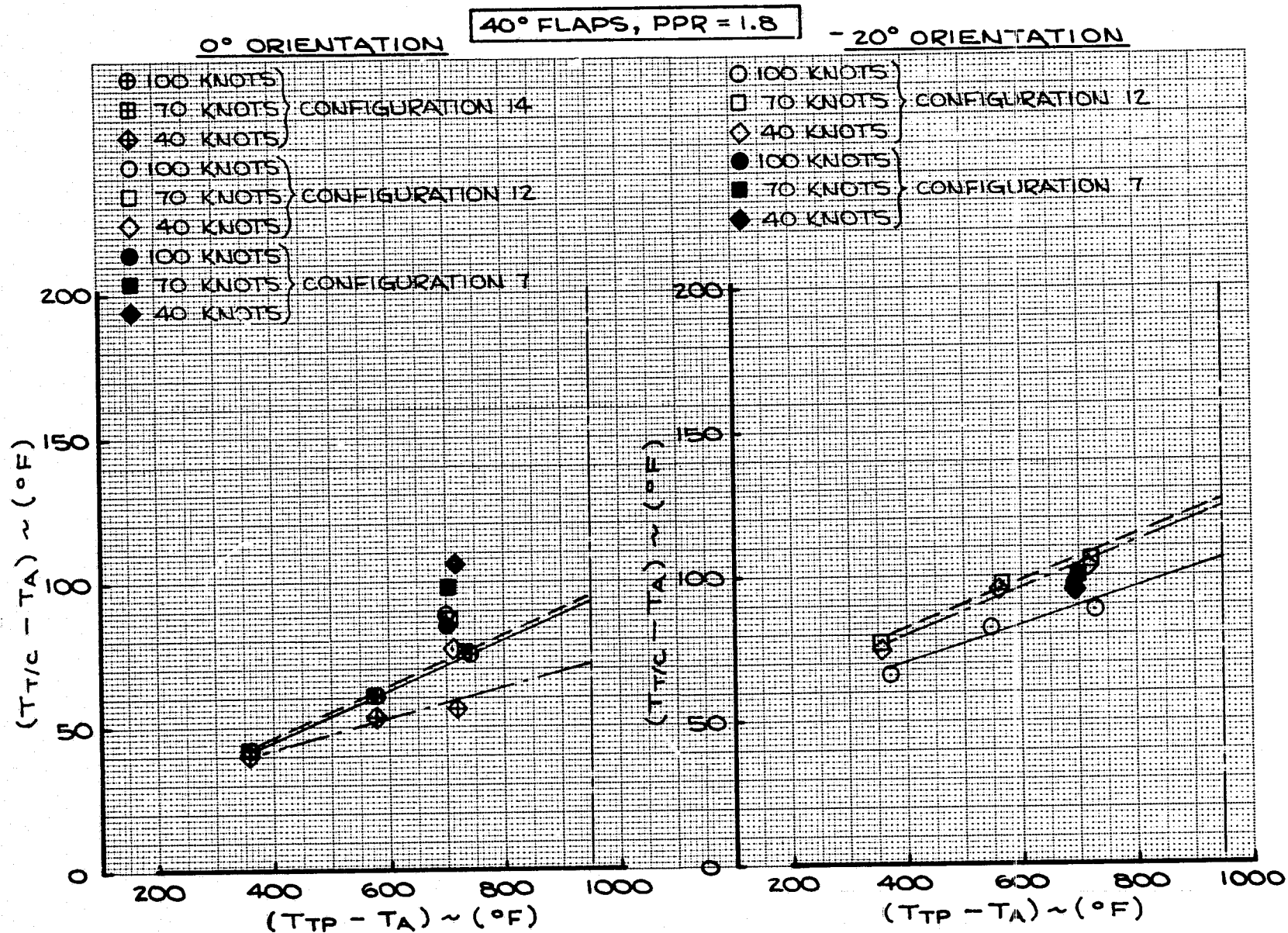
FIGURE 65 – IMPINGEMENT DATA FOR THERMOCOUPLE AT LOCATION 7
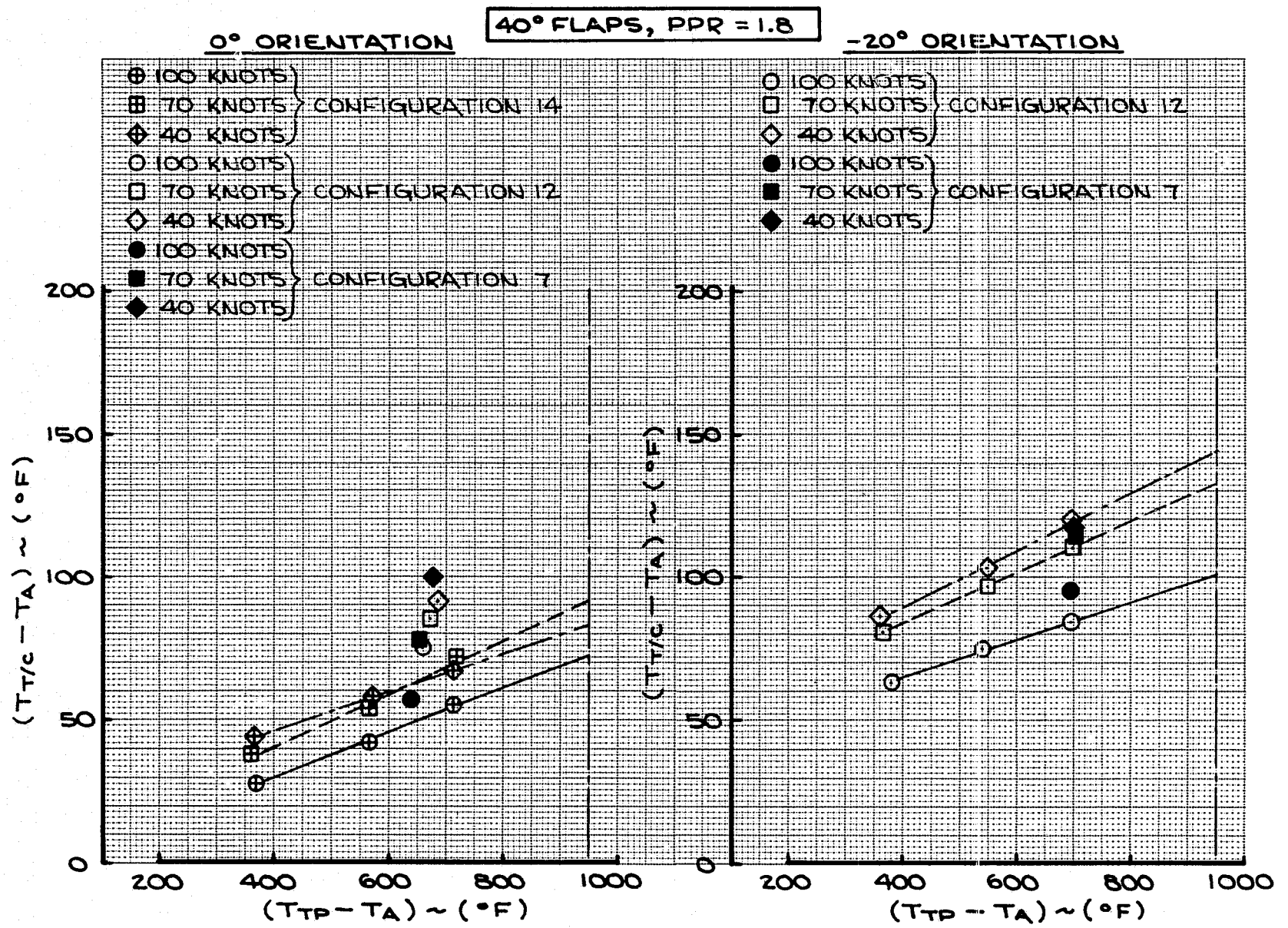
FIGURE 66 - IMPINGEMENT DATA FOR THERMOCOUPLE AT LOCATION 8
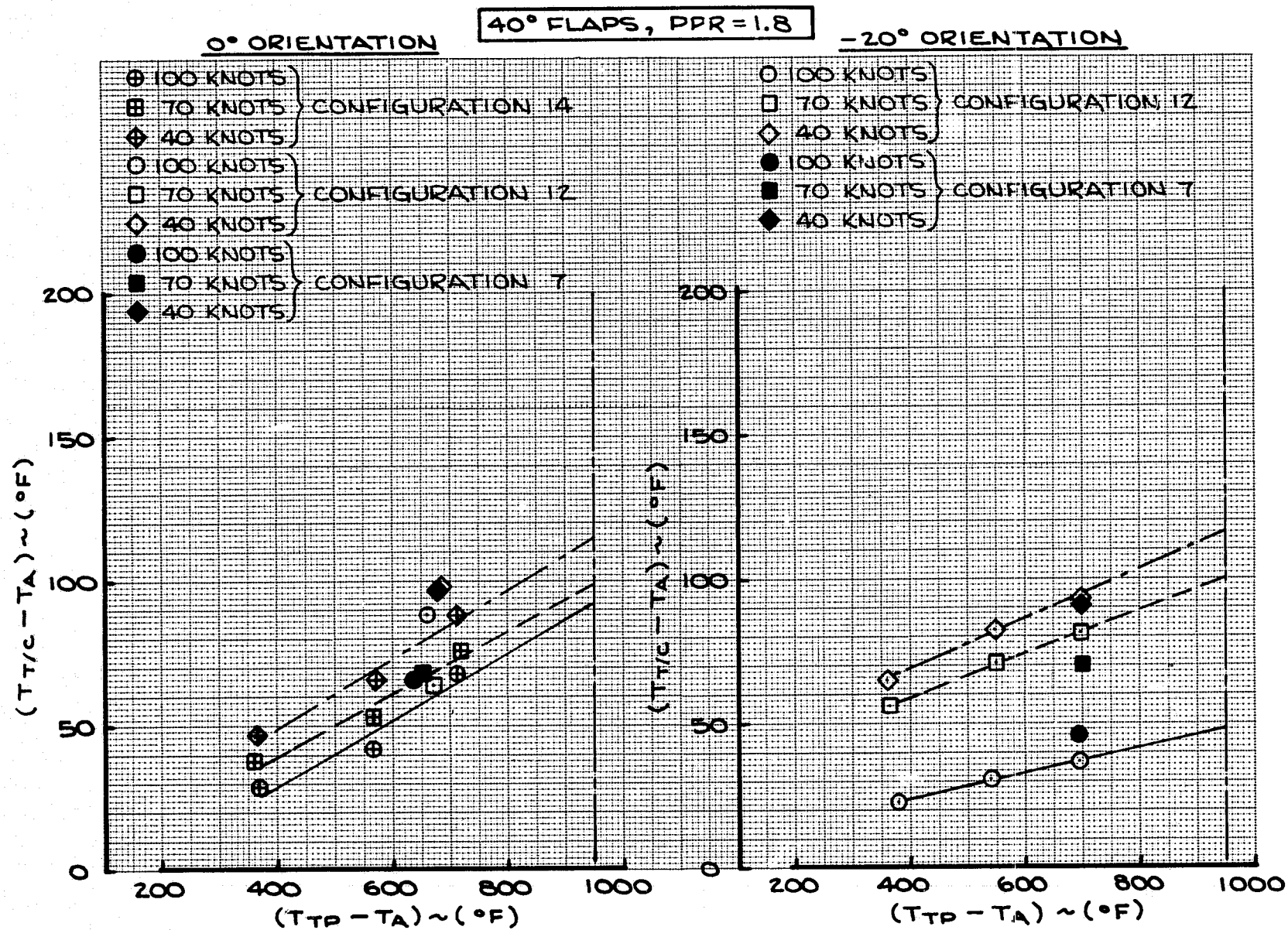
FIGURE 67 — IMPINGEMENT DATA FOR THERMOCOUPLE AT LOCATION 9
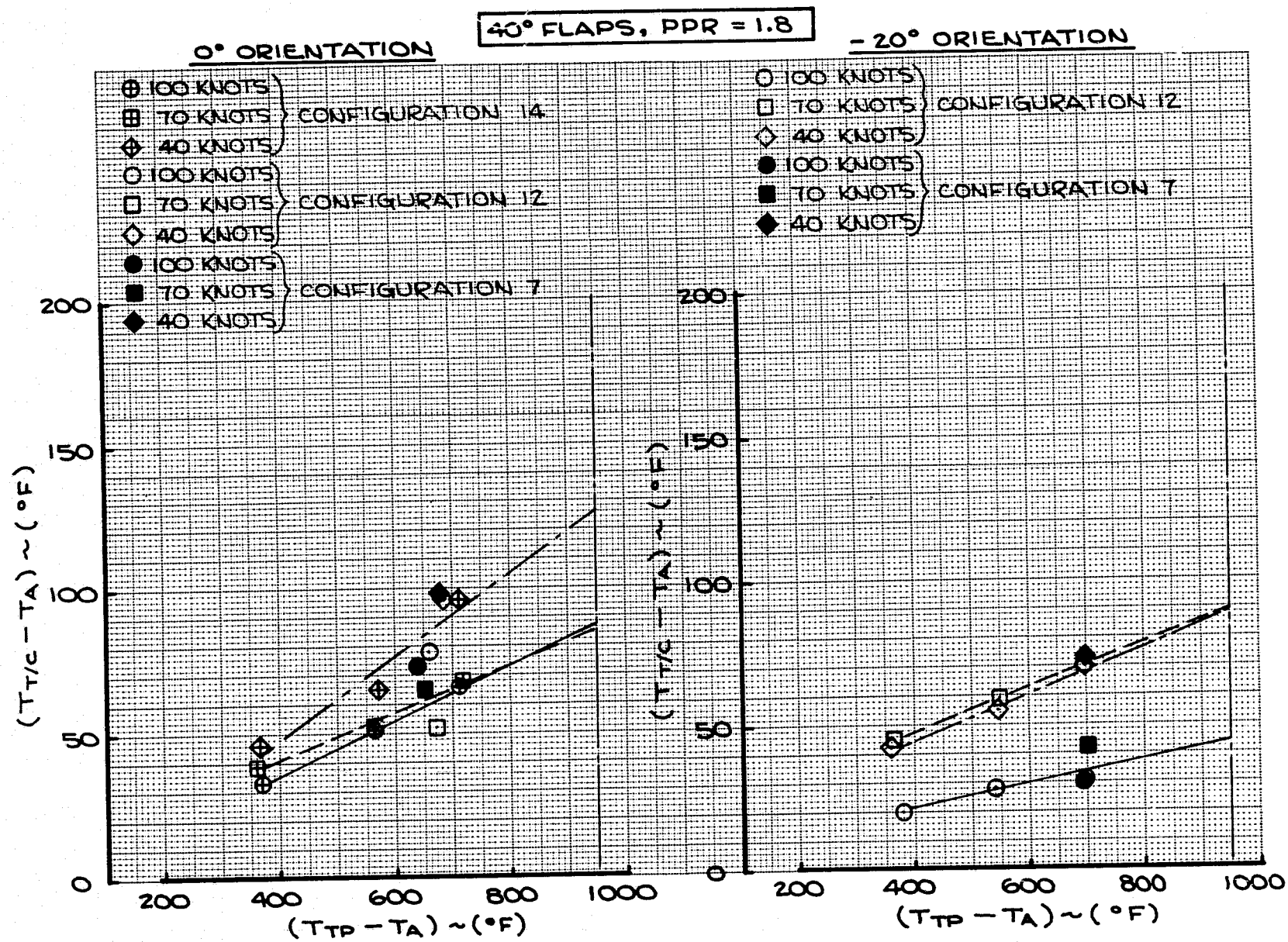
FIGURE 68 - IMPINGEMENT DATA FOR THERMOCOUPLE AT LOCATION 10
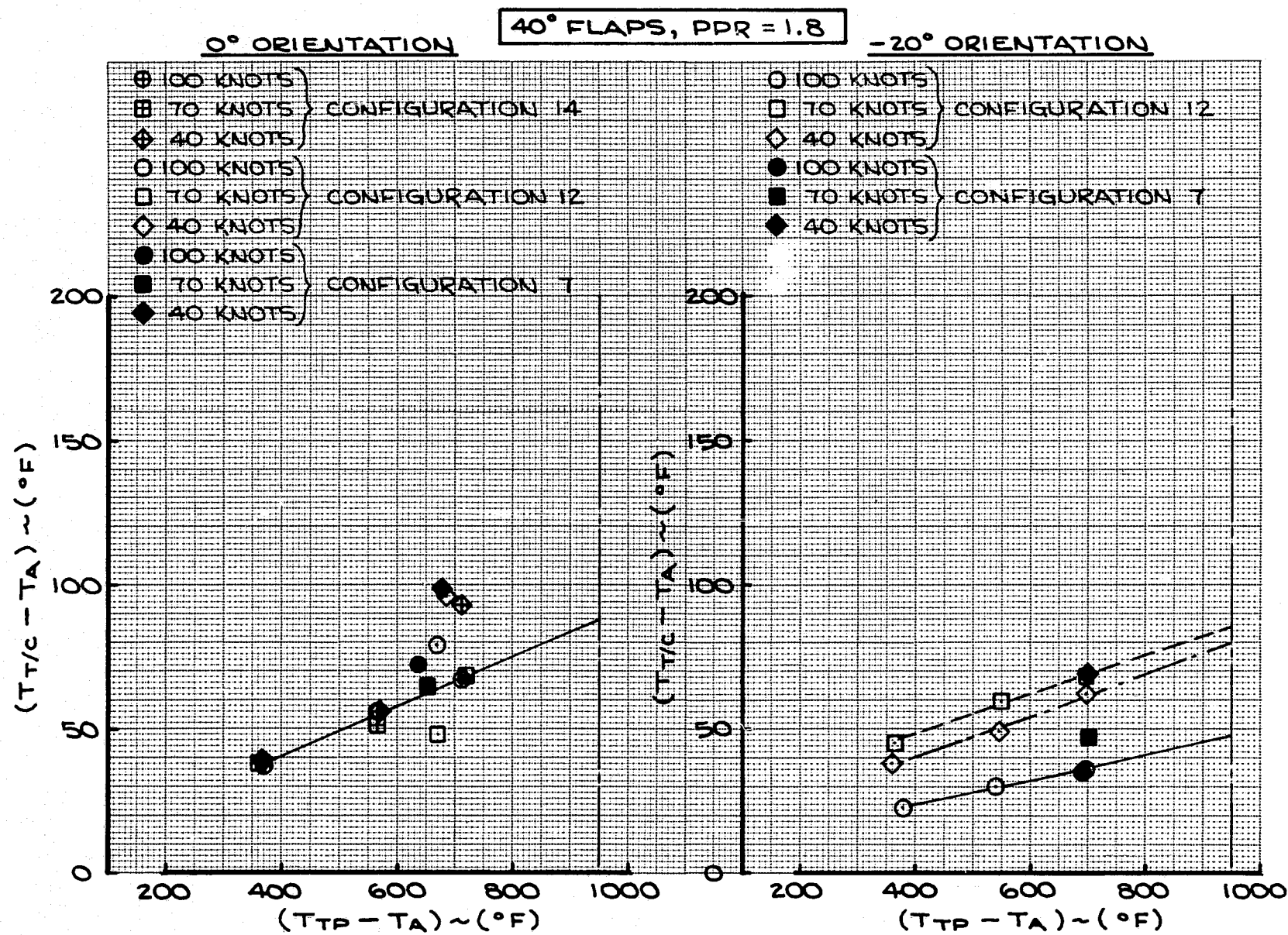
FIGURE 69 - IMPINGEMENT DATA FOR THERMOCOUPLE AT LOCATION 11

117
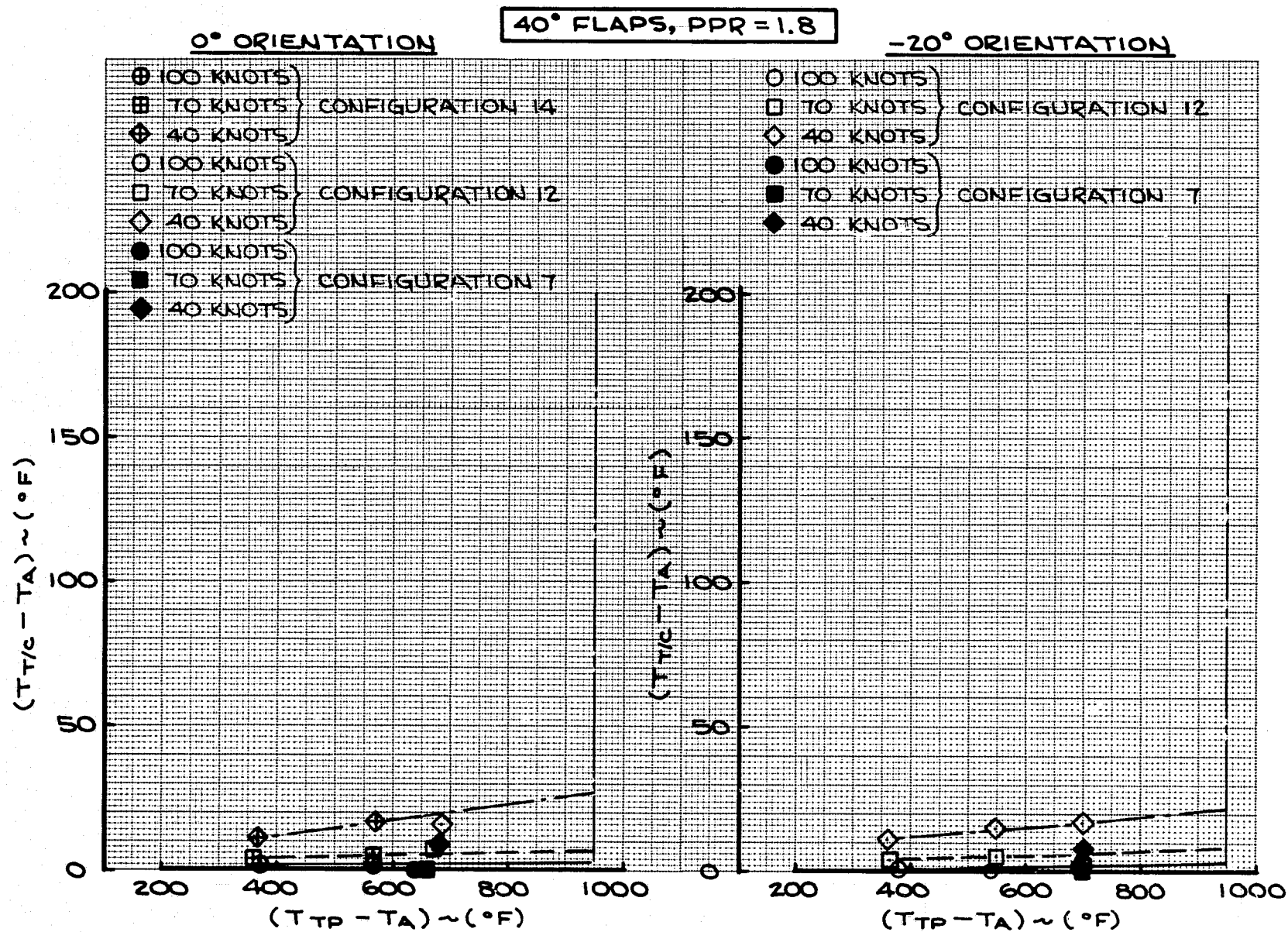
FIGURE 70 – IMPINGEMENT DATA FOR THERMOCOUPLE AT LOCATION 12
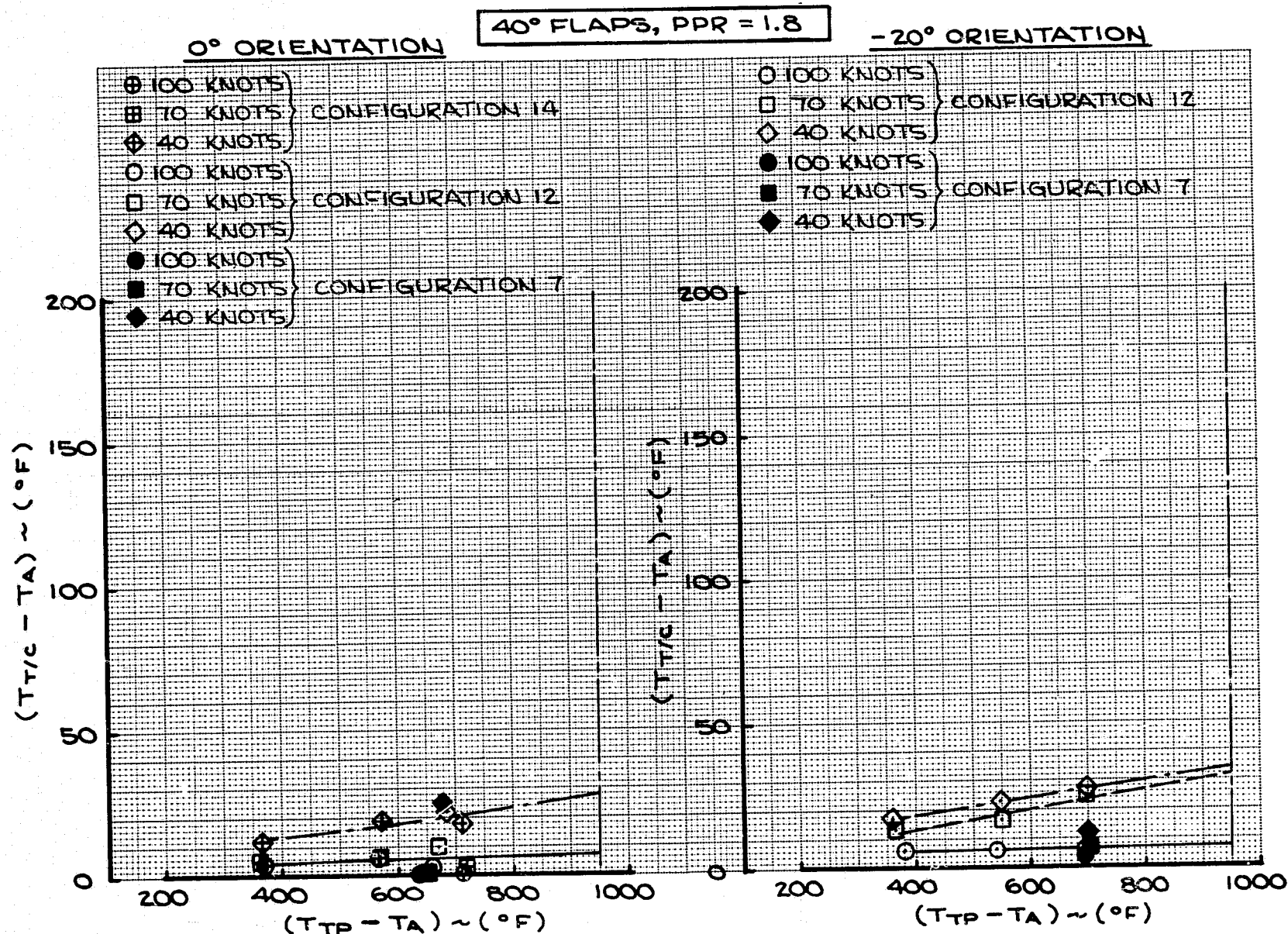
FIGURE 71 - IMPINGEMENT DATA FOR THERMOCOUPLE AT LOCATION 13
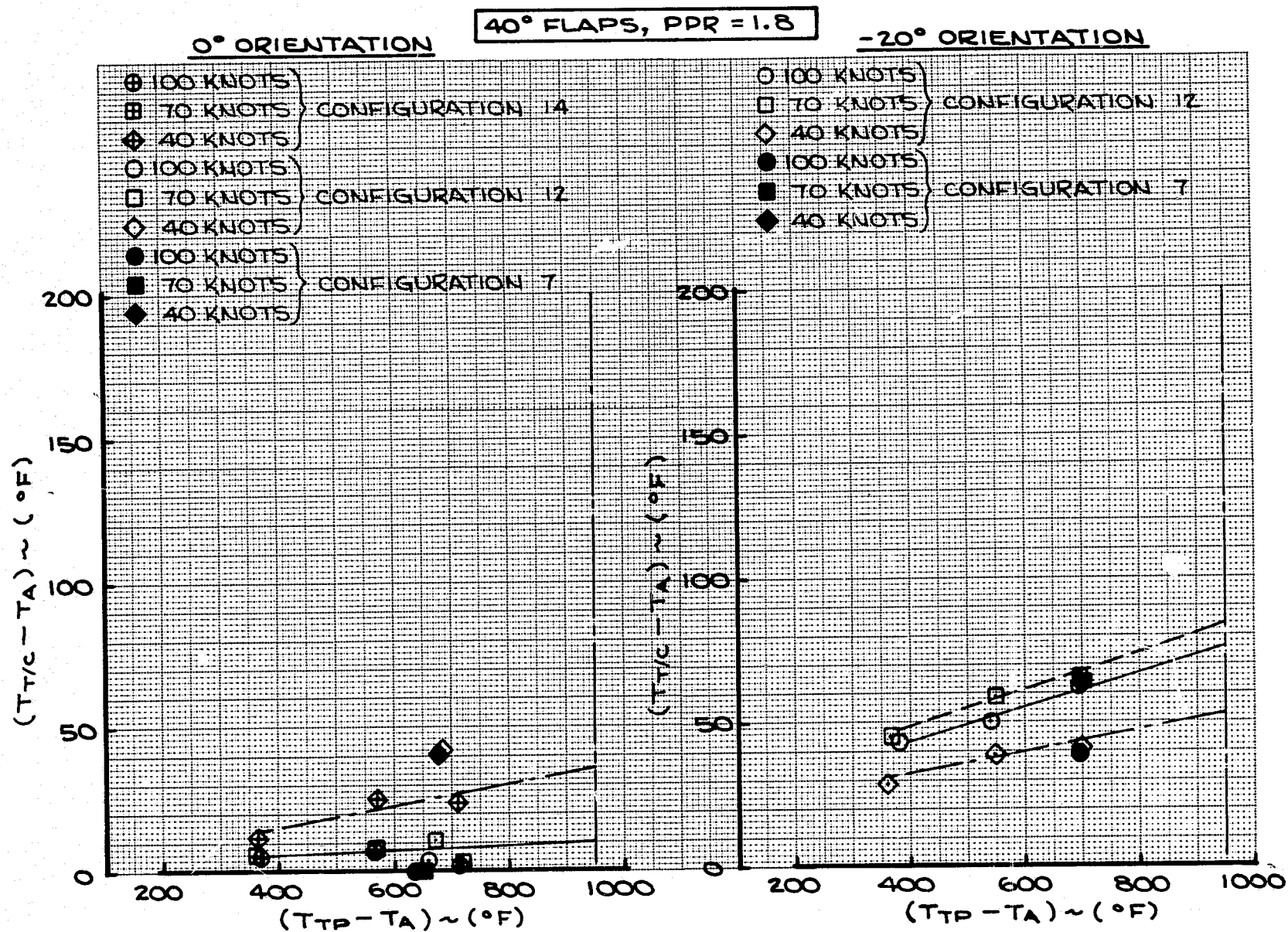
FIGURE 72 - IMPINGEMENT DATA FOR THERMOCOUPLE AT LOCATION 14
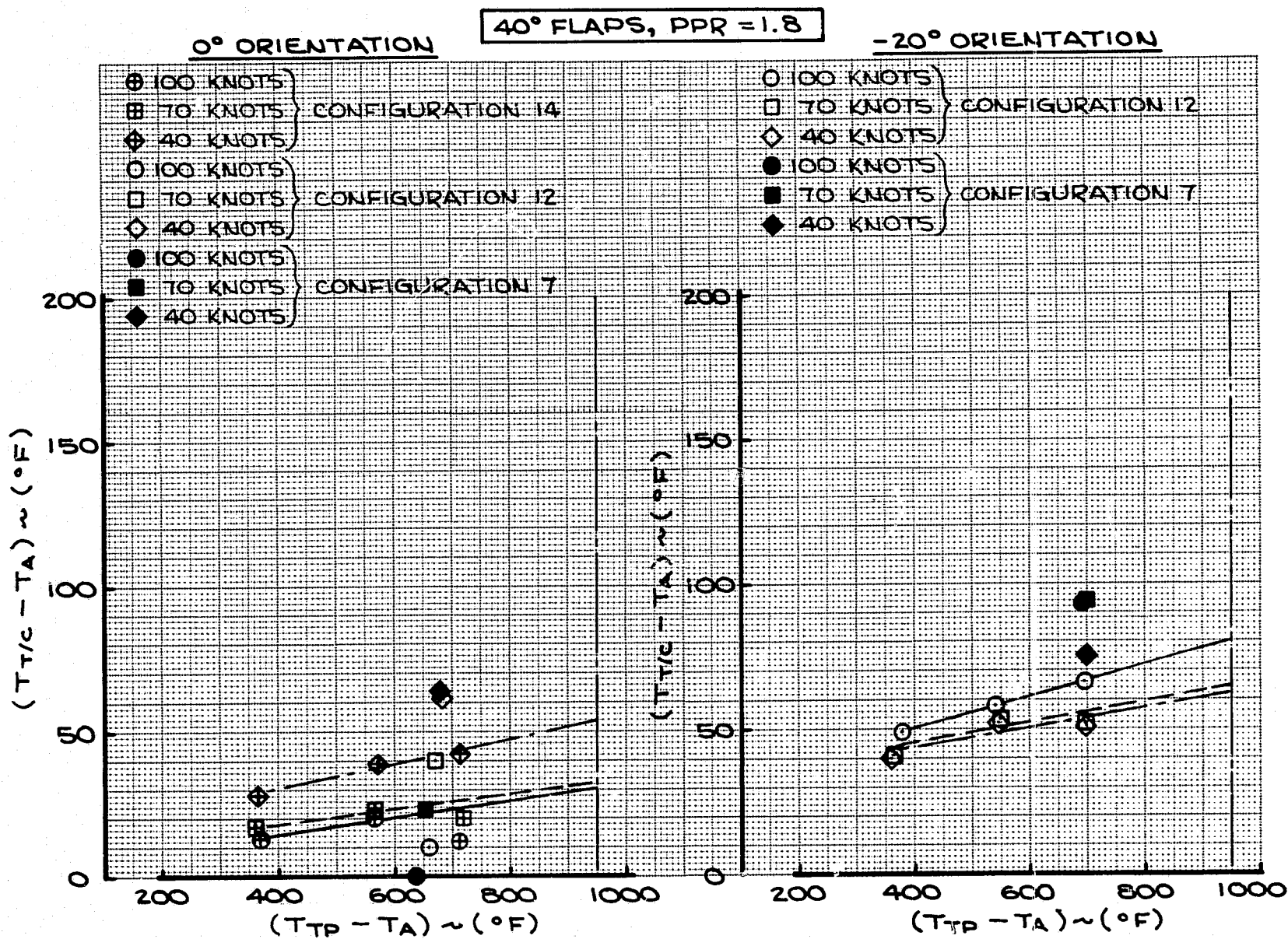
FIGURE 73 — IMPINGEMENT DATA FOR THERMOCOUPLE AT LOCATION 15
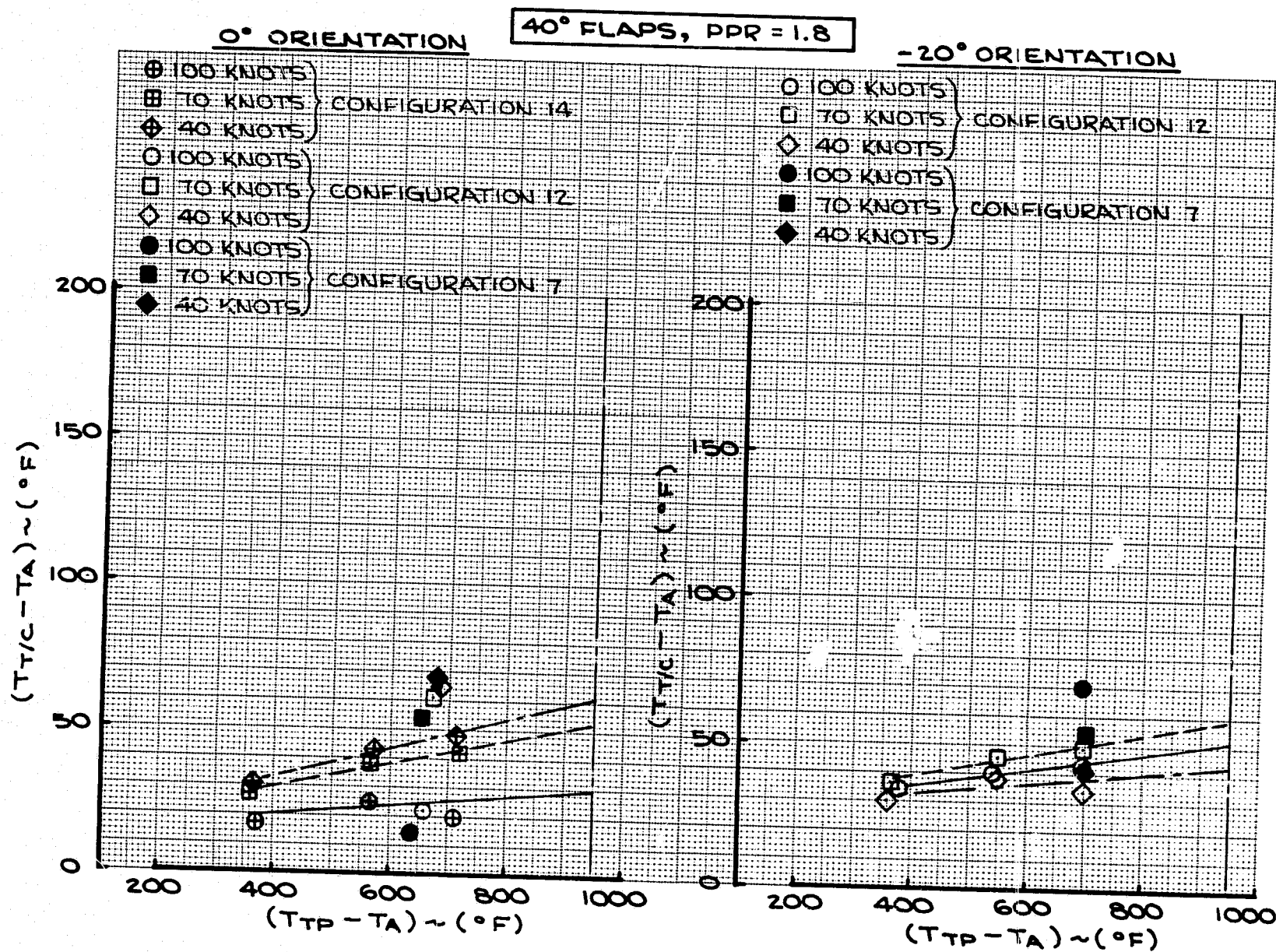
FIGURE **74** — IMPINGEMENT DATA FOR THERMOCOUPLE AT LOCATION 16
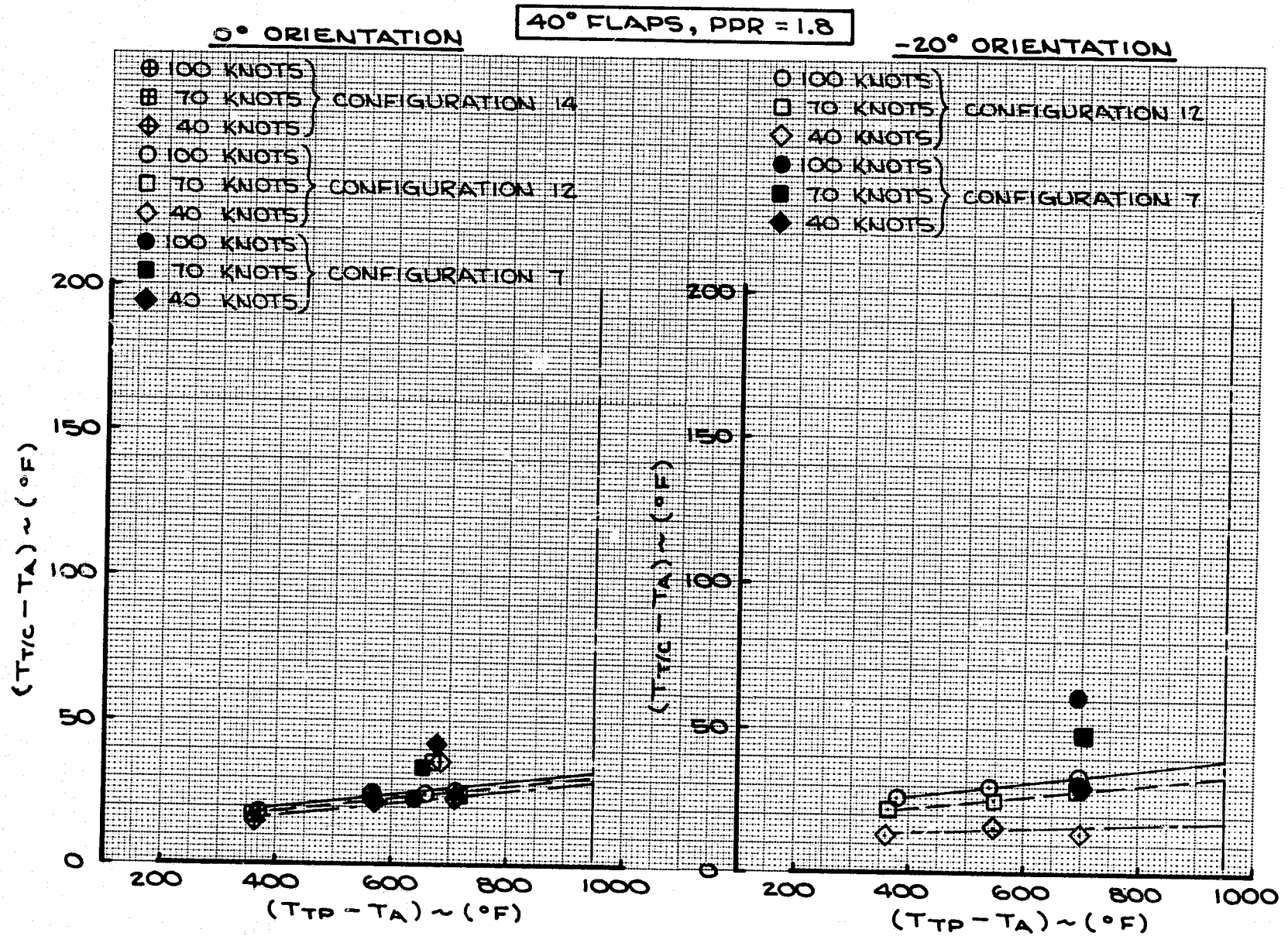
FIGURE 75 - IMPINGEMENT DATA FOR THERMOCOUPLE AT LOCATION 17
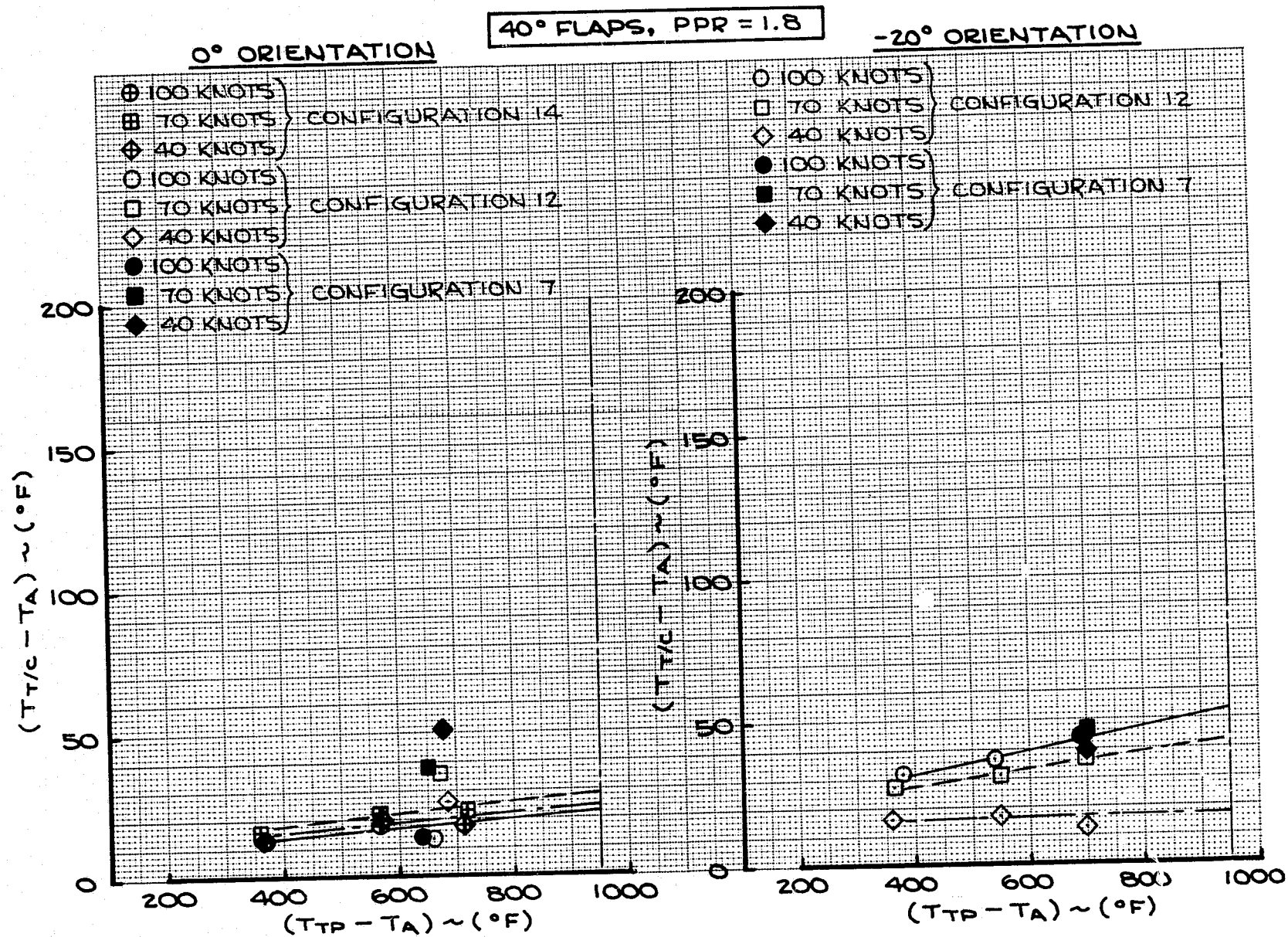
FIGURE 76 — IMPINGEMENT DATA FOR THERMOCOUPLE AT LOCATION 18
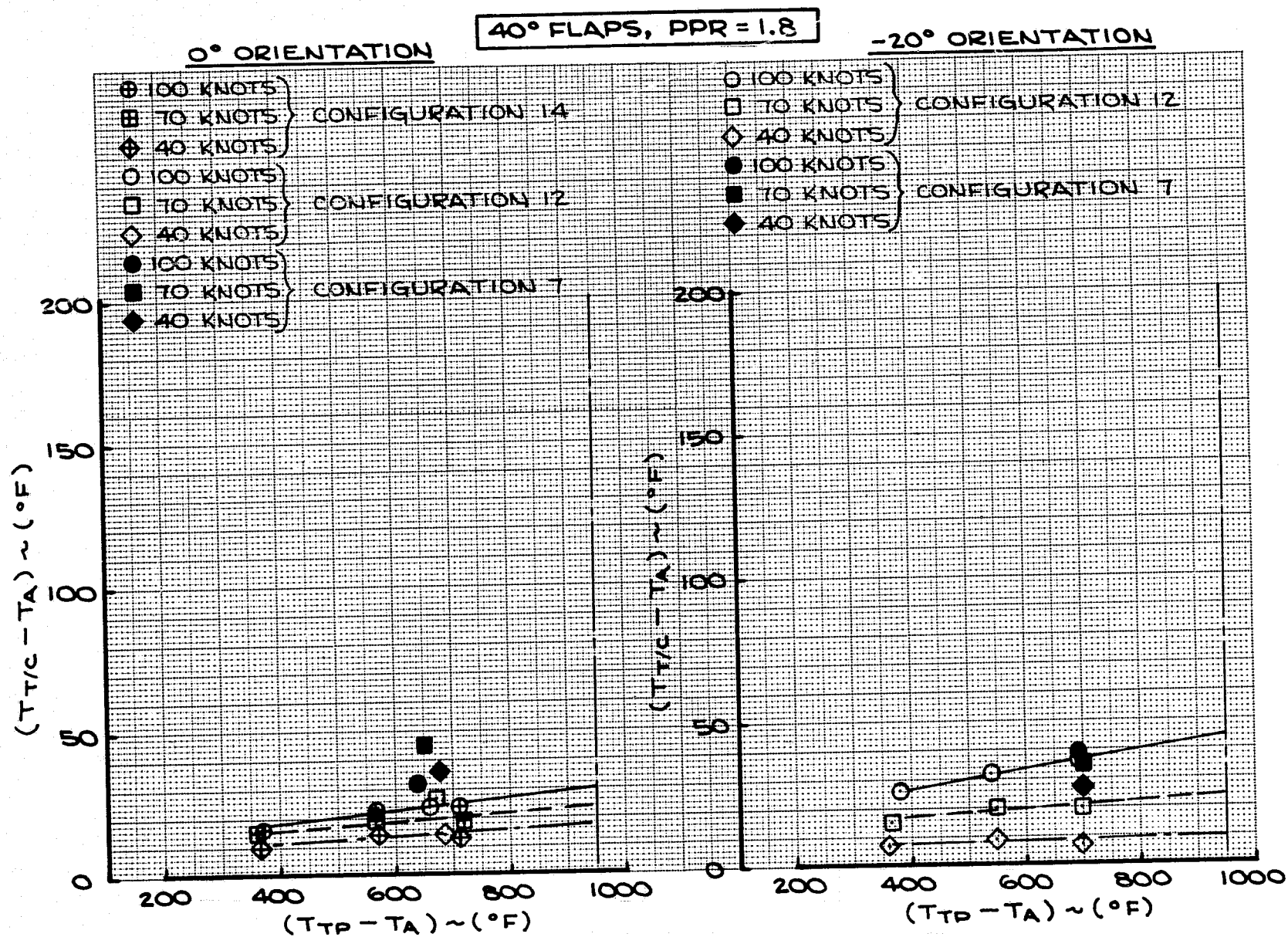
FIGURE 77 - IMPINGEMENT DATA FOR THERMOCOUPLE AT LOCATION 19
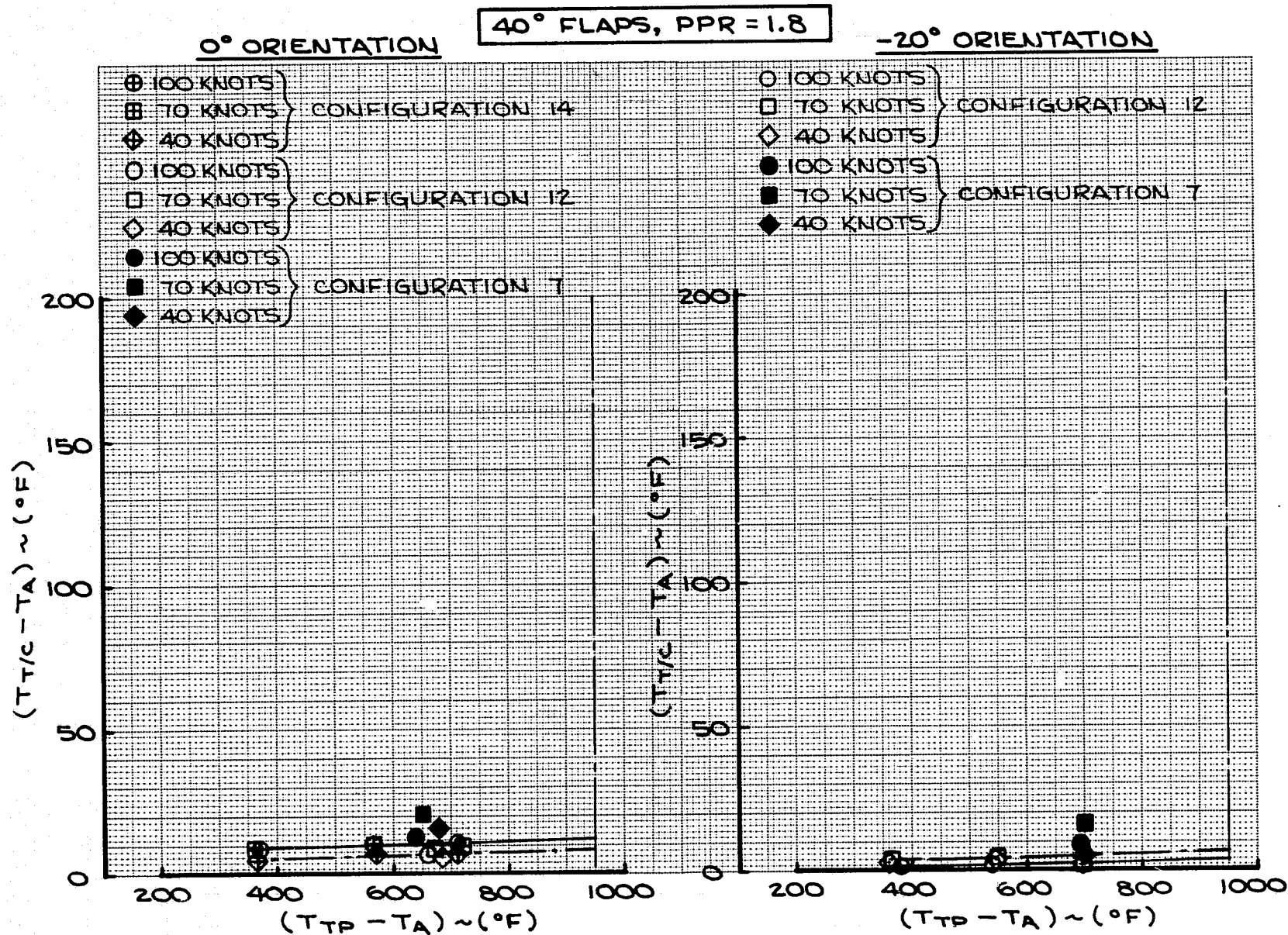
FIGURE 78 — IMPINGEMENT DATA FOR THERMOCOUPLE AT LOCATION 20

FIGURE **79** - EFFECT OF PRIMARY PRESSURE RATIO ON IMPINGEMENT TEMPERATURES

THERMOCOUPLE AT LOCATION 6
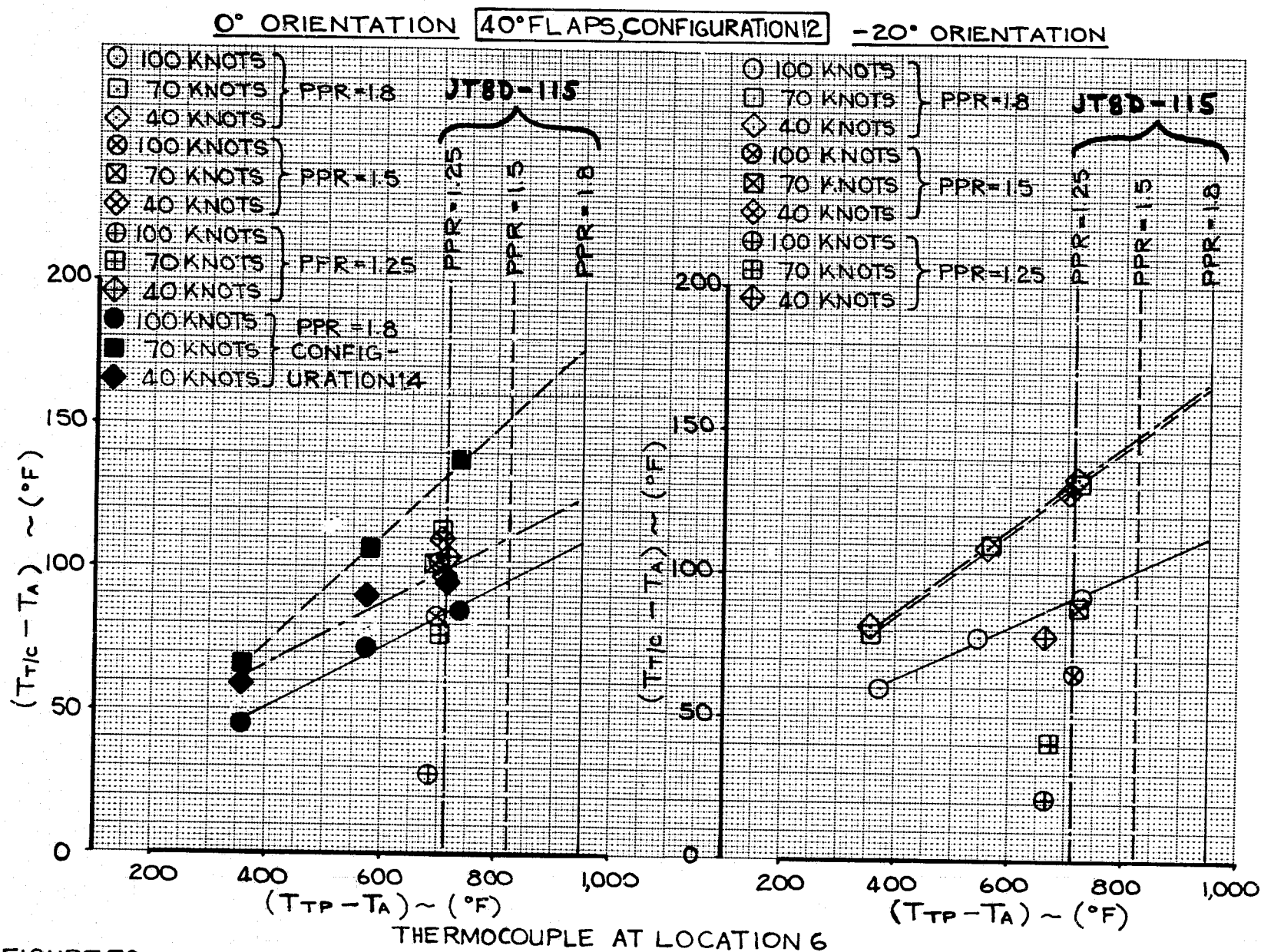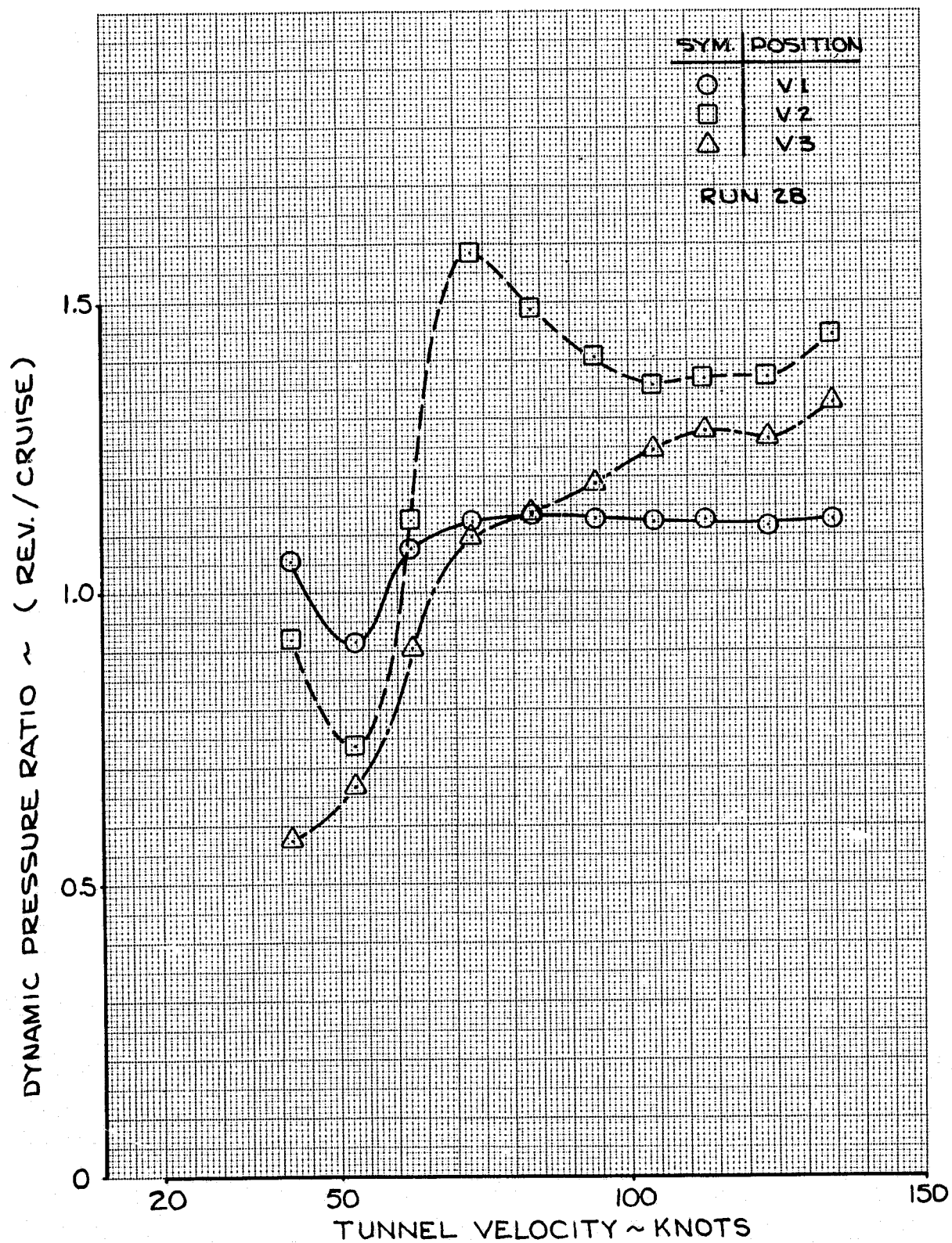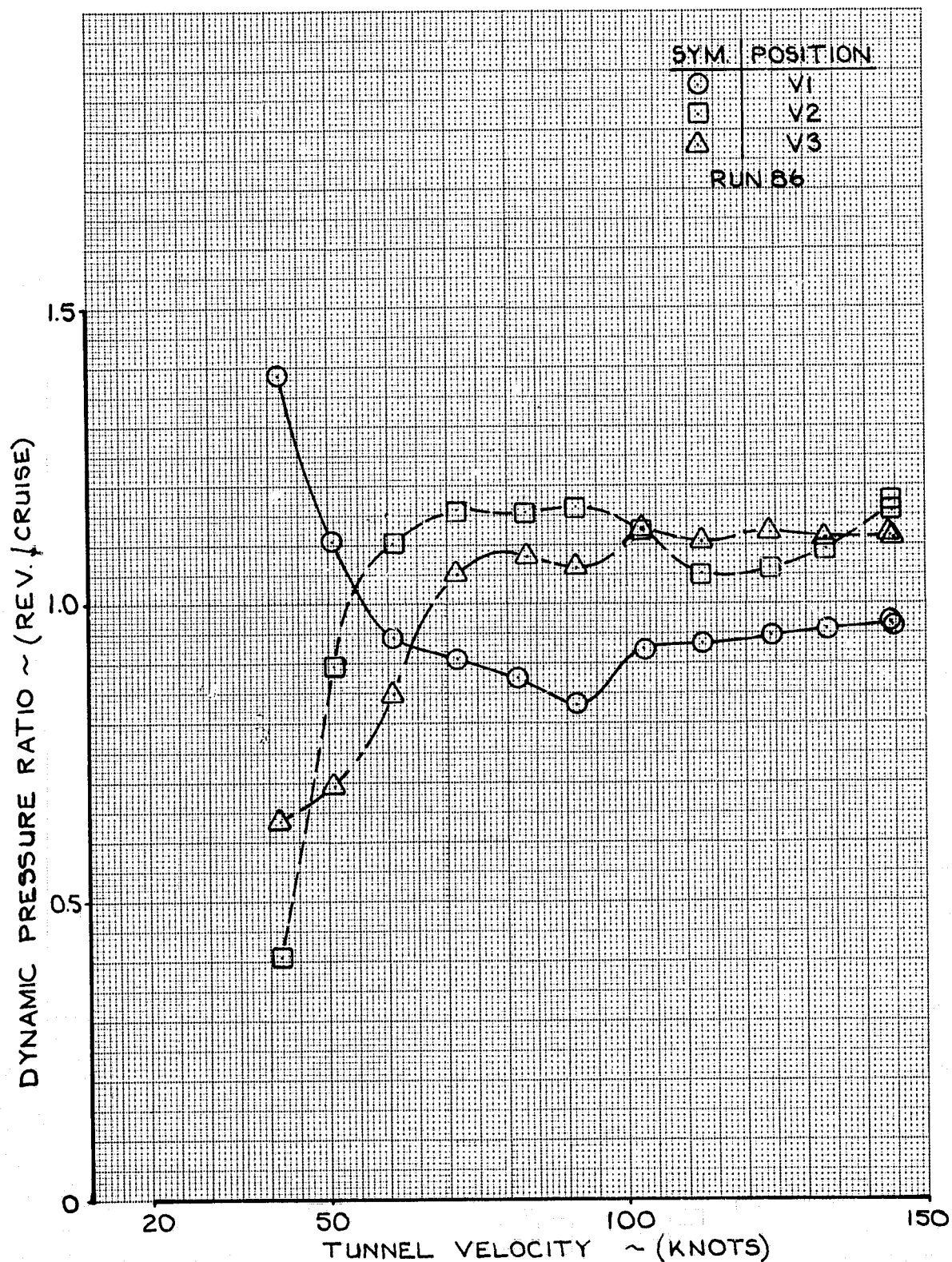
FIGURE 80 — VERTICAL TAIL DYNAMIC PRESSURE RATIOS; CONFIGURATION 1, 40° FLAPS, PPR = 1.8, +20° ORIENTATION
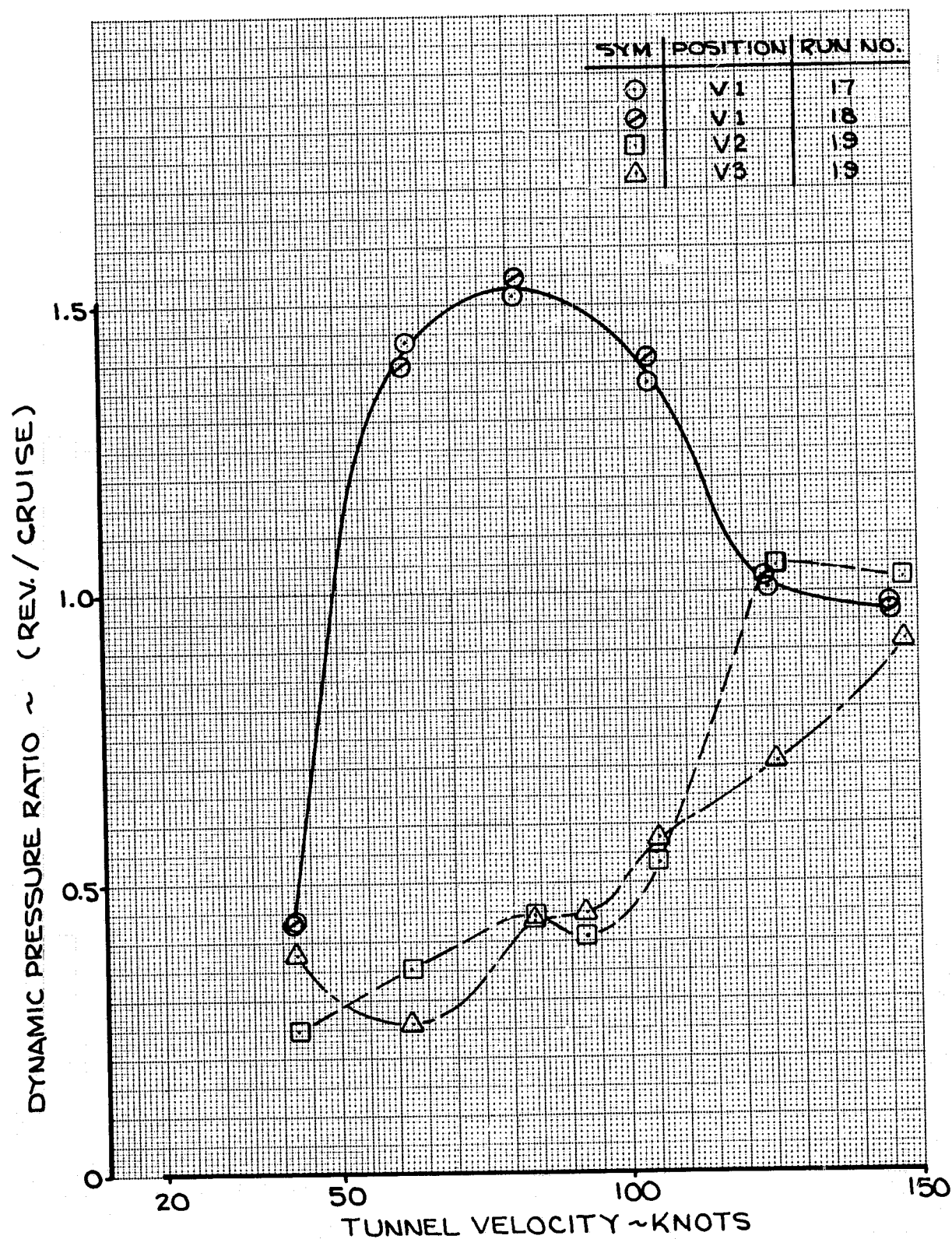
FIGURE 81 - VERTICAL TAIL DYNAMIC PRESSURE RATIOS; CONFIGURATION 1, 40° FLAPS, PPR=1.8, 0° ORIENTATION
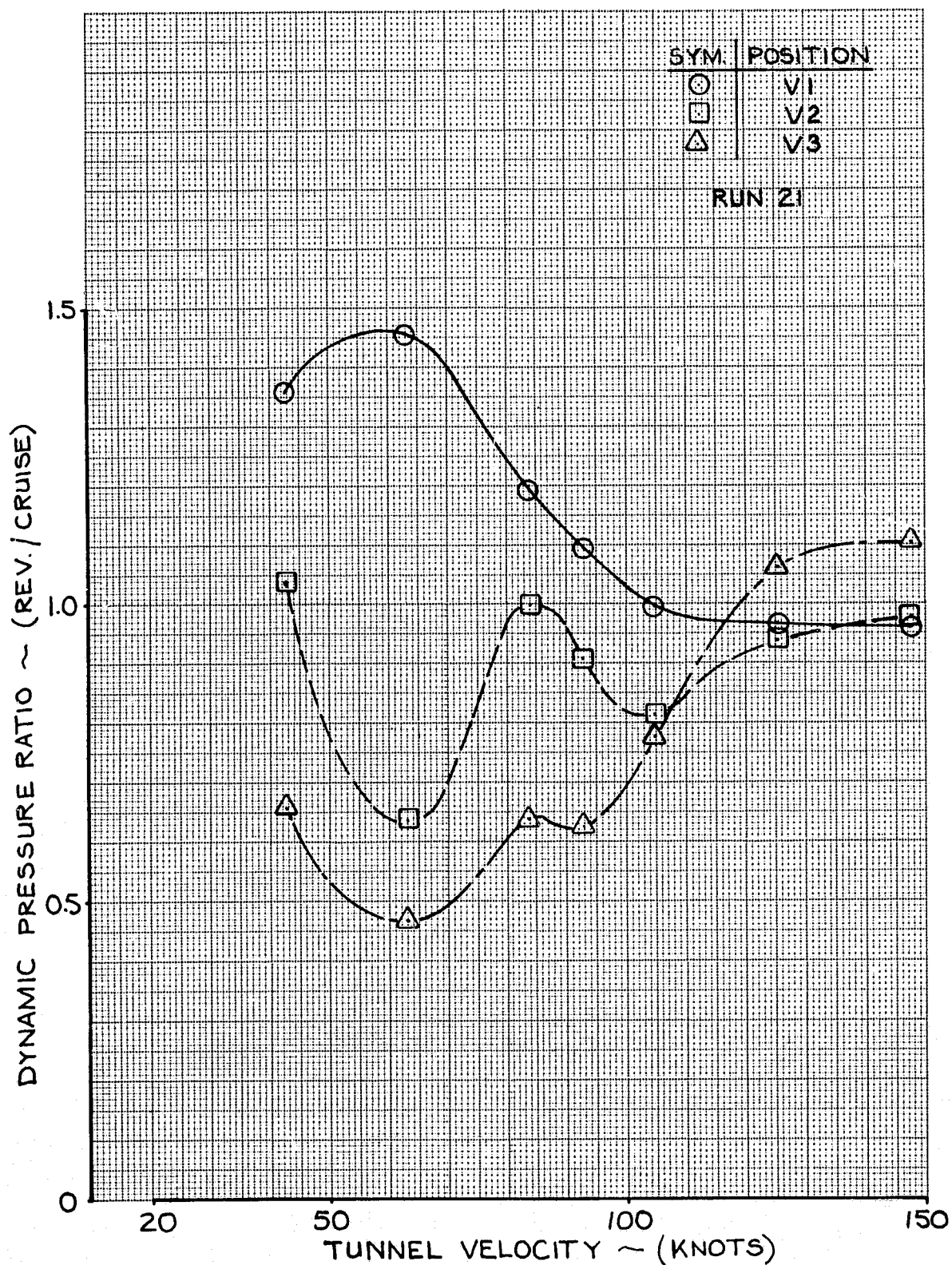
FIGURE 82 — VERTICAL TAIL DYNAMIC PRESSURE RATIOS;
CONFIGURATION 1, 40° FLAPS, PPR =1.5,
0° ORIENTATION.
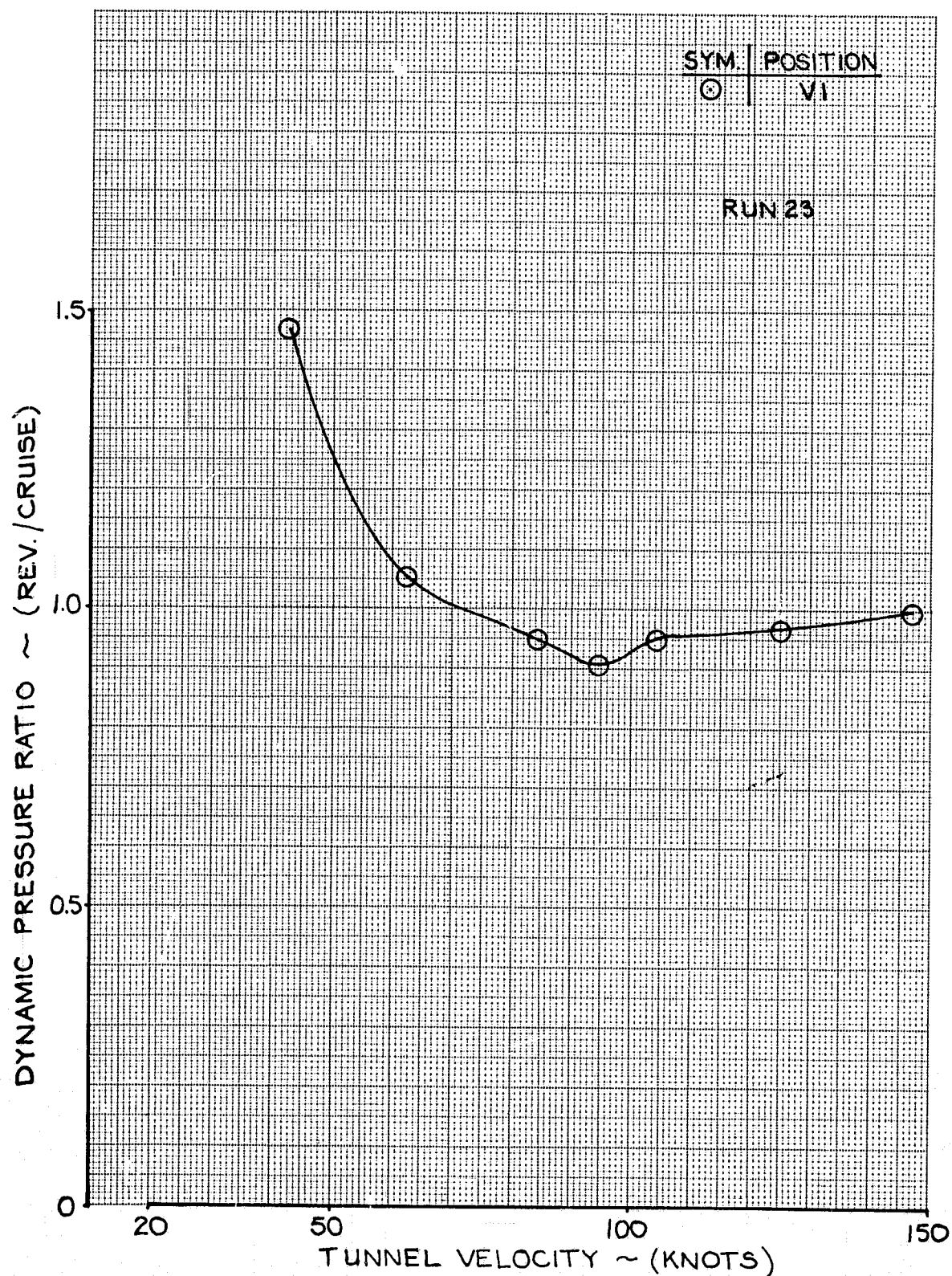
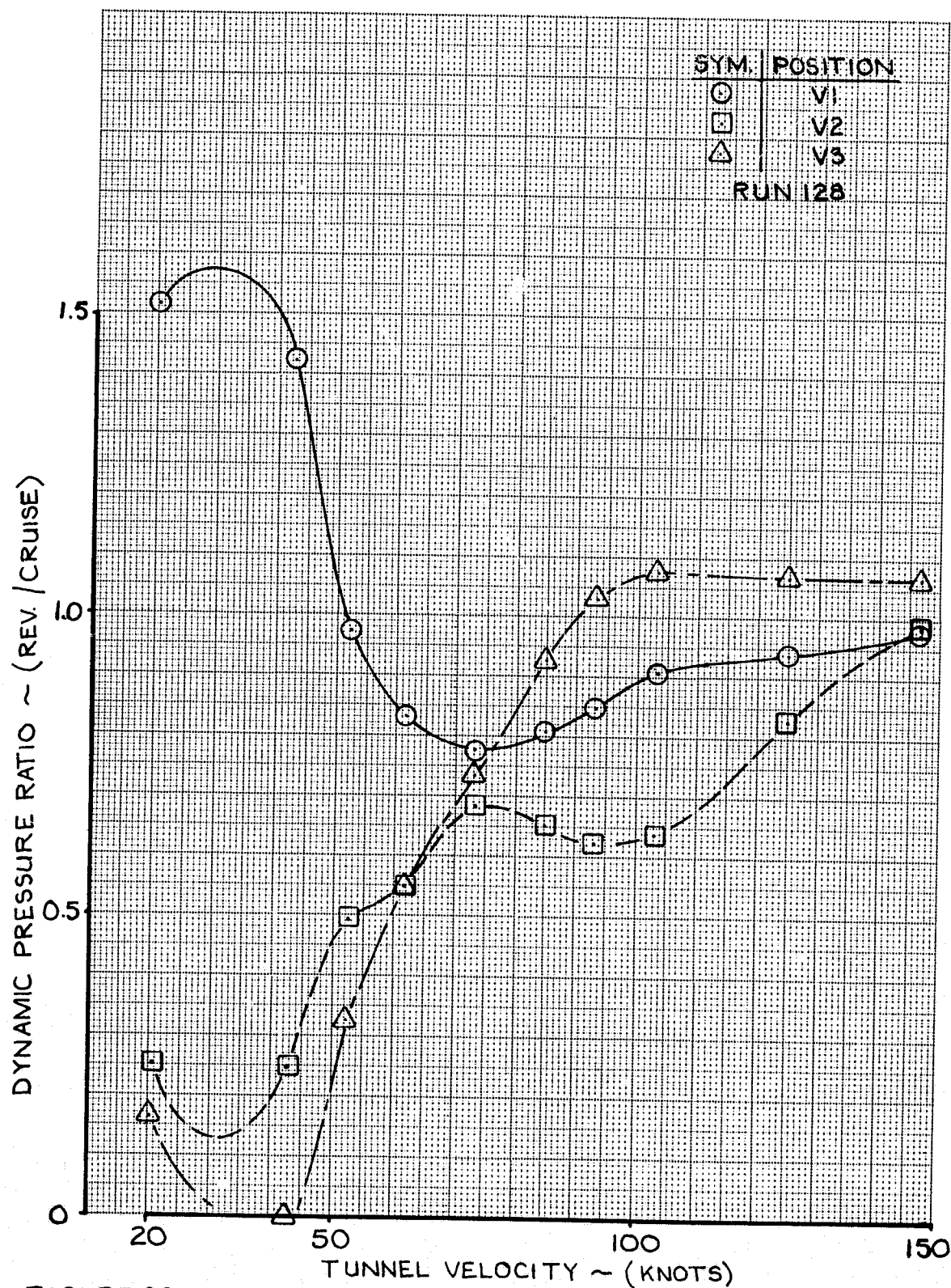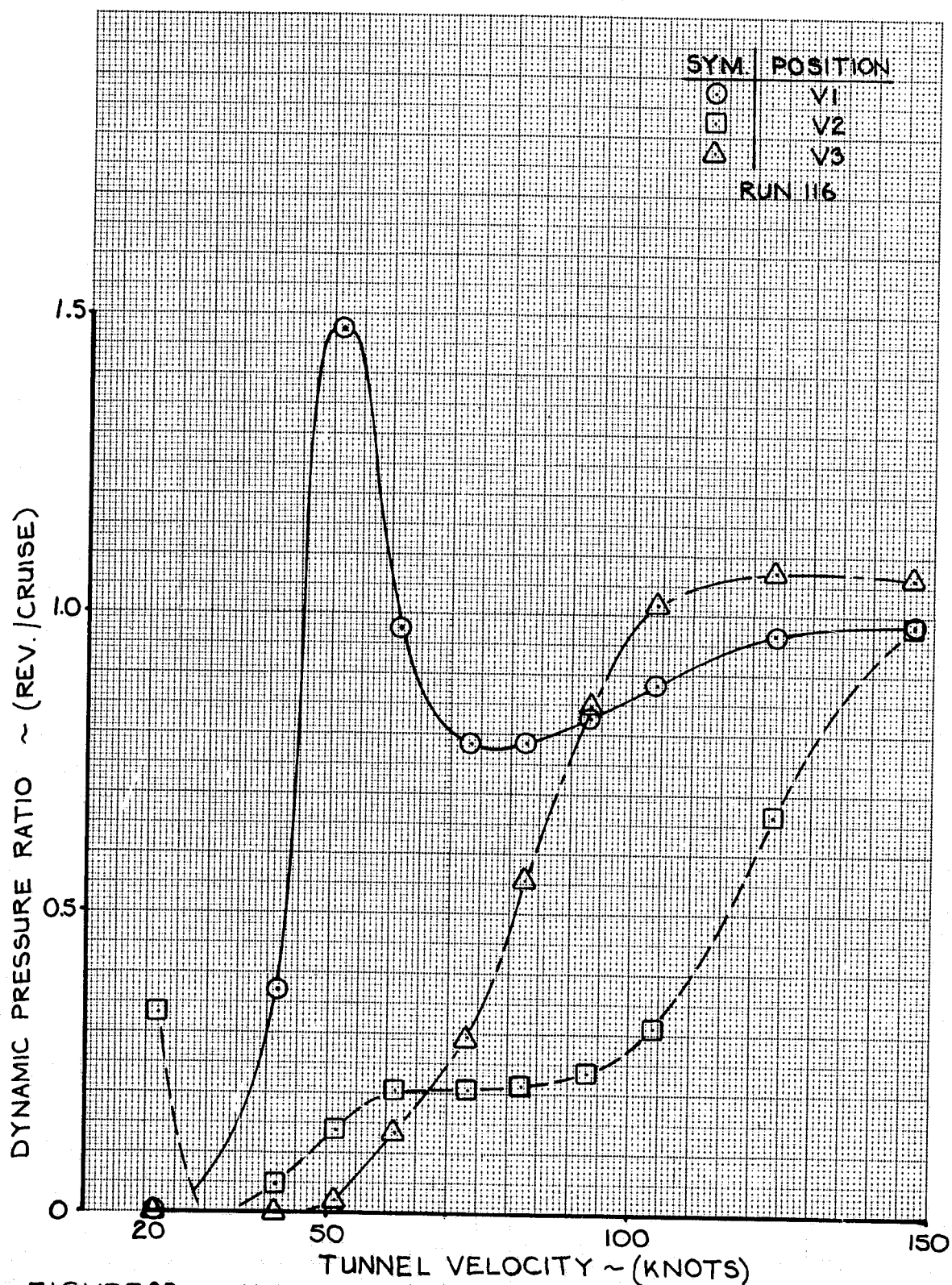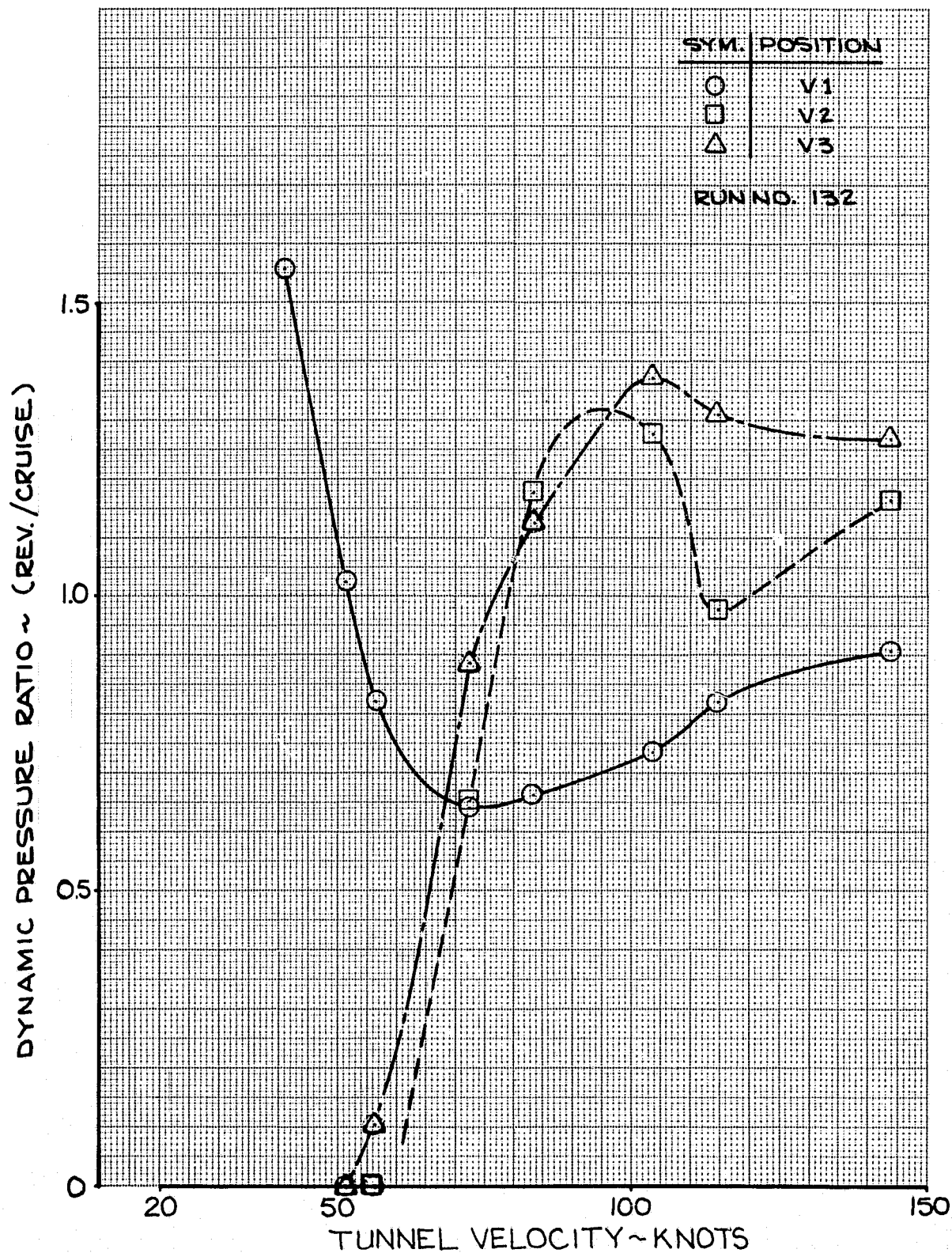FIGURE 83 — VERTICAL TAIL DYNAMIC PRESSURE RATIOS; CONFIGURATION 1, 40° FLAPS , PPR =1.25, 0° ORIENTATION.
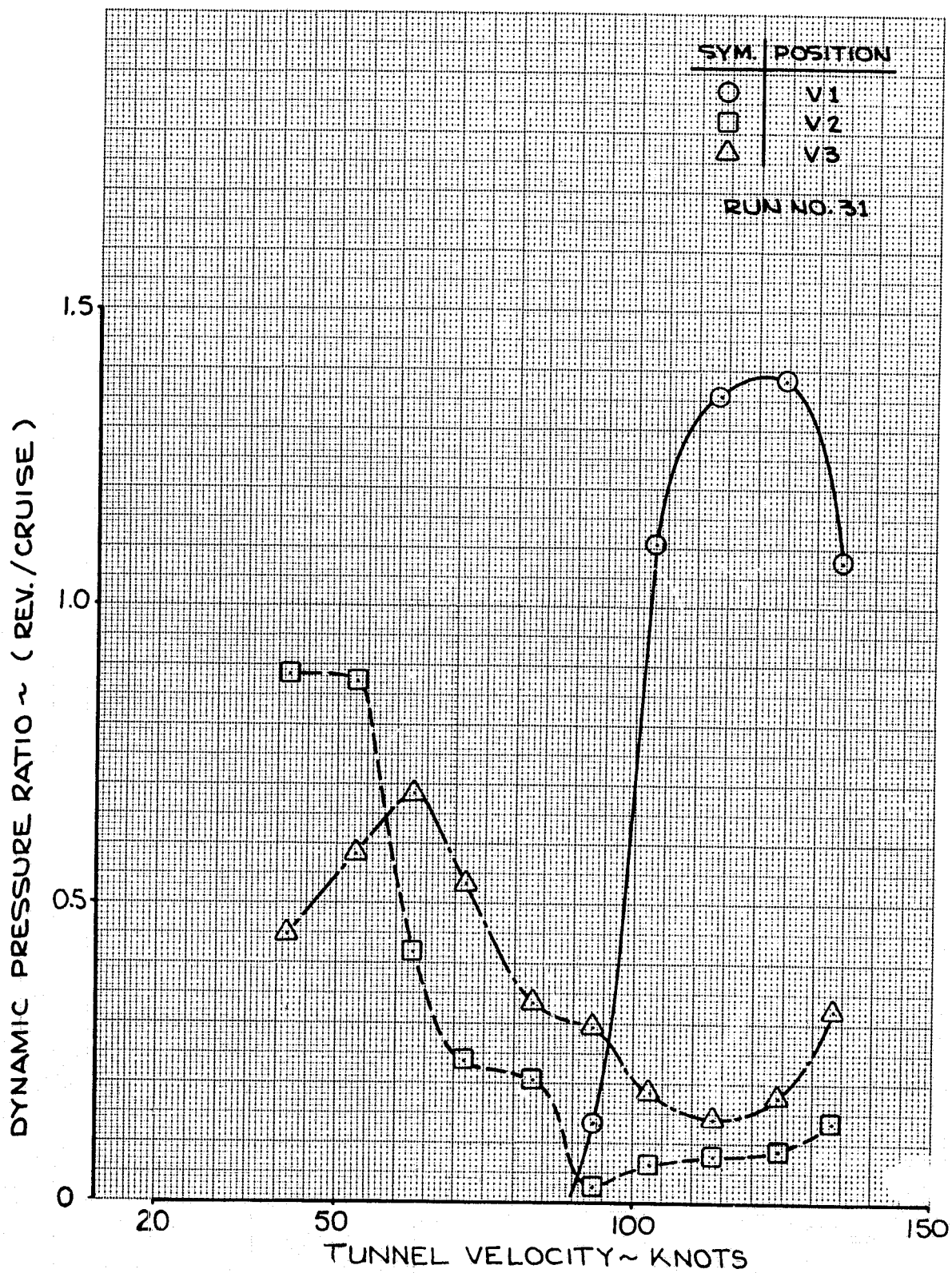
FIGURE 84 — VERTICAL TAIL DYNAMIC PRESSURE RATIOS;
CONFIGURATION 1, 40° FLAPS, PPR = 1.8,
− 20° ORIENTATION
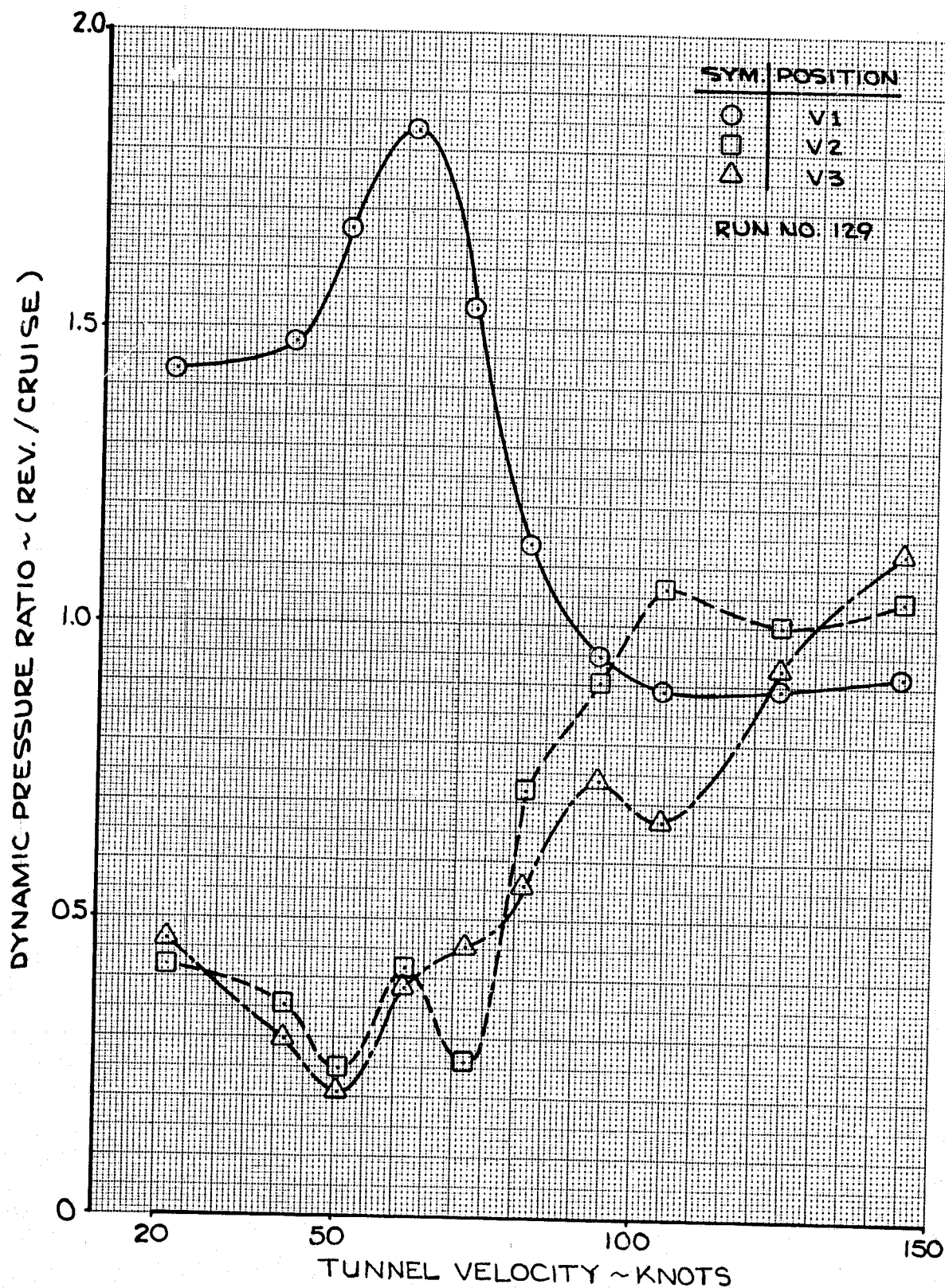
FIGURE **85** — VERTICAL TAIL DYNAMIC PRESSURE RATIOS; CONFIGURATION 12, 40° FLAPS, PPR = 1.8, 0° ORIENTATION
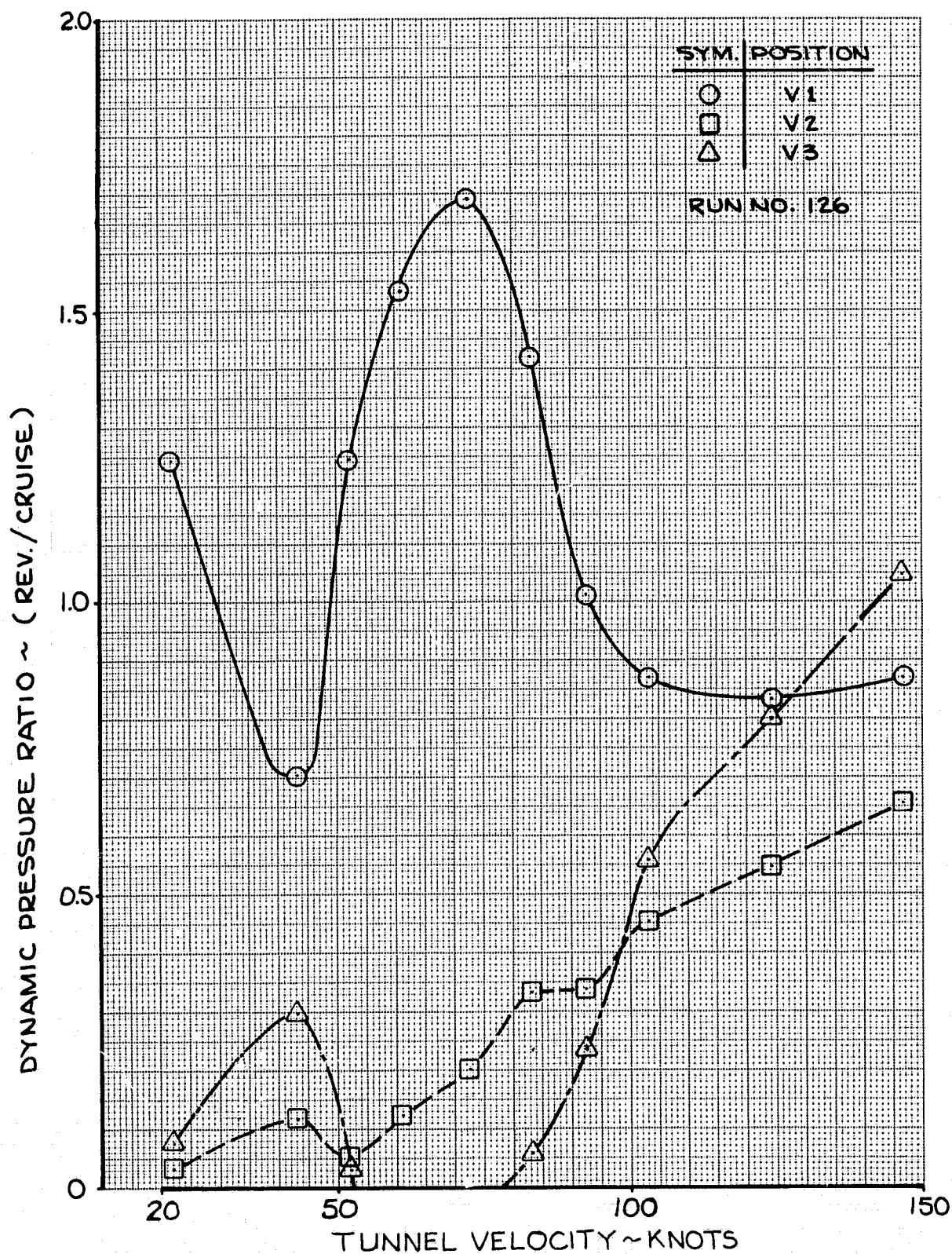
FIGURE 86 — VERTICAL TAIL DYNAMIC PRESSURE RATIOS;
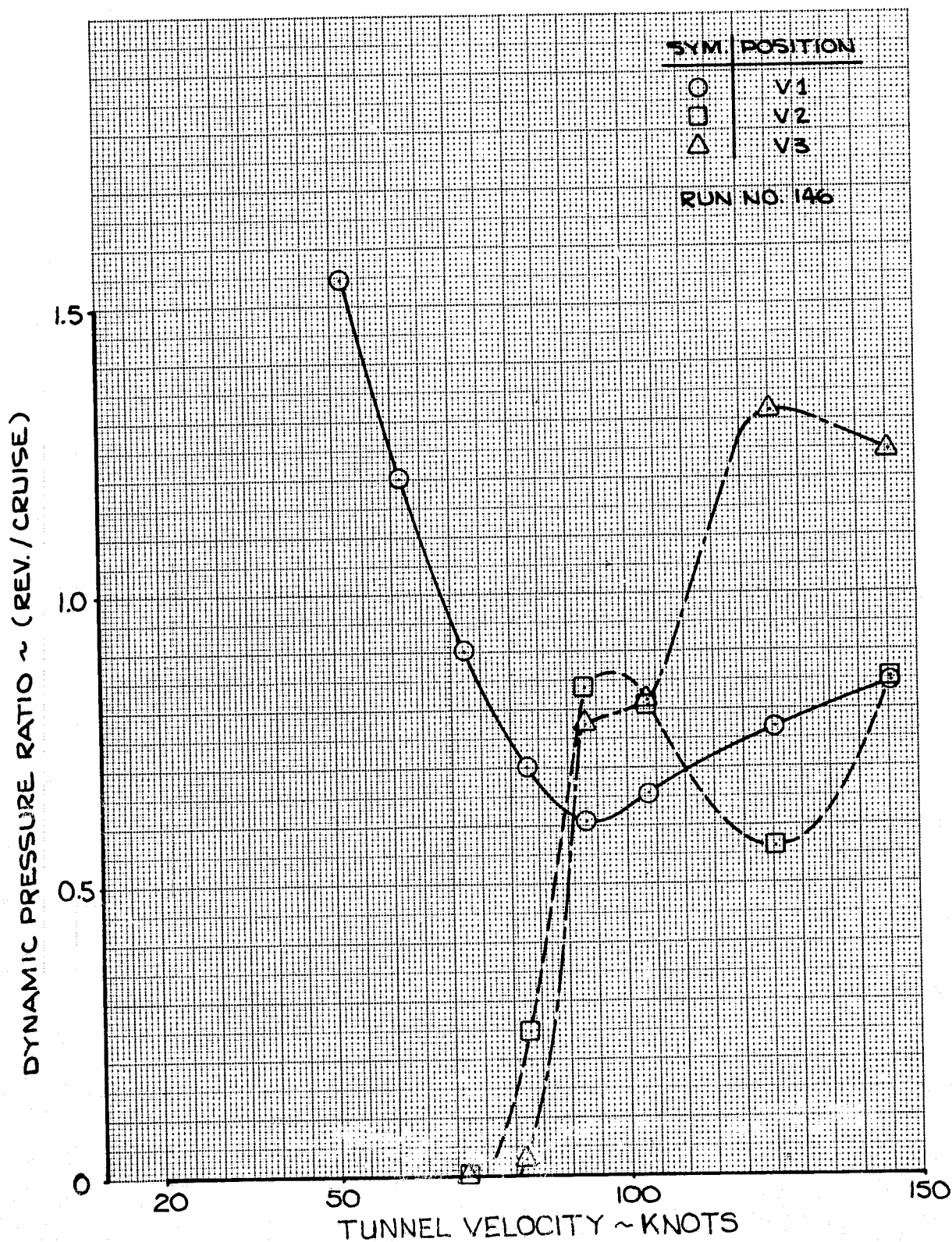CONFIGURATION 12, 40° FLAPS, PPR = 1.8,
-10° ORIENTATION
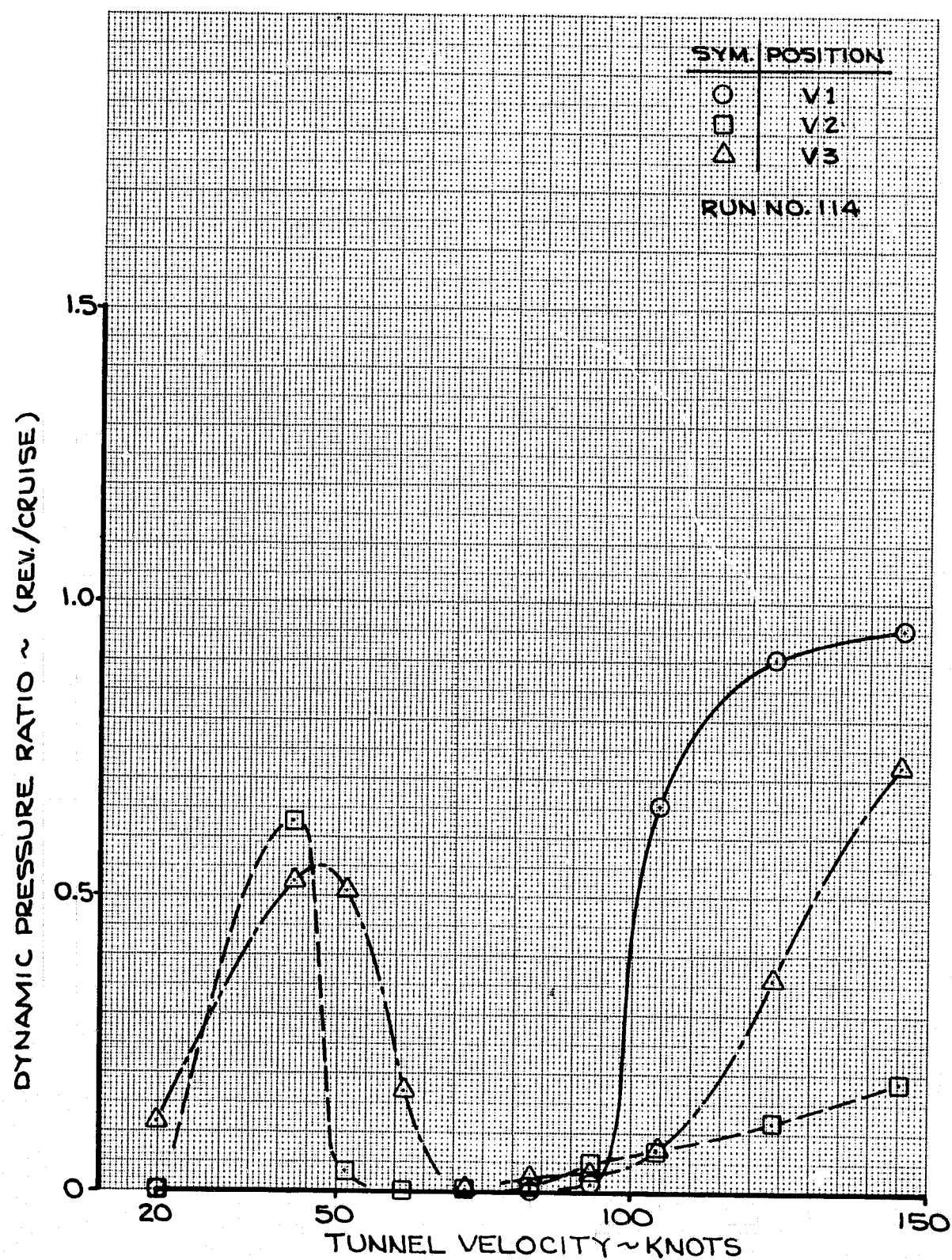
FIGURE **87** — VERTICAL TAIL DYNAMIC PRESSURE RATIOS;
CONFIGURATION 12, 40° FLAPS, PPR = 1.8,
-20° ORIENTATION
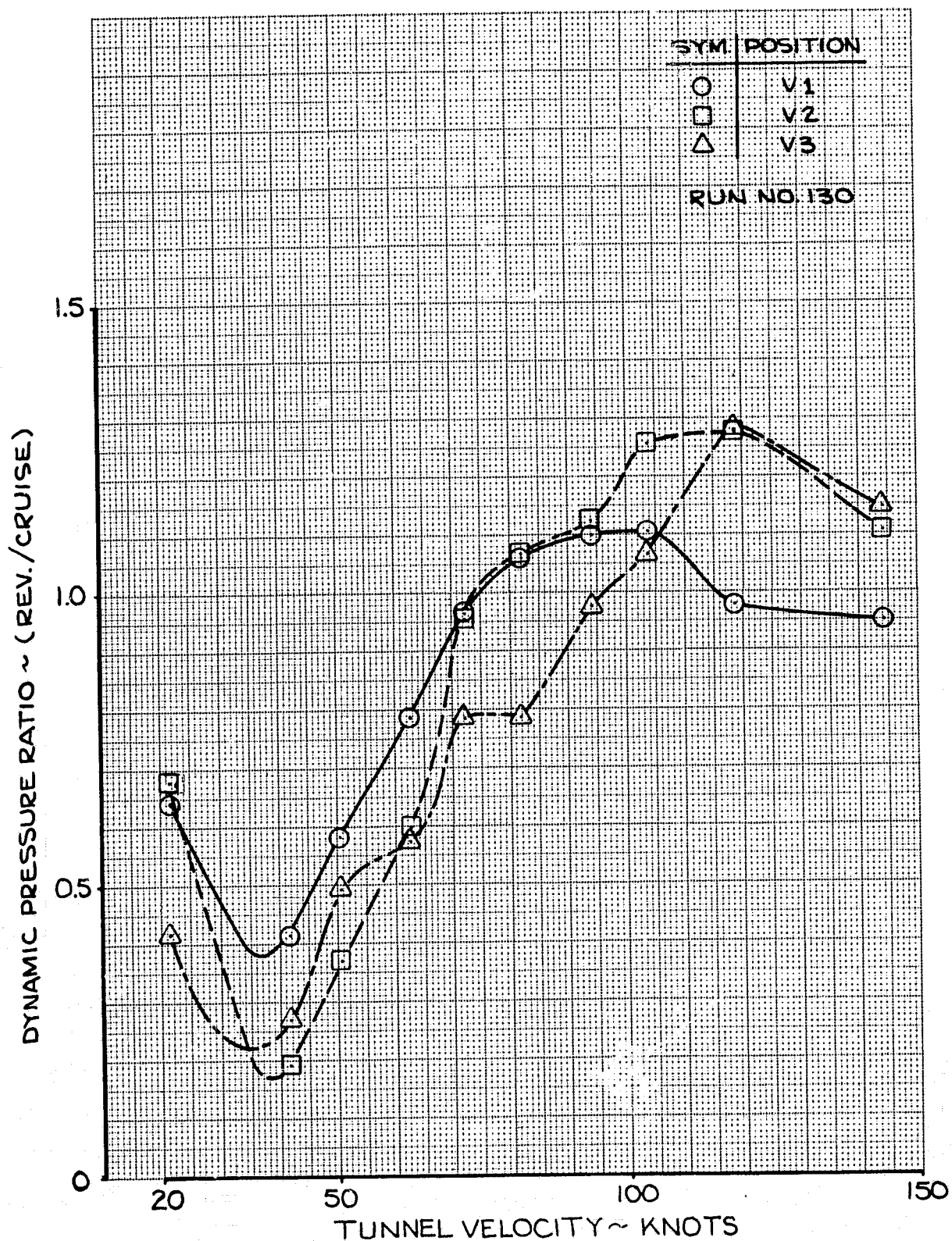
FIGURE 88 — VERTICAL TAIL DYNAMIC PRESSURE RATIOS;
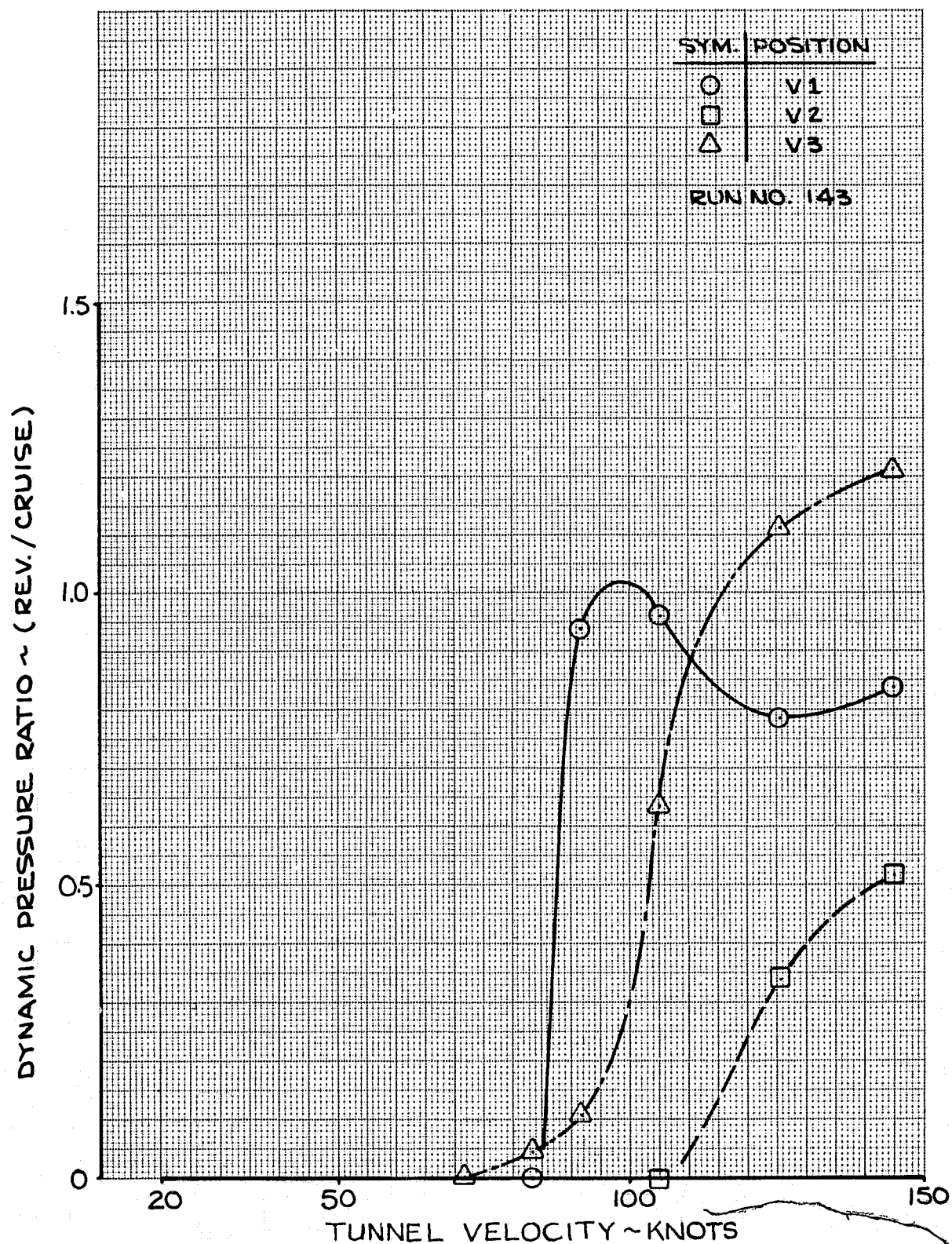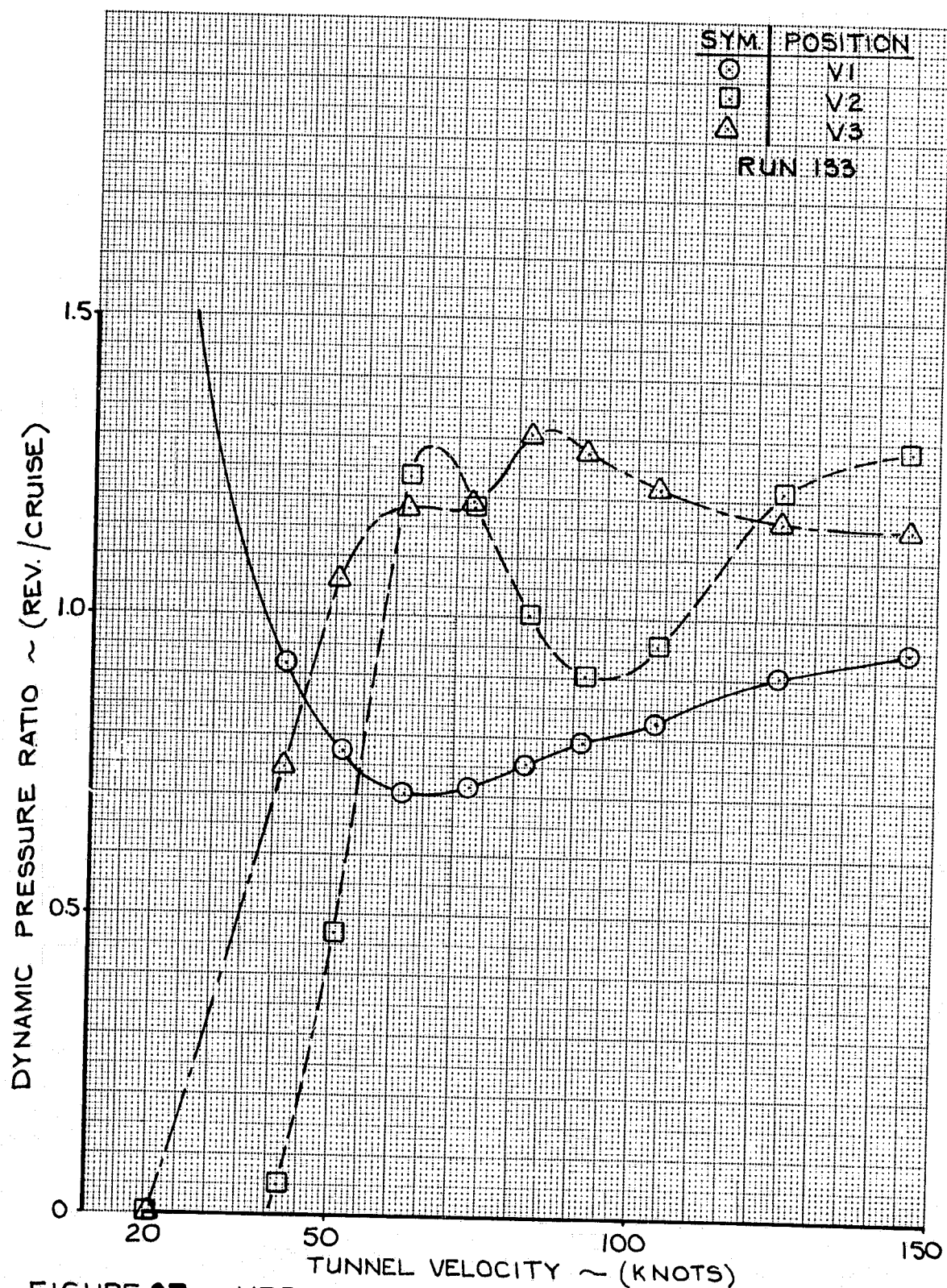CONFIGURATION 12, 40° FLAPS, PPR = 1.5,
0° ORIENTATION

136
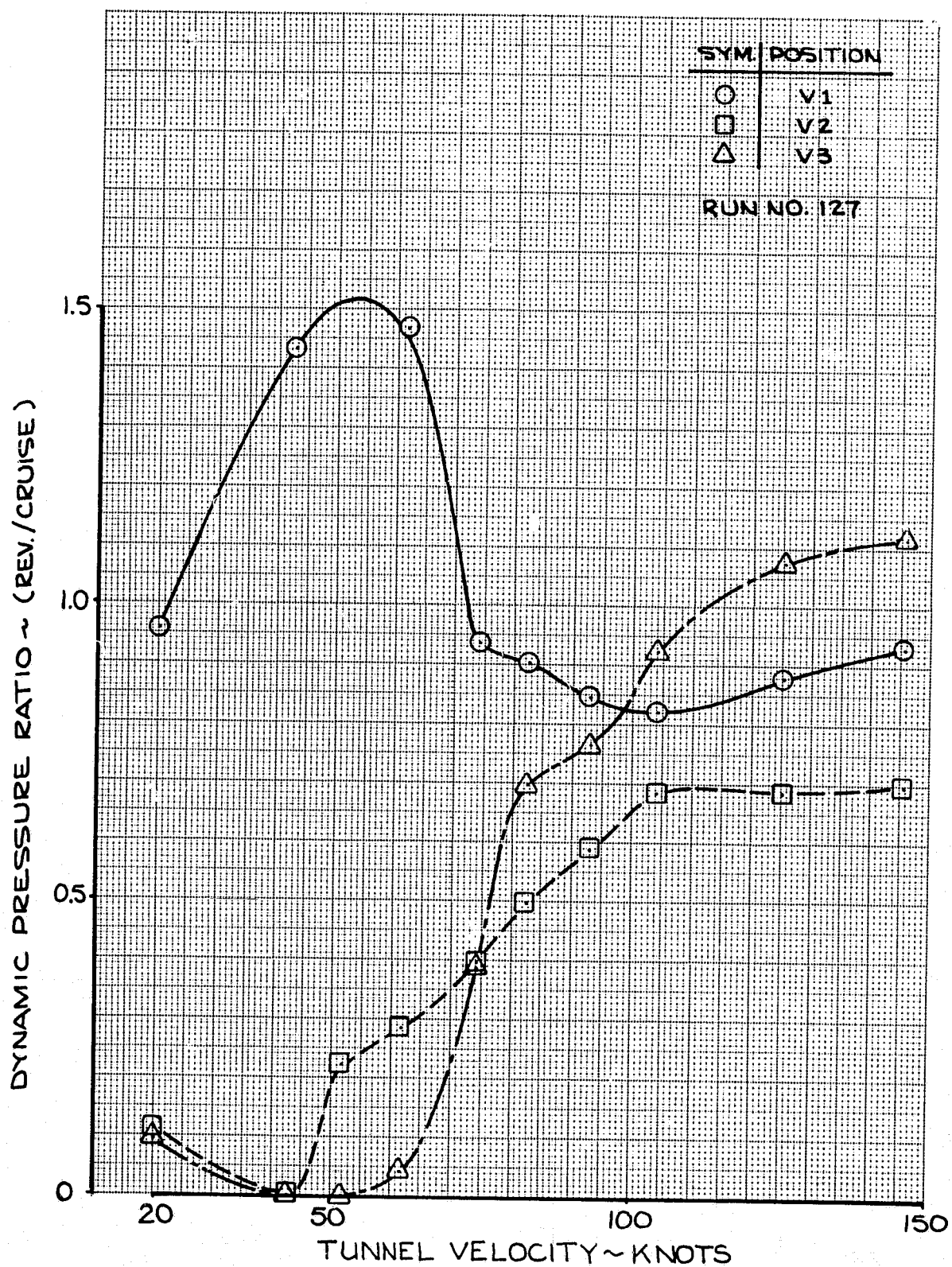
FIGURE 89 — VERTICAL TAIL DYNAMIC PRESSURE RATIOS; CONFIGURATION 12, 40° FLAPS, PPR = 1.5 −10° ORIENTATION
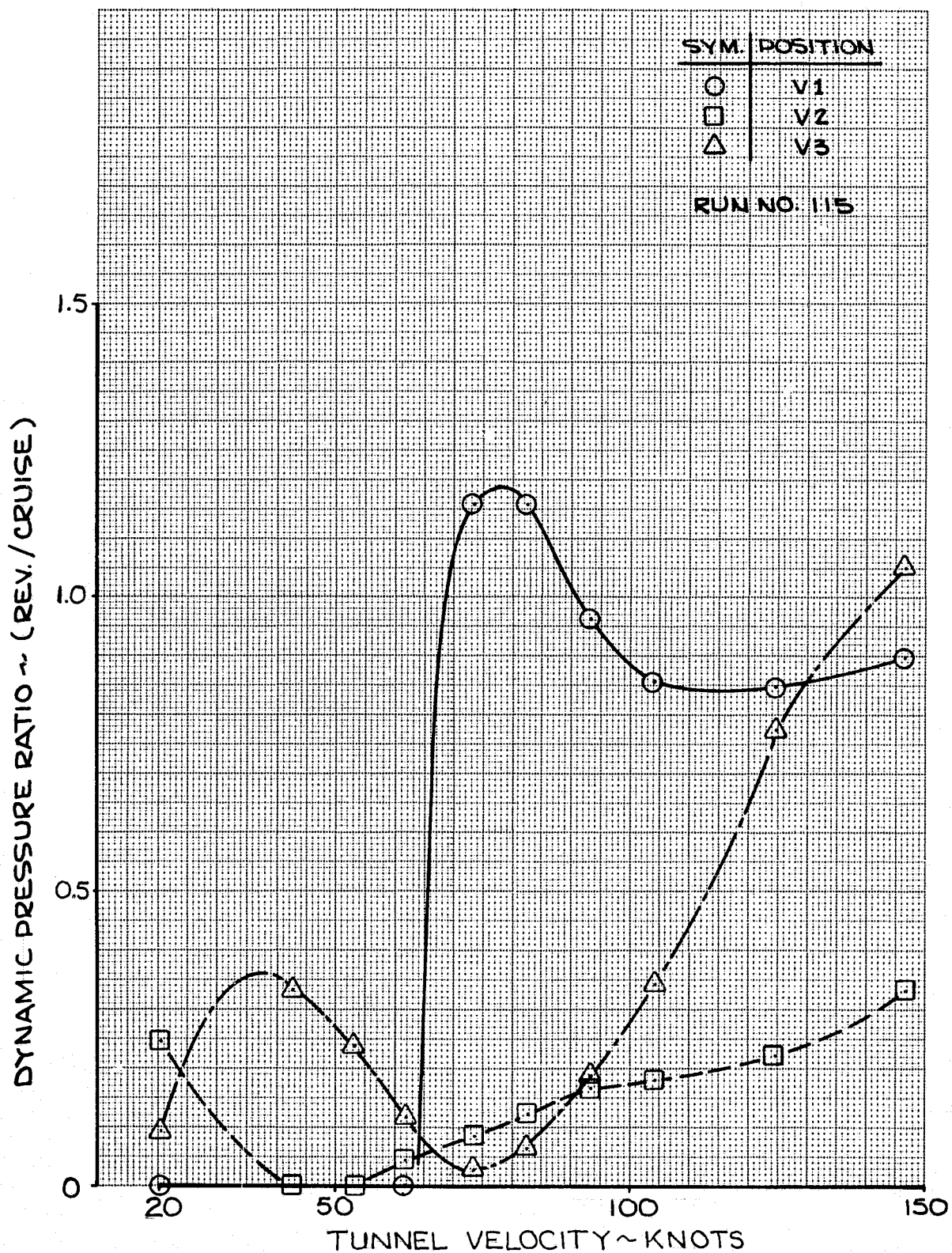
FIGURE **90** — VERTICAL TAIL DYNAMIC PRESSURE RATIOS;
CONFIGURATION 12, 40° FLAPS, PPR = 1.5,
− 20° ORIENTATION

138

FIGURE 91 — VERTICAL TAIL DYNAMIC PRESSURE RATIOS;
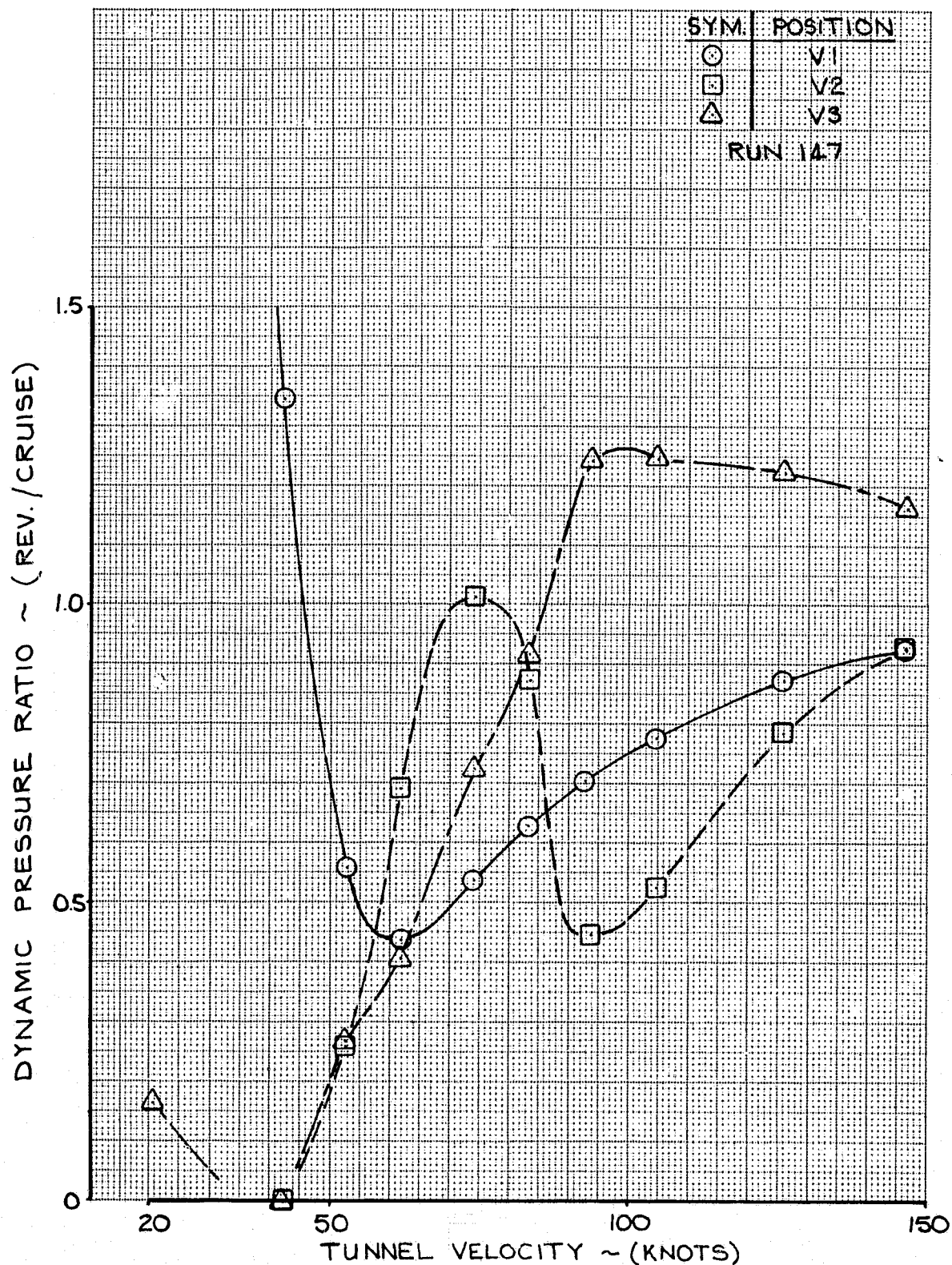CONFIGURATION 12, 40° FLAPS, PPR =1.25,
0° ORIENTATION.

FIGURE 92 — VERTICAL TAIL DYNAMIC PRESSURE RATIOS;
CONFIGURATION 12, 40° FLAPS, PPR = 1.25,
-10° ORIENTATION.

FIGURE 93 — VERTICAL TAIL DYNAMIC PRESSURE RATIOS;
CONFIGURATION 12, 40° FLAPS, PPR = 1.25,
− 20° ORIENTATION.

FIGURE 94 — VERTICAL TAIL DYNAMIC PRESSURE RATIOS;
CONFIGURATION 7, 40° FLAPS, PPR = 1.8,
0° ORIENTATION

FIGURE 95 - VERTICAL TAIL DYNAMIC PRESSURE RATIOS;
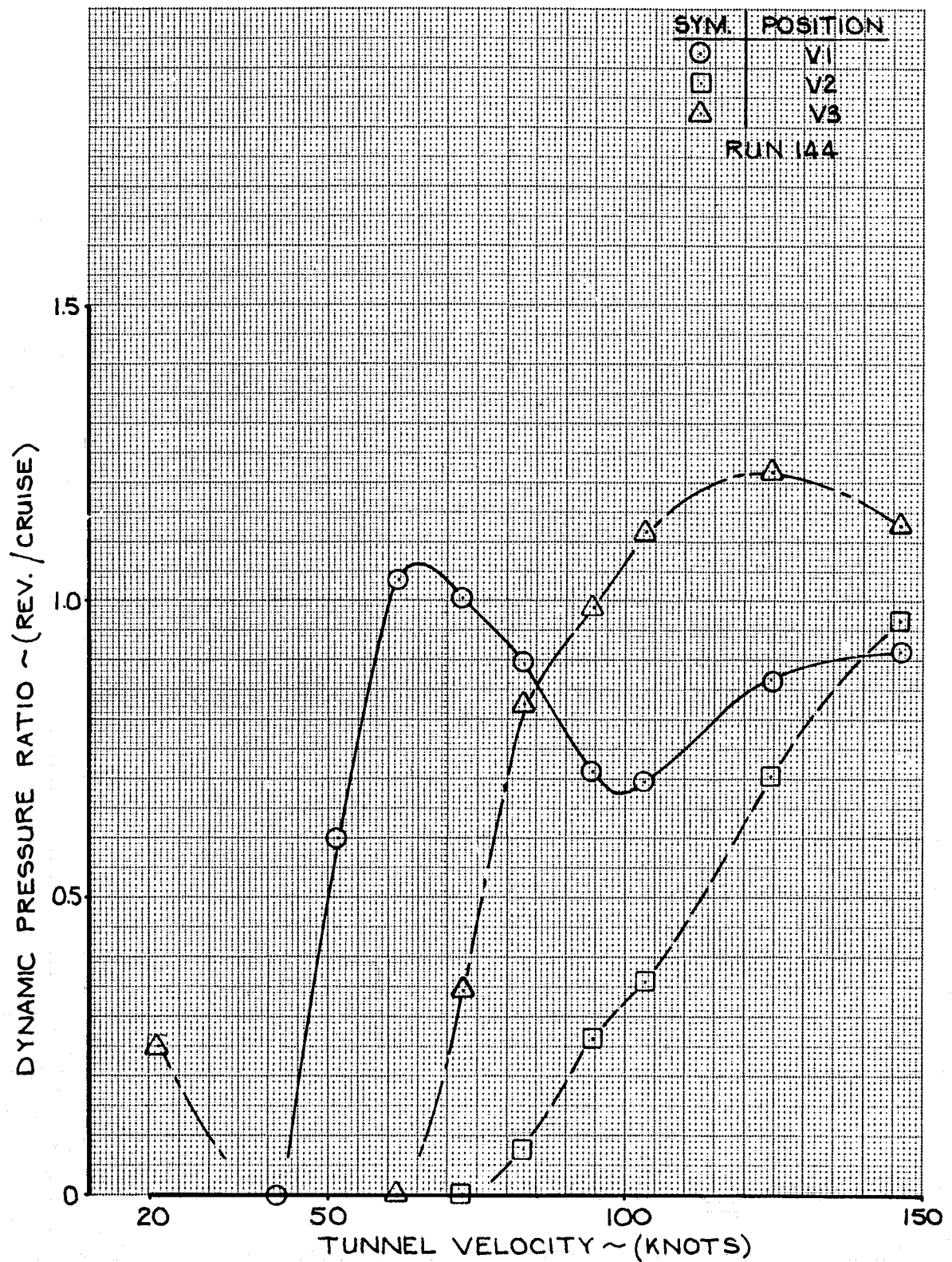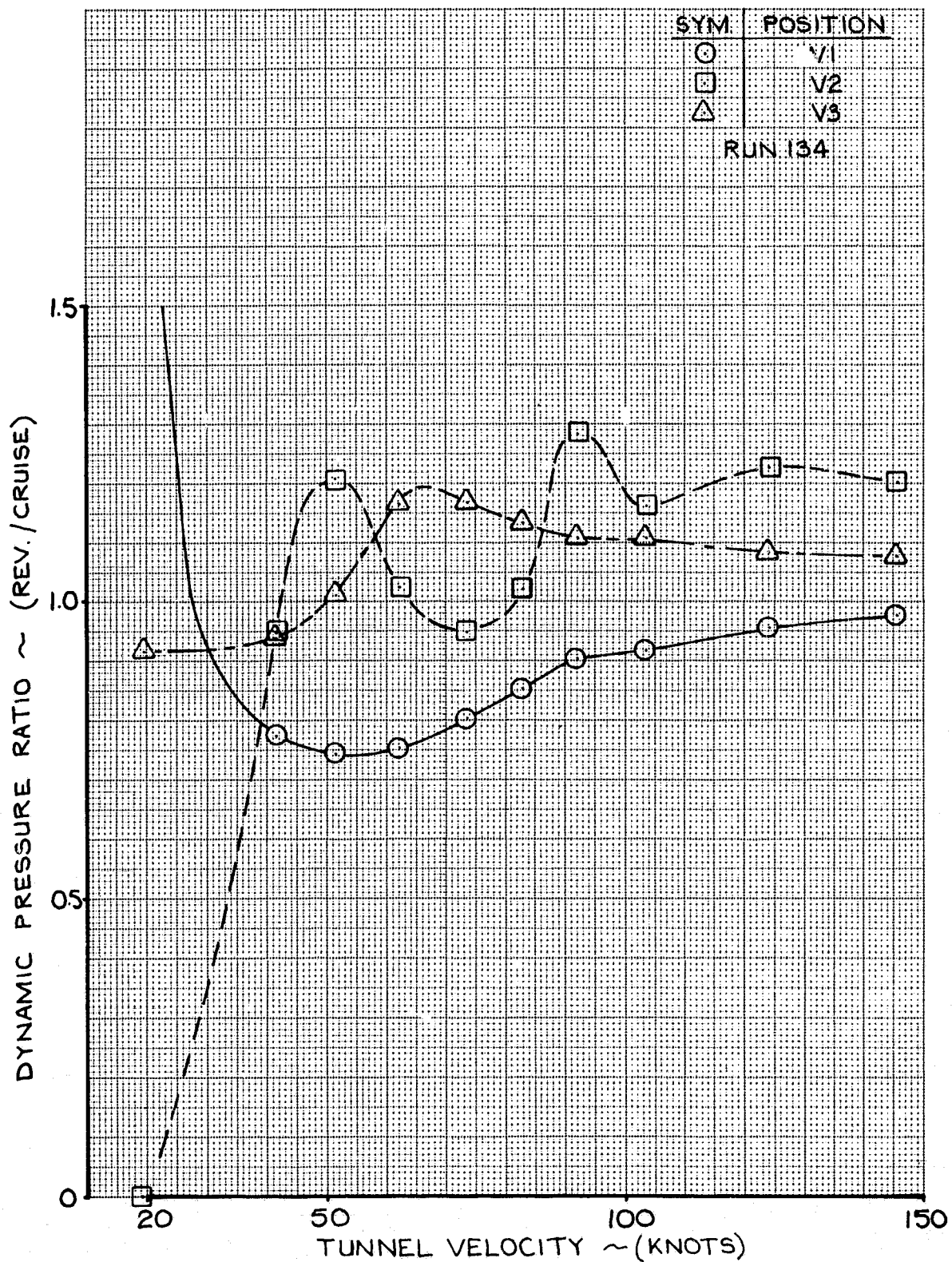CONFIGURATION 7, 40° FLAPS, PPR=1.8,
-10° ORIENTATION

143

FIGURE 96 - VERTICAL TAIL DYNAMIC PRESSURE RATIOS;
CONFIGURATION 7, 40° FLAPS, PPR = 1.8,
-20° ORIENTATION

FIGURE 97 — VERTICAL TAIL DYNAMIC PRESSURE RATIOS;
CONFIGURATION 7, 40° FLAPS, PPR = 1.5,
0° ORIENTATION.

FIGURE 98 — VERTICAL TAIL DYNAMIC PRESSURE RATIOS;
CONFIGURATION 7, 40° FLAPS, PPR = 1.5,
—10° ORIENTATION.

FIGURE 99 — VERTICAL TAIL DYNAMIC PRESSURE RATIOS;
CONFIGURATION 7 , 40° FLAPS, PP R =1.5,
−20° ORIENTATION.

FIGURE 100 — VERTICAL TAIL DYNAMIC PRESSURE RATIOS;
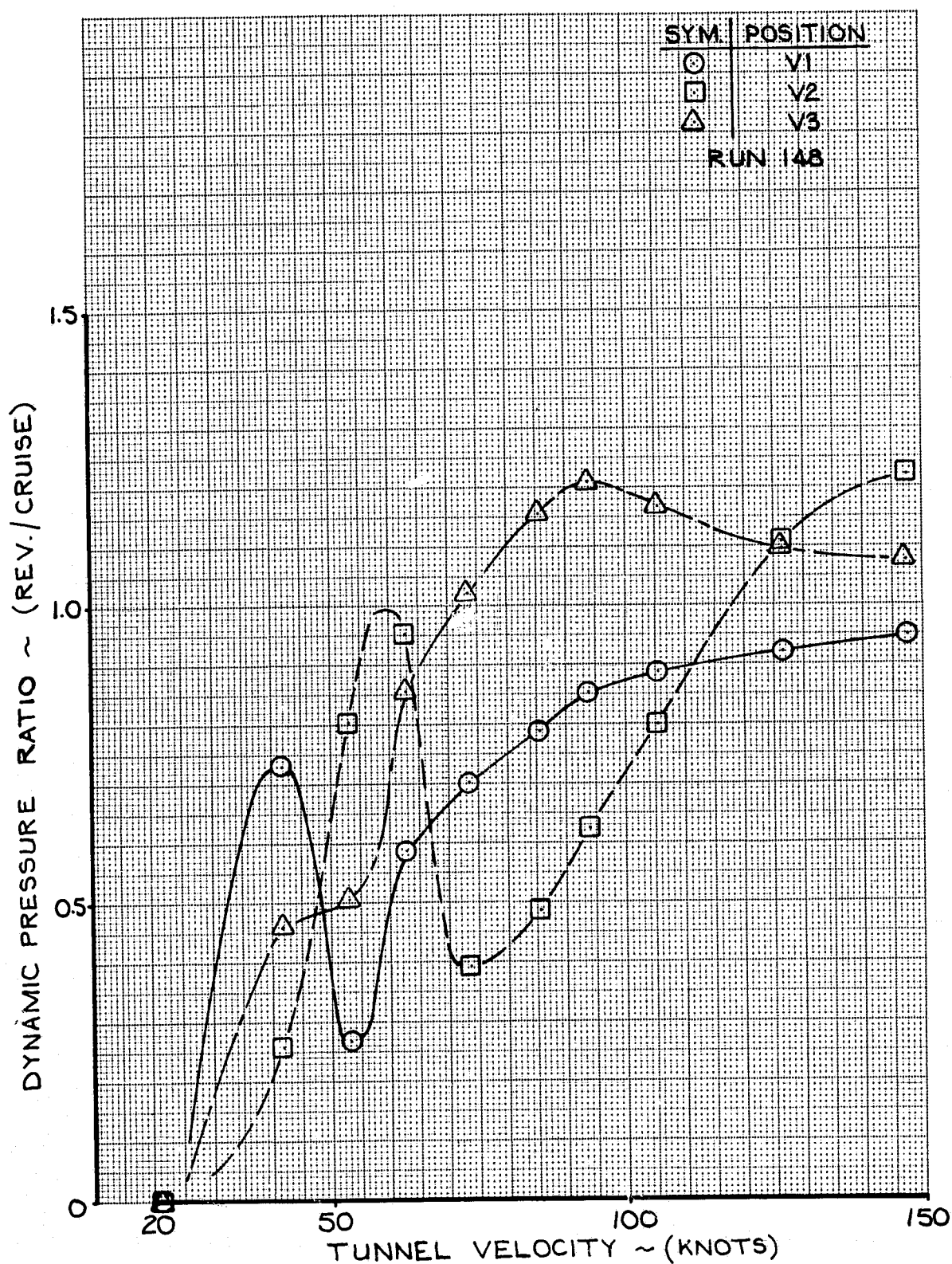CONFIGURATION 7, 40° FLAPS, PPR = 1.25,
ORIENTATION 0°.

FIGURE 101 — VERTICAL TAIL DYNAMIC PRESSURE RATIOS;
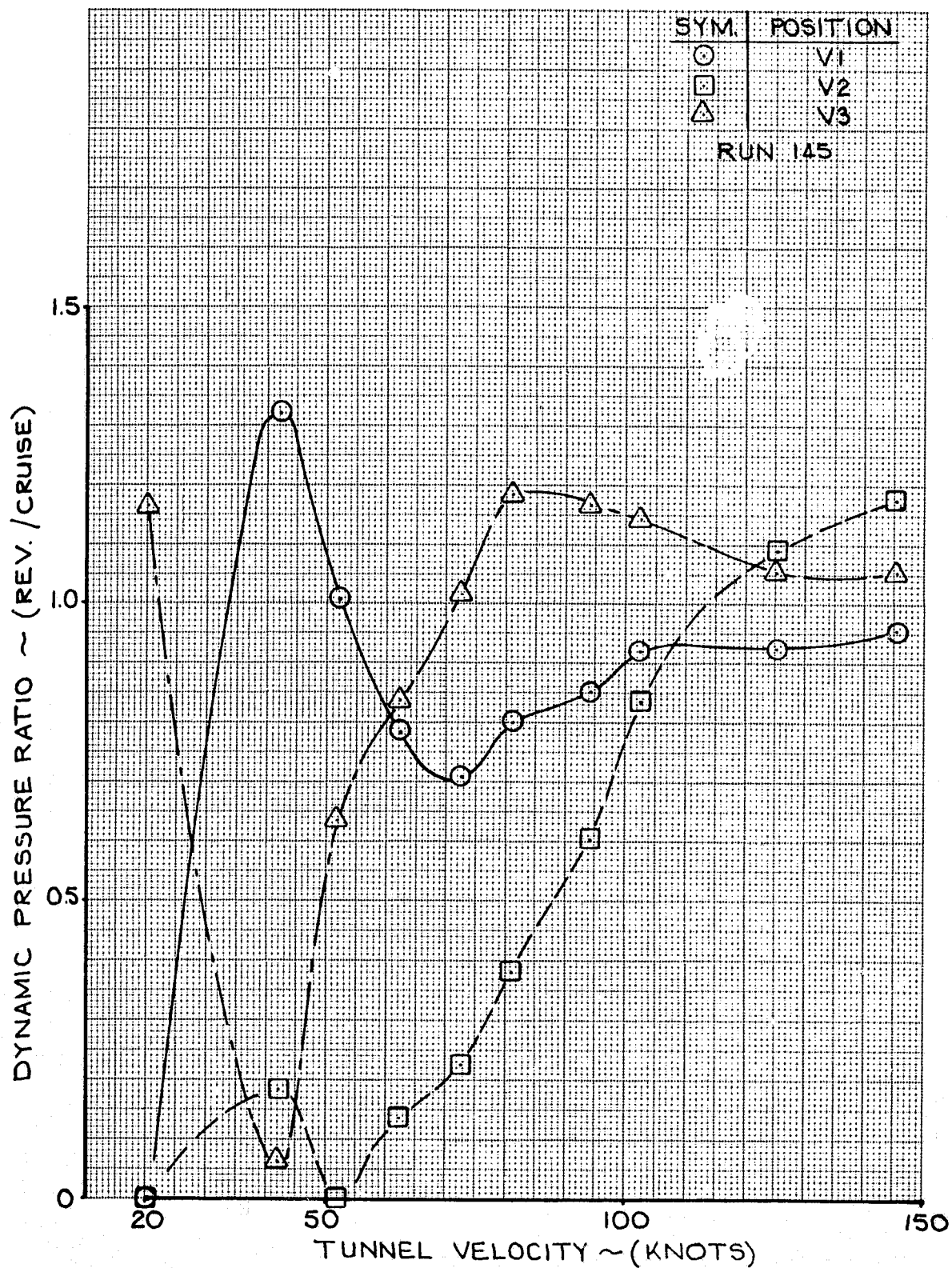CONFIGURATION 7, 40° FLAPS, PPR = 1.25,
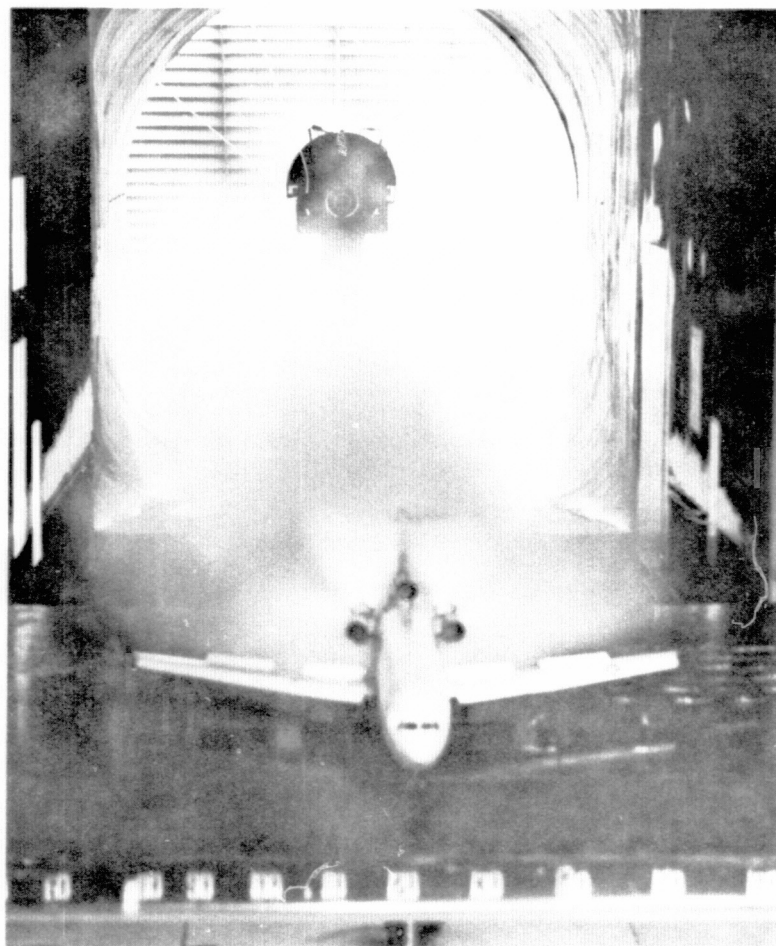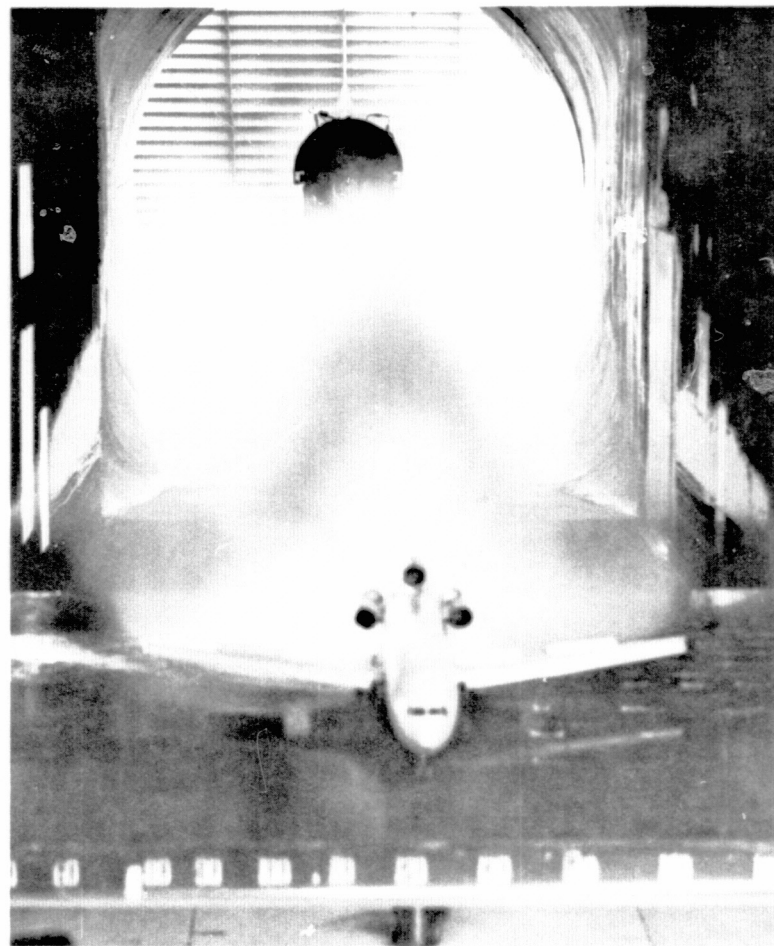ORIENTATION −10°.

FIGURE 102 — VERTICAL TAIL DYNAMIC PRESSURE RATIOS;
CONFIGURATION 7, 40° FLAPS, PPR =1.25
ORIENTATION −20°.

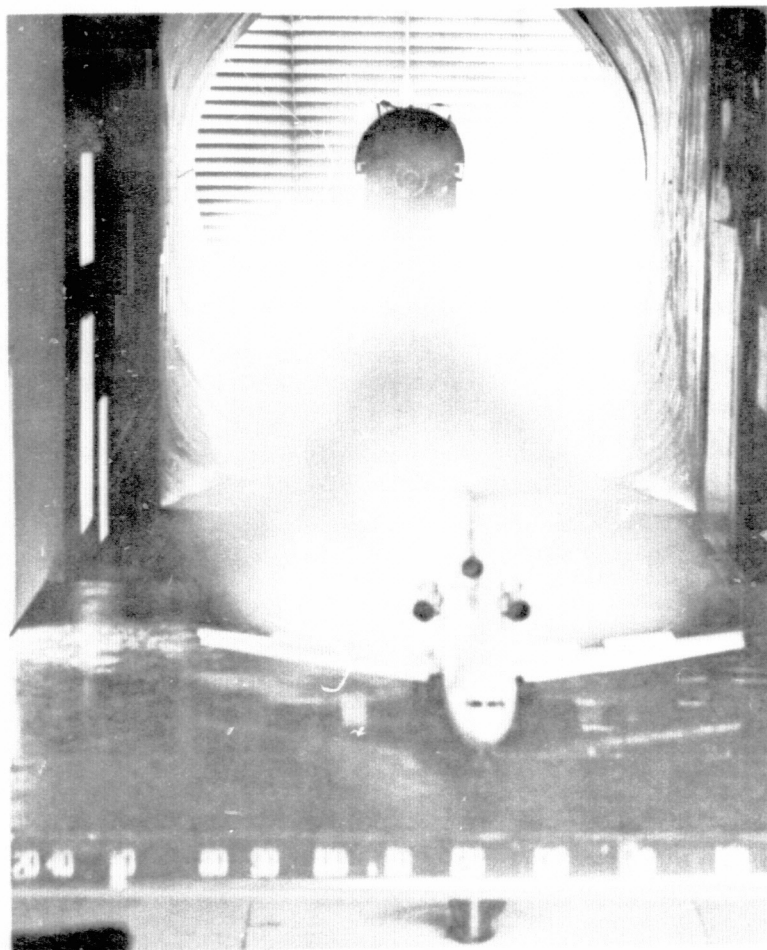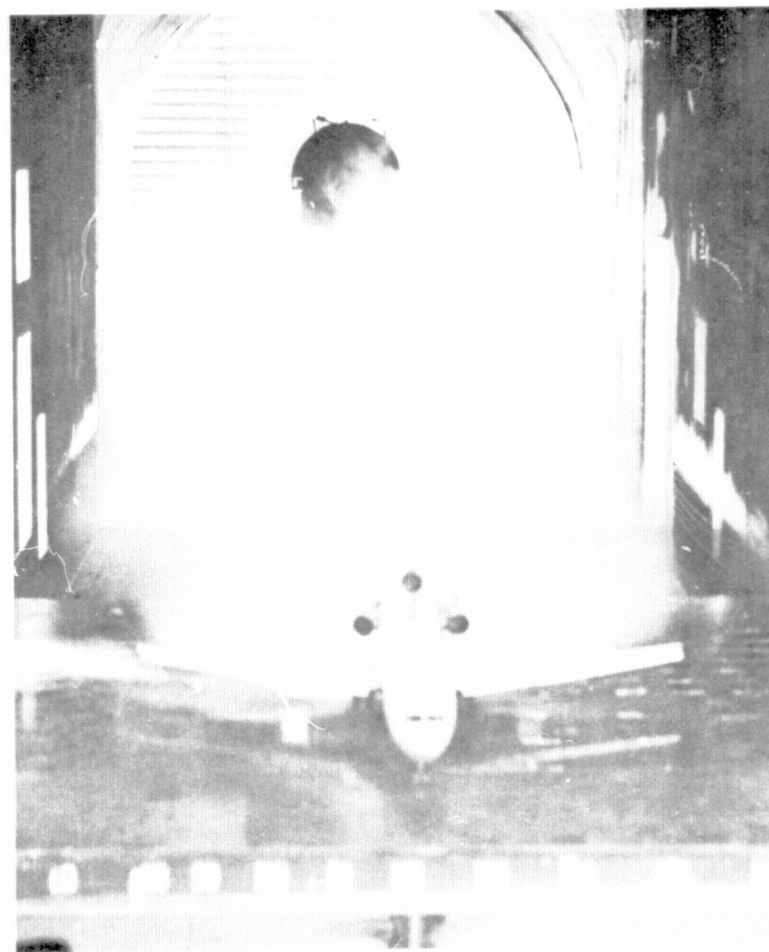0° T/R ORIENTATION   -20° T/R ORIENTATION

FIGURE 103. - FLOW VISUALIZATION, CONFIGURATION 12, PPR = 1.8, T.E. FLAPS = 40°, TUNNEL VELOCITY = 80 KNOTS

0° T/R ORIENTATION   -20° T/R ORIENTATION

FIGURE 104. - FLOW VISUALIZATION, CONFIGURATION 7, PPR = 1.8, T.E. FLAPS = 40°,
TUNNEL VELOCITY = 80 KNOTS

REFERENCES

1. Boeing Commercial Airplane Company, "Phase I 727 JT8D-109 Refan Nacelle and Airplane Integration Definition," D6-41170, June 1, 1973.

2. Boeing Commercial Airplane Company, "727 Airplane Target Thrust Reverser Static Performance Model Test for Refanned JT8D Engines," May 1974.

3. Pratt and Whitney Aircraft, "Phase I Engine Definition and Characteristics of the JT8D-100 Turbofan Engine," P&WA TM4713, Revised June 15, 1973.

4. Boeing Commercial Airplane Company, "Test Data Report of 727-JT8D-100 Refan Thurst Reverser Ingestion Model Test 2396," July 23, 1974.